FORMAL OPTIMIZATION OF HOVERING PERFORMANCE USING FREE WAKE LIFTING SURFACE THEORY

by

SONG-YOUNG CHUNG

FORMAL OPTIMIZATION OF HOVERING PERFORMANCE USING FREE WAKE LIFTING SURFACE THEORY

by

SONG-YOUNG CHUNG

Massachusetts Institute of Technology

Cambridge, Massachusetts 02139

February 1986

Prepared for:

NATIONAL AERONAUTICS AND SPACE ADMINISTRATION

AMES RESEARCH CENTER

UNDER GRANT NAG 2-275

ACKNOWLEDGMENTS

The author would like to express appreciation for the support provided for this research from grants under the Fulbright program and from NASA-Ames.

ABSTRACT

Free wake techniques for performance prediction and optimization of hovering rotor are discussed. The influence functions due to vortex ring, vortex cylinder, and source or vortex sheets are presented. The vortex core sizes of rotor wake vortices are calculated and their importance is discussed. Lifting body theory for finite thickness body is developed for pressure calculation, and hence performance prediction of hovering rotors. Numerical optimization technique based on free wake lifting line theory is presented and discussed. It is demonstrated that formal optimization can be used with the implicit and nonlinear objective or cost function such as the performance of hovering rotors as used in this report.

Table of Contents

LIST OF SYMBOLS

A : Hessian matrix

a : lift curve slope

A_{ij} : normal velocity influence coefficients due to source

A_{ik} : normal velocity influence coefficients doe to vortex

A_{11}, A_{12}, A_{13} : direction cosines of $\vec{t}_x$

A_{21}, A_{22}, A_{23} : direction cosines of $\vec{t}_y$

A_{31}, A_{32}, A_{33} : direction cosines of $\vec{t}_z$

b_{pk} : potential influence coefficients due to source

C_{pk} : potential influence coefficients due to doublet

C : blade chord

C_n : normal force coefficient

C_p : pressure coefficient or power coefficient

C_{ij} : tangential velocity influence coefficient due to source

C_{ik} : tangential velocity influence coefficient due to vortex

C_d : drag coefficient

C_ℓ : lift coefficient

C_T : thrust coefficient

C_Q : torque coefficient

d : vortex core diameter or size

E : elliptic integral of first kind

$\vec{e}_\phi$: azimuthal unit vector

$\vec{e}_r$: radial unit vector

F : elliptic integral of second kind or objective function

$\vec{F}$: force acting on lifting body

FMIN : value of objective function F at $\alpha = 0$

FV : value of objective function F at $\alpha = V$

FW : value of objective function F at $\alpha = W$

G : gradient vector of objective function F

H : approximate inverse of Hessian matrix A

h : spacing between ring vortices

$\vec{M}$: moment acting on lifting body

M : position where induced velocity is computed

M' : position of vortex

N : normal force acting on blade section

$\vec{n}$: unit normal vector to body surface

$\vec{P}$: axial momentum

Q : torque acting on rotor

R : blade radius

r : radial coordinate of ring vortex

r_{pq} : distance between singularity and field point

r_p : penalty parameter

S : search direction for minimization

T : thrust produced by rotor

$\vec{t}_x$, $\vec{t}_y$, $\vec{t}_z$: unit vectors of panel center coordinate

U : total velocity with respect to blade

U_∞ : free stream velocity

W_{pk} : potential influence coefficient due to doublet

W : wake surface

w : downwash

X_c : position of control point

X_v : position of concentrated vortex

X_i : design variable vector

z : axial coordinate of ring vortex

Greek Symbols

α : angle of attack or move parameter in search direction

$\delta(z)$: delta function

δ_{pk} : kronecker delta

ε : vortex core radius

η : normalized blade radius

γ : normalized bound circulation

Γ : bound circulation

θ : blade pitch angle

λ : normalized downwash

ϕ : azimuthal angle or velocity potential

ρ : air density

σ : solidity or source strength

ψ : Stokes stream function

ω : swirl angular velocity or vorticity

Ω : rotation velocity of rotor

CHAPTER 1
INTRODUCTION

1.1 Purpose

The best aerodynamic design of hovering helicopter rotor blades, propeller blades or wind turbine rotor blades can be achieved by the accumulated performance data, the engineering experience, and good performance analysis and design codes. A reliable aerodynamic performance analysis can be carried out by computational fluid dynamics. However, heuristic parametric analysis of many different configuration of blades by CFD is an expensive means of achieving good aerodynamic design.

A systematic method to achieve the best design is to set up a suitable quantity to maximize or to minimize. This quantity is combined into the objective function. When there are constraints which the best design should not violate, these constraints can be grouped into the penalty function with the objective function. When the penalty or cost function which the design should pay is minimized, the best design is achieved.

Usually the penalty function is a nonlinear function of a number of independent design parameters. Searching the best combination of the design variables to achieve the

minimum cost can be done numerically by various methods. Methods such as the steepest descent, conjugate direction, variable metric or quasi-Newton, and Newton's method can be used to minimize a function. The function minimization requires a performance analysis code to evaluate the penalty function at each design combination, the gradient or sensitivity calculation for methods such as conjugate direction or quasi-Newton method, and Hessian calculation for Newton's method. Hence the design computed by the combination of CFD and function minimization can not be better than the accuracy of the code. The codes used may be potential, Euler, or Reynolds averaged Navier-Stokes ones. Among potential flow codes one may distinguish between surface singularity type methods such as lifting line, lifting surface, panel method, and small disturbance or full potential finite difference method.

The optimum design of hovering helicopter or propeller blades can be achieved by minimizing the required power to sustain induced and profile drag while keeping the thrust constant. The penalty function for this problem is a combination of the objective function which is the required power and the constraint function which is the given thrust. This penalty function is suitable for converting a constrained function minimization to an unconstrained function minimization. In function minimization the

gradient calculation by direct perturbation of design variables can usually be done with less than 7 variables. Hence, a performance analysis code can be combined with a numerical optimization code, that is, function minimization code to determine the best combination of design variables. With more than 10 design variables the analytic gradient calculation code is a more powerful and accurate method for determining which design variables are best than finite difference methods.

The objective of this research is to compute the optimum chord and twist distribution of a hovering rotor. The methods used are lifting line and lifting surface theories coupled with a fast free wake model developed by Miller(ref.s 7-11). The profile drag is calculated by blade element theory using the effective angle of attack obtained from lifting line or surface theory. The objective function is the power due to induced and profile drag and the constraint function is the given thrust. The optimization code used are quasi-Newton method or conjugate gradient method. QNMDIF, the optimization code of quasi-Newton method developed by Kennely at NASA Ames, is used. This optimization code is combined with the performance analysis code of lifting line and lifting surface theories coupled with fast free wake model. Only the optimization using lifting line is performed and presented. During

optimization iteration the objective and constraint functions are computed by free wake lifting line theory exactly. In all optimizations the penalty function is used to convert the constrained optimization to the unconstrained optimization.

1.2 Technical Approach

The hovering rotor performances predicted by 3-D momentum and by free wake lifting line theory are compared in section (2.1). The bound circulation distribution obtained by 3-D momentum theory is very different from that found from free wake theory. The influence functions for a vortex ring, a vortex cylinder, a trailing vortex filament, and a rectangular vortex sheet or source are given in section (2.2). Also, in section (2.2) the swirl loss correction method is derived. In section (2.3) the free wake lifting line theory is shown to predict the results which are in good agreement with the experimental results of ATB tilt rotor of Ref.(6). The vortex core size of a hovering rotor is calculated and is shown to grow as the vortex ring moves further away from the rotor plane in section (2.4).

In section (3.1) vortex lattice and vortex panel lifting surface theories are derived and their applications to the hovering rotor are discussed. In section (3.2) the surface singularity method is shown to be the solution of Green's function applied to the rotor or the wing problems. The superposition method of sources and vortex sheets is derived for the pressure calculation and hence the performance prediction of any lifting body in section (3.3).

In section (3.4) the free wake geometry is computed by integrating the local velocity on the wake element with respect to the time after its generation by the blade. The overall results obtained by the application of the free wake surface singularity method to the hovering rotor and wings are shown and compared with past results in section (3.5).

In section (4.1) several different choices of the objective function and quadratic penalty functions are derived and the chosen seven different set of design variables are discussed. The direction of the function minimization is presented as the Quasi-Newton and Conjugate gradient method in section (4.2). Once the minimization direction is determined, the multi-dimensional problem becomes an one- dimensional minimization one. The parabolic line search technique is presented in section (4.3). In section (4.4) three types of rotor blade geometries are used for the formal optimization of the hovering performance. They are the rotor of Ref.68, which has the straight twist and a constant chord, a modified rotor, which has the straight twist and a taper ratio of 0.3. The rotor of Ref.68 is chosen because the experimental and theoretical results on bound circulation are available. The third rotor is a double twisted and tapered rotor.

1.3 Review Of Past Work

The vortex roll-up, or core size of the resulting vortex, and vortex motion are treated in Ref.s[1,2,3,4,5,30,31]. Free wake lifting line or surface theory was applied to the performance prediction of hovering rotor in Ref.s [7-14,24,28,29,35]. Surface singularity methods were used for the analysis of wing and rotor blade in Ref.s [15-22,27,33,34,36,55-63]. The review and applications of formal optimization techniques were presented in Ref.s [25,37,39,40,41,42,43,44,45,46,47,48]. The theoretical basis of numerical optimization was formulated in Ref.s [49,50,51,52,53,54]. The detailed review of all previous work are handled in the introduction to each chapter.

From all previous work the vortex motion, interaction to roll-up, the effect of vortex position on the rotor performance are well developed theoretically and the results are in good agreement with experimental data. Surface singularity methods were successful for the calculation of pressure field for the wing or rotor blade with fixed wake geometry. Several optimization program such as CONMIN, QNMDIF, or others were used to improve the aerodynamic and dynamic performance of wings, or rotors, or structures. In most cases the optimized results were only as good as the

heuristic and parameter optimization. Several theories on numerical optimization were presented and tested for the several explicit nonlinear objective functions.

CHAPTER 2
FREE WAKE LIFTING LINE THEORY AND VORTEX CORE SIZE OF ROTOR WAKE VORTICES

2.1 FREE WAKE MODEL

The wake of rotor blades is piled below the blades as shown in figure (2-1) unlike the wake of an ordinary wing which moves away from the wing. Since the effect of free wake vortices on the performance is very profound, a free wake analysis is necessary for the flow prediction of a wing which has leading or side edge vortices. For such wings the free wake results can be used as boundary conditions for the near field solutions of Euler or Navier-Stokes equation as done in Ref.(32).

The fast free wake model developed in Ref.s [7,8,9,10,11] are discussed in this section and was used for the formal optimization of hovering performance with lifting line or surface theory. The work done by the induced drag of rotor or wing appears as the kinetic energy due to trailing vortices as discussed in section (2-4). The study of the motion of trailing vortices is necessary for the determination and reduction of the induced drag and for the minimizatioin of the wake hazard to the following aircraft.

As developed in Ref.(7) the free wake is divided into three sections : the near wake attached to the blade on the

plane of rotation, an intermediate wake of rolled-up ring vortices, a far wake of semi-infinite vortex cylinders. The near wake is composed of a series of circular arc vortex filaments which span the half of the blade spacing. After leaving the blade as a vortex sheet, this distributed wake rolls up quickly according to the conservation of linear and angular momentum into helices which are approximated by vortex rings. The tip vortex is formed from the tip to the point of maximum bound circulation. A second roll up is assumed between this point of maximum circulation and the 15 percent spanwise position. The remaining circulation to the root rolls up into a third vortex. The effect of root vortex is neglected during the actual free wake calculation since its effect on the performance is negligible ,while making the solution converge slowly. The existence of the root vortex is doubtful for the hovering flight. There are four vortex rings in axial direction to represent the intermediate wake. The far wake consists of semi-infinite vortex cylinders starting at a distance from the rotor one vortex spacing below the last intermediate vortex. The geometry of this wake model is shown in Figure (2-1) taken from Ref.(7). Figure (2-2) shows the difference in predicted bound circulations between 3-D momentum theory and free wake lifting line theory. Table (1) and (2) present the results obtained by momentum theory and free wake

lifting line theory. In table (1) 10 spanwise divisions were used and in table (2) 15 spanwise divisions were used. In both tables CT and CP are thrust and power coefficients. CPI is the power coefficient due to the induced drag. FM is the figure of merit, CTR and CPR are thrust and power coefficients with wake rotation effect included.

2.2 DERIVATION OF INFLUENCE COEFFICIENTS AND MATRIX SOLUTION

(a) The velocities due to vortex ring or cylinder.

Ref.(7) gives the induced velocity due to a ring vortex derived by using the Biot-Sarvart law. The ring vortex has a radius of rR and an axial distance of z from the rotor blade of radius R as shown in figure. The vertical components of velocity induced at η due to a ring vortex of radius r is

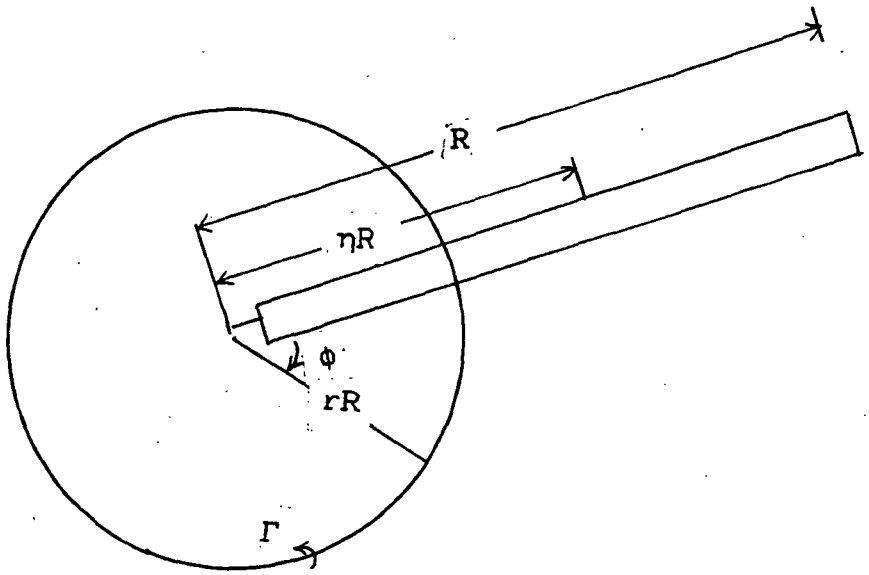

$$w = \frac{\Gamma}{4\pi R} \int_0^{2\pi} \frac{r(r - \eta\cos\phi)\, d\phi}{(\eta^2 + r^2 + z^2 - 2r\eta\cos\phi)^{3/2}} = \frac{\Gamma}{4\pi R} I_1$$

The radial component of induced velocity at η is

$$u = \frac{\Gamma}{4\pi R}\int_0^{2\pi} \frac{zr\cos\phi\, d\phi}{(\eta^2 + r^2 + z^2 - 2r\eta\cos\phi)^{3/2}} = \frac{\Gamma}{4\pi R} I_2$$

From ref.(7), I_1 and I_2 are given as follows.

$$I_1 = \sqrt{\frac{k^2}{r\eta}}\,[K - E\{1-0.5k^2(1+r/\eta)\}/(1-k^2)]$$

$$I_2 = \frac{z}{2\eta}\sqrt{\frac{k^2}{r\eta}}\,[E(2-k^2)/(1-k^2) - 2K]$$

where $k^2 = \dfrac{4r\eta}{(r+\eta)^2 + z^2}$

$$E = 1 + 0.5(F-0.5)(1-k^2) + (3/16)(F-1-1/12)(1-k^2)^2 + \ldots$$

$$K = F + 0.25(F-1)(1-k^2) + (9/64)(F-1-1/6)(1-k^2)^2 + \ldots$$

and $F = \ln\left(\dfrac{4}{\sqrt{1-k^2}}\right)$

The vertical velocity due to the far wake of semi-infinite cylinder at η is obtained by integrating equation (2-1) from z to ∞ .

$$w2 = \frac{1}{4\pi R}\frac{d\Gamma}{dz}\int_z^\infty\int_o^{2\pi} \frac{r(r-\eta\cos\phi)\, d\phi}{(\eta^2 + r^2 + z^2 - 2r\eta\cos\phi)^{3/2}}$$

$$= \frac{1}{4\pi R}\frac{d\Gamma}{dz}\int_0^{2\pi} \frac{r(r-\eta\cos\phi)}{\eta^2+r^2-2r\eta\cos\phi}\left[1-\frac{z}{(\eta^2+r^2+z^2-2r\eta\cos\phi)^{1/2}}\right]d\phi$$

$$= \frac{1}{4\pi R}\frac{d\Gamma}{dz}\int_0^{2\pi} I(\phi)\,d\phi$$

$$w2 = \frac{1}{4\pi R}\frac{d\Gamma}{dz}\sum_{i=1}^{N} I(\phi_i)\,\frac{2\pi}{N}\,,\quad \phi_i = \frac{2\pi}{N}(2i-1)$$

The radial velocity due to the far wake of semi-infinite cylinder is

$$u2 = \frac{1}{4\pi R}\frac{d\Gamma}{dz}\int_z^{\infty}\int_0^{2\pi} \frac{zr\cos\phi\,d\phi\cdot dz}{(\eta^2+r^2+z^2-2r\eta\cos\phi)^{3/2}}$$

$$= \frac{1}{4\pi R}\frac{d\Gamma}{dz}\int_0^{2\pi} \frac{r\cos\phi\,d\phi}{(\eta^2+r^2+z^2-2r\eta\cos\phi)^{1/2}}$$

$$= \frac{1}{4\pi R}\frac{d\Gamma}{dz}\frac{2}{k}\sqrt{\frac{r}{\eta}}\left[K(2-k^2)-2E\right]$$

(b) The velocity due to the trailing vortex filaments.

The velocity induced by a element of strength

$\vec{\Gamma} = \Gamma\left(1+\frac{x'}{\Delta x}\right)$ and length $\Delta S = 2\Delta x$ at point M(x,y,z)

is given in ref.(28) as follows.

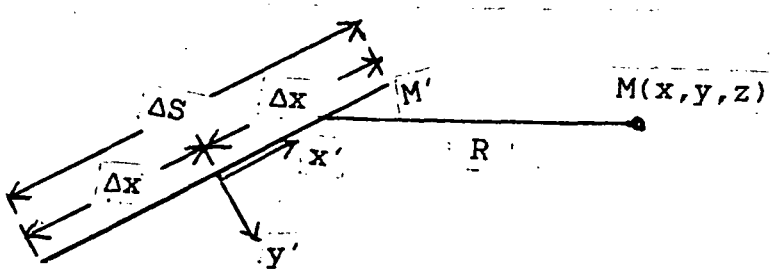

$$\vec{V} = -\frac{1}{4\Pi}\int_{-\Delta x}^{\Delta x} \frac{\overrightarrow{M'M} \times \Gamma(1 + x')\,\vec{i}}{R^3} dx'$$

Let $\vec{W}_S = -\frac{1}{4\Pi}\int_{-\Delta x}^{\Delta x} \frac{\overrightarrow{M'M} \times \Gamma\vec{i}}{R^3}\, dx'$

$$\vec{W}_v = -\frac{1}{4\Pi}\int_{-\Delta x}^{\Delta x} \frac{\overrightarrow{M'M} \times \Gamma x'\vec{i}}{R^3}\, dx'$$

Then, $W_{xs} = 0$

$$W_{ys} = -\frac{1}{4\Pi}\,\Delta S \cdot z \cdot \Gamma \cdot I_s$$

$$W_{zs} = \frac{1}{4\Pi}\,\Delta S \cdot y \cdot \Gamma \cdot I_s$$

$$W_{xv} = 0$$

$$W_{yv} = -\frac{1}{4\Pi}\,\Delta S \cdot z \cdot \Gamma \cdot \Delta x \cdot I_v$$

$$W_{zv} = \frac{1}{4\Pi}\,\Delta S \cdot y \cdot \Gamma \cdot \Delta x \cdot I_v$$

,where $I_s = \frac{1}{2\Delta x(y^2 + z^2)}\left[\frac{x + \Delta x}{R_1} - \frac{x - \Delta x}{R_3}\right]$

$$I_v = \frac{1}{2\Delta x^2(y^2 + z^2)}\left[\frac{R_0^2 + x\Delta x}{R_1} - \frac{R_0^2 - x\Delta x}{R_3}\right]$$

$$R_0 = \sqrt{x^2 + y^2 + z^2}$$

$$R_1 = \sqrt{(x + \Delta x)^2 + y^2 + z^2}$$

and $$R_3 = \sqrt{(x - \Delta x)^2 + y^2 + z^2}$$

The velocity induced by an vortex element of circular arc in near wake is given in ref.(29).

(c) The velocities due to a rectangular panel of vortex sheet or source.

The velocity induced by a rectangular vortex sheet is given in ref.(28) and one by a source in ref.(27) as follows. These velocities will be required later for a lifting body solution.

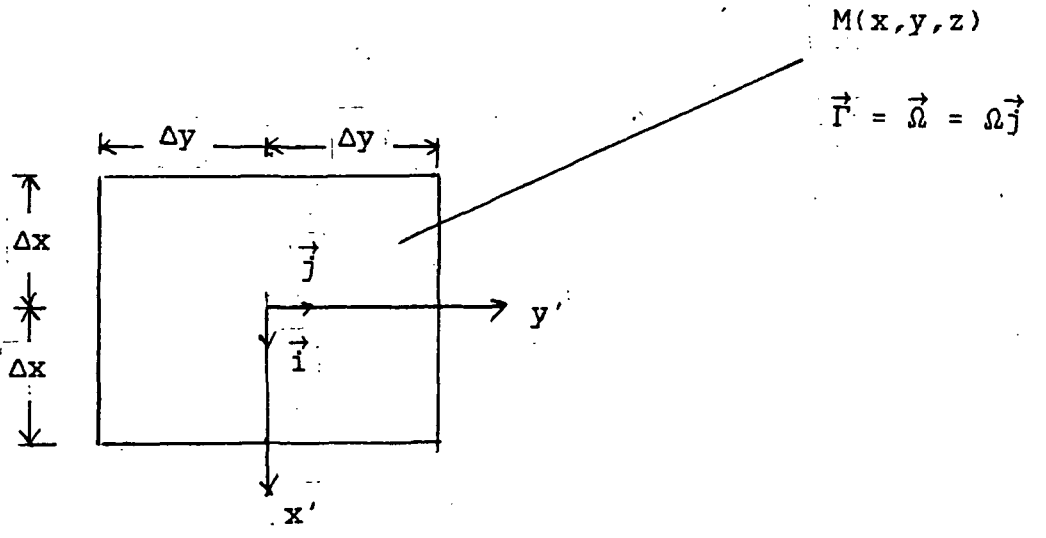

The velocity induced at M by a constant vortex panel is $\vec{W}_C(M)$

$$\vec{W}_c(M) \quad \left| \begin{array}{l} W_{xc} = \frac{\Omega}{4\Pi} J_1 \\ W_{yc} = 0.0 \\ W_{zc} = \frac{\Omega}{4\Pi} J_2 \end{array} \right.$$

The velocity induced at M by a constant source panel is $\vec{W}_S(M)$

$$\vec{W}_s(M) \quad \left| \begin{array}{l} W_{xs} = \frac{\sigma}{4\Pi} J_3 \\ W_{ys} = \frac{\sigma}{4\Pi} J_4 \\ W_{zs} = \frac{\sigma}{4\Pi} J_1 \end{array} \right.$$

Here, $J_1 = \arctan\left(\frac{-H_2}{zR_3}\right) - \arctan\left(\frac{-H_3}{zR_4}\right)$

$$+ \arctan\left(\frac{-H_4}{zR_2}\right) - \arctan\left(\frac{-H_1}{zR_1}\right)$$

$$J_2 = \ln\left[\frac{(y + \Delta y) + R_1}{(y - \Delta y) + R_3} \cdot \frac{(y - \Delta y) + R_4}{(y + \Delta y) + R_2}\right]$$

$$J_3 = \ln\left[\frac{R_1 + R_3 - 2\Delta y}{R_1 + R_3 + 2\Delta y} \cdot \frac{R_4 + R_2 + 2\Delta y}{R_4 + R_2 - 2\Delta y}\right]$$

and $J_4 = \ln\left[\frac{R_3 + R_4 + 2\Delta x}{R_3 + R_4 - 2\Delta x} \cdot \frac{R_2 + R_1 - 2\Delta x}{R_2 + R_1 + 2\Delta x}\right]$

Here, $H_1 = (y + \Delta y) \cdot (x + \Delta x)$

$$H_2 = (y - \Delta y) \cdot (x + \Delta x)$$

$$H_3 = (y - \Delta y) \cdot (x - \Delta x)$$

$$H_4 = (y + \Delta y) \cdot (x - \Delta x)$$

$$R_1 = \sqrt{(x + \Delta x)^2 + (y + \Delta y)^2 + Z^2}$$

$$R_2 = \sqrt{(x - \Delta x)^2 + (y + \Delta y)^2 + z^2}$$

$$R_3 = \sqrt{(x + \Delta x)^2 + (y - \Delta y)^2 + z^2}$$

$$R_4 = \sqrt{(x - \Delta x)^2 + (y - \Delta y)^2 + z^2}$$

The induced velocities with respect to a reference coordinate are obtained from the velocities with respect to panel center coordinate. Let three unit vectors of panel center coordinate be $\vec{t}_x$, $\vec{t}_y$ and $\vec{t}_z$ with respect to a reference coordinate. Then, the three unit vectors are given in terms of direction cosines, A_{nm}.

$$\vec{t}_x = (A_{11} , A_{12} , A_{13})$$

$$\vec{t}_y = (A_{21} , A_{22} , A_{23})$$

$$\vec{t}_z = (A_{31} , A_{32} , A_{33})$$

The velocity, $\vec{V}$ with respect to a reference coordinate is obtained by transforming the velocity, $\vec{W}$ with respect to panel center coordinate.

$$V_x = A_{11} W_x + A_{21} W_y + A_{31} W_z$$

$$V_y = A_{12} W_x + A_{22} W_y + A_{32} W_z$$

$$V_z = A_{13} W_x + A_{23} W_y + A_{33} W_z$$

(d) Matrix solution

The lift is related to the bound circulation by Kutta-Joukowski law.

$$L = 0.5 \rho U^2 a \alpha C = \rho U \Gamma \qquad \text{—— (2-2)}$$

$$\Gamma = 0.5 \left(\Omega^2 r^2 + w^2 \right)^{1/2} a C \left(\Theta + \frac{w}{\Omega r} \right) \qquad \text{—— (2-3)}$$

where Ω is the rotational velocity, r is the radius, w is the downwash, Θ is the pitch angle, a is the lift curve slope, C is the chord, Γ is the bound circulation, and α is the local blade angle of attack.

$$\frac{\Gamma}{\Omega R^2} = \gamma = 0.5 \left(\eta^2 + \lambda^2 \right)^{1/2} a \frac{C}{R} \left(\Theta + \frac{\lambda}{\eta} \right) \qquad \text{—— (2-4)}$$

where η is the normalized radius and λ is the normalized downwash. Then,

$$\lambda_i = A_{ij}\ \gamma_j \qquad \text{—— (2-5)}$$

A_{ij} are the influence coefficients which are the induced velocities on blade station, i, due to all trailing vortices of unit circulation on blade station, j.

$$\gamma_i^{k+1} = 0.5\ a\ \frac{C}{R}\ U_i^k\ (\Theta_i + A_{ij}\ \gamma_j^{k+1}\ /\eta_i\ ) \qquad \text{—— (2-6)}$$

$$[\ I - 0.5\ a\ \frac{C}{R}\ A_{ij}\ \ U_i^k\ /\eta_i\ ]\ \{\gamma_j\}^{k+1} = 0.5\ a\ \frac{C}{R}\ \ U_i^k\ \Theta_i \qquad \text{—— (2-7)}$$

$$[\ \alpha_{ij}\ ]^k\ \{\gamma_j\}^{k+1} = \{\beta_i\ \}^k \qquad \text{—— (2-8)}$$

Here, I is the unit matrix. The above linear system of equations are solved until $\{\ \gamma_i\ \}$ converges for the fixed wake geometry. Then a new wake geometry is obtained by integrating the local velocities on all wake vortices and a new influence coefficients are calculated from the new wake geometry. This procedure is repeated until the bound circulation distribution and the wake geometry are converged.

(e) Correction of the swirl loss to matrix solution.

By applying linear and angular momentum balance to a blade element of dr we obtain the following.

$dT = dm\ w' = 2\ dm\ w$, where $dm = \rho\ w\ 2\pi r\ dr$

$dT = 4\ \pi\rho\ w^2 r\ dr$

$dQ = dm\ \omega' r = 2\ dm\ wr \times r$

$$dQ = 4\ \pi\rho\ w\ \omega r^3\ dr$$

Here, dT and dQ are the blade element thrust and torque. ω is the local angular velocity due to swirl.

$$dC_T = \frac{4\ \pi\rho\ w^2 r\ dr}{\rho\pi\ R^2\Omega^2R^2} = 4\ \lambda^2\ \eta\ d\eta$$

$$dC_Q = \frac{4\ \pi\rho\ w\ \omega\ r^3\ dr}{\rho\pi\ R^2\Omega^2R^3} = 4\ \lambda\ \frac{\omega}{\Omega}\ \eta^3\ d\eta$$

For uniform λ, $C_T = 2\ \lambda^2$ and $C_Q = \lambda\ \frac{\omega}{\Omega}$

$$dC_Q = 4\ \lambda\ \frac{\omega}{\Omega}\ \eta^3\ d\eta$$

$$= 0.5\ \sigma\ [C_\ell\ \sin(\Theta - \alpha) + C_d\ \cos(\Theta - \alpha)]\ \eta(\eta^2 + \lambda^2)d\eta$$

$$\frac{\omega r}{\Omega R} = \frac{1}{8}\ \sigma\ [C_\ell\ \sin(\Theta - \alpha) + C_d\ \cos(\Theta - \alpha)]\ (\frac{\eta}{\lambda} + \frac{\lambda}{\eta})$$

Here, σ is the local solidity. The angle of attack correction due to swirl is, to first order,

$$\alpha_N = \Theta + \frac{w}{r(\Omega - \omega)}$$

This new angle of attack is used in computing the performance. Usually the swirl loss is negligible for the hovering flight and was neglected during the formal optimization.

2.3 APPLICATION TO JVX

A recent paper (ref.6) has presented experimental results on the hovering performance and wake geometry of a highly twisted rotor. It is the purpose of this section to show that the fast free wake model suggested in Ref.(10) and described more fully in Ref.s(7) and (8) appears to predict the observed wake geometry and the rotor performance over the operating range. Figure (2-6) shows the blade shape of ATB tilt rotor used in the calculation. Figure (2-3) compares the predicted radial contraction of tip vortices with the experimental results of Ref.(6). In Figure (2-4) the predicted axial positions of tip vortices are a little above the experimental results. This discrepancy is expected to disappear if the induced velocity below the following blade is computed behind the following blade. The average of the induced velocities on the blade and on the position below and behind the following blade represents the influence of the near wake of the following blade better than the average of the velocity immediately below the following blade. Fig.(2-5) compares the figure of merit obtained from present analysis with the experimental results in Ref.(6). The hovering performance of ATB tilt rotor is well predicted by the present free wake lifting line theory.

The good agreements with experiments show that the

present technique can be used for a parameter optimization or for a formal optimization of hovering performance. The execution time of the present program is about 10-20 seconds on VAX 750. The hovering condition has no free stream, that is, all flow quantities are the perturbations. Hence, it is the most severe test of the vortex theory. It is known that the vortex far(wake) geometry determined by following the local velocity satisfies the Euler equation. Hence, the strict calculation of the vortex position is important for the analysis of the flow field.

2.4 VORTEX CORE SIZE AND ITS IMPORTANCE

Vortex core size is a physical parameter which determines the potential flow region and the rotational flow region , or the inviscid flow and the viscous flow region in subsonic flow. In rotor aerodynamics the vortex core size is needed for the determination of the self induced velocity of a ring vortex which is given by Lamb (ref.66). For the representation of shear flows by vortices the vortex core size is needed to avoid the infinite velocity and hence the infinite kinetic energy in the flow field. In this section the work done by the induced drag is shown to be the kinetic energy carried by the vortices in the flow. A model for the prediction of the core diameter of a rolled-up far wake vortex of a lifting three dimensional wing was proposed by Spreiter and Sacks (ref. 1). They equated the downward momentum and the kinetic energy generated by the wing to those of the flow after roll-up to determine the spanwise position of the vortices and their core diameter. Ferziger (ref. 2) determined the vortex spacing to diameter ratio of the vortex array modelling an infinite free shear flow. He conserved the circulation and kinetic energy of the flow before and after roll-up. Landahl (ref. 3) obtained the radial position of vortices and the far wake core diameter of rotor wake vortices by conserving momentum and kinetic energy during roll-up and by using Prandtl's planar wake or

doubly infinite vortex ring model. Widnall (ref. 4) showed the invariants of vortex motion as conservation of momentum, angular momentum and kinetic energy. Wu et. al.(ref. 5) related the changes in the first and second moment of vorticity in the flow to the force on the body which generated the vortices. In the following the semi-infinite array of vortex rings is used to determine the core diameter of the interminate wake vortex ring. The momentum and kinetic energy by one revolution of the rotor were equated to those in the wake flow of one vortex ring spacing. The vortex ring was considered to be in solid-body rotation with potential flow outside the core (Rankine vortex).

The force and moment on the body are related to the derivative of the first and second moment of vorticity in the wake by Wu et. al.(ref. 5).

$$\vec{F} = \frac{\rho}{2}\frac{d}{dt}\int_V \vec{\omega} \times \vec{r}\, dV + \rho \frac{d}{dt}\int_B \vec{U}\, dB \quad \text{—— (2-9)}$$

$$\vec{M} = \frac{\rho}{3}\frac{d}{dt}\int_V \vec{r} \times (\vec{\omega} \times \vec{r})\, dV + \rho \frac{d}{dt}\int_B \vec{r} \times \vec{U}\, dB \quad \text{— (2-10)}$$

where ω is the vorticity and U is the velocity of the body. The volume V is the entire vortical region and the volume B is the region inside the solid body. When the solid body is steady, the moment of vorticity is equal to the momentum due to the rotor according to equation (2-9). To determine the moment of vorticity in the wake, a circular vortex sheet is considered which is generated by a rotating blade.

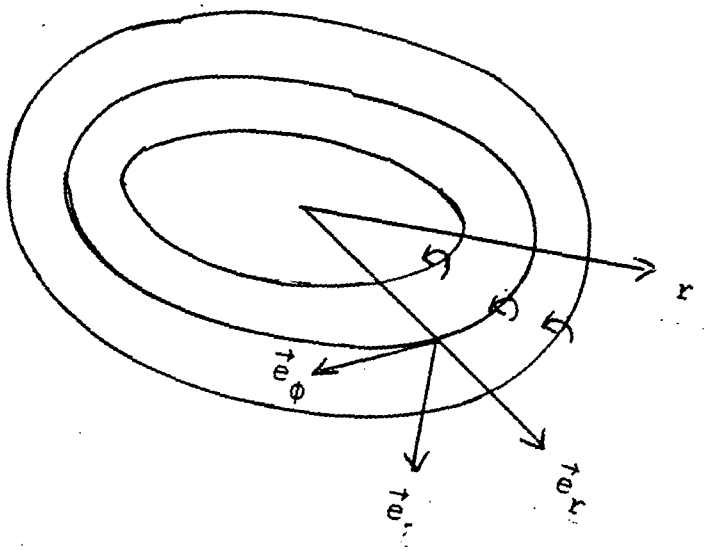

$$\vec{\omega} = \gamma(r,\phi)\,\delta(z)\,\vec{e}_\phi$$

$$\vec{r} = r\,\vec{e}_\phi$$

$$\vec{r} \times \vec{\omega} = r\,\vec{e}_r \times \gamma(r,\phi)\,\delta(z)\,\vec{e}_\phi$$

$$= r\,\gamma(r,\phi)\,\delta(z)\,\vec{e}_\phi$$

$$\vec{P} = 0.5\,\rho \int_V \vec{\omega} \times \vec{r}\, dV$$

$$= -0.5\,\rho \iiint r\,\gamma(r,\phi)\,\delta(z)\, r\, dr\, dz\, d\phi\, \vec{e}_k$$

$$= -0.5\,\rho \iint r^2\,\gamma(r,\phi)\, dr\, d\phi\, \vec{e}_k$$

$$\gamma(r,\phi) = \frac{d\Gamma}{dr}$$

$$\vec{P}_a = -\pi\rho \int_0^{R_0} r^2 \frac{d\Gamma}{dr}\, dr = 2\pi\rho \int_0^{R_0} r\,\Gamma(r)\, dr \quad \text{—— (2-11)}$$

The second moment of vorticity due to a circular vortex sheet is found to be zero by straightforward application of equation (2-10). The axial momentum associated with each vortex ring is

$$\vec{P}_a = \pi\rho\, \Gamma_0\, R^2$$

$$R^2 = \frac{2}{\Gamma_0} \int_0^{R_0} r\, \Gamma(r)\, dr \qquad \text{—— (2-12)}$$

To determine the kinetic energy of the ring vortex system we use the solution given by Lamb (1932) art. 161, for Stokes stream function for the potential flow outside the core of a single vortex ring.

$$\Psi = \Psi_0 = -\frac{\Gamma}{2\pi} (r_1 + r_2) \left[K(k) - E(k) \right] \qquad \text{—— (2-13)}$$

,where K and E are the complete elliptic integrals of the first and second kinds, respectly, and where

$$r_1 = \sqrt{z^2 + (r - r_0)^2}$$

$$r_2 = \sqrt{z^2 + (r + r_0)^2}$$

$$k = (r_2 - r_1)/(r_2 + r_1)$$

The velocity components are given by

$$u = \frac{1}{r} \frac{\partial \psi}{\partial z} \qquad \text{—— (2-14)}$$

$$w = -\frac{1}{r} \frac{\partial \psi}{\partial r} \qquad \text{—— (2-15)}$$

For the semi-infinite vortex ring system we thus have :

$$\psi = -\frac{\Gamma}{2\pi} \sum_{0}^{\infty} F_n \qquad \text{—— (2-16)}$$

where $F_n = (r_{1n} + r_{2n}) [K(k_n) - E(k_n)]$ —— (2-17)

$$r_{1n} = \sqrt{(z - nh)^2 + (r - R)^2} \qquad \text{—— (2-18)}$$

$$r_{2n} = \sqrt{(z - nh)^2 + (r + R)^2} \qquad \text{—— (2-19)}$$

$$k_n = (r_{2n} - r_{1n})/(r_{2n} + r_{1n}) \qquad \text{—— (2-20)}$$

The kinetic energy in one vortex spacing is

$$K = \pi\rho \iint (u^2 + w^2) \, dz \, r \, dr \qquad \text{—— (2-21)}$$

$$= \pi\rho \iint \left(w \frac{\partial\psi}{\partial z} - u \frac{\partial\psi}{\partial r}\right) dz \, dr$$

$$= \pi\rho \int_0^{\infty} w\psi \Big|_{z=-h/2}^{h/2} - \pi\rho \int_{-h/2}^{h/2} u\psi \Big|_{r=0}^{\infty} dz - \pi\rho \iint \psi w \, dz \, dr$$

$$= -\pi \rho \psi \Gamma \quad \text{by Lamb art. 162-1 (ref. 66)}$$

$$= \frac{r}{2} \Gamma^2 \sum_{0}^{\infty} F_n \qquad \text{—— (2-22)}$$

To determine the kinetic energy generated by the rotor, we compute the work done by the rotor to form one vortex ring. Each blade moves through azimuth $\phi = 2\pi/N$ to form one vortex. Thus the total work done to produce one ring is :

$$K_i = N \int_0^{2\pi/N} \int_0^{R_0} \rho U \Gamma \frac{w}{U} r \, d\phi \, dr \qquad \text{—— (2-23)}$$

For uniform downwash w and circulation Γ,

$$K_i = \rho \Gamma w \int_0^{R_0} r \, 2\pi \, dr = \pi \rho w \Gamma R_0^2 \qquad \text{—— (2-24)}$$

Here, w is the downwash on the rotor plane. Since w is doubled in the far wake,

$$\Gamma = 2 w h \qquad \text{—— (2-25)}$$

Thus, $$K_i = \frac{\rho}{2} \frac{\pi \Gamma^2 R_0^2}{h} \qquad \text{—— (2-26)}$$

,where h is the vortex spacing in the far wake.
To determine F_0 , we use the kinetic energy given by Lamb art. 163-6 due to a vortex ring at z = 0.

$$K_0 = \frac{\rho \Gamma^2}{2} R_0 \left[\ell n \frac{8}{\varepsilon / R_0} - \frac{7}{4} \right] \qquad \text{—— (2-27)}$$

$$F_0 = R_0 \left[\ell n \frac{8}{\varepsilon / R_0} - \frac{7}{4} \right] \qquad \text{—— (2-28)}$$

,where ε is the radius of the vortex core and R_0 is the radius of the ring vortex on the plane of rotor. Equating equations (2-22) and (2-26) with the use of equation (2-28) gives

$$\frac{\rho}{2} \frac{\pi \Gamma^2 R_0^2}{h} = \frac{\rho}{2} \Gamma^2 \{ R_0 \left(\ell n \frac{8}{\varepsilon / R} - \frac{7}{4} \right) + \sum^{\infty} F_n \}$$

$$\frac{\varepsilon}{R_0} = 8 \exp \left[G \left(\frac{R_0}{h} \right) - \frac{7}{4} - \pi \frac{R_0}{h} \right] \qquad \text{—— (2-29)}$$

,where $G = \frac{1}{R_0} \sum_{1}^{\infty} F_n (R_0 , 0)$, $2\varepsilon = d$

$$\frac{d_0}{h} = 16 \frac{R_0}{h} \exp\left[G\left(\frac{R_0}{h}\right) - \frac{7}{4} - \pi \frac{R_0}{h} \right] \qquad \text{—— (2-30)}$$

In equation (2-30), d is the diameter of the ring vortex and d_0 /h is the diameter to spacing ratio for the immediate vortex ring behind the blade. For the first vortex ring

$$\psi = - \frac{\Gamma}{2\pi} \sum_{-1}^{\infty} F_n , \quad F_0 = R_1 \left[\ell n \frac{8}{\varepsilon/R} - \frac{7}{4} \right] \qquad \text{—— (2-31)}$$

For the second vortex ring

$$\psi = - \frac{\Gamma}{2\pi} \sum_{-2}^{\infty} F_n , \quad F_0 = R_2 \left[\ell n \frac{8}{\varepsilon/R} - \frac{7}{4} \right] \qquad \text{—— (2-32)}$$

Likewise for the first vortex ring

$$G_1 = \frac{1}{R_1} \sum_{1}^{\infty} F_n(R_1 ,0) + \frac{1}{R_1} F_1 (R_1 ,0) \qquad \text{—— (2-33)}$$

and for the second vortex ring

$$G_2 = \frac{1}{R_2} \sum_{1}^{\infty} F_n (R_2,0) + \frac{1}{R_2} \sum_{-1}^{-2} F_n (R_2,0) \qquad \text{—— (2-34)}$$

In general, for the ith vortex ring

$$\frac{d_i}{h} = 16 \frac{R_i}{h} \exp \left[G_i \left(\frac{R}{h}\right) - \frac{7}{4} - \pi \frac{R_0}{h} \frac{R_0}{R_i} \right] \qquad \text{—— (2-35)}$$

,where $G_i = \frac{1}{R_i} \sum_{1}^{\infty} F_n (R_i ,0) + \frac{1}{R_i} \sum_{-1}^{-i} F_n (R_i ,0)$ —— (2-36)

From equation (2-35) the core sizes of ring vortices are computed using the free wake model in Ref.(7) and semi-rigid wake model. They are shown in fig.s (2-6) and (2-7). In the far wake the vortex core size approached that of Landahl (ref. 3). As the ring vortex moves away from the rotor, kinetic energy propagates outside the core due to the interactions between ring vortices and hence the core size grow. The core size grows to the value given by Landahl which is the possible maximum. The free wake model gives the smaller core size than the semi-rigid wake because the former contains the energy in smaller spacing than the latter. The bursting of the core will give larger core size than the Rankine core due to the conversion of kinetic energy into possible turbulent energy.

2.5 LIFTING LINE VS LIFTING SURFACE

Lifting line theory is based on Kutta-Joukowski law which is the relation between lift and circulation. The effective angle of attack can be defined when the trailing and shed vortices are trailed from the trailing edge of wing, blade, or airfoil. That is, lifting line theory is valid when there is no seperation from the side or leading edge of a lifting body. The free wake lifting line couples the exact relation between lift and circulation with the nonlinear motion of the vortices trailed from the trailing edge. Free wake lifting line theory gives the far field solution of Euler equation. Hence this solution can be used for the calculation of the pressure distribution around the blade, that is, for the near field solution. The near field can be obtained by lifting body theory, Euler or potential equation for inviscid flow and lifting body theory coupled with boundary layer calculation or Navier-Stokes equation for viscous flow. For low aspect ratio wings the vortices are trailed from the side or leading edge. In this case lifting surface theory uses the flow tangency condition on the surface with the free vortices from the side or leading edge.

Lifting line theory can not model the seperated vortices over the wing. But the lift used in lifting line

theory includes the leading edge suction and thickness effect in the lift. Lifting surface can not model the singularity on the leading edge or the leading edge suction. But the pressure distribution around the wing can be obtained by the lifting surface theory. The separated vortex can be placed on the surface for lifting surface theory. For the performance analysis of the rotor blades lifting line theory is better than lifting surface theory when there is no leading edge or side edge seperation of any importance. For the close encounter of the blade with the strong tip vortex the effective angle of attack for the lift calculation may not be valid. In present study lifting line, surface, and body theories were used. The lifting line solution was in better agreement with lifting body solution than lifting surface solution. In the comparison the distance between the blade and tip vortex was about 5 % of the blade radius. Lifting line appears to be better than lifting surface for the overall performance prediction of the rotor because of the use of the exact lift-circulation relationship of Kutta-Joukowski.

Table 1. Comparison of 3-D momentum theory and Free wake theory, with 10 spanwise division.

3-D MOMENTUM THEORY

NO. OF BLADES = 2 SOLIDITY =0.0382

CT =0.00408 CP =0.000279 FM =0.660 CT/CP =14.61

CTT =0.00400 CPI =0.000190

CVT1(LOCAL) =0.00050 CVT2(GLOBAL) =0.00500

CTR =0.00408 CPR =0.000281

ETA	CHORD	THETA	ALPHA	WLA	UT	CL	GAM
.150	.0600	0.1713E+02	0.7566E+01	-0.2448E-01	0.1520E+00	0.8453E+00	0.3854E-02
.250	.0600	0.1591E+02	0.8275E+01	-0.3281E-01	0.2521E+00	0.9064E+00	0.6857E-02
.350	.0600	0.1469E+02	0.8277E+01	-0.3872E-01	0.3521E+00	0.9001E+00	0.9509E-02
.450	.0600	0.1347E+02	0.7947E+01	-0.4297E-01	0.4520E+00	0.8611E+00	0.1168E-01
.600	.0600	0.1163E+02	0.7124E+01	-0.4693E-01	0.6018E+00	0.7696E+00	0.1390E-01
.750	.0600	0.9800E+01	0.6081E+01	-0.4845E-01	0.7516E+00	0.6560E+00	0.1479E-01
.825	.0600	0.8883E+01	0.5511E+01	-0.4836E-01	0.8264E+00	0.5941E+00	0.1473E-01
.875	.0600	0.8272E+01	0.5118E+01	-0.4799E-01	0.8763E+00	0.5516E+00	0.1450E-01
.925	.0600	0.7661E+01	0.4717E+01	-0.4737E-01	0.9262E+00	0.5083E+00	0.1412E-01
.975	.0600	0.7050E+01	0.4310E+01	-0.4648E-01	0.9761E+00	0.4643E+00	0.1360E-01

NB = 2 KIT = 1 RES. = 0.2487E-02
NB = 2 KIT = 2 RES. = 0.6850E-03
NB = 2 KIT = 3 RES. = 0.1086E-03
NB = 2 KIT = 4 RES. = 0.1156E-03
NB = 2 KIT = 5 RES. = 0.1097E-03
NB = 2 KIT = 6 RES. = 0.1103E-03
NB = 2 KIT = 7 RES. = 0.1099E-03
NB = 2 KIT = 8 RES. = 0.1090E-03
NB = 2 KIT = 9 RES. = 0.1077E-03
NB = 2 KIT = 10 RES. = 0.9794E-04
NB = 2 KIT = 11 RES. = 0.1010E-03
NB = 2 KIT = 12 RES. = 0.1004E-03
NB = 2 KIT = 13 RES. = 0.9947E-04
NB = 2 KIT = 14 RES. = 0.9824E-04
NB = 2 KIT = 15 RES. = 0.9674E-04
NB = 2 KIT = 16 RES. = 0.9583E-04
NB = 2 KIT = 17 RES. = 0.9693E-04
NB = 2 KIT = 18 RES. = 0.9782E-04
NB = 2 KIT = 19 RES. = 0.9848E-04
NB = 2 KIT = 20 RES. = 0.9899E-04
NB = 2 KIT = 21 RES. = 0.9932E-04
NB = 2 KIT = 22 RES. = 0.9945E-04
NB = 2 KIT = 23 RES. = 0.9944E-04
NB = 2 KIT = 24 RES. = 0.9928E-04
NB = 2 KIT = 25 RES. = 0.9893E-04
NB = 2 KIT = 26 RES. = 0.9851E-04
NB = 2 KIT = 27 RES. = 0.9790E-04
NB = 2 KIT = 28 RES. = 0.9722E-04
NB = 2 KIT = 29 RES. = 0.9633E-04
NB = 2 KIT = 30 RES. = 0.9531E-04
NB = 2 KIT = 31 RES. = 0.9431E-04
NB = 2 KIT = 32 RES. = 0.9301E-04
NB = 2 KIT = 33 RES. = 0.9176E-04
NB = 2 KIT = 34 RES. = 0.9033E-04
NB = 2 KIT = 35 RES. = 0.8866E-04
NB = 2 KIT = 36 RES. = 0.8727E-04
NB = 2 KIT = 37 RES. = 0.8539E-04
NB = 2 KIT = 38 RES. = 0.8348E-04
NB = 2 KIT = 39 RES. = 0.8202E-04

Table 1. -continued.

NO. OF BLADES = 2 SOLIDITY =0.0382

CT =0.00397 CP =0.000276 FM =0.639 CT/CP =14.35

CTT =0.00400 CPI =0.000188

CVT1(LOCAL) =0.00050 CVT2(GLOBAL) =0.00500

CTR =0.00397 CPR =0.000278

ETA	CHORD	THETA	ALPHA	WLA	UT	CL	GAM
.150	.0600	0.1713E+02	0.8377E+01	-0.2229E-01	0.1516E+00	0.9310E+00	0.4236E-02
.250	.0600	0.1591E+02	0.9175E+01	-0.2882E-01	0.2517E+00	0.1003E+01	0.7570E-02
.350	.0600	0.1469E+02	0.8859E+01	-0.3514E-01	0.3518E+00	0.9616E+00	0.1015E-01
.450	.0600	0.1347E+02	0.7887E+01	-0.4345E-01	0.4521E+00	0.8519E+00	0.1155E-01
.600	.0600	0.1163E+02	0.6112E+01	-0.5760E-01	0.6028E+00	0.6590E+00	0.1192E-01
.750	.0600	0.9800E+01	0.5192E+01	-0.6014E-01	0.7524E+00	0.5607E+00	0.1266E-01
.825	.0600	0.8883E+01	0.4930E+01	-0.5675E-01	0.8269E+00	0.5327E+00	0.1322E-01
.875	.0600	0.8272E+01	0.5203E+01	-0.4668E-01	0.8762E+00	0.5608E+00	0.1474E-01
.925	.0600	0.7661E+01	0.5840E+01	-0.2922E-01	0.9255E+00	0.6259E+00	0.1738E-01
.975	.0600	0.7050E+01	0.4858E+01	-0.3714E-01	0.9757E+00	0.5217E+00	0.1527E-01

ETA = normalized radius (= η)
CHORD = chord width (= C)
THETA = blade pitch angle (=θ)
ALPHA = angle of attack in degrees (=α)
WLA = normalized downwash (= λ)
UT = normalized total velocity with respect to blade(= $U_T/\Omega R$)
CL = lift coefficient (= C_l)
GAM = normalized bound circulation (= $\Gamma/\Omega R$)

Table 2. Comparison of 3-D momentum theory and Free wake Theory with 15 spanwise division.

3-D MOMENTUM THEORY

NO. OF BLADES = 2 SOLIDITY =0.0382

CT =0.00408 CP =0.000279 FM =0.660 CT/CP =14.62

CTT =0.00400 CPI =0.000190

CVT1(LOCAL) =0.00050 CVT2(GLOBAL) =0.00500

CTR =0.00408 CPR =0.000280

ETA	CHORD	THETA	ALPHA	WLA	UT	CL	GAM
.150	.0600	0.1713E+02	0.7566E+01	-0.2448E-01	0.1520E+00	0.8453E+00	0.3854E-02
.225	.0600	0.1622E+02	0.8189E+01	-0.3100E-01	0.2271E+00	0.8998E+00	0.6131E-02
.275	.0600	0.1561E+02	0.8320E+01	-0.3448E-01	0.2772E+00	0.9092E+00	0.7560E-02
.350	.0600	0.1469E+02	0.8277E+01	-0.3872E-01	0.3521E+00	0.9001E+00	0.9509E-02
.500	.0600	0.1286E+02	0.7707E+01	-0.4458E-01	0.5020E+00	0.8340E+00	0.1256E-01
.670	.0600	0.1078E+02	0.6657E+01	-0.4792E-01	0.6717E+00	0.7186E+00	0.1448E-01
.760	.0600	0.9678E+01	0.6007E+01	-0.4847E-01	0.7615E+00	0.6479E+00	0.1480E-01
.800	.0600	0.9189E+01	0.5704E+01	-0.4845E-01	0.8015E+00	0.6150E+00	0.1479E-01
.840	.0600	0.8700E+01	0.5394E+01	-0.4828E-01	0.8414E+00	0.5815E+00	0.1468E-01
.880	.0600	0.8211E+01	0.5078E+01	-0.4794E-01	0.8813E+00	0.5473E+00	0.1447E-01
.910	.0600	0.7844E+01	0.4838E+01	-0.4758E-01	0.9112E+00	0.5214E+00	0.1425E-01
.930	.0600	0.7600E+01	0.4676E+01	-0.4729E-01	0.9312E+00	0.5039E+00	0.1408E-01
.950	.0600	0.7356E+01	0.4514E+01	-0.4696E-01	0.9512E+00	0.4864E+00	0.1388E-01
.970	.0600	0.7111E+01	0.4351E+01	-0.4658E-01	0.9711E+00	0.4687E+00	0.1366E-01
.990	.0600	0.6867E+01	0.4186E+01	-0.4616E-01	0.9911E+00	0.4510E+00	0.1341E-01

NB = 2 KIT = 1 RES. = 0.4570E-02
NB = 2 KIT = 2 RES. = 0.6544E-03
NB = 2 KIT = 3 RES. = 0.8440E-03
NB = 2 KIT = 4 RES. = 0.1935E-03
NB = 2 KIT = 5 RES. = 0.1094E-03
NB = 2 KIT = 6 RES. = 0.1090E-03
NB = 2 KIT = 7 RES. = 0.1084E-03
NB = 2 KIT = 8 RES. = 0.1076E-03
NB = 2 KIT = 9 RES. = 0.1065E-03
NB = 2 KIT = 10 RES. = 0.1051E-03
NB = 2 KIT = 11 RES. = 0.1003E-03
NB = 2 KIT = 12 RES. = 0.1006E-03
NB = 2 KIT = 13 RES. = 0.9953E-04
NB = 2 KIT = 14 RES. = 0.9831E-04
NB = 2 KIT = 15 RES. = 0.9686E-04
NB = 2 KIT = 16 RES. = 0.9604E-04
NB = 2 KIT = 17 RES. = 0.9538E-04
NB = 2 KIT = 18 RES. = 0.9463E-04
NB = 2 KIT = 19 RES. = 0.9361E-04
NB = 2 KIT = 20 RES. = 0.9266E-04
NB = 2 KIT = 21 RES. = 0.9134E-04
NB = 2 KIT = 22 RES. = 0.9015E-04
NB = 2 KIT = 23 RES. = 0.8873E-04
NB = 2 KIT = 24 RES. = 0.8718E-04
NB = 2 KIT = 25 RES. = 0.8572E-04
NB = 2 KIT = 26 RES. = 0.8396E-04
NB = 2 KIT = 27 RES. = 0.8235E-04
NB = 2 KIT = 28 RES. = 0.8038E-04
NB = 2 KIT = 29 RES. = 0.7878E-04
NB = 2 KIT = 30 RES. = 0.7666E-04
NB = 2 KIT = 31 RES. = 0.7478E-04
NB = 2 KIT = 32 RES. = 0.7271E-04

Table 2. -continued.

NO. OF BLADES = 2 SOLIDITY =0.0382

CT =0.00394 CP =0.000277 FM =0.630 CT/CP =14.19

CTT =0.00400 CPI =0.000190

CVT1(LOCAL) =0.00050 CVT2(GLOBAL) =0.00500

CTR =0.00394 CPR =0.000279

ETA	CHORD	THETA	ALPHA	WLA	UT	CL	GAM
.150	.0600	0.1713E+02	0.8372E+01	-0.2230E-01	0.1516E+00	0.9306E+00	0.4234E-02
.225	.0600	0.1622E+02	0.9085E+01	-0.2742E-01	0.2267E+00	0.9954E+00	0.6769E-02
.275	.0600	0.1561E+02	0.9322E+01	-0.2961E-01	0.2766E+00	0.1016E+01	0.8433E-02
.350	.0600	0.1469E+02	0.8949E+01	-0.3458E-01	0.3517E+00	0.9710E+00	0.1025E-01
.500	.0600	0.1286E+02	0.7216E+01	-0.4890E-01	0.5024E+00	0.7776E+00	0.1172E-01
.670	.0600	0.1078E+02	0.5658E+01	-0.5968E-01	0.6727E+00	0.6107E+00	0.1232E-01
.760	.0600	0.9678E+01	0.5181E+01	-0.5948E-01	0.7623E+00	0.5595E+00	0.1280E-01
.800	.0600	0.9189E+01	0.5040E+01	-0.5776E-01	0.8021E+00	0.5446E+00	0.1310E-01
.840	.0600	0.8700E+01	0.5002E+01	-0.5404E-01	0.8417E+00	0.5405E+00	0.1365E-01
.880	.0600	0.8211E+01	0.5351E+01	-0.4374E-01	0.8811E+00	0.5760E+00	0.1522E-01
.910	.0600	0.7844E+01	0.5699E+01	-0.3389E-01	0.9106E+00	0.6114E+00	0.1670E-01
.930	.0600	0.7600E+01	0.5703E+01	-0.3062E-01	0.9305E+00	0.6115E+00	0.1707E-01
.950	.0600	0.7356E+01	0.5399E+01	-0.3227E-01	0.9505E+00	0.5793E+00	0.1652E-01
.970	.0600	0.7111E+01	0.4777E+01	-0.3936E-01	0.9708E+00	0.5129E+00	0.1494E-01
.990	.0600	0.6867E+01	0.3608E+01	-0.5618E-01	0.9916E+00	0.3876E+00	0.1153E-01

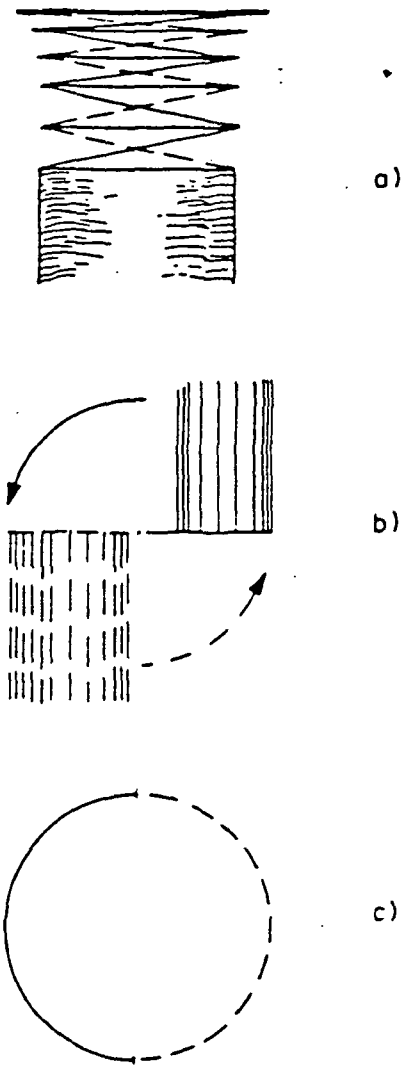

fig.2-1. Geometry of model using vortex rings and cylinders to represent the wake.

a) Side view of rotor wake model showing intermediate and far wakes formed from vortex spiral - 2 blades. Tip vortex only shown.

_____ Blade One ___ ___ Blade two

B) Plan view showing near wake

C) Formation of intermediate wake

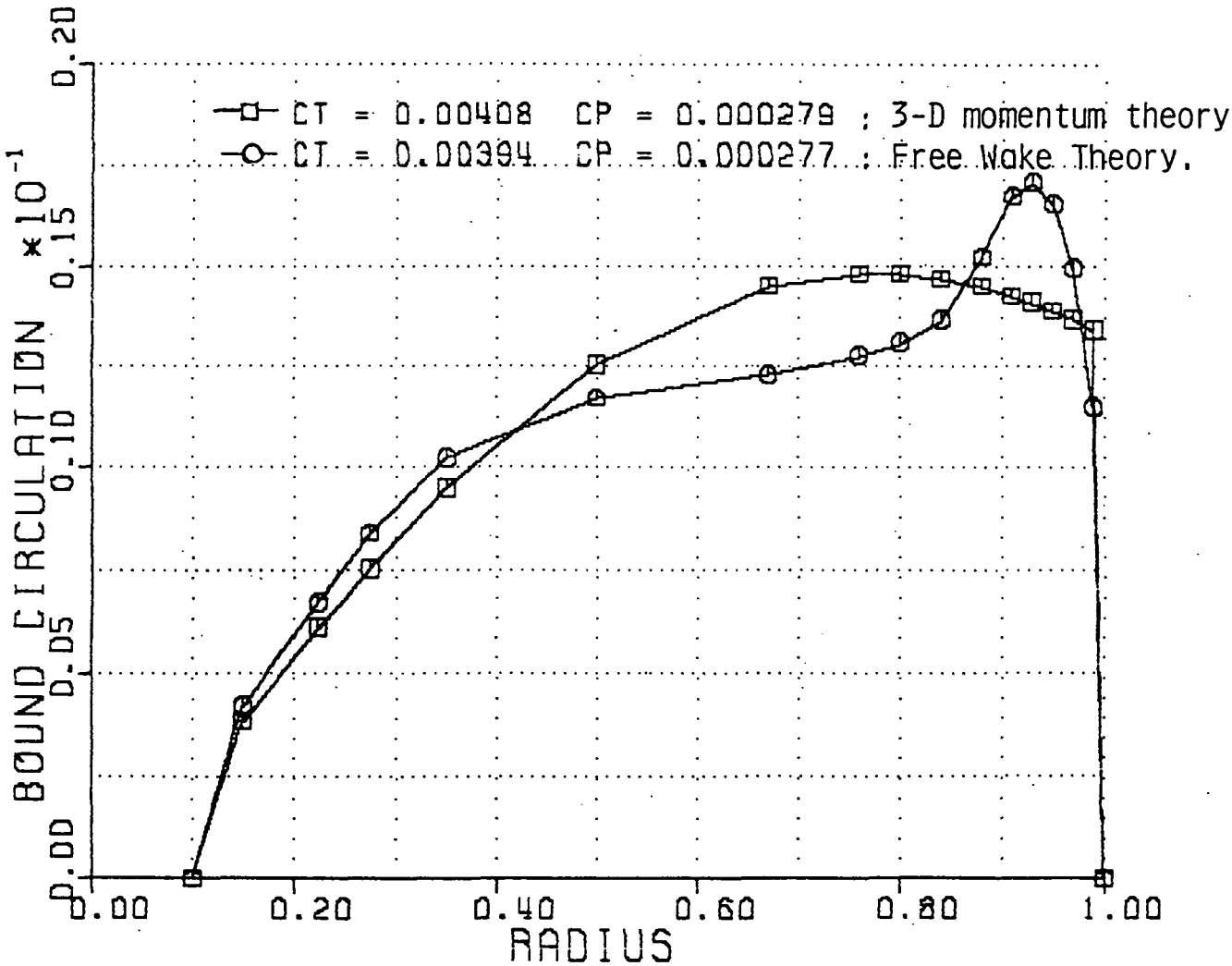

Figure 2-2. Comparison of Bound Circulations from Momentum Theory and Free Wake Lifting Line Theory.

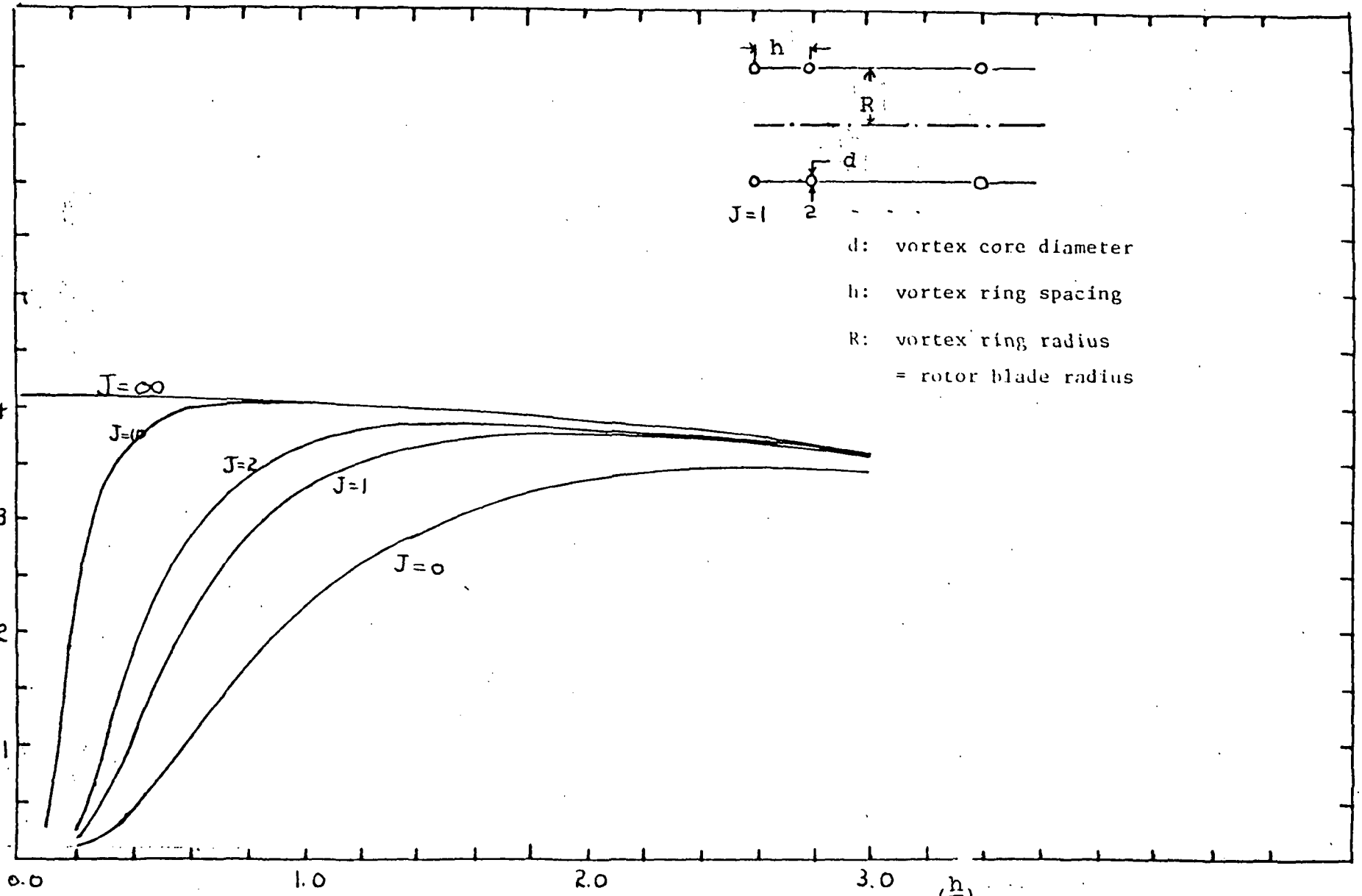

Figure 2-8. Vortex Core Diameter vs the Axial Spacing of Ring Vortex
(Semi-rigid wake model)

CHAPTER 3

SURFACE SINGULARITY METHODS FOR COMPUTING THE POTENTIAL FLOW OF HOVERING ROTOR WITH FREE WAKE GEOMETRY

In this chapter lifting line, lifting surface, and lifting body theories are applied to the aerodynamic analysis of hovering helicopter rotor with the calculation of free wake geometries. For lifting line theory the relationship of Kutta-Joukowski between bound circulation and downwash is solved iteratively untill the wake geometry is converged. The spiral wake of hovering rotor is represented by vortex rings and cylinders. Implicit-type wake geometry calculation is used to enhance the stability and convergence of wake geometry calculation. The radial and axial movement of intermediate ring vortices are computed exactly by integrating the downwash velocities on them directly below the blade while near wake is fixed on the plane of rotation and far wake of vortex cylinders is the continuation of intermediate wake.

For lifting surface and lifting body calculation intermediate and far wakes are treated as lifting line problem and the influence of near wake is treated as lifting surface or lifting body problems. For lifting surface solution vortex lattice method is used and for lifting body

solution the superposition method of sources and vortex sheets on the body surface of Hess and Smith (ref. 34) are applied. This means that the influence of wakes are computed on a quarter chord position of the blade for lifting line theory and on control point of each body surface element for lifting surface or body theory. In the analysis the rotor used by Johnson (ref. 35) is used for the comparison with Miller's results (ref. 7). Also, the wing of Boeing TR 17 of aspect ratio 2 is used to compare with the results in Ref. (33).

In section (3.1) vortex lattice method and vortex panel method are formulated for lifting surface solution. Also, the pressure coefficient formula for lifting surface theory is presented. In section (3.2) the mathematical basis of lifting surface and lifting body theory are formulated by applying Green's second identity to flow field. The matrix equations for unknown surface total potentials or perturbation potentials are derived which are the strengths of doublets on body surface. In section (3.3) lifting body theory of Hess and Smith using source and vortex are derived into a matrix equation which is the relationship between boundary conditions, Kutta conditions, and unknown strengths. The matrix equation is formulated from a system of linear equations obtained from descretizing Green's integral solution or from the superposition of surface

singularities. In section (3.4) the technique of free wake geometry calculation are discussed. In section (3.5) the engineering calcualtion of skin friction drag is derived for laminar or turbulent boundary layers of airfoil.

Miller, R.H. (ref. 7) used the simplified free wake model of infinite line vortices or ring vortices below the rotor to replace helical vortices. In both cases the semi-infinite near wake was attached to the blade on the plane of rotation for the rotor of two blades. He had three line or ring vortices in intermediate wake and three semi-infinite vortex sheets or vortex cylinders in far wake and used the Betz roll-up for line vortices. These two or three dimensional simplified free wake model predicted tip vortex positions in close agreement with experiments. Miller, R.H. (ref. 8) investigated the effect of bound circulation and the extent of intermediate wake on vortex position. He found that the wake contracted, then expanded, and became wavy when far wake was eliminated. Simplified models was in agreement with the more complete solutions. Miller, R.H. (ref. 9) showed that ideal figure of merit decreased when vortex core size was decreased, or when wake rotation was included, or when number of spirals in the far wake was increased. Miller, R.H. (ref. 10) suggested the simplified approach for the first time in which the spiral wake was replaced by line vortices or ring vortices which

were shown to have a closed form solution for the induced velocities at any location.

Brower, M.(ref. 12) compared lifting surface (vortex Lattice) and lifting line solutions for the blade interactions with curved or straight vortex lines. He found that lifting surface solution predicted lower bound circulation than lifting line solution. Brower, M. (ref. 13) computed the bound circulation of hovering helicopter rotor using lifting line theory and free wake model of filament vortices. The wake was divided into near wake of 70 degrees, intermediate wake of three filament vortices over 740 degrees, far wake of three semi-infinite vortex cylinders. His predicted thrust coefficients were a little lower than the experimental results. The calculated wake contraction was less than the experiments, which he suggested was due to inner line vortices. Tanuwidjaja, A. (ref. 14) investigated the effects of free wake models on hovering performance prediction. He used vortex sheets in near and intermediate wake regions. He found that the free wake model which used vortex sheets in near wake and four line vortices in intermediate wake was in better agreement with experiments than one which used vortex sheets in near and intermediate wakes. Also, he neglected the distortion of inner sheets in near wake of that model.

Kocurek,J.D. et. al. (ref. 15) computed the

hovering performance with circulation coupled prescribed wake lifting surface theory. The axial and radial settling rates of tip and inner vortices were expressed as a function of the tip vortex strength and the number of blades. They also computed lifting line and lifting surface solution and found that leading edge suction obtained by lifting surface solution was higher than one obtained by lifting line solution near the blade tip region. Lifting surface theory with higher leading edge suction underpredicted the lift coefficient compared to lifting line theory. Shenoy, K.R. and Gray, R.B. (ref. 16) computed the surface vorticity distribution of thick bladed hovering rotors. They used lifting line theory with a prescribed wake to calculate the effective angle of attack. From starting the two-dimensional airfoil surface vorticity at the effective angle of attack they solved the three dimensional potential flow by iterating until the surface vorticity strength became the total surface vorticity due to blade surface vorticity, prescribed wake vortices, and free stream.

Djojodihardjo, R.H. and Widnall, S.E. (ref. 17) developed a numerical method using only doublet (or vorticity) distribution for the calculation of unsteady potential flow. They used a quadratic distribution of doublet only along the chord and computed two kinds of influence coefficients for the surface velocity and

potential. Although they gave results about the impulsive starting of airfoil and wings, they did not give formulas for two-dimensional problem. Preuss, R.D. et. al. (ref. 18) developed the potential flow solution for wind turbines and hovering helicopter rotors using Green's function method. For lifting surface problem the unknowns were potential discontinuities and for a lifting body problem the unknowns were surface potential strengths. They found that lifting surface solution underpredicted the blade lift, compared to lifting body solution and that 3 chordwise and 10 spanwise lifting surface elements were enough to achieve the required accuracy. For the lifting body configuration solution the strengths of surface sources were known and the strengths of surface doublets, that is, the perturbation potential strengths were unknowns to be determined by the normal flow boundary condition. They found that the airloads acting on wind turbine blades due to shear wind was oscillatory in the same form as the shear wind. Clark, D.R. (ref.19) reviewed the previous potential flow panel code with seperated region modelled by constant vorticity panel. A bluff body was modelled by distribution of sources and linear vorticity and the body surface vorticity was zero after the seperation line with all vorticity going into the flow field.

Johansson, B.C. (ref.20) showed that the effect of

compressibility for a helicopter rotor in vertical climb, hovering, and for a propeller was a Prandtl-Glauert correction on a lift curve slope with the effective angle of attack computed by the compressible flow downwash for a lifting line theory. Johnson, W.(ref. 21) derived the linearized equation for the acceleration potential in a coordinate where an oblique convecting vortex interaction with an infinite wing appeared as steady flow. As a function of free stream Mach number and the skew angle of the convecting line vortex he derived elliptic kernal which related the acceleration to the downwash. He calculated peak section lift for incompressible flow as a function of vortex height from an infinite wing. Bristow, D.R. et. al. (ref.22) combined 3-D surface panel method with multiple geometry perturbations to compute the potential flow for a series of different geometries. Their surface panel method used the constant source of known strength and a quadratic doublet on each panel with zero interior perturbation potential condition. From the linear relationship between the doublet(potential) strength and the boundary condition on each control point they obtained the derivative matrix of the surface potential with respect to geometry perturbations.

Tai,T.C. et. al. (ref.25) computed the optimum round trailing edge geometry for the highest lift of circulation

control airfoils. In their analysis the potential flow was computed by surface vortex panel method with the Kutta condition of specified circulation due to blowing. Three baseline geometries of round trailing edge were used as design variables for the search of the highest lift. The viscous effect of blowing formed a separation bubble at the trailing edge. At the upper and lower ends of the separation bubble the zero pressure difference determined the circulation around the airfoil. But the predicted lift was dependent on panel arrangements and hence the circulation was not uniquely determined. It is unlikely that circulation control airfoils are as effective as airfoils of chord change even though the lift to drag ratio is high due to the reduction in drag by jet flow. Mcveigh, M.A. et. al. (ref.23) showed that the tapered tip had the highest figure of merit for hovering performance among tested tip shapes. They found that low solidity rotor had the higher figure of merit than the high solidity one for the same thrust coefficient and the same tip speed. But as the tip speed is decreased, it is expected that the high solidity rotor has a higher induced power, hence a higher figure of merit than a low solidity one.

Roberts,T.W. and Murman,E.M. (ref. 24) derived the potential finite difference equation for axisymmetric flow beneath hovering rotor by using mass conservation with

potential jumps due to vortex branch cuts. By subtracting the local potential due to a ring vortex they computed the velocity induced on that ring vortex due to all other vortices and then they added the self induced velocity to get the convecting velocity. Therefore the convecting velocity of a ring vortex was not dependent on the grid size. They found that relatively a few vortices were required to adequately determine the downwash on the rotor. Liu, et. al. (ref. 26) solved the vorticity-stream function equation in cylindrical coordinate, while neglecting circumferential variations, for the vortical flow beneath the rotor plane. They found that the roll-up and inboard movement of vorticity occured very rapidly and that the maximum vorticity decayed to 0.8 from 1.0 after 180 degree rotation.

3.1 VORTEX LATTICE AND VORTEX PANEL

LIFTING SURFACE THEORY

Vortex lattice method places the concentrated vortex on a quarter point of each panel and the control point on a three quarter point of each panel. This arrangement of vortex and control points will give the exact value of the overall circulation as follows.

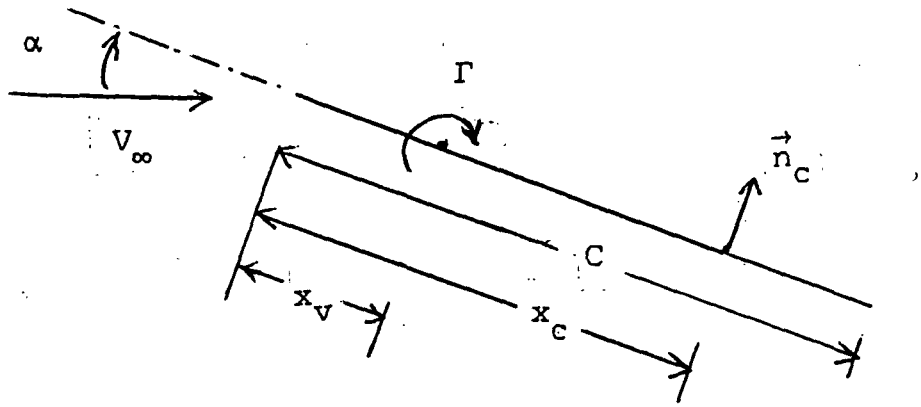

$$\frac{\Gamma}{2\Pi\ (x_v - x_c)} = -\ \vec{V}_\infty \cdot \vec{n} = -\ V_\infty \alpha$$

$$\Gamma = 2\pi V_\infty \alpha (x_c - x_v) = 2\Pi V_\infty \alpha d \qquad - \qquad (3\text{-}1)$$

The circulation distribution of the plate airfoil at angle

of attack α is $\gamma(x)$.

$$\gamma(x) = 2V_\infty \alpha \sqrt{\frac{c - x}{x}} \qquad \text{——— (3-2)}$$

The overall circulation is Γ.

$$\Gamma = V_\infty \alpha \pi c \qquad \text{——————— (3-3)}$$

By equating equations (3-1) and (3-3) we obtain the vortex position to give the same circulation for γ = constant panel as flat plate.

$$x_c - x_v = \frac{c}{2} \qquad \text{——————— (3-4)}$$

In ref.(36) it was pointed out that vortex lattice method underestimated the strength of vortex near the leading edge compared to equation (3-2). Therefore, let us consider the vortex panel method. Insted of concentrated vortex, we distribute a constant vortex sheet.

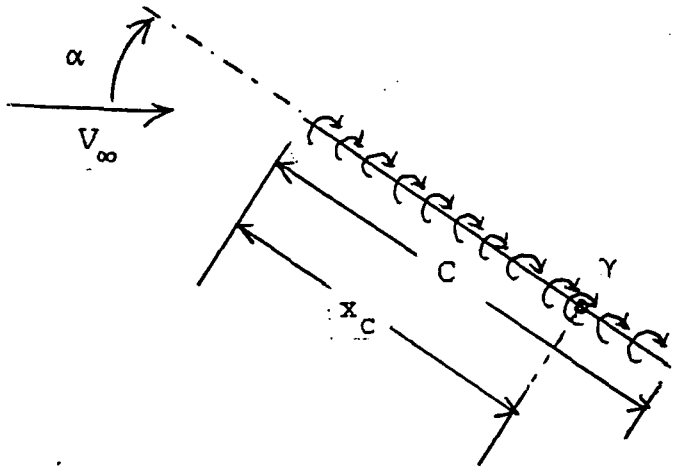

$$\frac{1}{2\pi}\int_0^c \frac{\gamma}{(x - x_c)}dx = -\vec{V}_\infty \cdot \vec{n} = -V_\infty \alpha$$

$$\frac{1}{2\pi}\int_0^c \frac{\gamma}{x - x_c}\,dx = \frac{\gamma}{2\pi}\ln\left\{\frac{x_c - c}{-x_c}\right\}$$

$$\gamma \ln\left(\frac{c - x_c}{x_c}\right) = -V_\infty \alpha 2\pi$$

$$\gamma = \frac{-V_\infty \alpha\, 2\pi}{\ln\left(\frac{c - x_c}{x_c}\right)} \qquad \text{——— (3-5)}$$

$$\gamma \cdot c = \Gamma = -\frac{2\pi\, V_\infty \alpha\, c}{\ln\left(\frac{c - x_c}{x_c}\right)} \qquad \text{——— (3-6)}$$

By equating equations (3-3) and (3-6) we obtain

$$x_c = \frac{c}{1 + \frac{1}{e^2}} = 0.8808\ c \qquad \text{——— (3-7)}$$

The vortex sheet strength predicted by vortex panel method should represent the strength to match equation (3-2). Hence

$$\gamma\,(x_v) \cdot c = 2V_\infty\, \alpha\sqrt{\frac{c - x_v}{x_v}} \cdot c = \Gamma \qquad \text{—— (3-8)}$$

By equating equations (3-3) and (3-8) we obtain the

vortex position.

$$x_v = \frac{c}{1 + \frac{\pi}{4}^2} = 0.2884c \qquad \text{(3-9)}$$

The vortex strength predicted by equations (3-1) or (3-6) should be used as the strength at the location $x_v = 0.2884c$ Then the underestimation of vortex strength by vortex lattice method is expected to disappear.

The sensitivity of the vortex strength on control point location for one panel is obtained from equations (1) and (6).

From equation (1),

$$\frac{d\Gamma}{dX_c} = V_\infty \alpha \, 2 \, \Pi$$

From equation (6),

$$\frac{d\Gamma}{dX_c} = \frac{- 2\Pi \, V_\infty \, \alpha C^2}{X_c \, (C - X_c) \left[\ell n \left\{ \frac{C-X_c}{X_c} \right\} \right]^2}$$

Vortex lattice method is less sensitive to control point location than vortex panel method for one panel. But as the number of panels increases, the vortex panel method is less sensitive to control point location than vortex lattice method. Hence ,vortex panel method is expected to give better results for three dimensional flow, for example, for hovering rotor, than vortex lattice method. Both method satisfy the Kutta condition implicitly.

The pressure coefficient, C_p , is calculated as follows.

$$p + 0.5\,\rho U^2 = p_\infty + 0.5\rho\Omega^2 r^2 \qquad \text{——— (3-10)}$$

Ω is the rotational speed of the rotor and r is the radius. On the suction surface $U = u + 0.5\,\gamma$ and on the pressure surface $U = u - 0.5\,\gamma$. u is the total tangential velocity on the surface and γ is the local strength of vortex sheet.

$$C_{p\pm} = 1 - \left(\frac{u}{\Omega R \eta} \pm \frac{\gamma}{\Omega\, R\, \eta} \right)^2 \qquad \text{——— (3-11)}$$

where η is the normalized radius. By integrating the pressure distribution the normal section force, N , of lifting surface is calculated as $N = C_n \cdot 0.5\rho\Omega^2 r^2 c$. Since $C_\ell = a\,\alpha$, $\alpha_1 = C_n / a$ as a first approximation where α is the angle of attack, a is the lift curve slope, and C_ℓ is the lift coefficient.

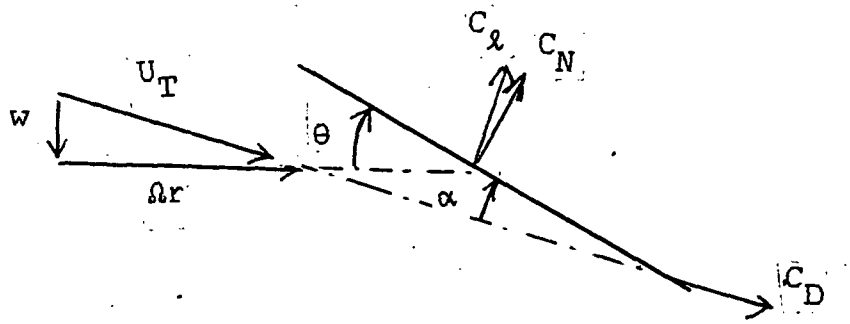

$$\text{arc tan}\left(\frac{w}{\Omega r}\right) = \Theta - \alpha \quad \text{from the figure}$$

$$w / (\Omega r) = \lambda/\eta = \tan(\Theta - \alpha)$$

$$\lambda_1 = \eta \tan(\Theta - \alpha_1)$$

By Kutta-Joukowski law normal force N should act perpendicular to the velocity U_T.

$$C_\ell = \frac{N}{0.5\rho U_T^2 c} = \frac{C_n}{1 + \lambda_1^2}$$

Then the new angle of attack is $\alpha = C_\ell / a$. The power coefficient of rotor is C_p.

$$C_p = 0.5\sigma \int_{\eta_T}^{1} \{C_\ell \sin(\Theta - \alpha) + C_d \cos(\Theta - \alpha)\} \eta(\eta^2 + \lambda^2)\, d\eta \quad -(3\text{-}12)$$

The thrust coefficient of rotor is C_T.

$$C_T = 0.5\sigma \int_{\eta_T}^{1} \{C_\ell \cos(\Theta - \alpha) - C_d \sin(\Theta - \alpha)\}(\eta^2 + \lambda^2)\, d\eta \quad -(3\text{-}13)$$

Here, σ is the solidity and λ is the inflow ratio.

Also, $C_d = C_{d0} + C_{dk}\, \alpha^2 = 0.014 + 0.5\, \alpha^2$

3.2 DERIVATION OF METHOD

The second form of Green's theorem is

$$\iiint_R (\phi_1 \nabla^2 \phi_2 - \phi_2 \nabla^2 \phi_1)\, dV$$

$$= \iint_S \vec{n}.(\phi_1 \nabla \phi_2 - \phi_2 \nabla \phi_1)\, dS \qquad \text{—— (3-14)}$$

where R is the region bounded by the closed surface S and $\vec{n}$ is the outward unit normal. Let us consider the region outside a wing as shown in figure.

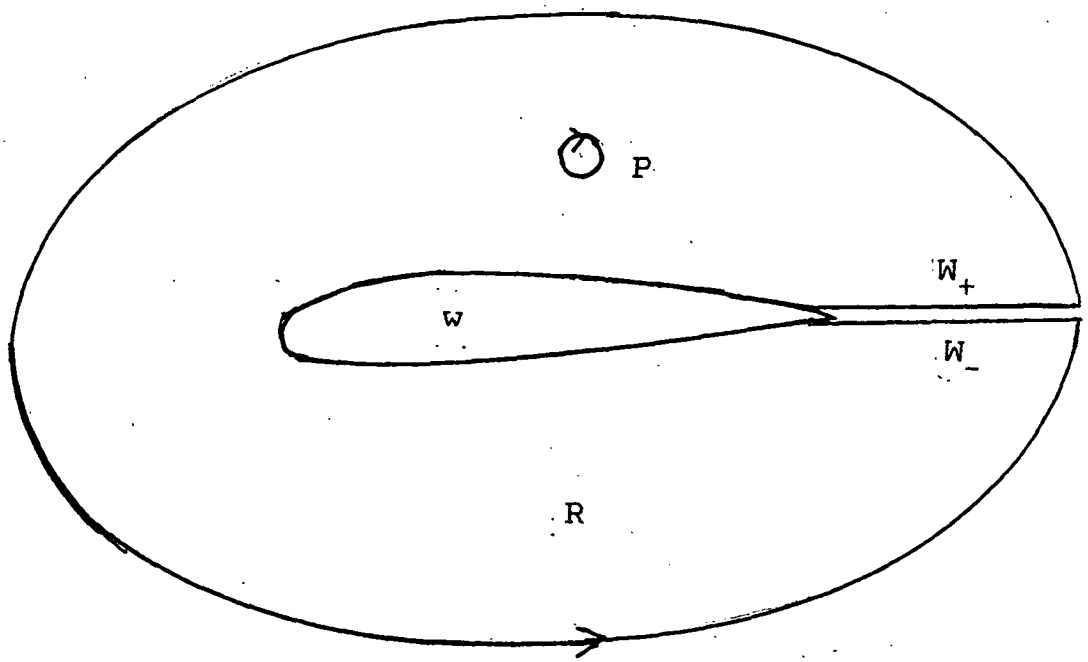

Let $\phi_1 = \phi$ and $\phi_2 = \dot{x} = 1/r$. Then $\nabla^2\phi_1 = 0$ in region R and and $\nabla^2\phi_2 = 0$ except at a point P. Let us exclude the point P

from the region R. Then the first integral in equation (3-14) is zero. At a point P

$$\iint_p \vec{n}.\left(\phi\nabla\frac{1}{r} - \frac{1}{r}\nabla\phi \right) dS$$

$$= \lim_{r\to o} \int \left(\frac{\phi}{r^2} - \frac{1}{r}\nabla\phi \right) r\, d\Omega = -4\Pi\phi_p \qquad \text{---- (3-15)}$$

$$\iint_S \vec{n}.(-\phi\nabla\frac{1}{r} + \frac{1}{r}\nabla\phi)dS = -4\Pi\phi_p$$

, if p is inside of R.

$= 0$, if p is outside of R.

S =Body surface + Wake = B + W.

On the wake surface W,

$$\iint_S \vec{n}.\left(\frac{1}{r}\nabla\phi \right) dS =$$

$$\int_{W_+} \frac{1}{r}\frac{\partial\phi_u}{\partial n}dS - \int_{W_-} \frac{1}{r}\frac{\partial\phi_\ell}{\partial n}dS = 0$$

On the wake surface the normal velocity is continuous. Hence,

$$\phi_p = \frac{-1}{4\Pi}\iint_B \left(\frac{1}{r}\nabla\phi - \phi\nabla\frac{1}{r}\right).\vec{n}\, dS$$

$$+ \frac{1}{4\Pi}\iint_W \left(\phi_u - \phi_\ell \right)\nabla\frac{1}{r}.\vec{n}\, dS \qquad \text{---- (3-16)}$$

Let ϕ_1 be the velocity potential inside of the wing.

$$0 = \frac{1}{4\pi} \iint_B \left(\frac{1}{r}\nabla\phi_1 - \phi_1 \nabla\frac{1}{r}\right).\vec{n}\, dS \qquad \text{——} \qquad (3\text{-}17)$$

Adding equations (3-16) and (3-17) we obtain

$$\phi_p = -\frac{1}{4\pi} \iint_B \frac{1}{r} (\nabla\phi - \nabla\phi_1).\vec{n}\, dS$$

$$+ \frac{1}{4\pi} \iint_B (\phi - \phi_1)\nabla\frac{1}{r} .\vec{n}dS + \frac{1}{4\pi} \iint_W (\phi_u - \phi_\ell)\nabla\frac{1}{r}.\vec{n}dS \quad — (3\text{-}18)$$

If we set $\phi = \phi_1$ on the body surface, we get potential due due to source distribution and circulation $\Gamma = \phi_u - \phi_\ell$.

$$\phi_p = -\frac{1}{4\pi} \iint_B \frac{1}{r}(\nabla\phi - \nabla\phi_1).\vec{n}dS + \frac{1}{4\pi} \iint_W (\phi_u - \phi_\ell)\nabla\frac{1}{r}.\vec{n}dS$$

$$\phi_p = -\frac{1}{4\pi}\iint_B \frac{\sigma}{r}dS + \frac{1}{4\pi}\iint_W \Gamma\nabla\left(\frac{1}{r}\right).\vec{n}dS \qquad \text{——} \qquad (3\text{-}19)$$

Here, $\frac{1}{4\pi}\frac{\partial}{\partial n}\left(\frac{1}{r}\right)$ is the potential due to a doublet.

$$\frac{\partial\phi_p}{\partial n_p} = -\vec{V}.\vec{n}_p = -\frac{1}{4\pi}\iint_B \sigma\frac{\partial}{\partial n_p}\left(\frac{1}{r_{pq}}\right)dS_q$$

$$+ \frac{1}{4\pi}\iint_W \Gamma\frac{\partial}{\partial n_p}\frac{\partial}{\partial n_q}\left(\frac{1}{r_{pq}}\right)dS_q \qquad \text{——} \qquad (3\text{-}20)$$

The velocity due to doublet can be replaced by the velocity due to vortex. Then the vortex of circulation of Γ can be distributed on the wing surface or on the camber surface.

If we let $\nabla\phi \cdot \vec{n} = \nabla\phi_l \cdot \vec{n}$, then we get the potential due to doublet distribution only.

$$\phi_p = \frac{1}{4\pi}\iint_B (\phi - \phi_l)\nabla(\frac{1}{r}).\vec{n}dS$$

$$+ \frac{1}{4\pi}\iint_W (\phi_u - \phi_\ell)\nabla(\frac{1}{r}).\vec{n}dS \qquad \text{——— (3-21)}$$

When the wing has zero thickness, the normal velocity across the wing is continuous. We get the potential due to doublet only. From equation (3-16) we can get the expression for the total potential Φ.

$$\Phi_p = \phi_{\infty p} - \frac{1}{4\pi}\iint_B (\frac{1}{r}\nabla\phi - \phi\nabla\frac{1}{r}).\vec{n}dS$$

$$+\frac{1}{4\pi}\iint_W (\phi_u - \phi_\ell)\nabla(\frac{1}{r}).\vec{n}\, dS \qquad \text{——— (3-22)}$$

Here ϕ_∞ is the potential due to the free stream. Let ϕ be the total potential Φ. THen $\nabla\Phi \cdot \vec{n} = 0$ on body surface.

$$\Phi_p = \phi_{\infty p} + \frac{1}{4\pi}\iint_B \Phi\nabla(\frac{1}{r}).\vec{n}\, dS$$

$$+ \frac{1}{4\pi}\iint_W (\Phi_u - \Phi_\ell)\nabla(\frac{1}{r}).\vec{n}\, dS \qquad \text{——— (3-23)}$$

Let p be the point on the wing surface. Then equation(3-23) becomes

$$\frac{1}{2\pi}\iint_{B-p}\Phi\nabla\left(\frac{1}{r}\right).\vec{n}dS + \frac{1}{2\pi}\iint_{W}(\Phi_u - \Phi_\ell)\nabla\left(\frac{1}{r}\right).\vec{n}dS - \Phi_p + 2\phi_{\infty p} = 0 \quad -(3\text{-}24)$$

For a numerical solution of equation (3-24), we represent the surface and wake by a number of flat quadrilateral panels and we assume the singularity distribution is constant over each panel. Equation(3-24) is applied at a central control point on the under side of each surface panel.

$$[\delta_{pk} - C_{pk} - W_{pk}]\{\Phi_k\} = \{2\phi_{\infty k}\} \qquad \text{——} \quad (3\text{-}25)$$

where δ_{pk} is the kronecker delta.

$$C_{pk} = \left[\frac{1}{2\pi}\int_{S_k}\frac{\partial}{\partial n}\left(\frac{1}{r}\right)dS_k\right], \quad p \neq k$$

$$W_{pk} = \left[\pm\frac{1}{2\pi}\int_{S_w}\frac{\partial}{\partial n}\left(\frac{1}{r}\right)dS_w\right]$$

$W_{pk} = 0$ for the segments not in contact with the trailing edge.

From equation (3-23) we obtain

$$\frac{\partial\Phi_p}{\partial n_p} = \vec{V}_\infty.\vec{n}_p + \frac{1}{4\pi}\iint_{B}\Phi\frac{\partial}{\partial n_p}\frac{\partial}{\partial n_q}\left(\frac{1}{r}\right)dS_q$$

$$+\frac{1}{4\pi}\iint_{W}(\Phi_u - \Phi_\ell)\frac{\partial}{\partial n_q}\frac{\partial}{\partial n_w}\left(\frac{1}{r}\right)dS_w \qquad \text{——} \quad (3\text{-}26)$$

Since doublet is equivalent to vortex, the surface distribution

of vortex can replace the doublet distribution. The strength of vortex is the surface tangential velocity since Φ is the total potential.

When P is the point on the wing surface, equation (3-16) becomes

$$-\frac{1}{4\pi}\iint_{B}\frac{1}{r}\nabla\phi.\vec{n}dS+\frac{1}{4\pi}\iint_{B-p}\phi\nabla(\frac{1}{r}).\vec{n}dS$$

$$+\frac{1}{4\pi}\iint_{w}(\phi_u-\phi_l)\nabla(\frac{1}{r}).\vec{n}dS=\frac{1}{2}\phi_p \qquad \text{——} \quad (3\text{-}27)$$

Using the same approach as equation (3-25) we obtain

$$[\delta_{pk}-C_{pk}-W_{pk}]\{\phi_k\}=[b_{pk}]\{(\frac{\partial\phi}{\partial n_k})\} \qquad \text{——} \quad (3\text{-}28)$$

$$C_{pk}=[\frac{1}{2\pi}\int_{S_k}\frac{\partial}{\partial n}(\frac{1}{r})dS_k],\ p\neq k$$

$$W_{pk}=[\pm\frac{1}{2\pi}\int_{S_w}\frac{\partial}{\partial n}(\frac{1}{r})\,dS_w]$$

$W_{pk}=0$ for the segments not in contact with the trailing edge.

$$b_{pk}=[-\frac{1}{2\pi}\int_{S_k}\frac{1}{r}\,dS_k]$$

In equation (3-24) we set $\Phi=\phi_\infty+\phi$.

$$-\phi_p + \phi_{\infty p} + \frac{1}{2\pi}\iint_{B-p}(\phi_\infty + \phi)\nabla(\frac{1}{r}).\vec{n}\ dS$$

$$+\frac{1}{2\pi}\iint_{W}(\phi_u - \phi_\ell)\nabla(\frac{1}{r}).\vec{n}dS = 0$$

$$\phi_p - \frac{1}{2\pi}\iint_{B-p}\phi\nabla(\frac{1}{r}).\vec{n}dS - \frac{1}{2\pi}\iint_{W}(\phi_u - \phi_\ell)\nabla(\frac{1}{r}).\vec{n}dS \quad \text{——(3-29)}$$

$$= \phi_{\infty p} + \iint_{B-p}\phi_\infty\nabla(\frac{1}{r}).\vec{n}\ dS$$

The numerical implementation of this equation is

$$[\delta_{pk} - C_{pk} - W_{pk}]\{\phi_k\} = [\delta_{pk} + C_{pk}]\{\phi_{\infty k}\} \quad \text{——(3-30)}$$

3.3 LIFTING BODY THEORY

Among the various formulations presented in section (3.2) the method of Hess and Smith in ref.(34) was used in the lifting body potential flow computation of wings and rotor. The method of Hess and Smith can be derived from equation (3-20) as follows. There are N normal flow boundary conditions to determine N source strengths, σ_j , for N surface panels of the lifting body. There are also K Kutta conditions of equal pressure on lower and upper panels nearest to the trailing edge to determine K vortex sheet strengths, γ_k , for K spanwise sections of the lifting body. The normal velocity at control point i can be expressed in matrix form.

$$\left[A_{ij} \, , \, A_{ik} \right] \begin{pmatrix} \sigma_j \\ \gamma_k \end{pmatrix} = \{w_i\} \qquad i = 1, \cdots, N \qquad \text{——————} \quad (3\text{-}31)$$

$$\text{where} \quad A_{ij} = \left[-\frac{1}{4\pi} \iint_{S_j} \nabla_i \left(\frac{1}{r_{ij}} \right) dS_j \right] \cdot \vec{n}_i \qquad \text{———} \quad (3\text{-}32)$$

$$\text{and} \quad A_{ik} = \left[-\frac{1}{4\pi} \iint_{S_k} \frac{\vec{r}_{ik} \times \vec{\Gamma}_k}{r_{ik}^3} \, dS_k \right] \cdot \vec{n}_i \qquad \text{———} \quad (3\text{-}33)$$

The magnitude of $\vec{\Gamma}_k$ is unit for the surface panel S_k , increases

linearly along the side edge of panels according to Helmholtz law, and stays constant in the wake. The perturbation tangential velocity at control point i is $\{ v_i \}$.

$$\{ v_i \} = [C_{ij} , C_{ik}] \begin{Bmatrix} \sigma_j \\ \gamma_k \end{Bmatrix} \quad \text{——— (3-34)}$$

where $$C_{ij} = \left[-\frac{1}{4\pi} \iint_{S_j} \nabla_i \cdot \left(\frac{1}{r_{ij}} \right) dS_j \right] \cdot \vec{t}_i \quad \text{——— (3-35)}$$

$$C_{ik} = \left[-\frac{1}{4\pi} \iint \frac{\vec{r}_{ik} \times \vec{\Gamma}_k}{r_{ik}^3} dS \right] \cdot \vec{t}_i \quad \text{—— (3-36)}$$

$\vec{n}_i$ and $\vec{t}_i$ are the normal and tangential unit vectors on control point i. The Kutta condition gives K additional equations in addition to N equations given by equation (3-31)

$$[C_{iu,j} , C_{iu,k}] \begin{Bmatrix} \sigma_j \\ \gamma_k \end{Bmatrix} + \vec{U}_\infty \cdot \vec{t}_{iu}$$

$$= [C_{i\ell,j} , C_{i\ell,k}] \begin{Bmatrix} \sigma_j \\ \gamma_k \end{Bmatrix} + \vec{U}_\infty \cdot \vec{t}_{i\ell} \quad \text{——— (3-37)}$$

Here, i is the control point of the panel touching the trailing edge.

$$[(C_{iu,j} - C_{i\ell,j}) \; (C_{iu,k} - C_{i\ell,k})] \begin{Bmatrix} \sigma_j \\ \gamma_k \end{Bmatrix}$$

$$= \left(\vec{U}_\infty \cdot \vec{t}_{i\ell} - \vec{U}_\infty \cdot \vec{t}_{iu} \right)$$

Let $A_{ij} = C_{iu,j} - C_{i\ell,j}$, $A_{ik} = C_{iu,k} - C_{i\ell,k}$

and $w_i = \vec{U}_\infty \cdot \vec{t}_{i\ell} - \vec{U}_\infty \cdot \vec{t}_{iu}$ for $i = N+1,\cdots,N+K$.

Then, $\left[A_{ij} , A_{ik} \right] \begin{Bmatrix} \sigma_j \\ \gamma_k \end{Bmatrix} = \{ w_i \}$, $i = 1,\cdots,N+K$ — (3-38)

The solution of this matrix equation gives N source and K vortex strengths. For the rolled-up vortex trailed between station k and k+p, the strength of this vortex is $\Gamma_k - \Gamma_{k+p}$. The influence coefficients at control point i due to this rolled-up vortex is B_{ik} . Then $C_{ik} = C_{ik} + B_{ik}$ and $C_{i,k+p} = C_{i,k+p} - B_{ik}$. Equation (3-34) gives the perturbation tangential velocity at control point i. From Bernoulli's equation we can determine the pressure distribution.

3.4 CALCULATION OF ROTOR FREE WAKE GEOMETRY

For rotor performance analysis using lifting line, lifting surface, and lifting body theories, the wake geometry is divided into near wake, intermediate wake, and far wake. The near wake consists of concentrated circular vortex filaments attached to the blade trailing edge and spans to the half of the blade spacing from each blade on the plane of rotation. The number of vortex filaments in near wake depends on the number of spanwise divisions of the blade. The intermediate wake usually consists of four ring vortices in axial direction and three inner ring vortices in radial direction with the root vortex suppressed. The far wake consists of semi-infinite vortex cylinders whose number depends on the inner ring vortices in intermediate wake. During lifting surface and lifting body representation of the rotor blade, the blade bound circulation is considered to be concentrated on a quarter chord line of the blade for the calculation of free wake geometry. During free wake geometry computation the near wake is considered to roll-up instantaneously on the plane of rotation according to the conservation of linear momentum. The radial positions of rolled-up vortices are determined as follows.

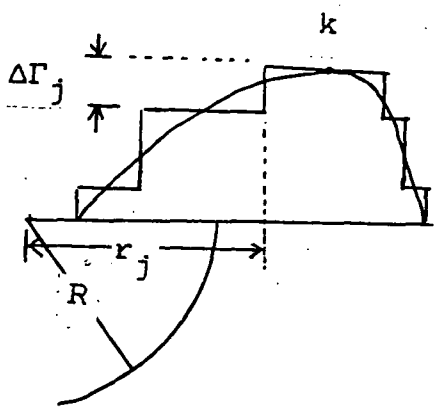

$$(\Gamma_k - \Gamma_1) R^2 = \sum_{j=1}^{k} r_j^2 \Delta\Gamma_j$$

where R is the radial position of rolled-up vortex, $\Delta\Gamma_j$ the strength of the trailing vortex filament, and r_j the radial coordinate of the trailing vortex filament.

From the root to 15 % radius of the blade span the root vortex is considered to be formed and then is suppressed. From 15 % radius to the position of the maximum bound circulation a second inner vortex is rolled-up. From the position of the maximum bound circulation to the blade tip the tip vortex is formed. The rolled-up near wake was used to compute the induced velocities on the rolled-up near wake vortex, while the entire near wake was used to compute the induced velocities on the blade or intermediate wake. The

induced velocities on the blade and beneath each blade are computed. The average of these two velocities multiplied by the blade spacing determines the position of intermediate ring vortex. Since the influence of near wake vortex filaments is computed only on and beneath the blade,the near wake is extended to form ring vortices and the half of the velocity due to ring vortex is the induced velocities on blade and wake.

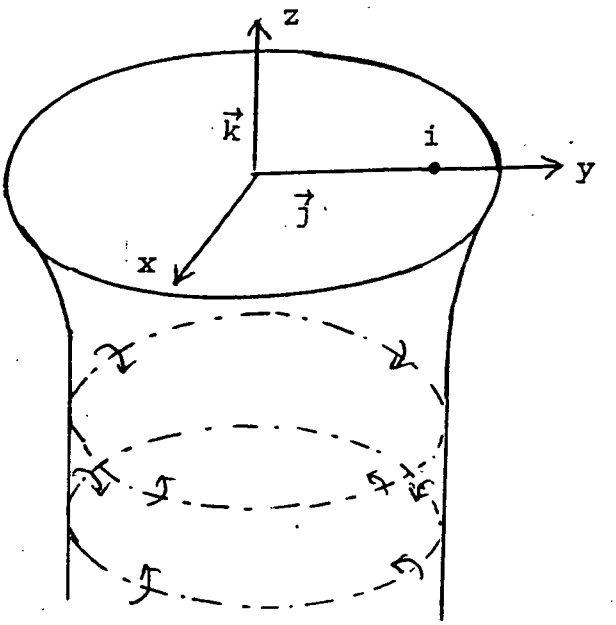

On the position, i, of the quarter chord line of the blade, or intermediate wake the induced velocities are $(w_i \vec{k} + v_i \vec{j})$.

$$w_i^{n+1} = A^n_{zi,j}\ \gamma_j^{n+1} \quad , \quad v_i^{n+1} = A^n_{yi,j}\ \gamma_j^{n+1}$$

where γ_j are the strength of bound circulation, $A_{yi,j}$ and $A_{zi,j}$ are the y- and z- direction induced velocities due to all

trailing vortices from bound circulation, j, of unit strength. i covers all spanwise stations of the blade and all positions of intermediate vortices. The influence coefficients $A_{zi,j}$ and $A_{yi,j}$ are computed from the wake geometry of (n)th iteration. The bound circulation of (n+1)th iteration is computed by applying the boundary condition of no flow normal to body for lifting surface and lifting body theory or Kutta-Joukowski law for lifting line theory. The wake geometry of (n+1)th iteration is computed by intergrating the downwash on wake positions. When the variation of the bound circulation is less than 0.5% for all sections independently, the iteration stops. For the computation of free wake geometry by lifting line theory the initial wake geometry is generated from semi-rigid wake model obtained by local momentum theory. For lifting surface and lifting body theory the wake geometry starts from the lifting line results. The influence coefficients on a quarter chord line due to intermediate and far wakes are taken to be those over all chordwise panel points. This means that the blade is treated as lifting line for intermediate and far wakes during lifting surface and lifting body calculation.

3.5 RESULTS AND DISCUSSION

In this section we discuss lifting body solution for a thin airfoil and wings, and lifting line, lifting surface, and lifting body solutions for the rotor used in Ref.(68). In figure (3-1) to (3-5) lifting body and Euler solutions for a thin airfoil of 1% thickness and vortex panel and exact solutions of a plate are compared. As the thickness approaches zero, source and sink of the lifting body solution become of equal strength and approaches doublet. Figure (3-1) shows that suction side pressure near the leading edge are overpredicted compared to the exact solution of figure (3-2) as the thickness approaches zero. Euler solution of Ref.(32) in figure (3-3) is in good agreement with figure (3-2). Vortex panel solution in figure (3-4) is in good agreement with the exact solution in figure (3-5). Lifting body solutions from figure (3-6) to figure (3-9) for a rectangular wing of Boeing TR 17 of aspect ratio =2 demonstrated that they are in good agreement with the solutions of Ref.(33). In Ref.(33) doublet distribution on camber surface and source distribution on body surface were used instead of one vortex and source distribution on body surface used in the present method.

Figure (3-10) to (3-13) show lifting body solutions for a rectangular wing of NACA 0012 of aspect ratio of 6 which are in close agreement with experiments in Ref.(67). But at the wing tip region the rolling-up vortex from the side edge passes above the wing surface slightly inboard from the tip. Hence the experimental results are different from the theoretical results of the fully attached flow near the wing tip. Figure (3-10) to (3-12) shows that the boundary layer growth gives higher negative pressure near the wing leading edge. Figure (3-14) to (3-23) compares lifting surface and lifting body solutions of NACA 0012 sections for a rotor used in Ref.(68) with wake geometry computed by free wake lifting line theory. In all figures thickness give rise to higher surface velocities compared to surface of zero thickness and hence lowers the surface pressure. Also, thickness gives higher leading edge suction and hence increases the bound circulation. Vortex lattice lifting surface theory underestimates the leading edge suction, while lifting body theory using chordwise panels less than 50 panels overestimates the leading edge suction. Figure (3-24) shows the wake geometry computed by free wake lifting line, lifting surface, lifting body theories, and one computed in Ref.(7). Except for the free wake lifting body solution, wake geometries are in close agreement with each other. Higher circulation due to thickness and due to the finite

number of panels was coupled to wake geometry to move ring vortices further downward for lifting body solution. Bound circulation distribution are shown in figure (3-25), which are obtained by lifting line, lifting surface, lifting body theory with the same wake geometry computed by free wake lifting line theory. The peak bound circulation due to lifting body is the highest among the three solutions and lifting line shows the higher peak circulation than lifting surface solution. From the figure this difference seems to be due to the different leading edge suction due to thickness and due to the finite number of chordwise panels for the lifting body solution. In figure (3-26) bound circulation obtained by free wake lifting line and free wake extended lifting line* are in close agreement except the peak circulation. Free wake lifting body solution gives much higher circulation than two other solution partly due to nonlinear coupling of thickness with free wake geometry. Figure (3-27) compares the bound circulation obtained in Ref.(7) with one obtained by the present method and by using the same geometry used in Ref.(7), and with one obtained by the present method with free wake geometry. They are in almost exact agreement. Figure (3-28) shows the effect of far wake and intermediate wake on bound circulation and performance coefficients. Far wake has a about 10 % effect on the performance coefficients and intermediate wake has

*Single panel lifting surface solution (Weissinger)

very strong influence on the performance of the rotor. When there is only near wake, the thrust coefficients increases and the required power coefficients decreases very much. Figures (3-29) and (3-30) compares the bound circulations obtained by lifting line, surface, and body theories coupled with free wake calculations. Lifting body solution gives about 10 % higher bound circulation due to the thickness effect coupled with free wake geometry. As the number of panels used in lifting body solution is extrapolated to an infinite number, the thickness effect gives about 7 % higher circulation than lifting line solution which used the lift curve slope of 0.98*6.283. In Figure (3-31) the induced drag for the wing of NACA 0012 and aspect ratio =6 converges as the chordwise number of panels increases to 50. Hence, the differences between lifting line and lifting body in figure (3-24) to figure (3-30) will become less than those shown in figures if the chordwise number of panels becomes above 50.

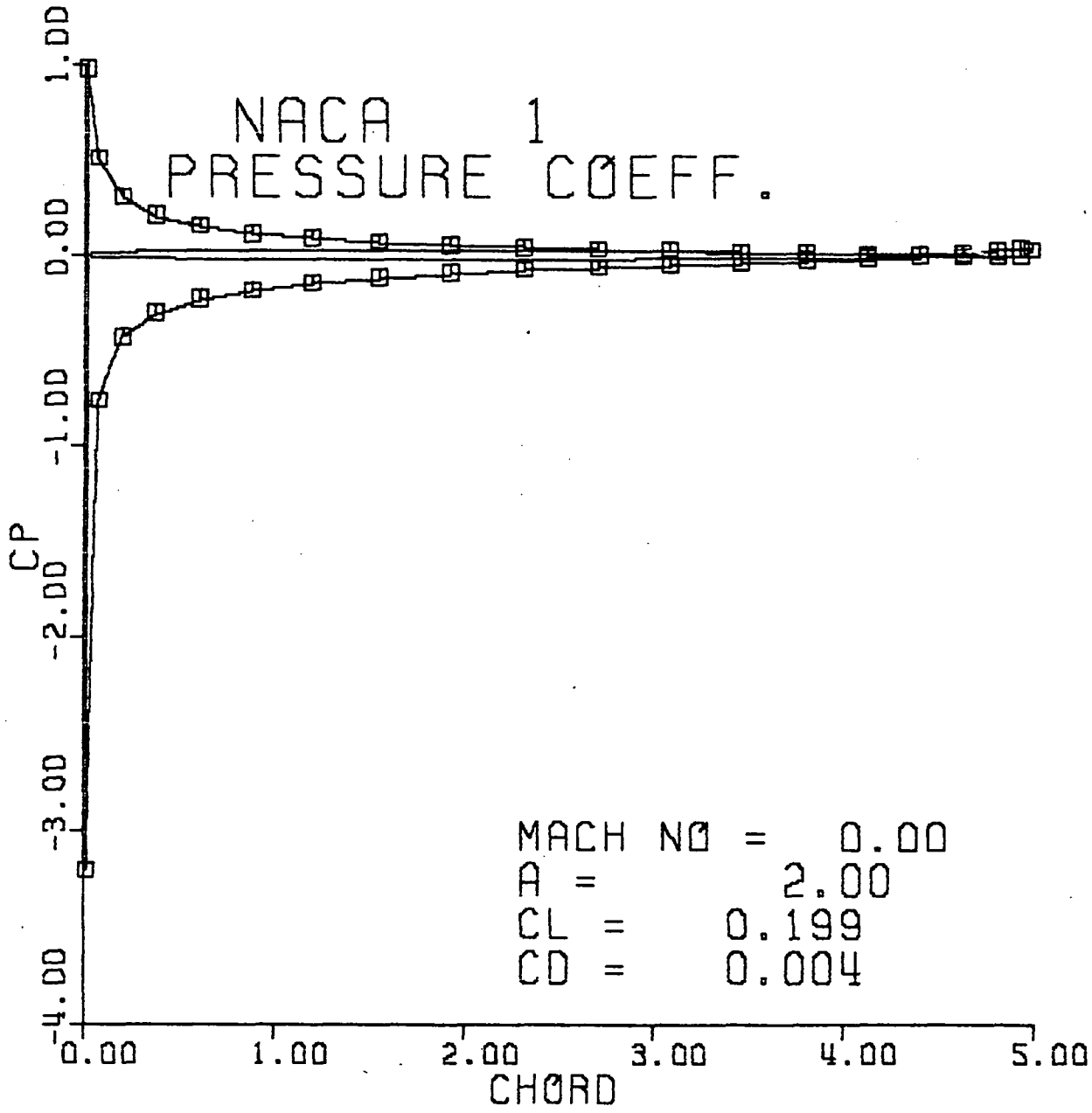

Figure 3-1. Lifting Body Solution of an Airfoil

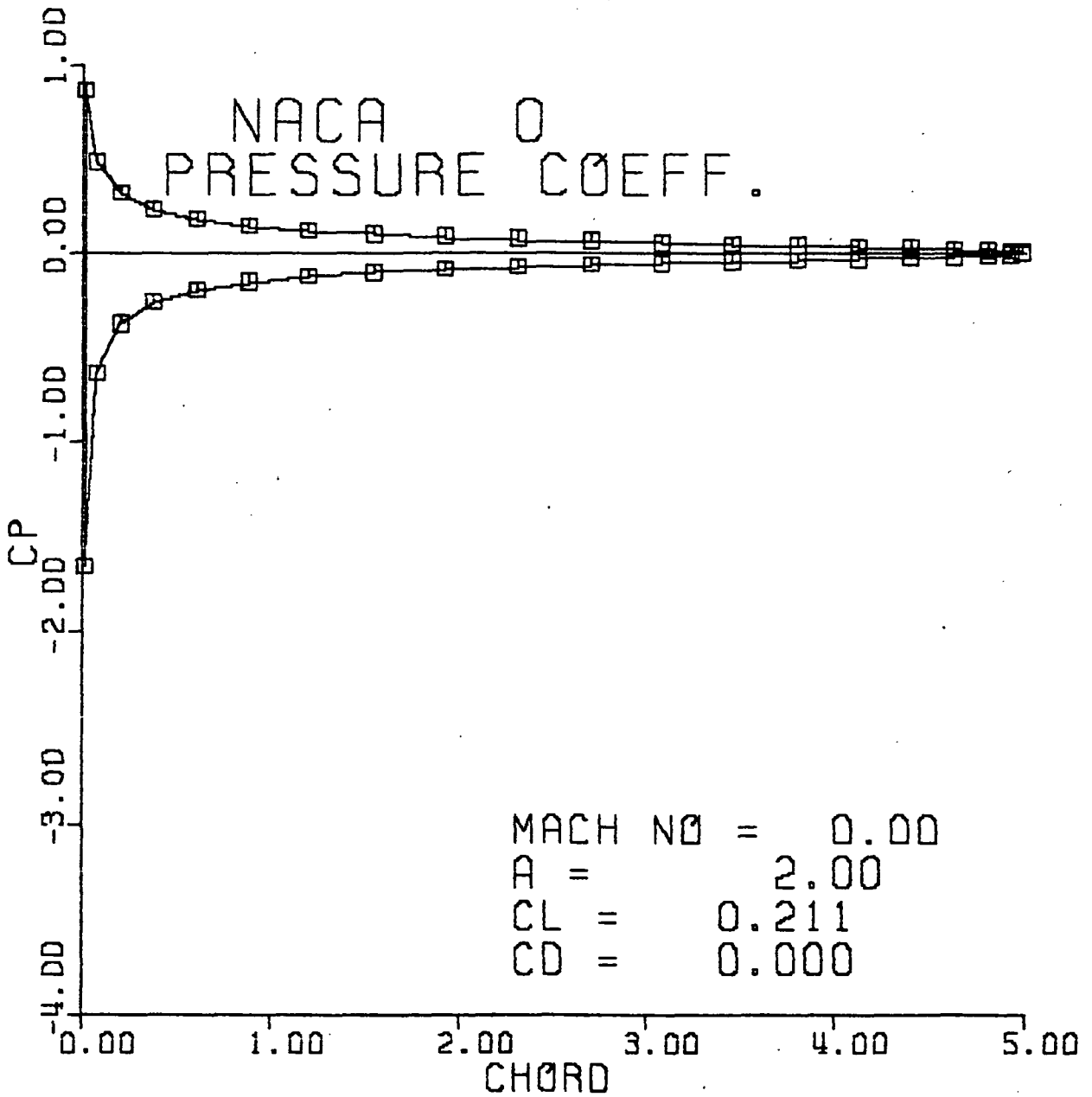

FIGURE 3-2 EXACT SOLUTION OF A PLATE AIRFOIL

FIGURE 3-3 EULER SOLUTION OF THIN AIRFOIL

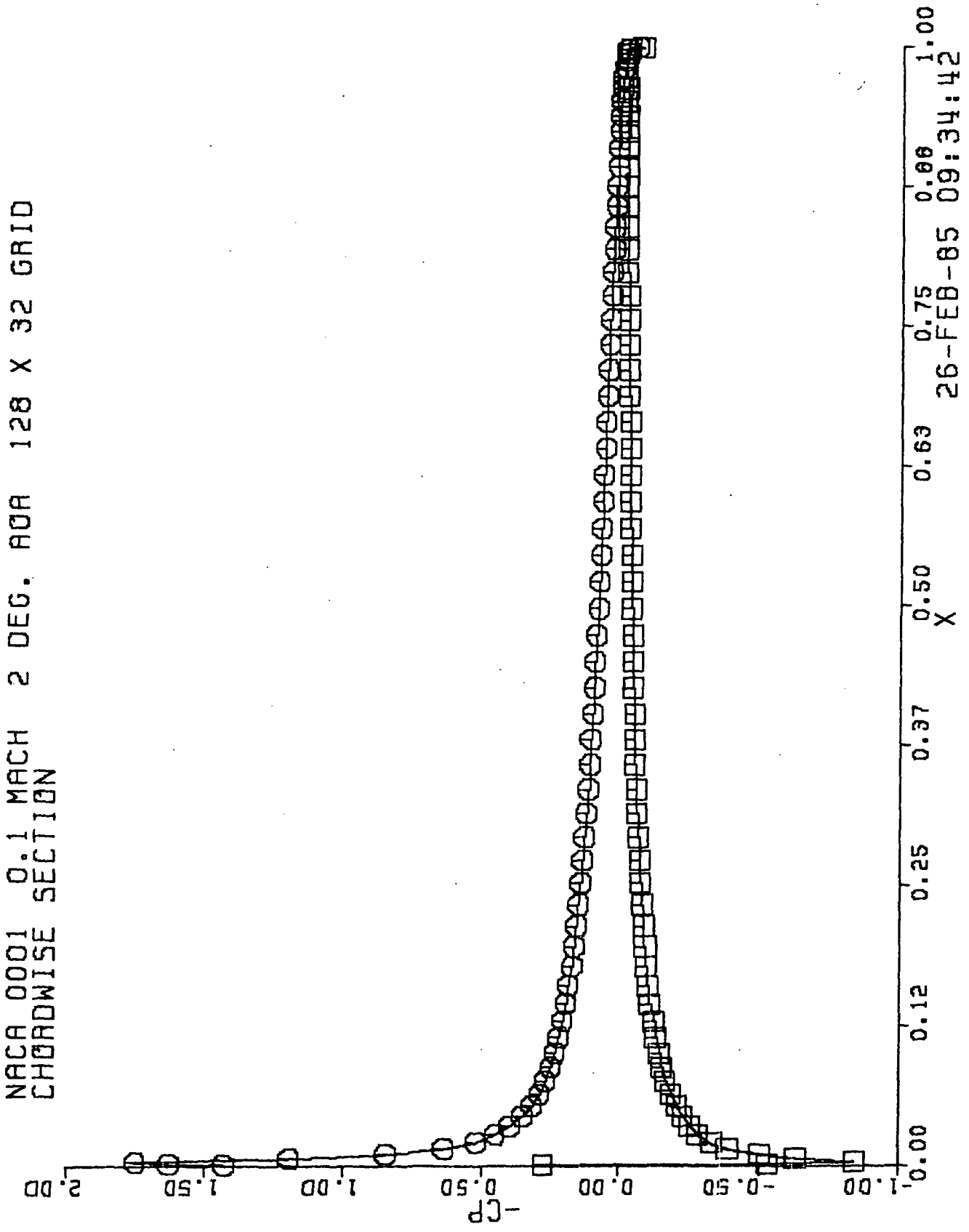

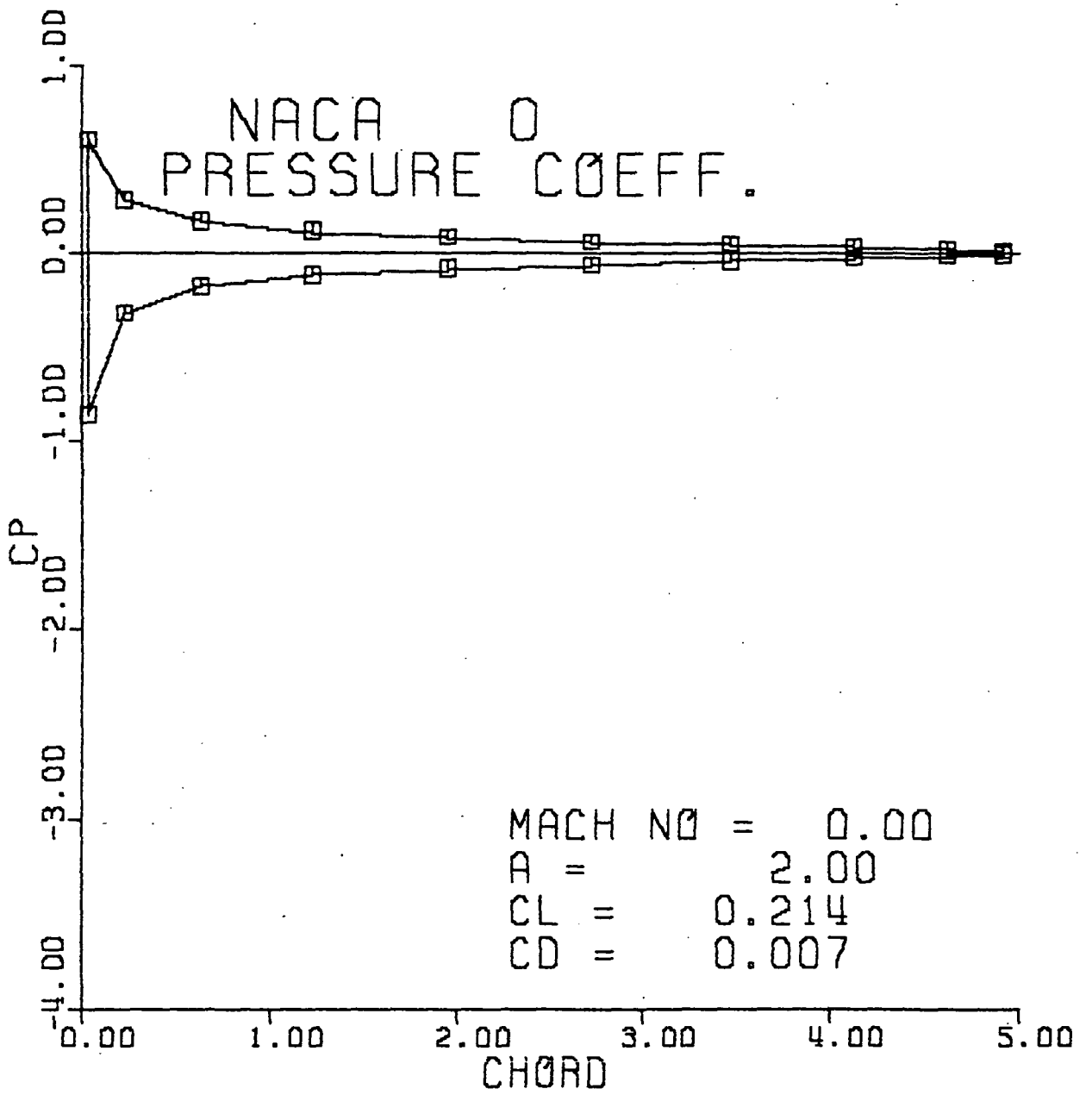

FIGURE 3-4 VORTEX PANEL SOLUTION OF A PLATE

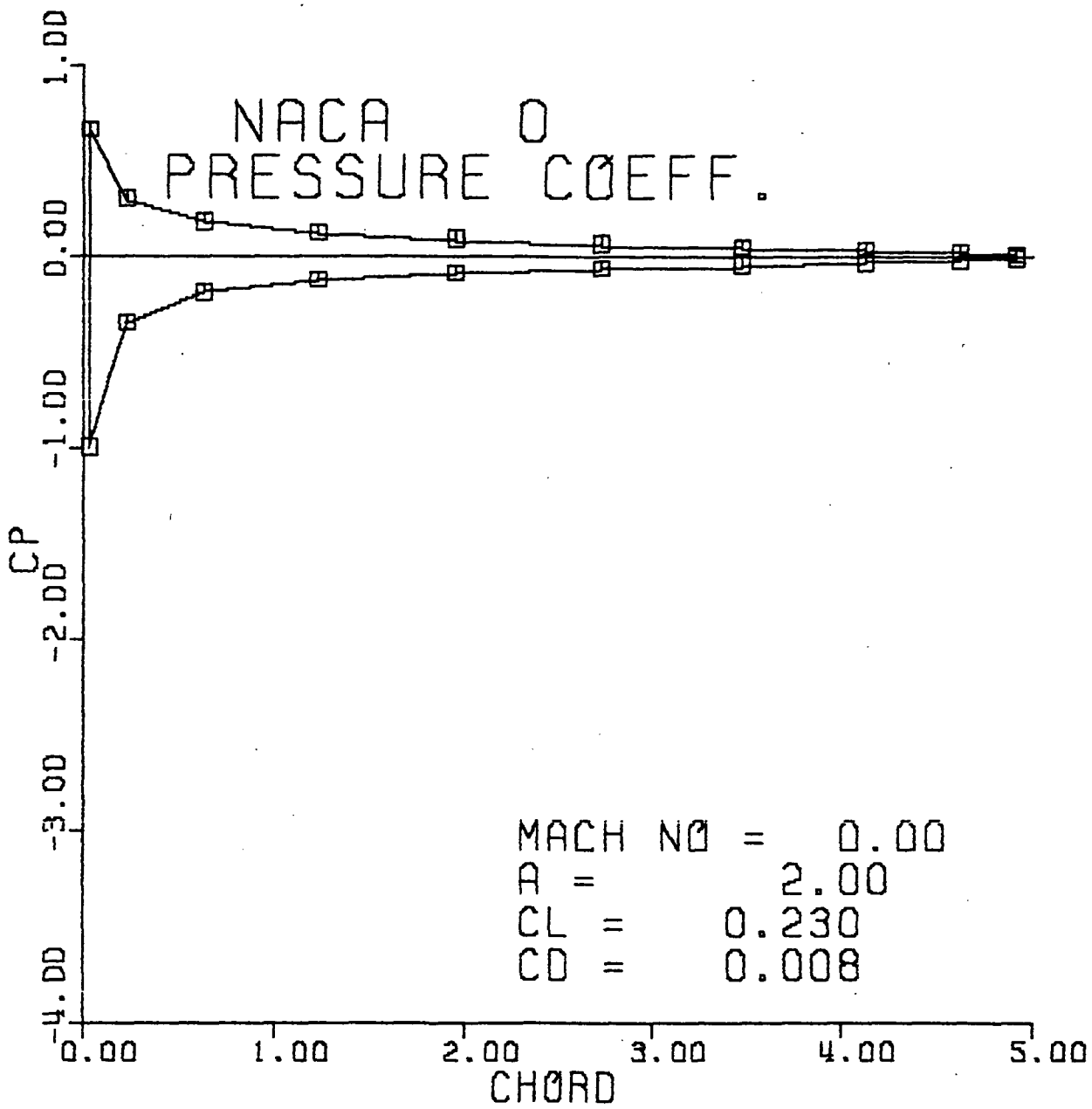

FIGURE 3-5. EXACT SOLUTION OF A PLATE AIRFOIL AT THE SAME CHORDWISE POSITIONS AS FIGURE 3-4.

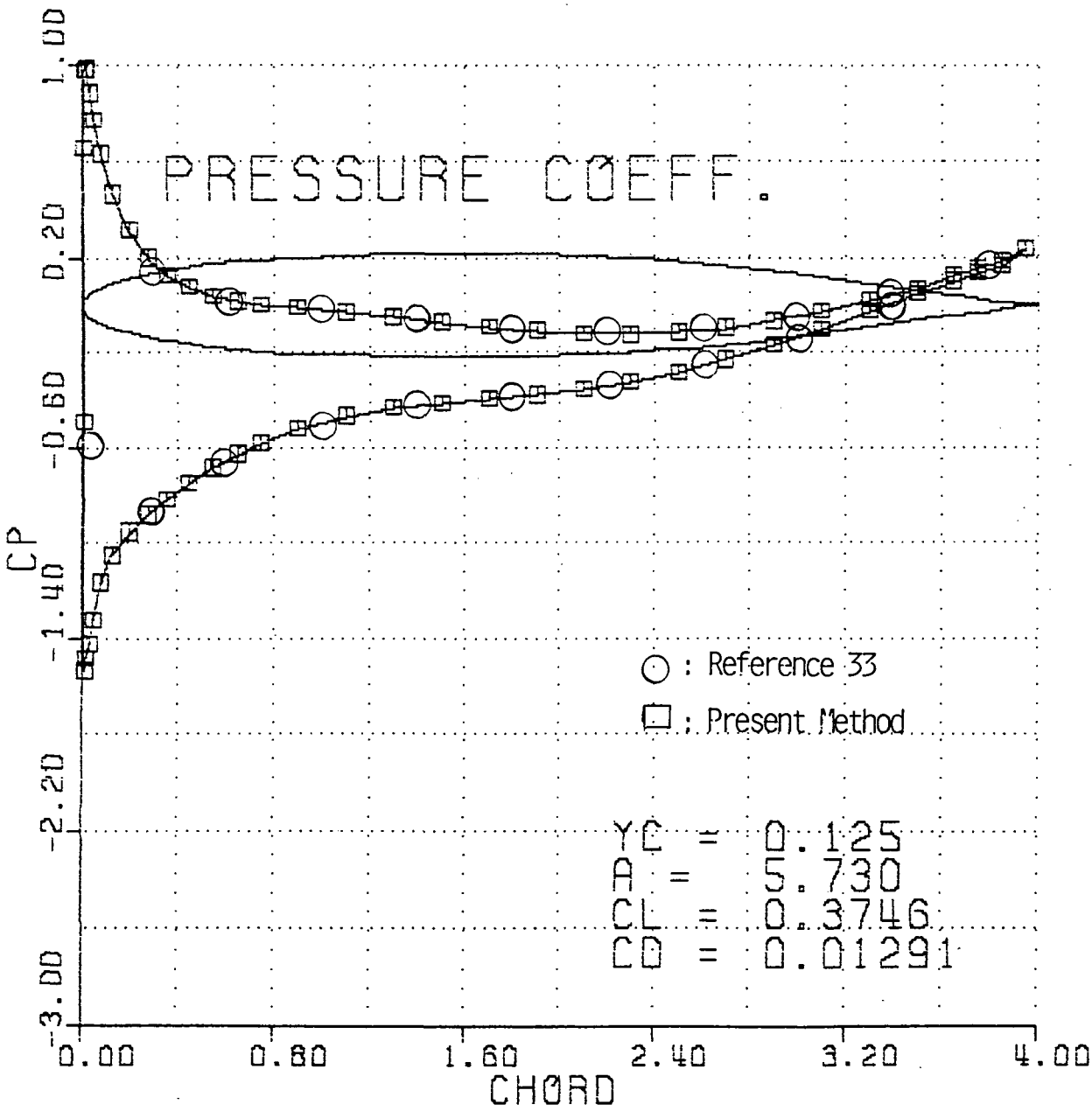

Figure 3-6. Lifting Body Solution of Boeing TR 17 Wing at η= 0.125.

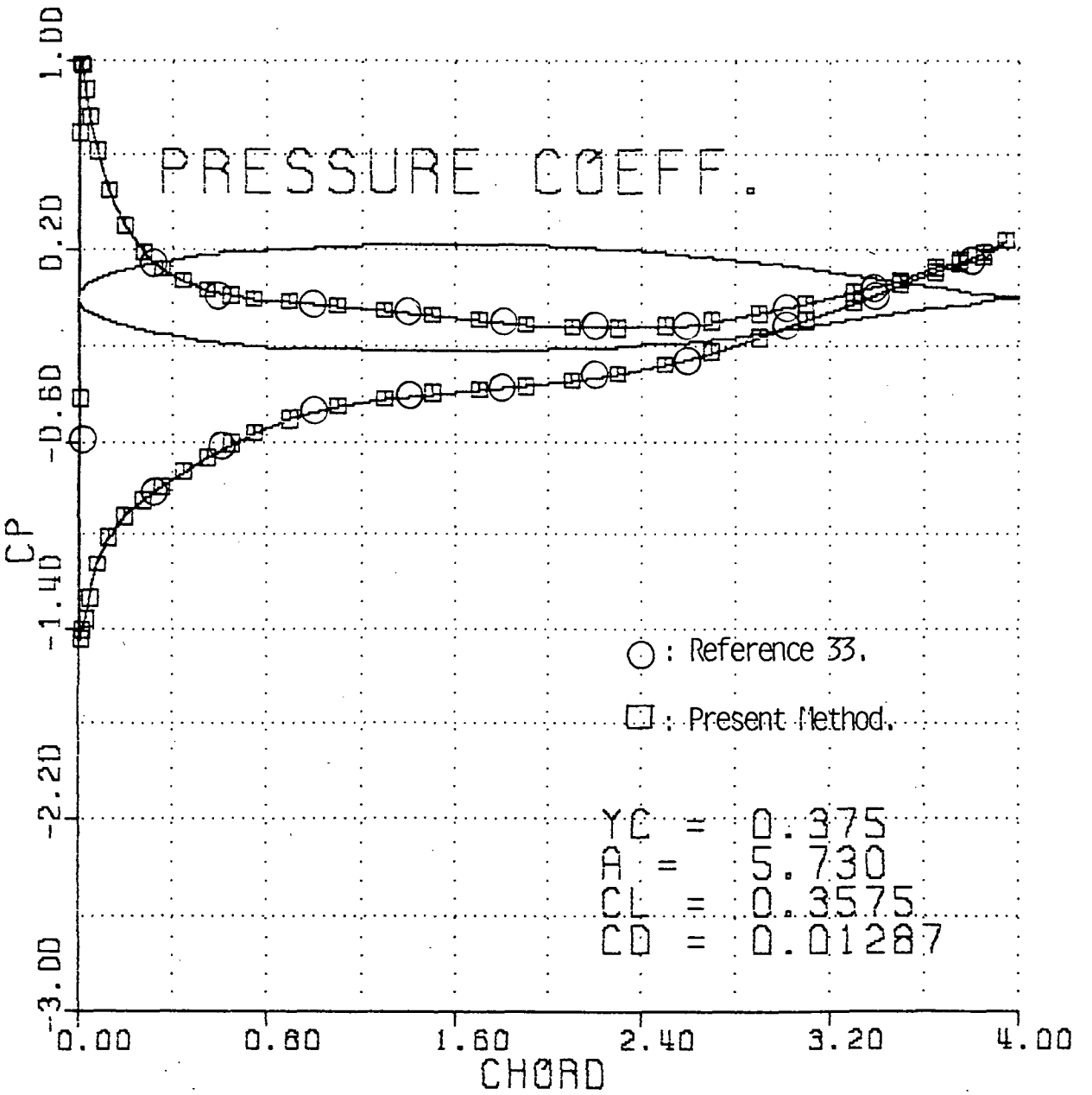

Figure 3-7. Lifting Body Solution of Boeing TR 17 Wing at η= 0.375.

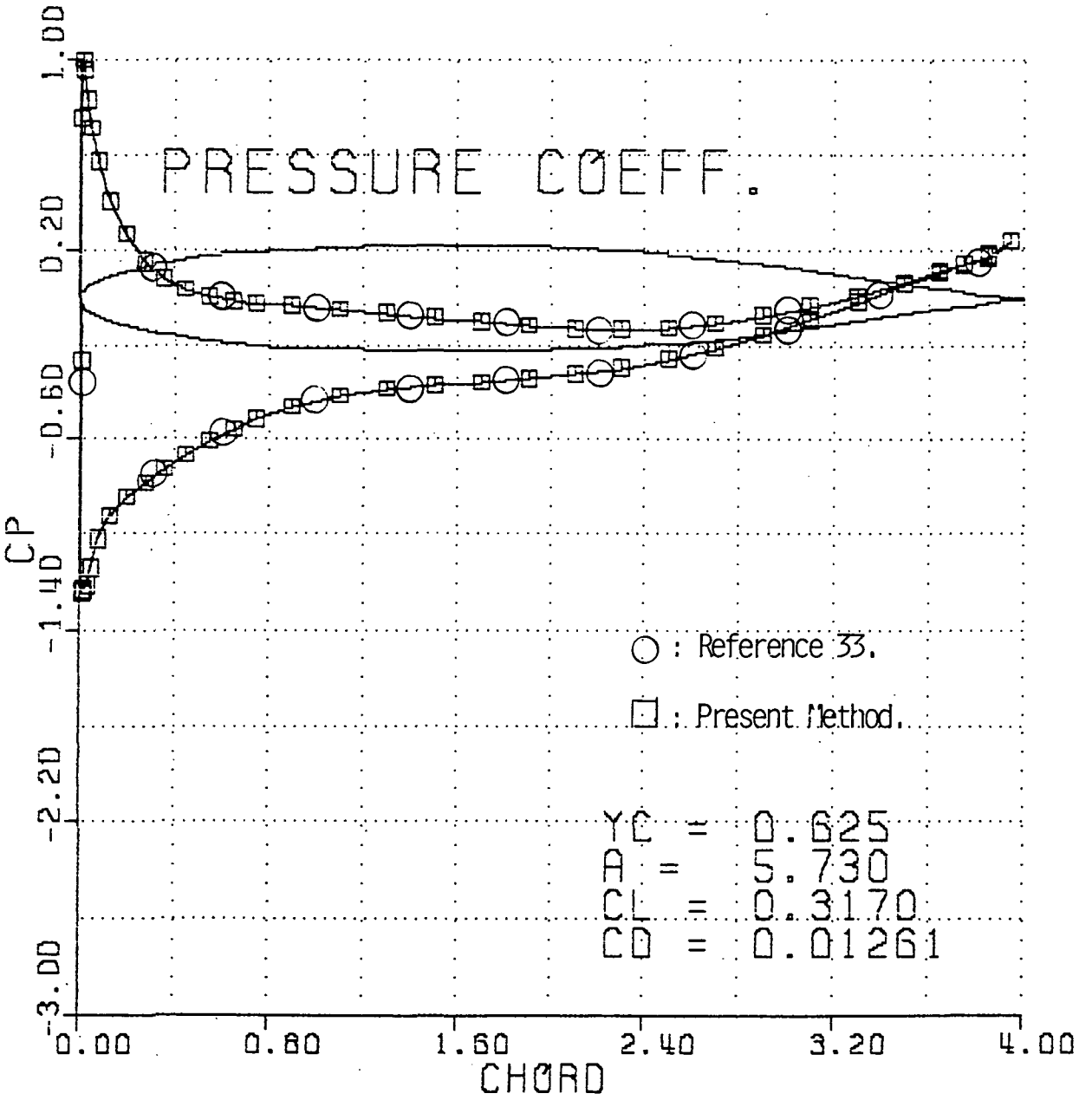

Figure 3-8. Lifting Body Solution of Boeing TR 17 Wing at η = 0.625.

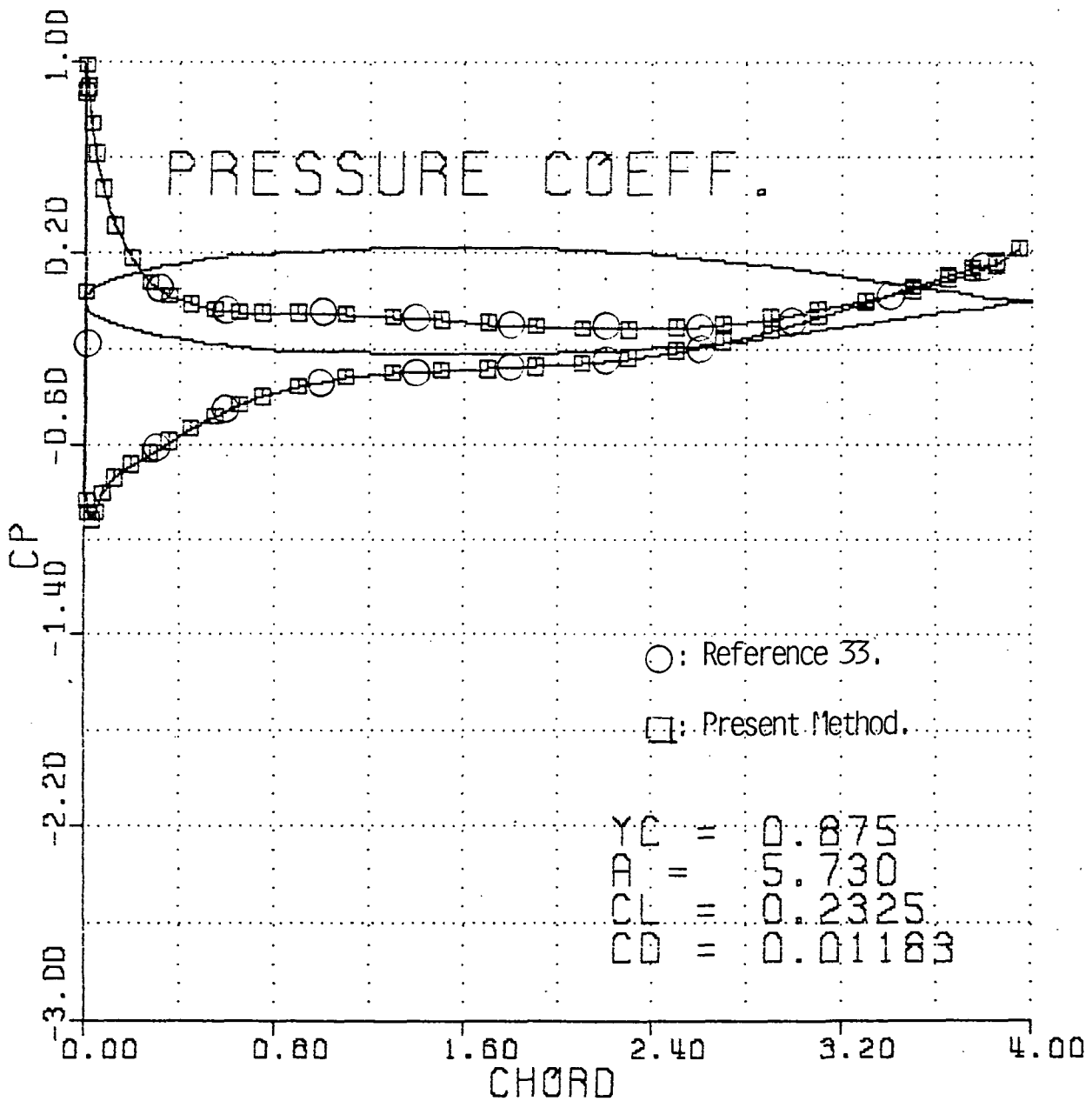

Figure 3-9. Lifting Body Solution of Boeing TR 17 Wing at η=0.875.

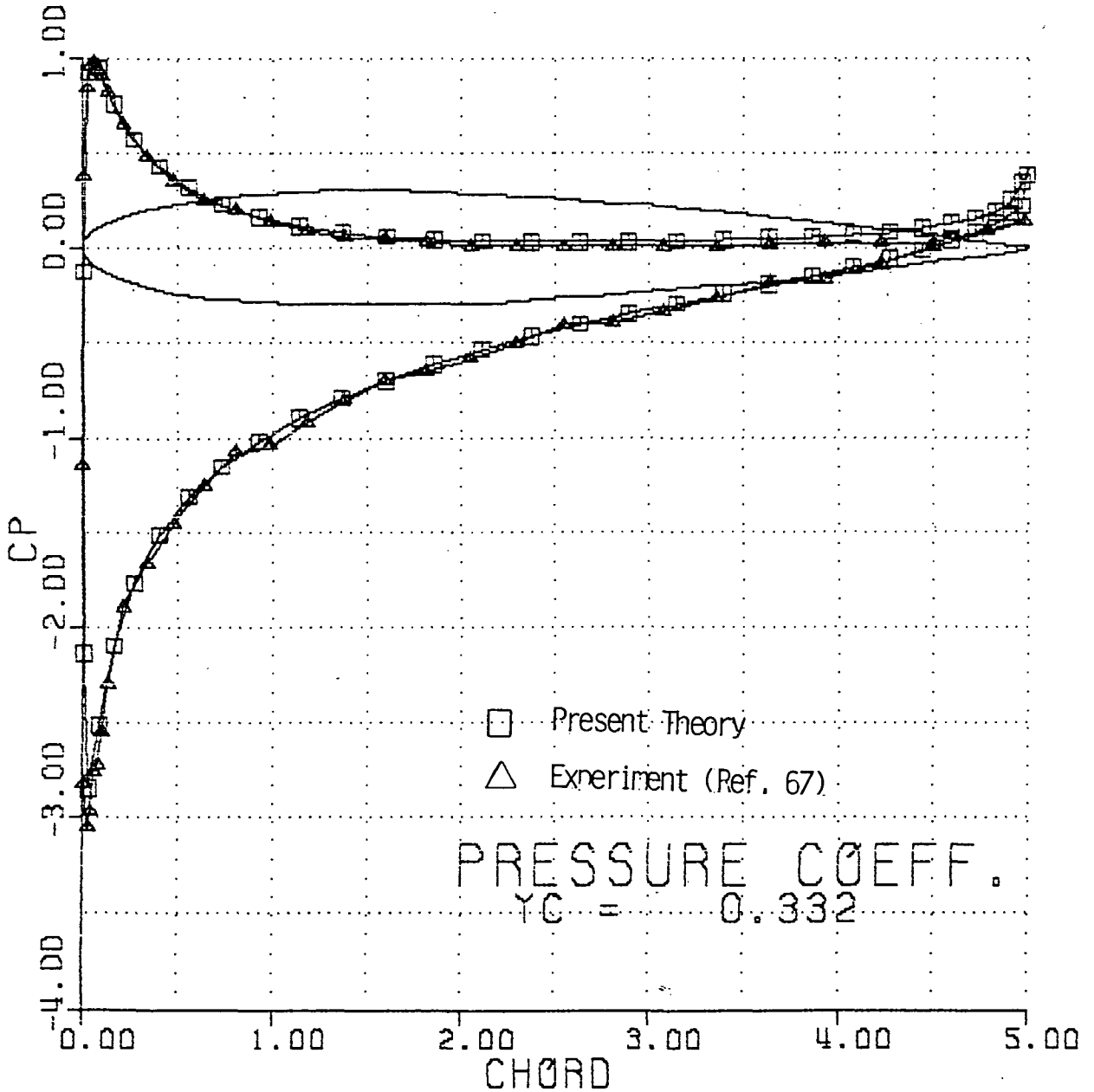

Figure 3-10. Lifting Body Solution of a Rectangular Wing of NACA 0012 at $\eta = 0.332$.

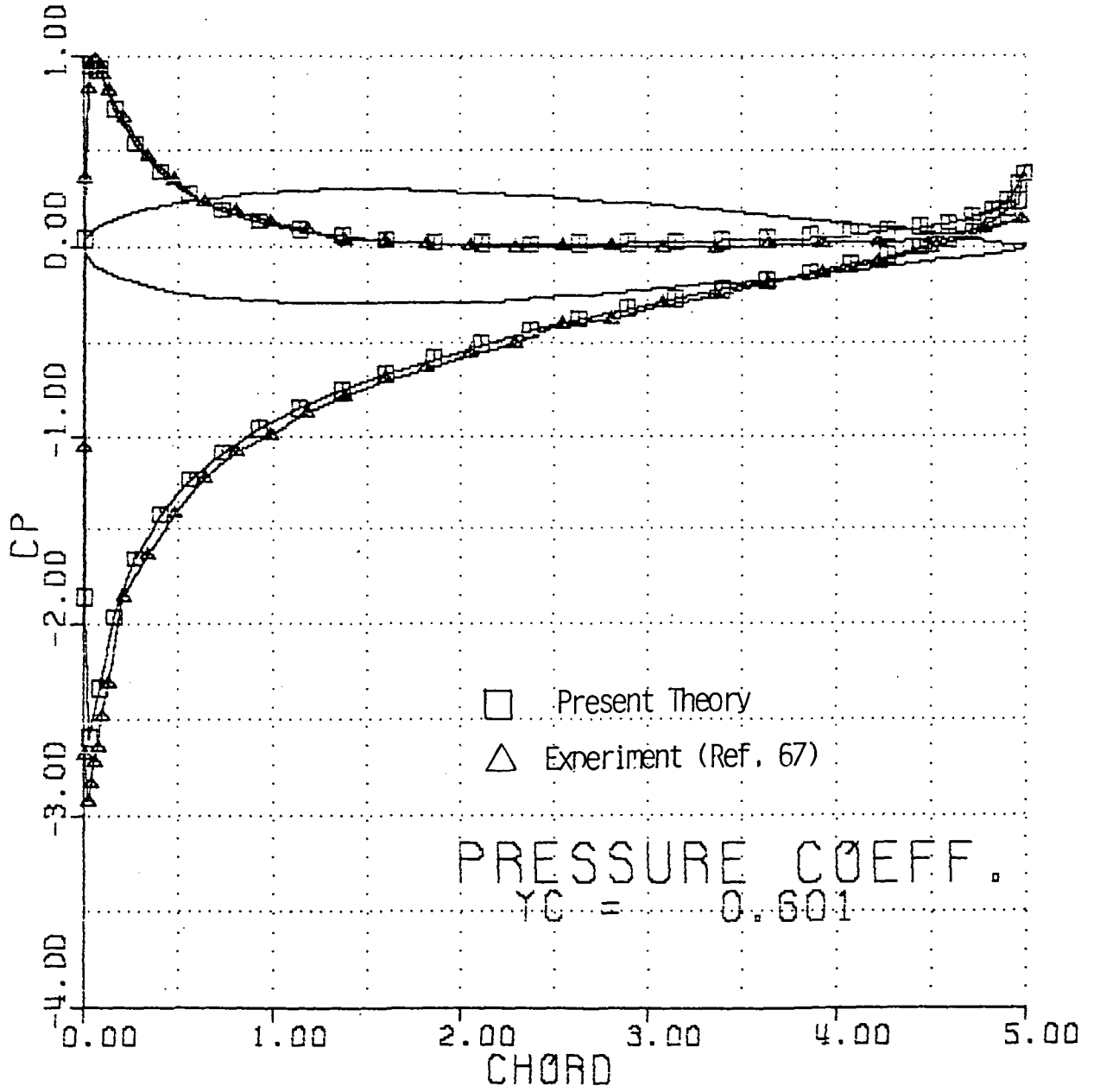

Figure 3-11. Lifting Body Solution of a Rectangular Wing of NACA 0012 at η = 0.601.

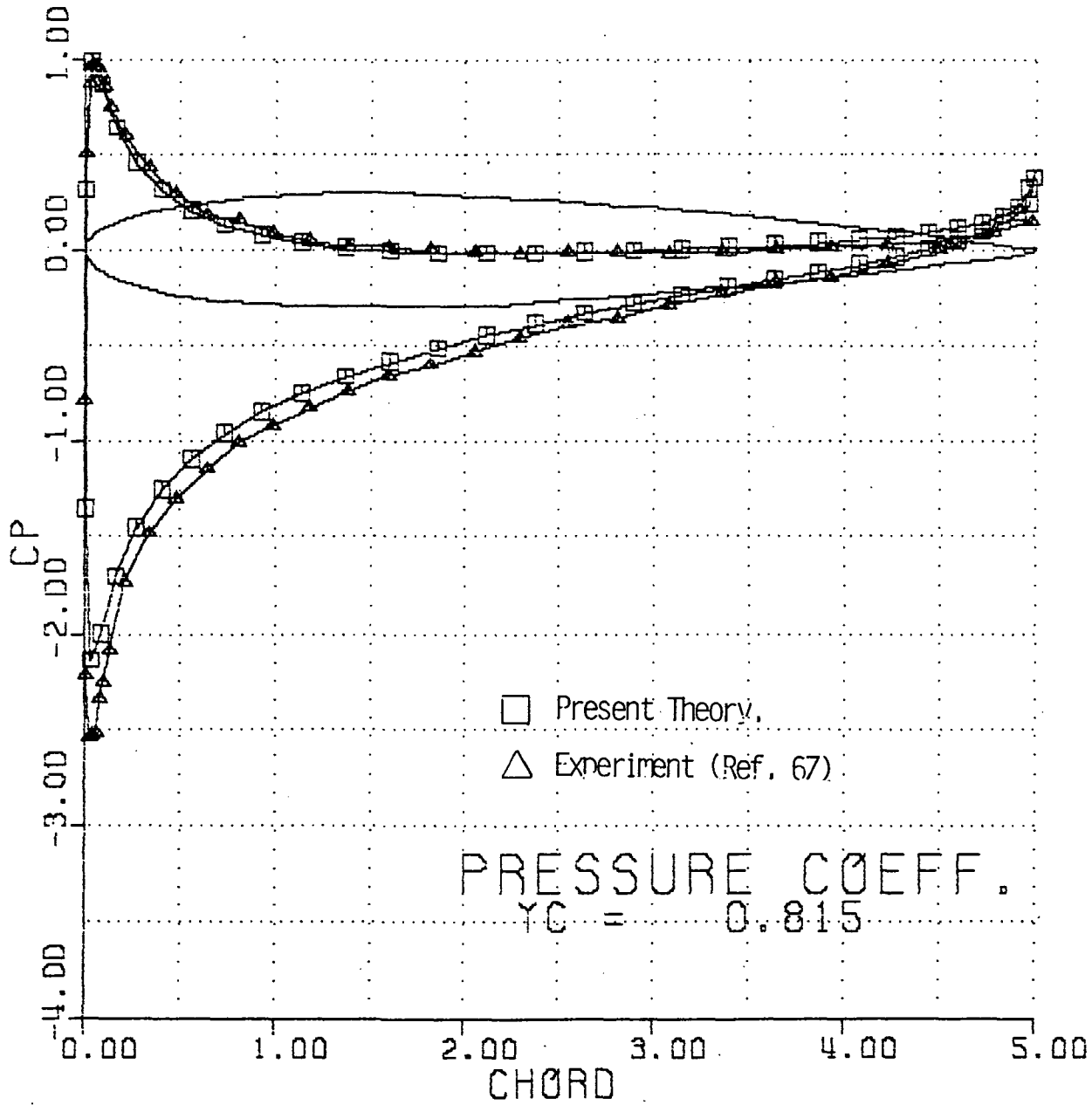

Figure 3-12. Lifting Body Solution of a Rectangular Wing of NACA 0012 at η=0.815.

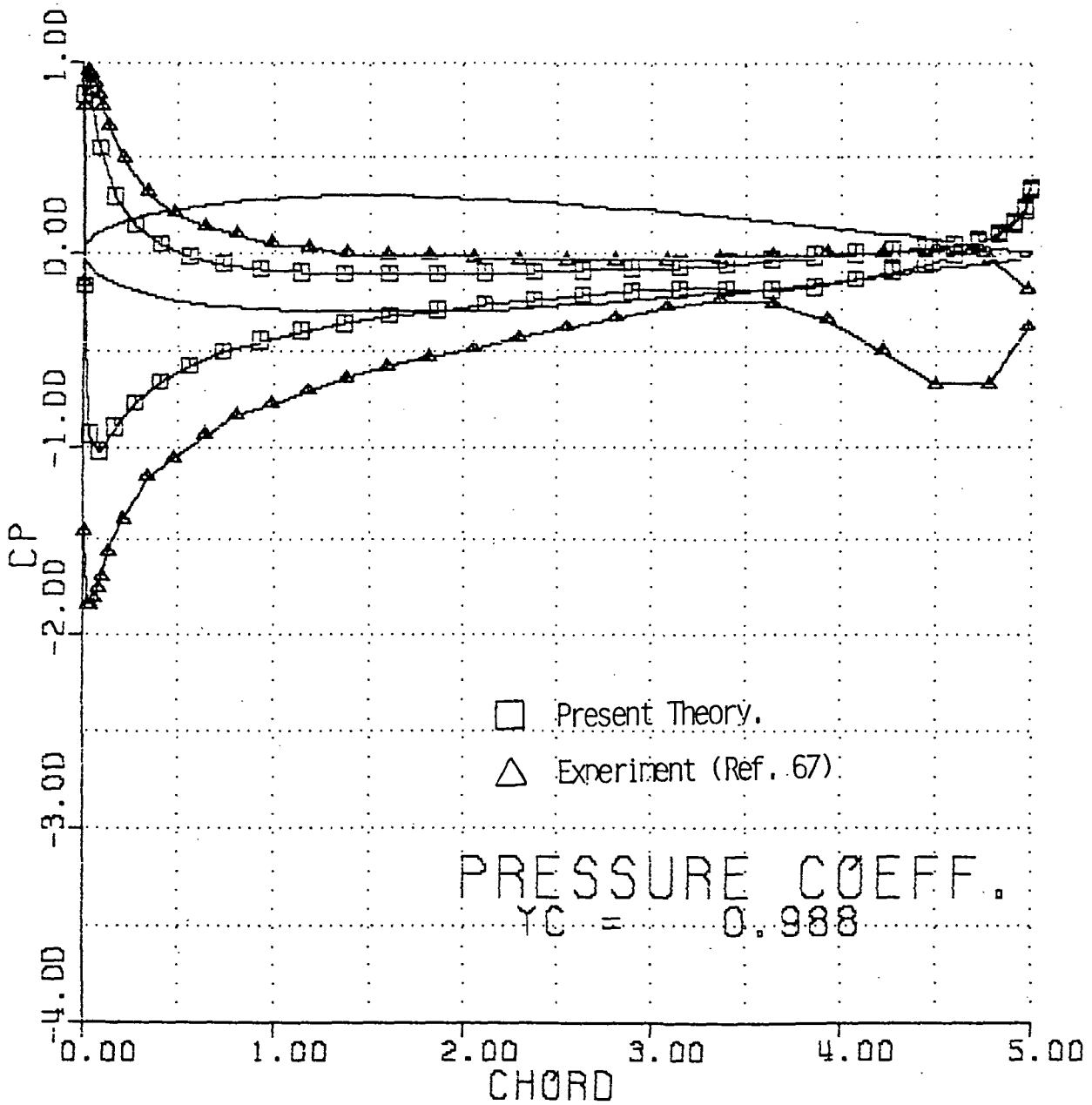

Figure 3-13. Lifting Body Solution of a Rectangular Wing of NACA 0012 at η=0.988.

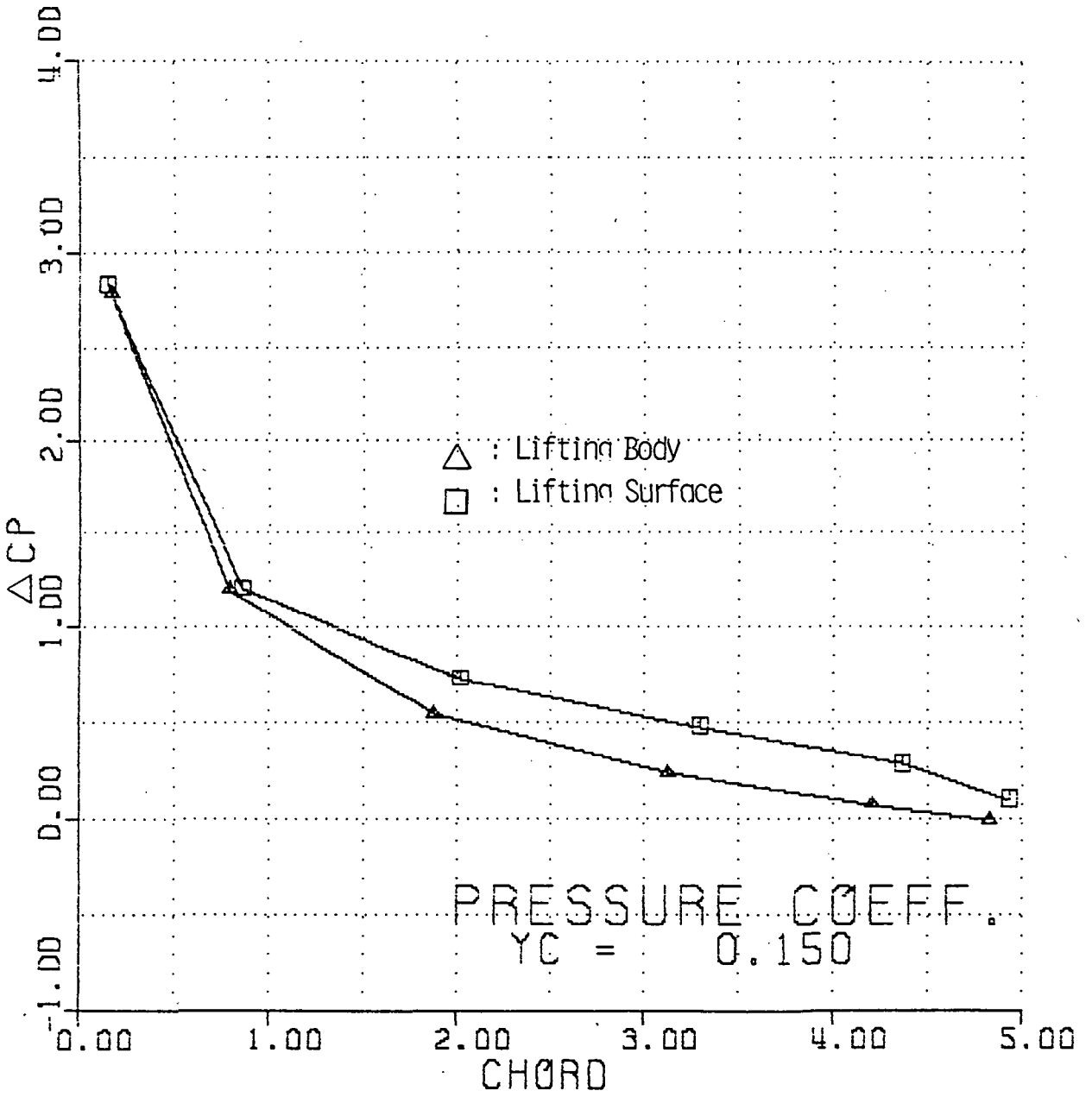

Figure 3-14. Lifting Body and Surface Solution of Rotor of Ref. 68.

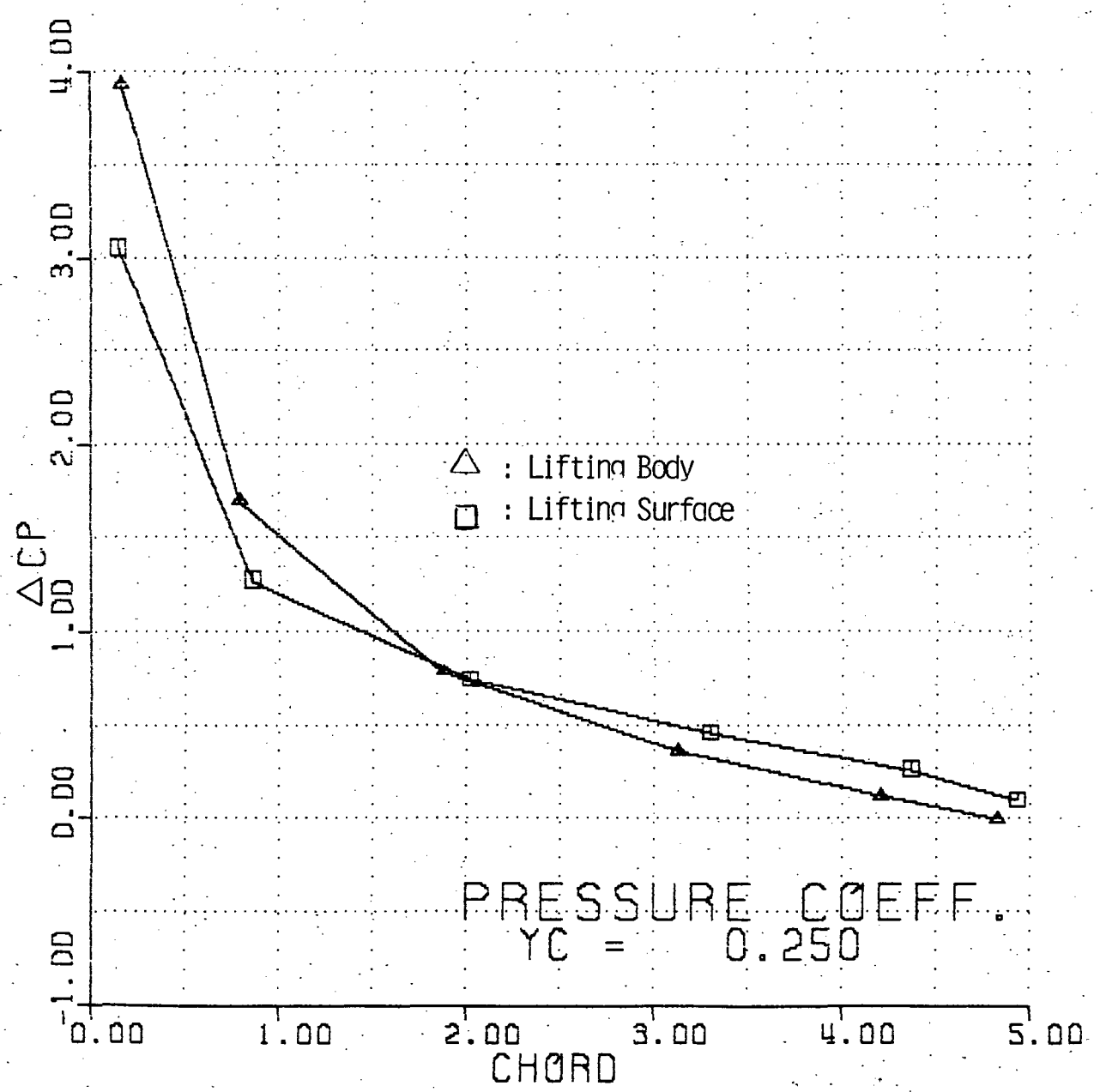

Figure 3-15 Lifting Body and Surface Solution of Rotor of Ref. 68.

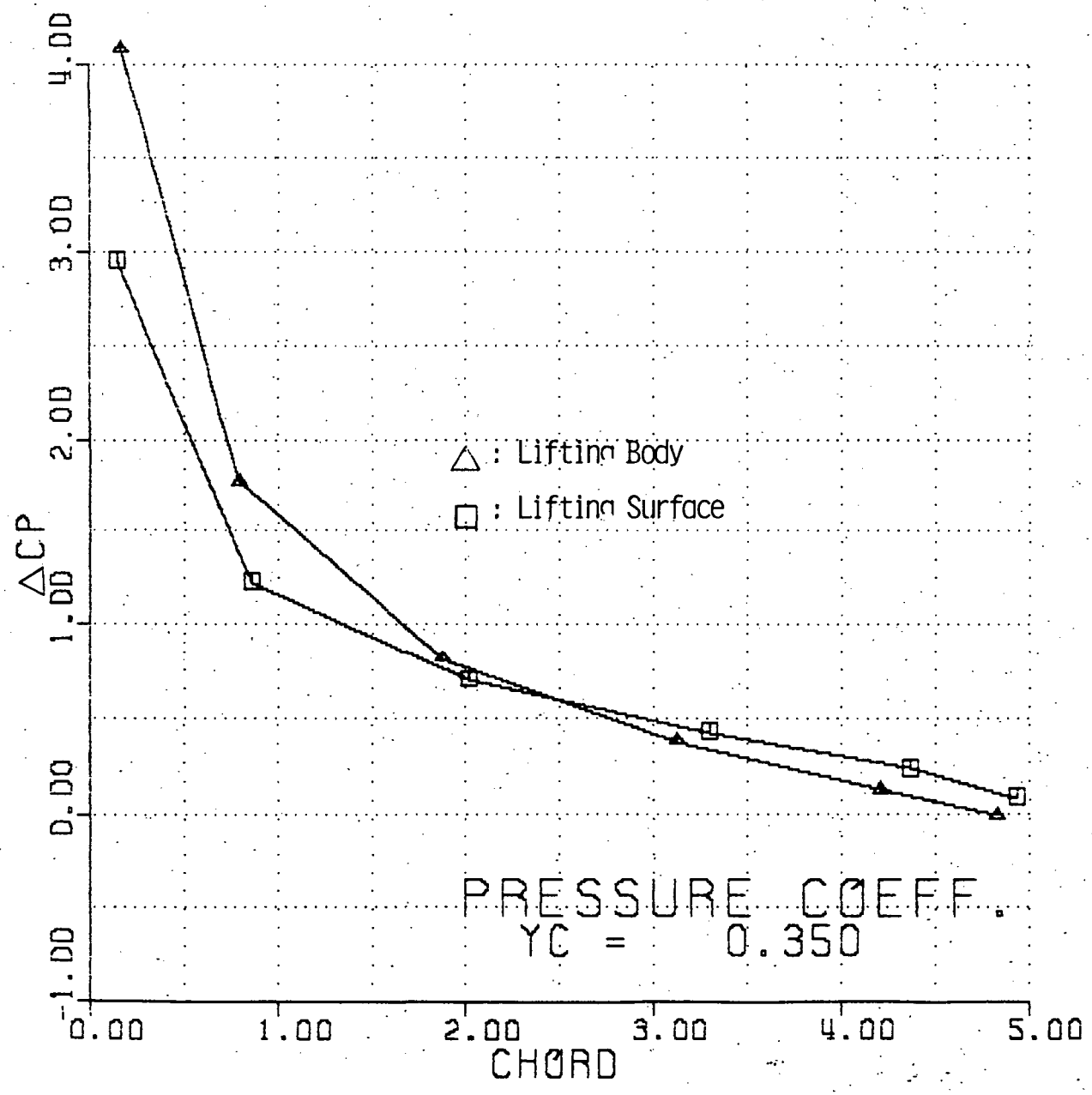

Figure 3-16. Lifting Body and Surface Solution of Rotor of Ref. 68.

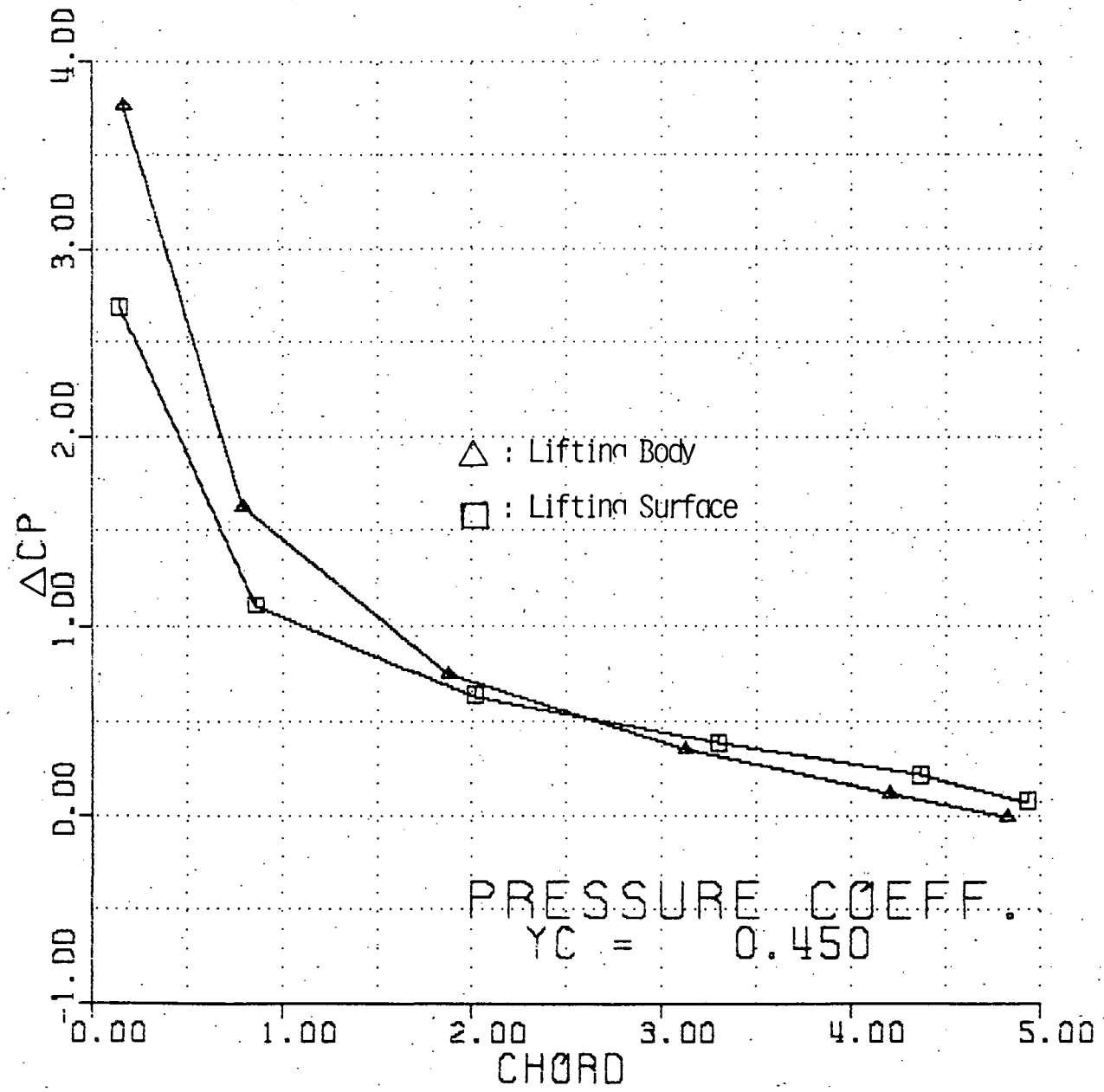

Figure 3-17. Lifting Body and Surface Solution of Rotor of Ref. 68.

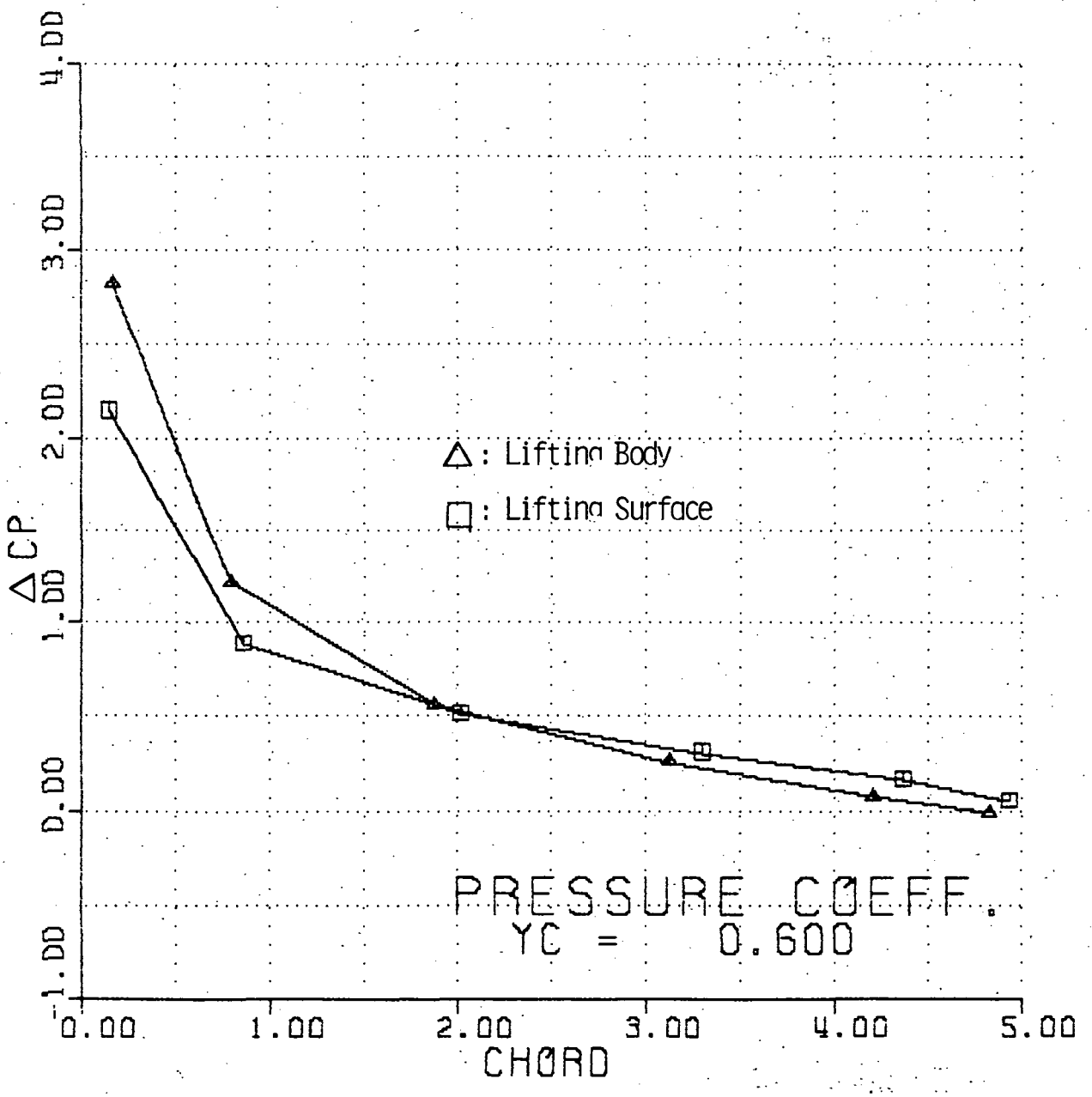

Figure 3-18. Lifting Body and Surface Solution of Rotor of Ref. 68.

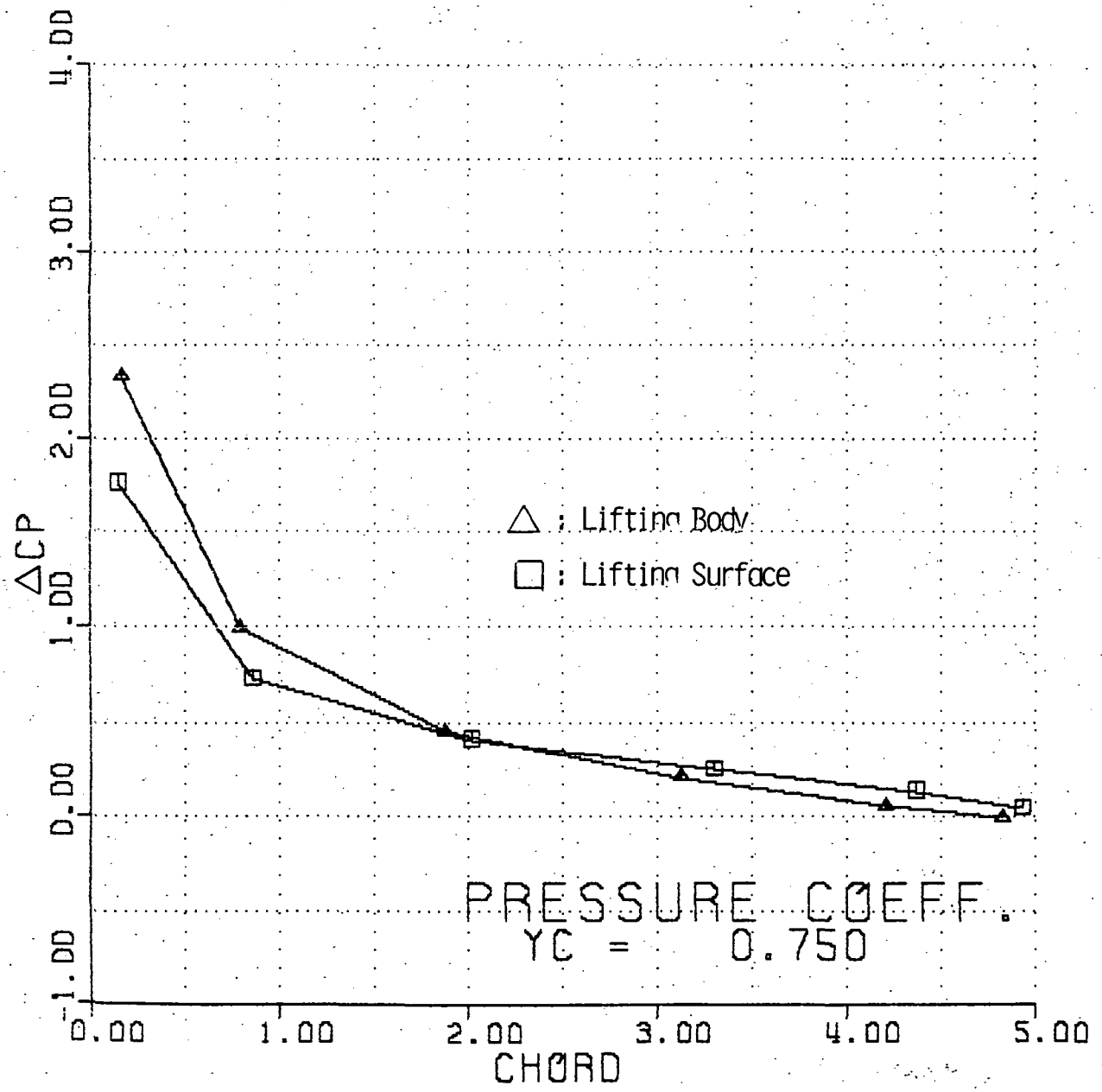

Figure 3-19. Lifting Body and Surface Solution of Rotor of Ref. 68.

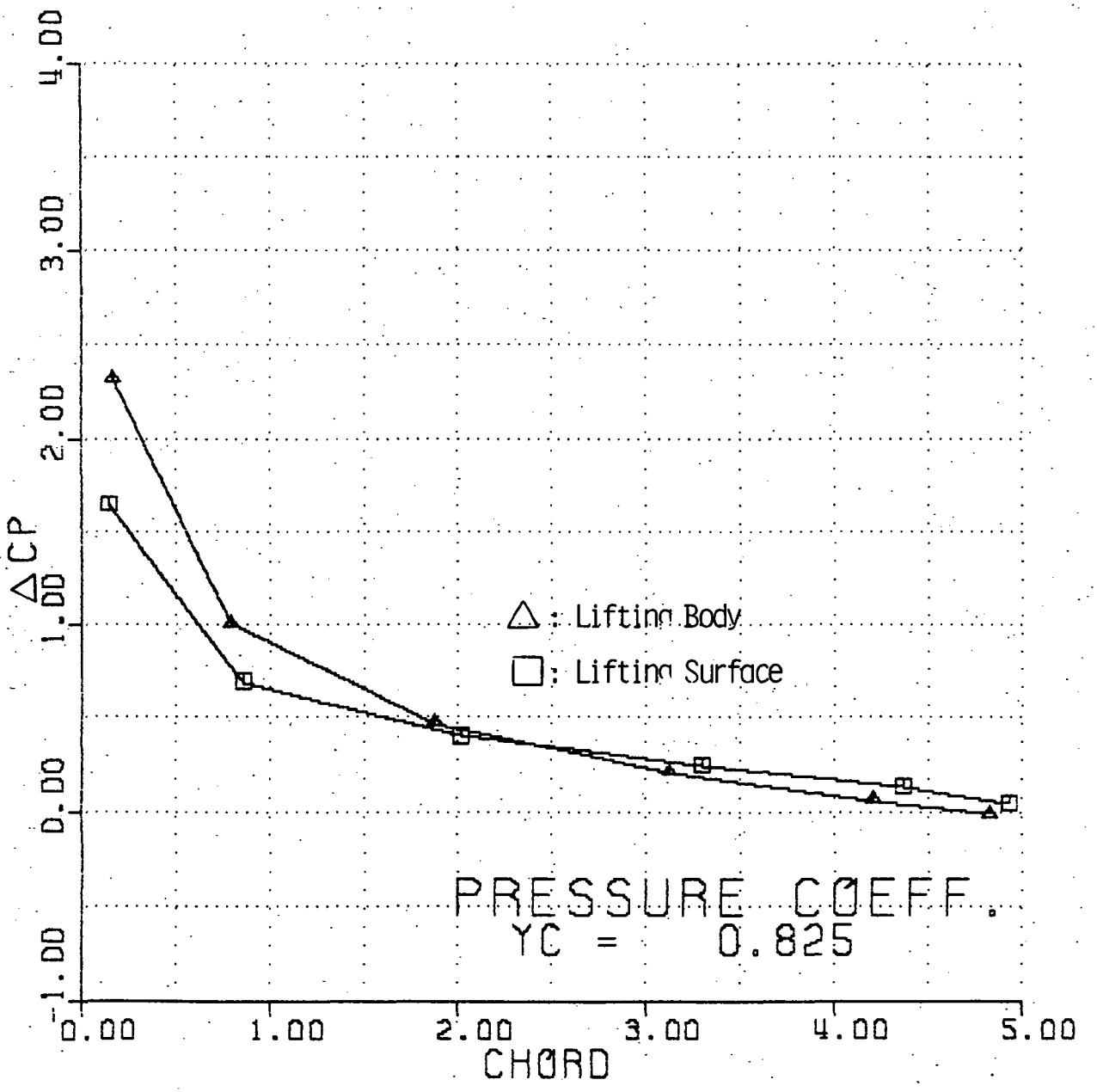

Figure 3-20. Lifting Body and Surface Solution of Rotor of Ref. 68.

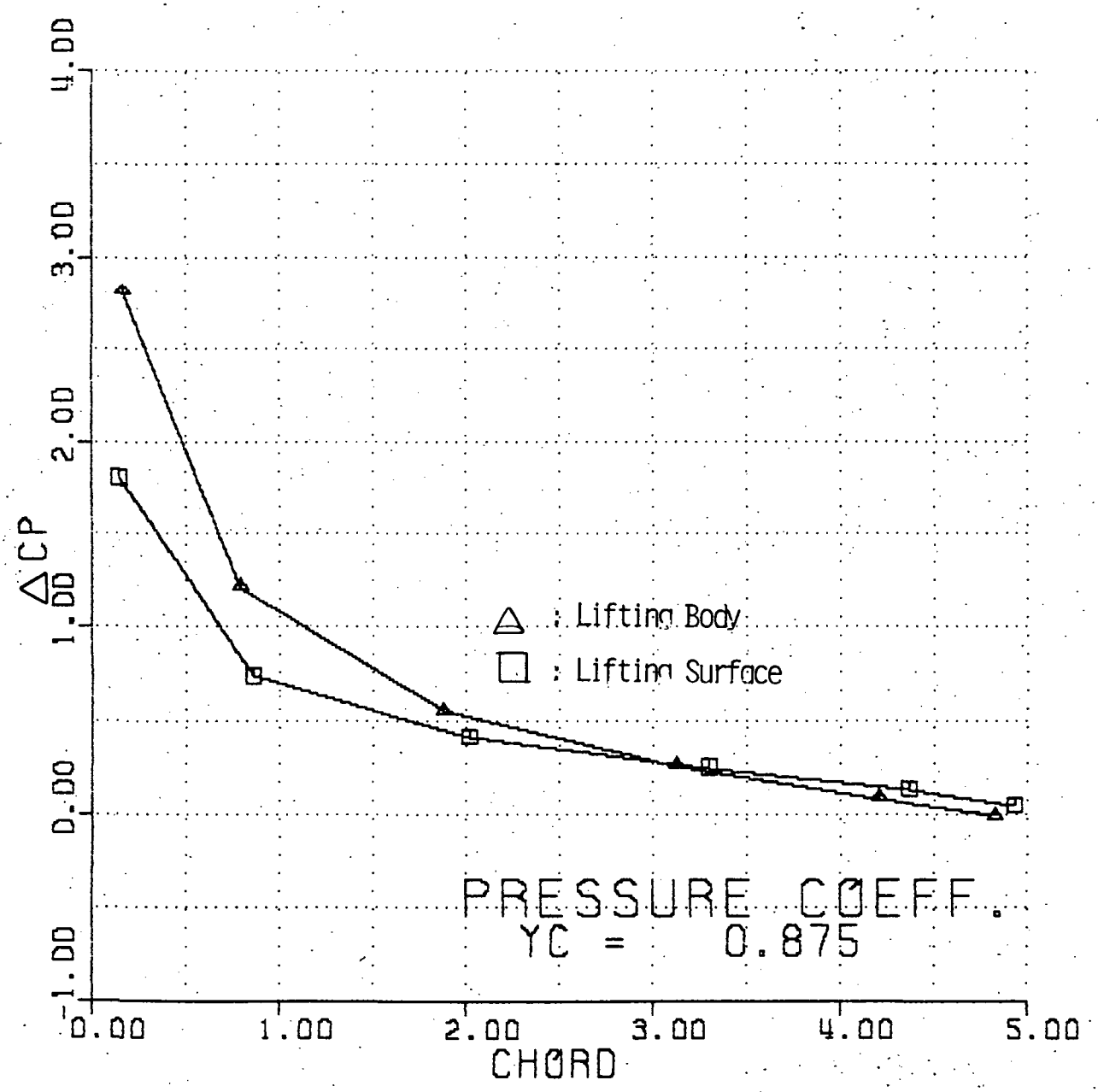

Figure 3-21. Lifting Body and Surface Solution of Rotor of Ref. 68.

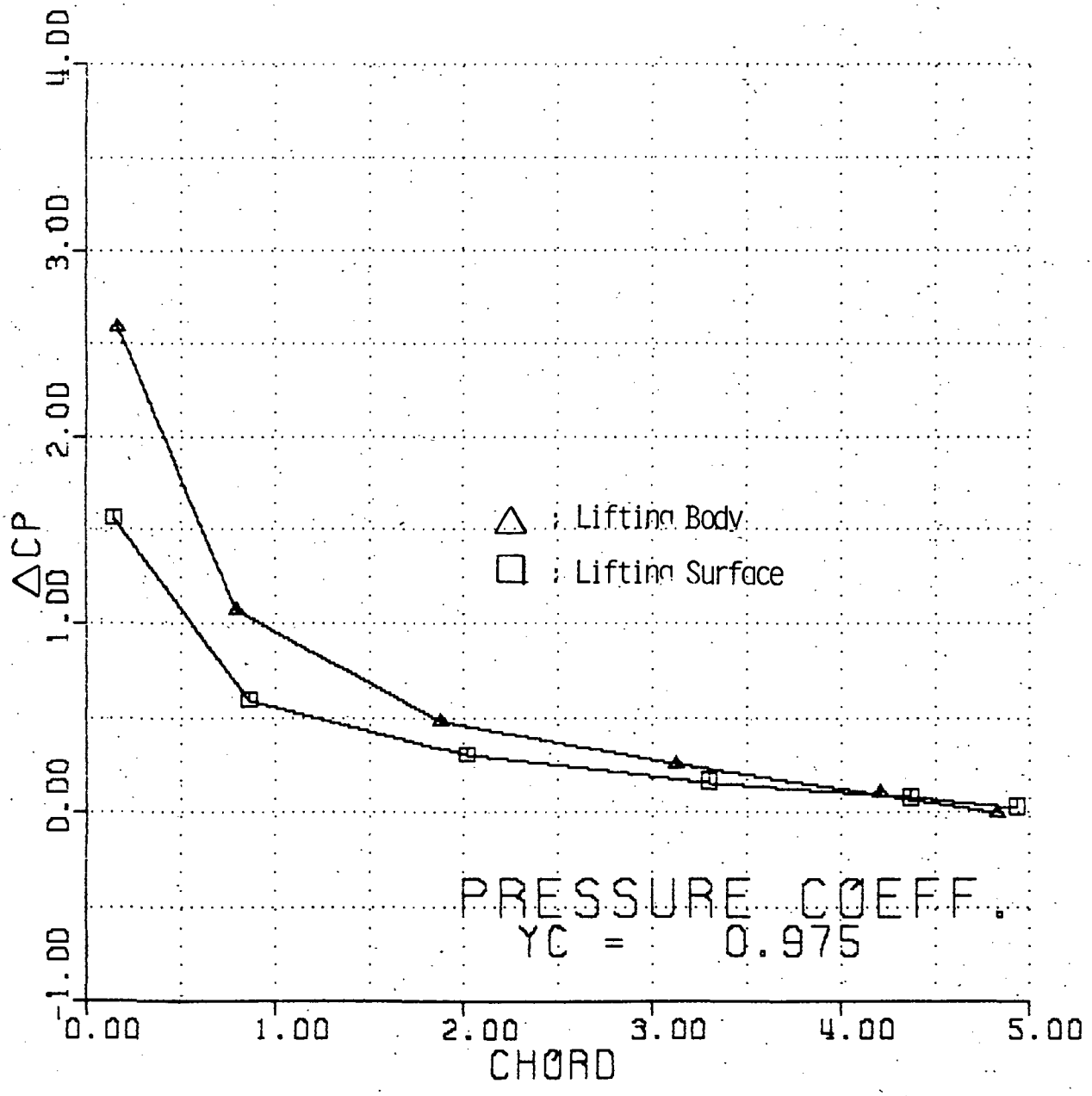

Figure 3-22. Lifting Body and Surface Solution of Rotor of Ref. 68.

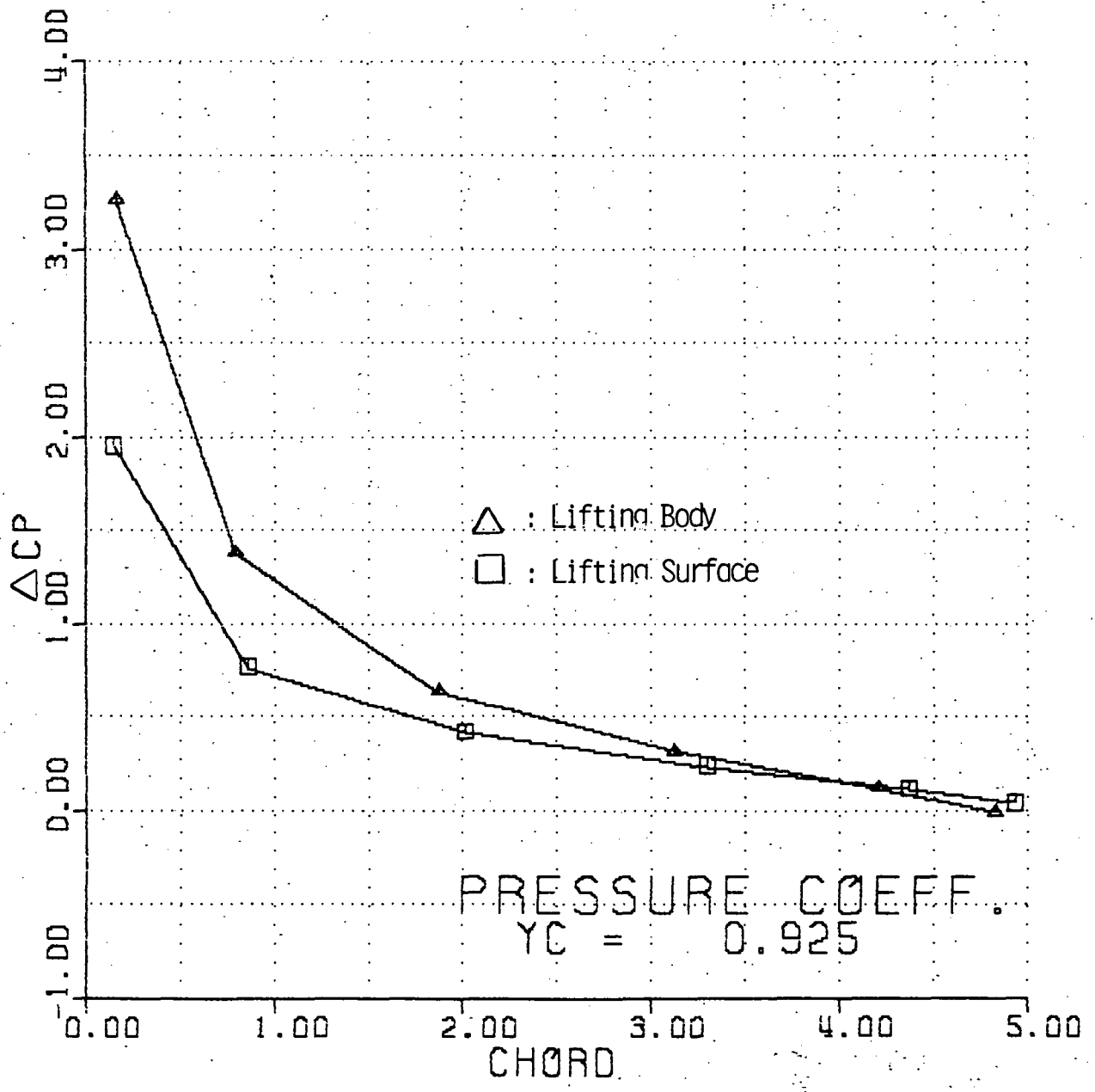

Figure 3-23. Lifting Body and Surface Solution of Rotor of Ref. 68.

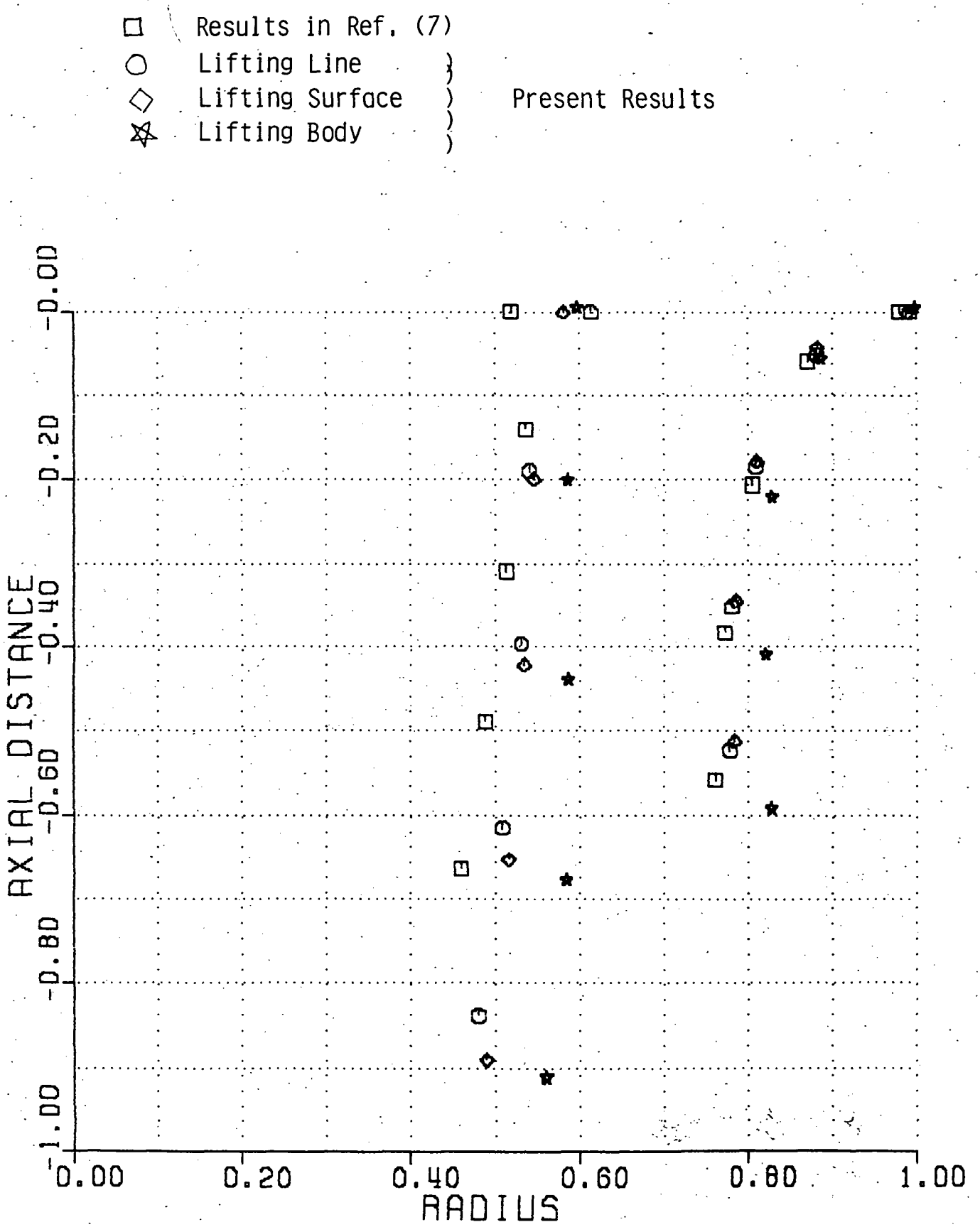

Figure 3-24 Comparison of Free Wake Geometry Calculation Results.

"Page missing from available version"

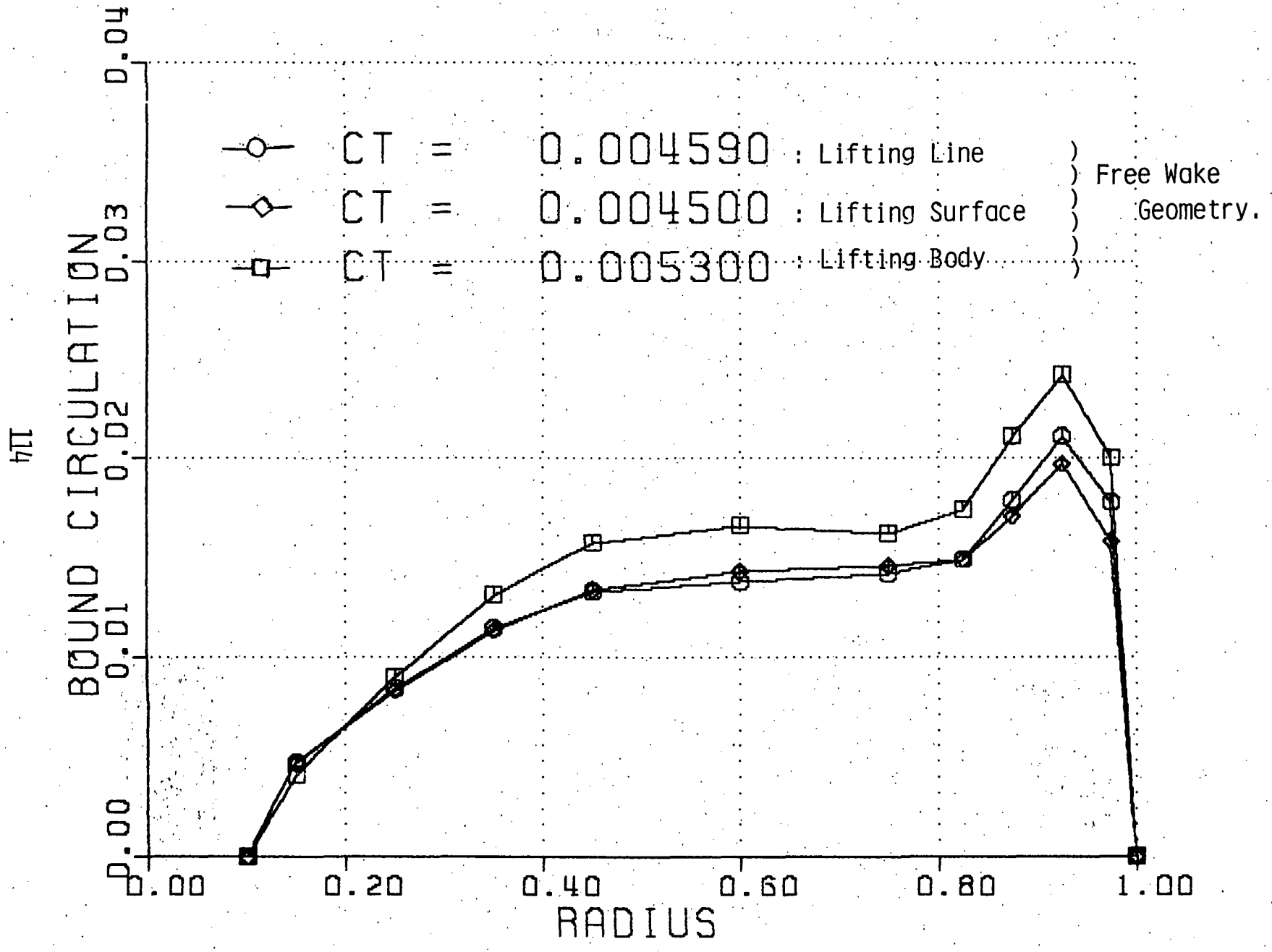

Figure 3-26. Comparisons of Bound Circulations Obtained by Using Free Wake Geometry

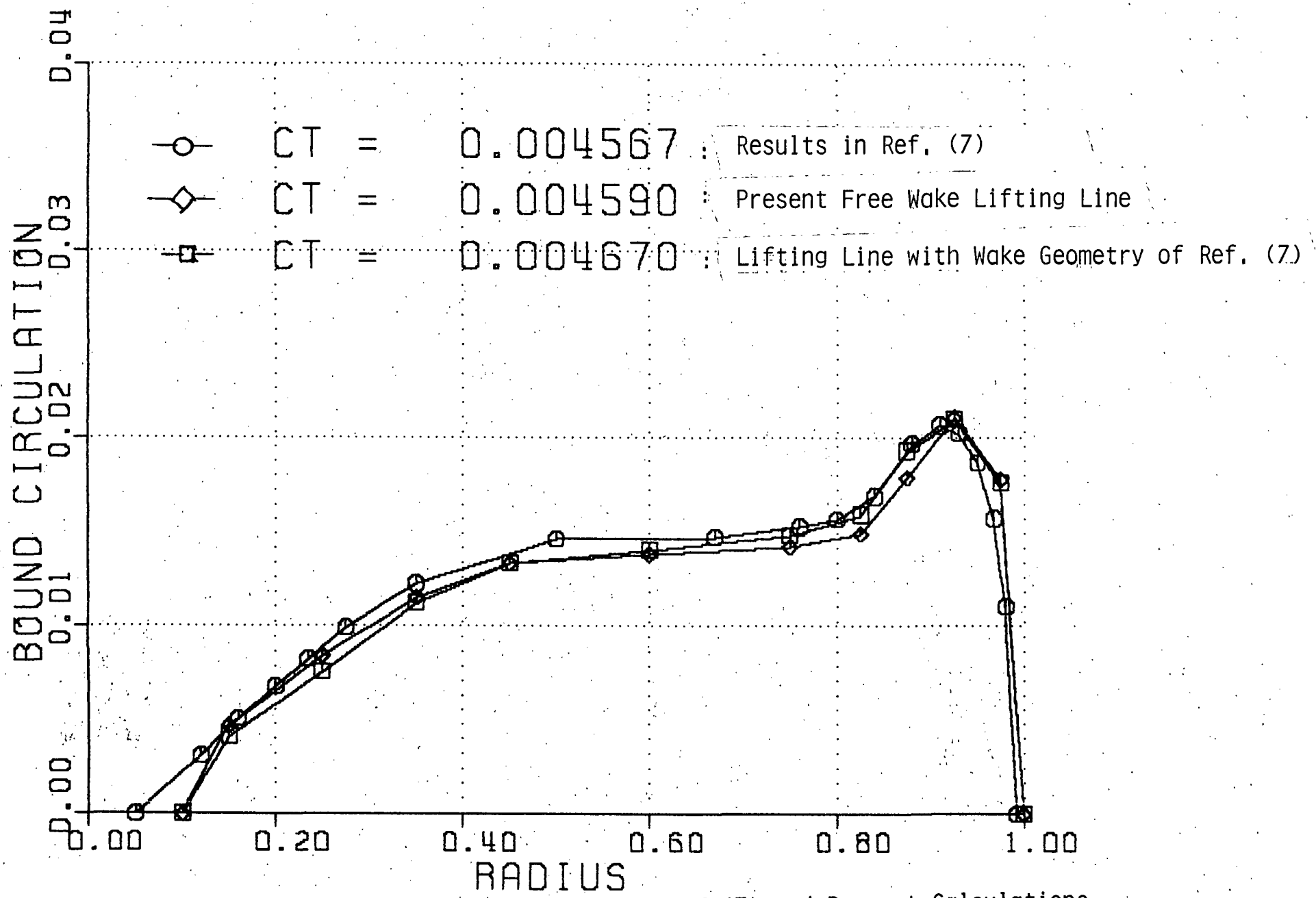

Figure 3-27. Comparisons of Bound Circulations of Ref.(7) and Present Calculations.

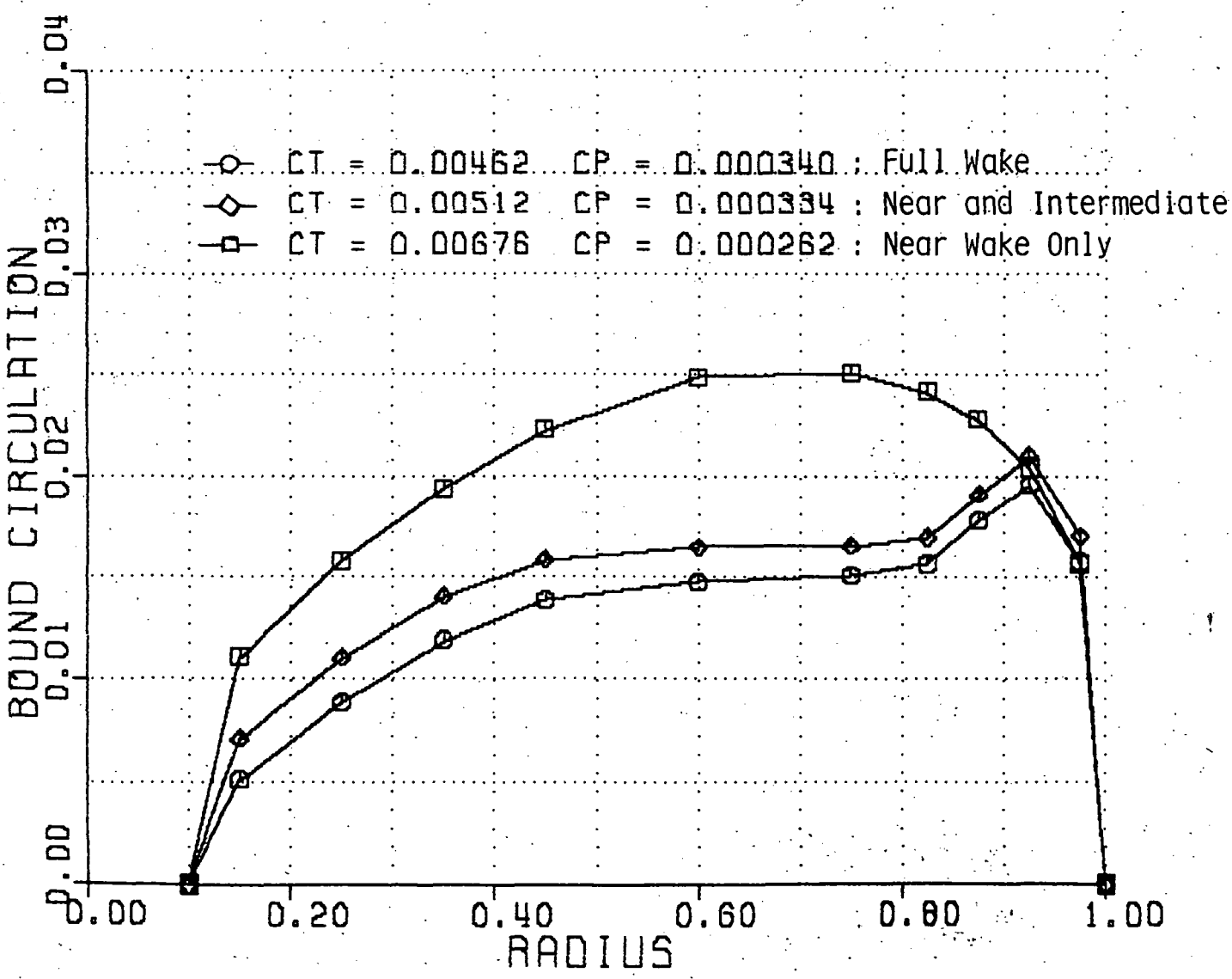

Figure 3-28. Effect of Wake on Bound Circulation.

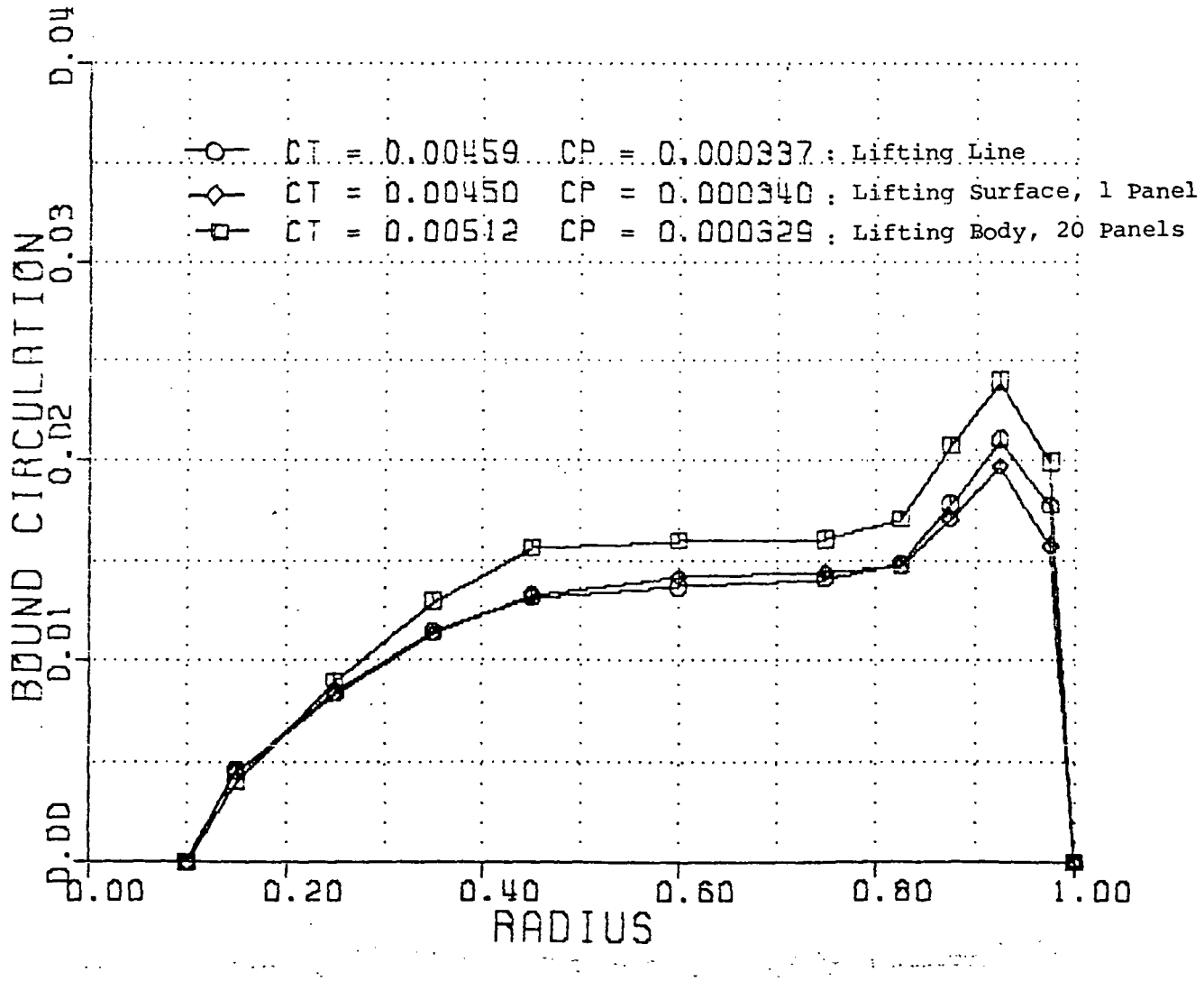

Figure 3-29. Comparisons of Bound Circulations Using Free Wake Geometry

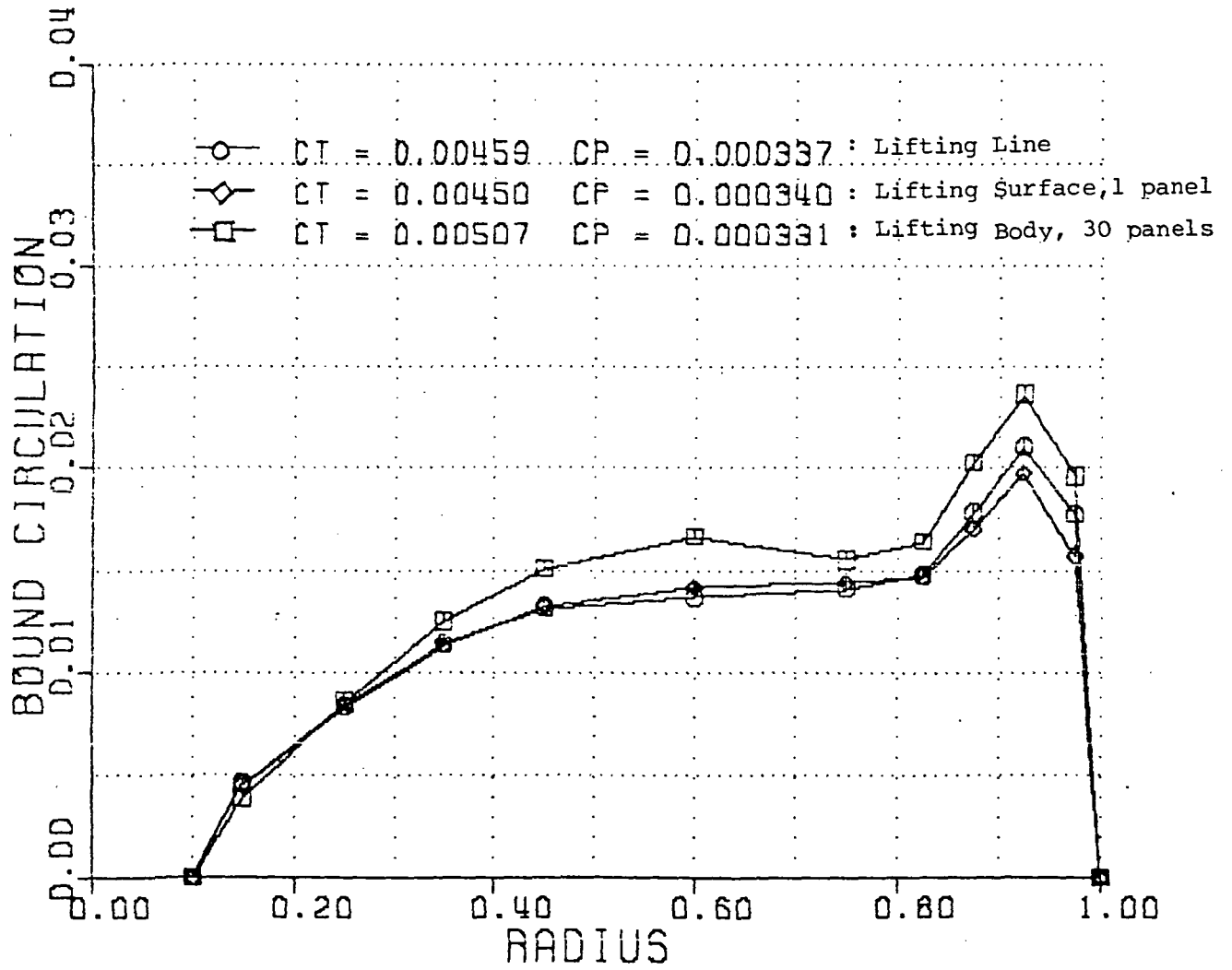

Figure 3-30. Comparisons of Bound Circulations Using Free Wake Geometry

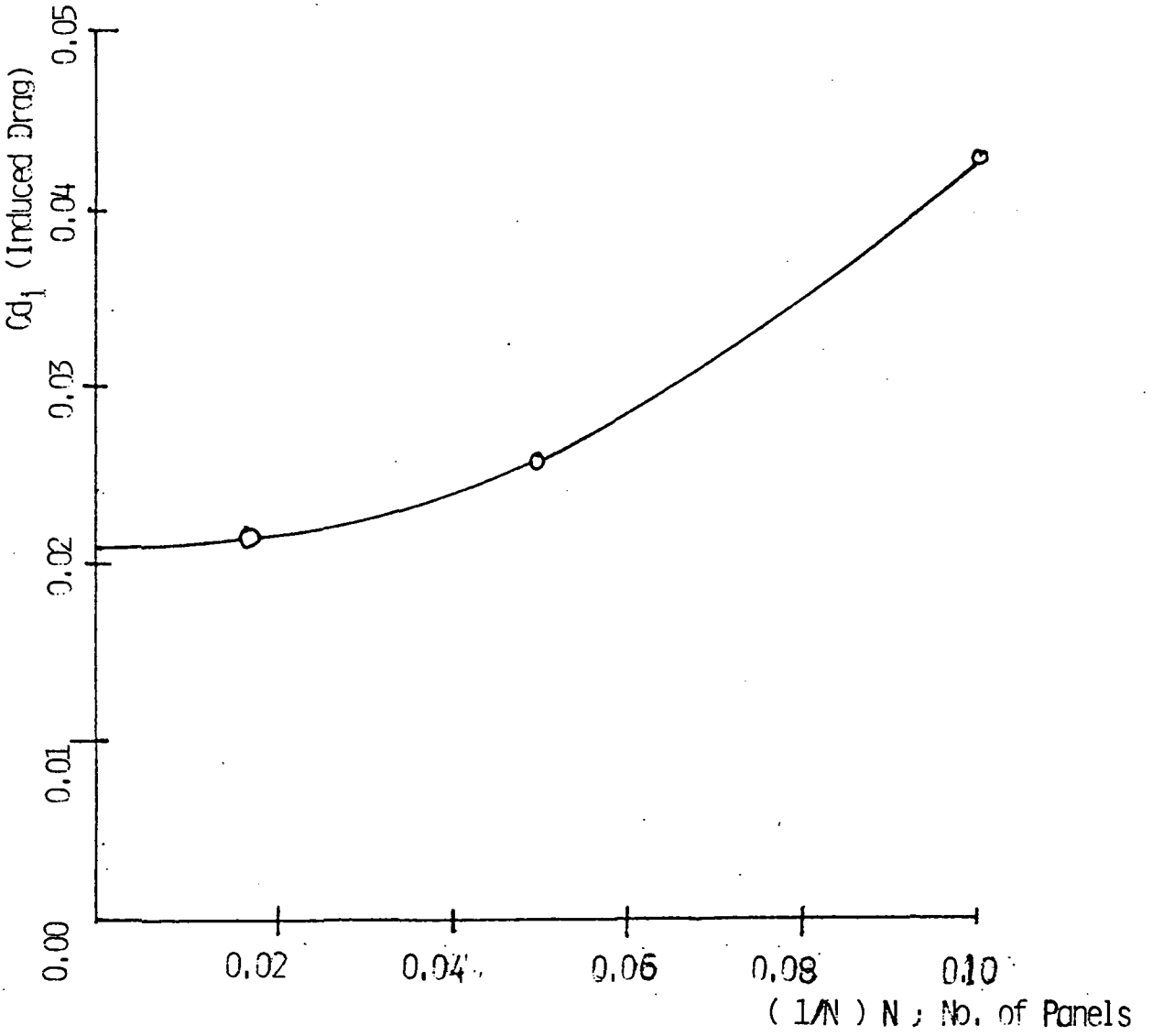

Figure 3-31. Convergence of the Induced Drag Vs No. of Chordwise Panels.

CHAPTER 4
NUMERICAL OPTIMIZATION OF HOVERING PERFORMANCE

In this chapter the review of the papers on the optimization theories and of their applications on the aerodynamic design of rotor blade and wing are presented. Theories on the optimization are formulated and these theories are extended to the numerical solution of nonlinear simultaneous equations in Appendix C. Finally the results of the optimization for hovering rotor blade are discussed.

Liebst,B.S. (ref.37) derived the kinetic energy of wind turbine blade from the coordinate transformation of the inertial coordinate to the blade coordinate to obtain blade velocities during flapping, lagging, and pitching motion. He obtained the full nonlinear blade equation of motion by using Lagrange's equation with the system kinetic and potential energy determined. To obtain the optimum tip section pitch controller he used the penalty integral which was the sum of a quadratic in the state and a quadratic in the control, took the variations of this integral, and equated all coefficients of variations to be zero for the global minimum condition. By implementing the pitch control he decreased the blade bending moments and noise, while

increasing average power output of wind turbine. McCormick, B.W. (ref. 38) computed the optimum bound circulation distribution of several swept propellers by applying the constant pitch condition in the far wake. He found that the swept propeller has a higher bound circulation than the straight propeller for the optimum condition of the constant pitch in the far wake. Chang, L.K. and Sullivan, J.P. (ref. 39) computed the optimum twist of the several propellers of given shape using the penalty function with Davidon-Fletcher-Powell's method for the search direction and with the extended lifting line theory. Ashley (ref, 40) reviewed many papers on aeronautical uses of optimization such as aerodynamics ,structures, and flight trajectory optimizations. He mentioned that the use of aerodynamic optimization was less successful than those of flight trajectory, or structural optimization.

Murman, E.M. and Chapman, G.T.(ref. 41) mentioned how to select the objective function, constraint function, and design variables for aerodynamic design by numerical optimization. They reviewed many papers on aerodynamic optimization and cited the CONMIN optimizating algorithm which was a gradient type constrained minimization algorithm. Vanderplaats. ,et. al. (ref. 42) considered the problem of maximizing the lift with a wave drag constraint at transonic speeds using the combination of

conjugate gradient direction and feasible direction algorithm. Peteers, M.F. (ref. 43) considered the problem of reducing the computation time for the gradient calculation during optimization. He was able to reduce the computation time by reducing the size of the computational domain for aerodynamic analysis during the gradient calculation. He reduced the computation time by using the small disturbance potential solver and the above mentioned method but was not able to do so by the full potential equation solver for aerofoils. Larson, Greg (ref .44) was able to reduce the computation time by restricting the number of aerodynamic analysis iterations per optimization iteration using a full potential equation solver for transonic airfoil design. He used an optimizer QNMDIF developed by Kennelly at NASA Ames which used a quasi-Newton method for the search direction calculation during a function minimization.

Miura, H. (ref. 45) reviewed applications of multivariable search techniques in five categories of helicopter design problems; conceptual and preliminary design, rotor system design, airframe structures design, and flight trajectory planning. Friedmann, P.P. and Shanthakumaran, P. (ref. 46) applied formal optimization technique to vibration reduction of helicopter rotor blades in forward flight. The maximum peak to peak value of the

oscillatory vertical hub shears or the oscillatory hub moment due to blade flapwise bending was used as an objective function. The sequential unconstrained minimization techniques, based on extended interior penalty function and a modified Newton method, was used. They found that the modification of section properties near blade tip and the addition of nonstructural mass at the elastic axis resulted in considerable reduction of vibratory hub loads and blade mass, compared to the blade of uniform properties. Walsh, J.L., et. al. (ref. 47) applied a formal optimization for helicopter rotor blade design using momentum theory for the hover analysis and rotorcraft flight simulation computer program, C-81, for forward flight analysis. They combined the analysis programs with CONMIN optimizer program of ref. (53). The objective function was the required horsepower for the hover and the constraints were the drag coefficients and horsepower required during forward flight and pull-up maneuver. They were able to obtain the rotor geometry which had the performance as good as that of heuristic design with ten times shorter time than the heuristic design. For AH-64 rotor the hover horsepower was governed by the horsepower required for forward flight. For UH-1 helicopter the hover horsepower with the given design gross weight was governed by the drag coefficients for the forward flight and the pull-up maneuver. In both

designs the rotor had 290 RPM with the blade radius of 24 feet for AH-64 and 324 RPM with the blade radius of 24 feet for UH-1. Consentino, G.B. and Holst, T.L. (ref. 48) combined a transonic wing flow analysis program with a quasi-Newton unconstrained optimization algorithm, QNMDIF, for the numerical optimization of transonic wing configurations. The lift to drag was increased by 27.64 % for Lockheed C-141B wing and by 85.72 % for Cessna model 650 wing by changing the upper surface wing geometry. At each spanwise sections of the wing there were three or four movable points with all the rest of the points fixed. Cubic splines were used through immovable and movable points. The vertical positions of the movable points at three spanwise stations became twelve or nine design variables.

Broyden, C.G. (ref. 49) defined Quasi-Newton method as methods in which the search direction for minimization approaches to the direction of Newton method as the minimum of the function is approached. He proposed several Quasi-Newton methods which are exact if the Hessian matrix is symmetric and nonsingular. Fletcher, R. and Reeves, C.M. (ref. 50) proposed quadratically convergent method which used only the gradient vectors for the search direction in contrast to Quasi-Newton method which used the approximation for the inverse of Hessian matrix at each search direction calculation. Fletcher, R. and Powell,

M.J.D. (ref. 51) gave the search direction vector which was quadratically convergent and approached Newton's method near the minimum. He used cubic interpolation given by Davidon to obtain a minimum along the search line. Topping, B.H.V. and Robinson, D.J. (ref. 54) gave brief descriptions of three mathematical programing methods for nonlinear optimization techniques. These are sequential linear programing (SLP), feasible direction method (FDM), and sequential unconstrained minimization technique (SUMT). They applied the above three techniques to the minimization of portal frame weight and found that FDM was the most inefficient technique.

4.1 Objective Function Formulation And Design Variables

Hovering performance of helicopter rotor can be measured by the thrust produced from unit horsepower, that is, T/P. Then,

$$\frac{T}{P} = \frac{C_T}{C_P \, \Omega R}$$

Hence, the objective function, F , to be minimized can be set

$$F = -\frac{C_T}{C_P} \quad \text{or} \quad F = \frac{C_P}{C_T}$$

When $F = C_P / C_T$ is used, the optimization code produces the result of negative thrust, that is, downward thrust for some design variables. When $F = - C_T / C_P$ is used, the optimizer produces the result of zero power coefficient, that is, zero disk loading. In both cases, if the design variables are two tip pitch angles and two tip chords or five tip pitch angles which were the cases run here, the optimizer produces the minimum of the objective function, F, with respect to design variables.

When design variables are chosen to give the overall minimum of F, the negative thrust, or, the zero disk loading is obtained by the optimizer, depending on F. Hence, the constraint on the thrust coefficient is needed. With the nonlinear constraint of fixed thrust coefficient the problem becomes the constrained optimization. The problem can be stated as follows.

Find the minimum of $F(X_i)$

,where X_i , i =1, $\cdots$ N ; design variables

$X_{i\ell} < X_i < X_{iu}$; side constraints

and $h_k(X_i) = 0$; k nonlinear equality constraints.

The constrained optimization can be converted into a unconstrained optimization using the penalty function method. The ordinary quadratic penalty function $P(X_i)$ is given by

$$P(X_i) = r_p \sum_{k=1}^{\ell} [h_k(X_i)]^2$$

Then a new objective function, $\Phi(X_i)$, is

$$\Phi(X_i) = F(X_i) + P(X_i)$$

$$\Phi(X_i, r_p) = C_P/C_T + r_p (C_{TT} - C_T)^2$$

,where C_{TT} is the given thrust coefficient, C_T is the current thrust coefficient, and r_p is the penalty parameter. r_p is determined by the requirement that $F(X_i)$ and $P(X_i)$ should be the same order of magnitude. For example, if C_p/C_T is $0(10^{-1})$ and $(C_{TT} - C_T)$ is $0(10^{-3})$, then r_p is $0(10^5)$.

The various formulations of the penalty function are given in Ref.(52). If we use a small penalty parameter, C_P/C_T is minimized while the equality constraint of $C_T = C_{TT}$ is violated. If we use a large penalty parameter,

C_P / C_T goes to a suboptimal value while the constraint is satisfied. Hence, we vary r_p during the optimization from a small value to a large value. With the variable penalty parameter this approach is called the sequential unconstrained minimization technique (SUMT). During the initial run of the optimizing program r_p is fixed, that is, $r_p = r_0 = 10000.$ or $100000.$ Then, r_p is varied, that is, $r_{p+1} = \gamma\, r_p$ and $\gamma = 1.3$ where p is the iteration count.

The first category of design variables considered are pitch angle ,or chord width, or both at each spanwise station. With ten divisions of the blade span there are ten pitch angles as design variables for the given chord or ten chord widths as design variables for the given pitch distribution. From the tip section to any specified station of the blade, pitch angles and chord widths are design variables.

(1) $X_i = C_i$ for $i = 1, \cdots, N$

(2) $X_i = \theta_i$ for $i = 1, \cdots, N$

(3) $X_i = C_i$ for $i = 1, \cdots, N/2$

$X_i = \theta_i$ for $i = N/2 + 1, \cdots, N$

For a second category of design variables a double twisted and tapered blade was chosen for the optimization with 5 design variables. For this blade the initial blade geometry is as follows.

(4) $X_1 = \Delta\theta_1 = 0.25$; root twist.

$X_2 = \Delta\theta_2 = 0.15$; tip twist.

$X_3 = \eta_{twist} = 0.75$; position of taper and double twist.

$X_4 = C_{root} = 0.0729$; root chord.

$X_5 = C_{tip} / C_{root} = 0.3$; taper ratio.

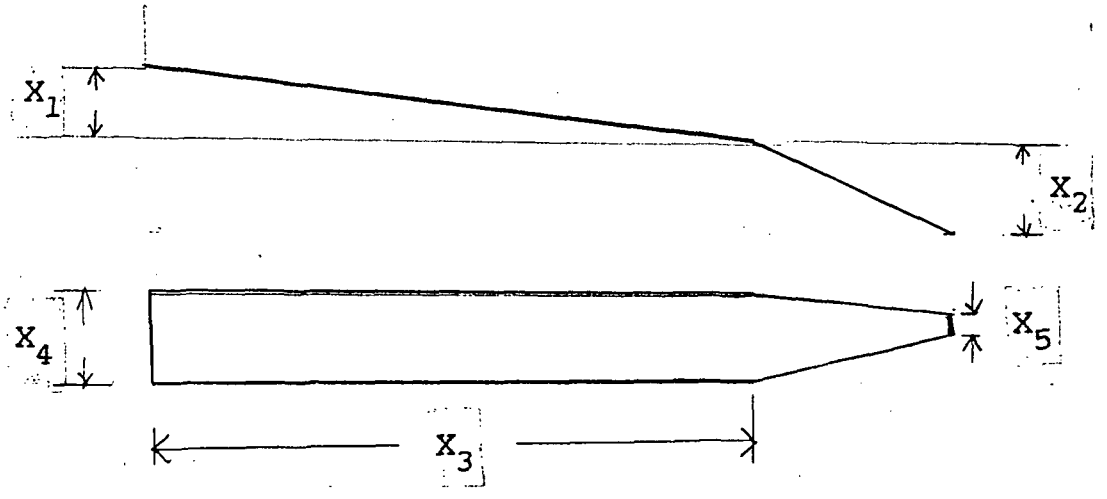

Definition of Design Variables for Category 2

Then the blade pitch and chord distribution of the second try are obtained as follows.

For $\eta \leq X_3$, $C = X_4$

$$\theta = X_2 + \frac{(X_3 - \eta)}{X_3} X_1$$

For $\eta > X_3$, $C = X_4 \left\{ X_5 + \frac{1 - \eta}{1 - X_3} (1 - X_5) \right\}$

$$\theta = \frac{(1 - \eta)}{(1 - X_3)} X_2$$

The side constraints are

$$X_1, X_2, X_4, X_5 > 0 \text{ and } 1.0 > X_3 > 0.1$$

Here C and θ are each the chord and the pitch angles and η is the normalized radius.

Then, for a third design problem, three set of design variables are used with the initial geometry of rotor of Ref.(68). First the collective pitch and the straight twist are used as design variables. Second the collective pitch, straight twist, taper ratio, and the position of the taper are used as four design variables. Third the collective pitch, tip twist, root twist, taper ratio, and the position of taper and double twist are used as five design variables. These are summarized as follows.

(5) $X_1 = \theta$; collective pitch.

$X_2 = \Delta\theta$; straight twist.

(6) $X_1 = \theta$; collective pitch.

$X_2 = \Delta\theta$; straight twist.

$X_3 = \eta_{taper}$; position of taper.

$X_4 = C_{tip} / C_{root}$; taper ratio.

(7) $X_1 = \theta$; collective pitch.

$X_2 = \Delta\theta_1$; tip twist.

$X_3 = \eta_{taper}$; position of taper and twist.

$X_4 = \Delta\theta_2$; root twist.

$X_5 = C_{tip}/C_{root}$; taper ratio.

(8) X_1 to X_5 are the same as the case (7).

X_6 = root chord

The side constraints are same as the case (4).

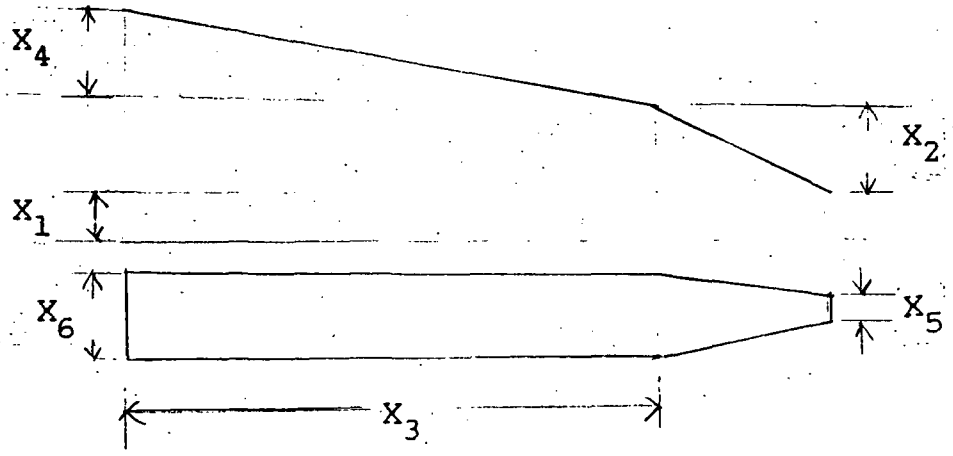

Definition of Design Variables for Category 3

4.2 Search Direction Calculation Using Quasi Newton or Conjugate Gradient Method

The search direction vector of a quasi-Newton method is given in Ref.(49). We define A as a Hessian matrix of the objective function F. Then A is given as follows.

$$A = \begin{bmatrix} \frac{\partial^2 F}{\partial X_1 \partial X_1} & \frac{\partial^2 F}{\partial X_1 \partial X_2} & \cdots & \frac{\partial^2 F}{\partial X_1 \partial X_N} \\ \vdots & \ddots & & \vdots \\ \frac{\partial^2 F}{\partial X_N \partial X_1} & \cdots & & \frac{\partial^2 F}{\partial X_N \partial X_N} \end{bmatrix}$$

We define G as the gradient vector of the objective function and S as the search direction vector for the minimization.

$$S = - A^{-1} G \quad ; \text{ Newton method.}$$

But A^{-1} is approximated in the quasi-Newton method as H and is given in Ref. (51) as follows. In the following P is the iteration count.

$$S = - A^{-1} G \cong - H G$$

$$H^{p+1} = H^p + A^p + B^p$$

,where $$A^p = \frac{|\sigma^p\rangle\langle\sigma^p|}{\langle\sigma^p|y^p\rangle}$$

$$,B^p = \frac{-H^p|y^p\rangle\langle y^p|H^p}{\langle y^p|H^p|y^p\rangle}$$

$$|\sigma^p\rangle = |X^{p+1}\rangle - |X^p\rangle = \alpha^p |S^p\rangle$$

and $|y^p\rangle = |G^{p+1}\rangle - |G^p\rangle$

$|\sigma^p\rangle$ is a vector while $\langle\sigma^p|$ is the transpose of $|\sigma^p\rangle$.

QNMDIF ,which is used for the optimization, is a parameter optimizing program with complementary Davidon-Fletcher-Powell update. The updating formulas are given for the approximated Hessian matrix or for the inverse of the Hessian matrix in Ref. (44). The method of conjugate gradients is given in Ref. (50) as follows.

$$S^{p+1} = -G^{p+1} + \frac{|G^{p+1}|^2}{|G^p|^2} S^p$$

$$X^{p+1} = X^p + \alpha S^p$$

α is chosen such that $F(X^p + \alpha S^p)$ gives its minimum with respect to positive α

The momentum theory gives the uniform downwash to be the optimum condition for the minimum induced power. The constant downwash can be obtained with the free wake lifting line theory by varying the chord or pitch as follows. The circulation is related to the pitch and the downwash.

$$\Gamma = \pi C \Omega r \left(\Theta + \frac{w}{\Omega r} \right)$$

$$\Gamma_{opt} = \pi C_{fix} \Omega R \eta \left(\Theta + \frac{\lambda}{\eta} \right)$$

$$d\Theta + \frac{d\lambda}{\eta} = 0$$

$$\frac{d\Theta}{d\lambda} = -\frac{1}{\eta}$$

Then, $\Theta^{p+1} = \Theta^{p} + \frac{d\Theta}{d\lambda}(\lambda_{opt} - \lambda^{p})$

From the momentum theory, $\lambda_{opt} = \sqrt{C_T/2}$

$$\Gamma_{opt} = \pi C \Omega R \eta \left(\Theta_{opt} + \frac{\lambda}{\eta} \right)$$

$$dC \left(\Theta_{opt} + \frac{\lambda}{\eta} \right) + C \frac{d\lambda}{\eta} = 0$$

$$\frac{dC}{d\lambda} = -C \frac{1}{\eta \Theta_{opt} + \lambda}$$

or $$\left.\frac{dC}{d\lambda}\right|_{\lambda=\lambda_{opt}} = -C \frac{1}{\eta \Theta_{opt} + \lambda_{opt}}$$

Then $C^{p+1} = C^{p} + \frac{dC}{d\lambda}(\lambda_{opt} - \lambda^{p})$

$$C^{p+1} = C^{p} \frac{\eta \Theta_{opt} + \lambda^{p}}{\eta \Theta_{opt} + \lambda_{opt}}$$

To get a uniform downwash Θ^{p} or C^{p} is updated until λ^{p} becomes λ_{opt}.

4.3 One Dimensional Line Search To Find A Minimum.

Line search is to find α which minimizes the value of objective function, $F(X^p + \alpha S^p)$, with respect to positive value of α for the fixed direction of the descent S. In QNMDIF the line search procedure is to fit a parabolic curve through three points of α or two points and a slope of F with respect to α. When the program starts the line search procedure, it estimates α as follows.

$$F(X^p + \alpha S^p) = F(X^p) + \alpha \nabla F^p \cdot S^p = F_{opt}$$

,where $|S| = 1$, F_{opt} is the input which is considered to be the minimum, and ∇F is the gradient of the function F at p th iteration.

$$F_c + \alpha \frac{dF}{d\alpha} = F_{opt}$$

$$\alpha = -(F_c - F_{opt}) / \frac{dF}{d\alpha}$$

F_c is the current value of F.

The minimum is obtained as follows when there are two values of F and a slope of F.

The notations used in QNMDIF are used here.

$$F = Q \alpha^2 + 2 S \alpha + R$$

$$\frac{dF}{d\alpha} = 2\,Q\,\alpha + 2\,S$$

$$\frac{d^2F}{d\alpha^2} = 2\,Q$$

In order that F has a minimum Q should be positive.

$F = FW$ at $\alpha = W$

$\frac{dF}{d\alpha} = GTP$ at $a = W$

$F = FMIN$ at $\alpha = 0$

Then, $FW = Q\,W^2 + 2\,S\,W + R$

$GTP = 2\,Q\,W + 2\,W$

$FMIN = R$

From the above three relations,

$$Q = -\frac{1}{W^2}\,(FW - FMIN - W \cdot GTP)$$

$$2\,S = \frac{2}{W}\,(FW - FMIN) - GTP$$

F has a minimum at $\alpha = -S/Q$.

When there are three values of F, the minimum is obtained as follows.

$F = FW$ at $\alpha = W$.

$F = FV$ at $\alpha = V$.

$F = FMIN$ at $\alpha = 0$.

Then, $FW = Q\,W^2 + 2\,S\,W + R$

$$FV = Q\,V^2 + 2\,S\,V + R$$

$$FMIN = R$$

Let $x = Q\,V^2W + 2\,S\,V\,W$ and $y = Q\,W^2V + 2\,S\,V\,W$.

Then,

$$Q = \frac{y - x}{V\,W\,(W - V)}$$

$$S = \frac{xW - yV}{2\,V\,W\,(W - V)}$$

$$\alpha_{min} = - S/Q$$

If F has decreased sufficiently,or α_{MIN} is very small after any decrease of F, then the line search is successful. QNMDIF goes to the search direction calculation after the success of the line search. If the line search has failed with the forward difference calculation of the gradient, it does the central difference calculation of the gradient and goes back to the line search. If the line search was a failure with the central difference calculation of the gradient, QNMDIF stops with the message of the line search failure. The convergence criteria for the optimization is the condition that the norm of the gradient is very small. In some cases the norm of the gradient vector was not zero while the objective function did not decrease. But the signs of all components of the gradient vector were changed during the previous two iterations. This means the objective function had a steep valley.

4.4 Results And Discussion

To test the optimization program the momentum theory is used for the performance analysis. The design variables are 10 pitch angles at all spanwise stations with the objective function F = -0.1 CT/CP. Table 4 shows the output of the optimization program which converges after 5 iterations. The downwash and the circulation are nearly constant over the span as expected. The initial blade geometry for the results of Table 4 is the rotor of Ref.(68) shown in Figure (4-1). Figure (4-2) shows the optimum chord distribution obtained from the momentum theory with profile drag where 10 chord widths are the design variables while the linear twist is given and fixed. Here the chord bulges towards the root because the linear twist is not the optimum pitch. In figure (4-2) CT went up and CT went down from the initial values. Fig.s (4-3) and (4-4) show the effect of profile drag on the optimum pitch distribution obtained from 3-D momentum theory. The effect of the profile drag is to reduce the pitch angle near the blade root. By momentum theory there is a clear optimum pitch distribution for fixed chord distribution and optimum chord distribution for fixed pitch distribution, while zero loading by having zero chord is the optimum by vortex theory. Therefore the constraint

on thrust was not needed in the momentum calculction but was required for vortex theory.

The optimum rotor to give the minimum induced power is the rotor which has a constant circulation or a constant downwash according to the classical vortex theory using the rigid wake geometry. Table 3 shows the results for constant downwash obtained by changing the pitch distribution for the free wake lifting line theory. The resulting pitch distribution is shown in Fig.(4-5). The bound circulation distribution is shown in Fig.(4-6). The summary of tables are shown in Table of Optimization with thrust to power coefficient ratios and thrust coefficients (CT/CP, CT). The CT/CP from momentum theory for a straight linear twisted rotor (Ref. 68) was 13.8 at CT=0.00471 (Table 3). The optimized pitch (say 1/r) for constant downwash gave CT/CP=14.4 at CT=0.00328 (Table 4), but when compared at same CT, there is very little difference from the initial rotor. The constant downwash results from free wake theory gave CT/CP=13.4 at CT=0.00376 ,which was constrained to have same downwash as the one by momentum theory (Table 3).

We will now consider results using the free wake lifting line theory with the QNMDIF optimizer. Constant chord and variable twist results (Table 5) gave CT/CP=14.25 at CT=0.00422. Since this is at higher CT compared to the constant downwash result of CT/CP=13.4 and CT=0.00376, when lower CT is expected, obviously constant downwash is not

optimum. This is also qualitatively evident from Fig. 4-17 (Table 5). Table 5 shows the result of optimization where 5 section pitch angles near the tip are used. The initial blade geometry is the rotor of Ref.(68) shown in Fig.(4-1). The objective function(OBJ) is F = CP/CT. The pitch angles near the tip has decreased as a result of the optimization as shown in Fig.(4-17). But the thrust coefficient is decreased while CP/CT is decreased from 0.073 to 0.070. Therefore, in table 6 the thrust coefficient is added into the objective function in the form of a quadratic penalty function. The given and fixed thrust coefficient is CT= 0.00422 and the initial thrust coefficient is CT= 0.00459. The design variables are 5 section pitch angles near the tip. The objective function is F = 10.CP/CT + 100000.*(CTT - CT)**2. The objective function has decreased from 0.7454 to 0.6467 in Table 6. The downwash on the tip section is reversed, that is, becomes upwash.

Adding taper gave 14.7 for CT/CP at CT=0.00416 close to one of Table 5 in Table 7 and Fig. (4-18). With constraint on thrust CT/CP=13.9 in Table 8. Table 7 shows the results of optimization where the initial blade geometry is the rotor of Ref.(68) and the design variables are two section pitch angles and two chord widths near the blade tip. In table 7 the objective F (now =- CT/CP) has decreased from -13.67 to -14.74 with the result of a tapered and double twisted rotor as shown in Fig.(4-18) by optimization. In

table 8 the same trend is shown with the constraint on the thrust. In Table 9 switch to more stations gave similar results as Table 8.

As a result of previous unpublished heuristic studies * the blade geometry of taper and double twist shown in Fig. (4-7) was found to be optimum and is used for the heuristic parameter optimization. Fig.s (4-8) and (4-9) show the bound circulation distributions at various thrust coefficients obtained by varying the root chord width while keeping the twist and taper ratio constant. CT/CP increases as a result of the decrease in the root chord. Fig.(4-10) compares the bound circulation distributions at the same thrust coefficients between the tapered and double twisted blade and the constant chord and linear twisted blade. The bound circulation distribution which has the peak near the tip has the higher power coefficient than that having the peak around the center of the blade. The downwash of the tapered and double twisted blade has become the upwash near the blade tip. That is, the blade is in vortex ring condition at the tip. In vortex ring condition the maximum residual in bound circulation does not decrease below the convergence criterion which requires that the change in circulation between iterations should be less than 0.5 % of local circulation.

Fig.(4-11) shows CT/CP for the rotors shown in Fig.(4-1) and in Fig.(4-7) with various pitch and fixed

* Ref. 69

chord. Fig.(4-11) shows that there is an optimum pitch which gives the maximum of CT/CP with a fixed chord, while zero loading is the optimum with zero chord. Fig.(4-12) compares CT/CP for the tapered and double twisted rotor of Fig.(4-7) with that for the tapered and straight twisted rotor of Fig.(4-13). Both blade chords used in Fig.(4-12) are varied to get different thrust coefficients. The tapered and straight twisted rotor is shown to be better than the double twisted and tapered rotor. With the initial geometry of the rotor of Fig.(4-1) the optimized rotor is computed by using the design variable sets of (5), (6), (7) and (8) in section (4.1). For the sets of design variable (5) and (6) rotor of Fig.(4-1) does not change with the constraint on CTT = 0.00459 of the initial geometry and with objective function F = CP/CT + r_p*(CTT-CT)**2, r_p =1.3*r_{p-1} ,and r_0 =100000.0. For the case of 5 design variables of the set (7) tip pitch angles are reduced, that is, the blade is double twisted as a result of the optimization as shown in Fig.(4-20) and in Table (11). For the case of 6 design variables of the set (8) root chord is reduced, that is, the rotor has a lower solidity and a higher ratio of thrust to power coefficient as a result of the optimization as shown in Table 9. In Fig.(4-14) the tapered and double twisted rotor of Fig.(4-7) is as good as the straight twisted and constant chord rotor of Fig.(4-1). Fig.(4-15) compares CT/CP of the rotor of Fig.(4-7) to that

obtained by the present optimization with the design variables set (4) in section (4.1). The rotor of Fig.(4-7) is in vortex ring condition and hence the gradient calculation tend to be inaccurate. Hence, only one optimization result is better than the initial rotor used. The rotor blade which produces the better performance than the initial rotor has only the slightly decreased root twist compared to the initial rotor. Fig.(4-16) compares the bound circulation distributions for the rotors of Fig.(4-7), Fig.(4-13) and that obtained by the formal optimization. Among them the bound circulation result of the formal optimization has the peak circulation at the middle of the span and the best CT/CP. Double twisted and tapered rotor gave CT/CP=15.946 but at CT=0.0035 (Fig. 4-19 and Table 10) compared to 15.78 for heuristic rotor (Fig. 4-7) by the formal optimization with design variables set (8) of the section (4-3). Fig. (4-11) shows that the effect of going to CT=0.00416 reduces CT/CP very slightly. This is clearly optimum and gives about 5% difference.

Table 3. Results Obtained to Give Constant Downwash.

(a) Momentum Theory Results for Rotor of Fig.(4-3)

NO. OF BLADES = 2 SOLIDITY =0.0464

CT =0.00471 CP =0.000342

CTT =0.00459 CPI =0.000234

CVT1(LOCAL) =0.00050 CVT2(GLOBAL) =0.00500

ETA	CHORD	THETA	ALPHA	WLA	UT	CL	GAM
.150	.0729	0.1713E+02	0.7310E+01	−0.2597E−01	0.1522E+00	0.7751E+00	0.4300E−02
.250	.0729	0.1591E+02	0.7932E+01	−0.3504E−01	0.2524E+00	0.8469E+00	0.7791E−02
.350	.0729	0.1469E+02	0.7928E+01	−0.4150E−01	0.3525E+00	0.8486E+00	0.1090E−01
.450	.0729	0.1346E+02	0.7610E+01	−0.4614E−01	0.4524E+00	0.8157E+00	0.1345E−01
.600	.0729	0.1163E+02	0.6823E+01	−0.5047E−01	0.6021E+00	0.7320E+00	0.1606E−01
.750	.0729	0.9798E+01	0.5821E+01	−0.5214E−01	0.7518E+00	0.6249E+00	0.1712E−01
.825	.0729	0.8881E+01	0.5271E+01	−0.5204E−01	0.8266E+00	0.5660E+00	0.1705E−01
.875	.0729	0.8274E+01	0.4895E+01	−0.5165E−01	0.8765E+00	0.5257E+00	0.1679E−01
.925	.0729	0.7660E+01	0.4507E+01	−0.5096E−01	0.9264E+00	0.4840E+00	0.1634E−01
.975	.0729	0.7047E+01	0.4113E+01	−0.4998E−01	0.9763E+00	0.4417E+00	0.1572E−01

(b) Free Wake Results to Give Constant Downwash, $WLA=\sqrt{CT/2}$

NO. OF BLADES = 2 SOLIDITY =0.0464

CT =0.00376 CP =0.000281

CTT =0.00459 CPI =0.000181

CVT1(LOCAL) =0.00050 CVT2(GLOBAL) =0.00500

ETA	CHORD	THETA	ALPHA	WLA	UT	CL	GAM
.150	.0729	0.3350E+02	0.1608E+02	−0.4708E−01	0.1572E+00	0.1615E+01	0.9254E−02
.250	.0729	0.2177E+02	0.1107E+02	−0.4723E−01	0.2544E+00	0.1160E+01	0.1076E−01
.350	.0729	0.1561E+02	0.7930E+01	−0.4722E−01	0.3532E+00	0.8356E+00	0.1075E−01
.450	.0729	0.1171E+02	0.5727E+01	−0.4716E−01	0.4525E+00	0.6030E+00	0.9944E−02
.600	.0729	0.8016E+01	0.3545E+01	−0.4691E−01	0.6018E+00	0.3697E+00	0.8108E−02
.750	.0729	0.6069E+01	0.2473E+01	−0.4714E−01	0.7515E+00	0.2593E+00	0.7100E−02
.825	.0729	0.6644E+01	0.3323E+01	−0.4787E−01	0.8264E+00	0.3574E+00	0.1076E−01
.875	.0729	0.8331E+01	0.5131E+01	−0.4892E−01	0.8764E+00	0.5600E+00	0.1788E−01
.925	.0729	0.9235E+01	0.6212E+01	−0.4885E−01	0.9263E+00	0.6742E+00	0.2276E−01
.975	.0729	0.7697E+01	0.4851E+01	−0.4846E−01	0.9762E+00	0.5247E+00	0.1867E−01

Table 4. Optimization Results Obtained by Using Momentum Theory. $F = -C_T / (10.\ C_p)$, Design Variables = 10 Pitch Angles.

NO. OF BLADES = 2 SIGT =0.0464 SIG =0.0464

CT =0.00471 CP =0.000342 OBJ = -0.1379E+01

CTT =0.00471 CPI =0.000234 CVT1(LOCAL) =0.00050 CVT2(GLOBAL) =0.00500

ETA	CHORD	THETA	ALPHA	WLA	UT	CL	GAM
.150	0.7288E-01	17.1314	7.3097	-0.2597E-01	0.1522E+00	0.7751E+00	0.4300E-02
.250	0.7288E-01	15.9110	7.9320	-0.3504E-01	0.2524E+00	0.8469E+00	0.7791E-02
.350	0.7288E-01	14.6906	7.9278	-0.4150E-01	0.3525E+00	0.8486E+00	0.1090E-01
.450	0.7288E-01	13.4645	7.6102	-0.4614E-01	0.4524E+00	0.8157E+00	0.1345E-01
.600	0.7288E-01	11.6310	6.8227	-0.5047E-01	0.6021E+00	0.7320E+00	0.1606E-01
.750	0.7288E-01	9.7976	5.8210	-0.5214E-01	0.7518E+00	0.6249E+00	0.1712E-01
.825	0.7288E-01	8.8808	5.2714	-0.5204E-01	0.8266E+00	0.5660E+00	0.1705E-01
.875	0.7288E-01	8.2735	4.8953	-0.5165E-01	0.8765E+00	0.5257E+00	0.1679E-01
.925	0.7288E-01	7.6604	4.5071	-0.5096E-01	0.9264E+00	0.4840E+00	0.1634E-01
.975	0.7288E-01	7.0474	4.1129	-0.4998E-01	0.9763E+00	0.4417E+00	0.1572E-01

NO. OF BLADES = 2 SIGT =0.0464 SIG =0.0464

CT =0.00333 CP =0.000232 OBJ = -0.1436E+01

CTT =0.00471 CPI =0.000138 CVT1(LOCAL) =0.00050 CVT2(GLOBAL) =0.00500

ETA	CHORD	THETA	ALPHA	WLA	UT	CL	GAM
.150	0.7288E-01	17.2873	7.4040	-0.2613E-01	0.1523E+00	0.7850E+00	0.4356E-02
.250	0.7288E-01	16.1258	8.0758	-0.3536E-01	0.2525E+00	0.8622E+00	0.7933E-02
.350	0.7288E-01	14.7296	7.9552	-0.4158E-01	0.3525E+00	0.8515E+00	0.1094E-01
.450	0.7288E-01	13.0258	7.2937	-0.4517E-01	0.4523E+00	0.7818E+00	0.1288E-01
.600	0.7288E-01	8.3132	4.4334	-0.4069E-01	0.6014E+00	0.4758E+00	0.1043E-01
.750	0.7288E-01	6.6077	3.5152	-0.4052E-01	0.7511E+00	0.3774E+00	0.1033E-01
.825	0.7288E-01	6.9414	3.8539	-0.4450E-01	0.8262E+00	0.4139E+00	0.1246E-01
.875	0.7288E-01	6.1685	3.3660	-0.4283E-01	0.8760E+00	0.3615E+00	0.1154E-01
.925	0.7288E-01	5.4661	2.9248	-0.4105E-01	0.9259E+00	0.3141E+00	0.1060E-01
.975	0.7288E-01	4.8598	2.5488	-0.3935E-01	0.9758E+00	0.2738E+00	0.9736E-02

NO. OF BLADES = 2 SIGT =0.0464 SIG =0.0464

CT =0.00325 CP =0.000226 OBJ = -0.1438E+01

CTT =0.00471 CPI =0.000133 CVT1(LOCAL) =0.00050 CVT2(GLOBAL) =0.00500

ETA	CHORD	THETA	ALPHA	WLA	UT	CL	GAM
.150	0.7288E-01	17.4919	7.5283	-0.2635E-01	0.1523E+00	0.7981E+00	0.4430E-02
.250	0.7288E-01	16.3755	8.2437	-0.3572E-01	0.2525E+00	0.8800E+00	0.8099E-02
.350	0.7288E-01	14.6951	7.9309	-0.4151E-01	0.3525E+00	0.8489E+00	0.1090E-01
.450	0.7288E-01	12.4158	6.8567	-0.4380E-01	0.4521E+00	0.7350E+00	0.1211E-01
.600	0.7288E-01	8.3520	4.4604	-0.4082E-01	0.6014E+00	0.4787E+00	0.1049E-01
.750	0.7288E-01	6.6673	3.5567	-0.4076E-01	0.7511E+00	0.3819E+00	0.1045E-01
.825	0.7288E-01	6.0248	3.2075	-0.4060E-01	0.8260E+00	0.3445E+00	0.1037E-01
.875	0.7288E-01	5.6020	2.9695	-0.4023E-01	0.8759E+00	0.3189E+00	0.1018E-01
.925	0.7288E-01	5.3732	2.8601	-0.4060E-01	0.9259E+00	0.3072E+00	0.1037E-01
.975	0.7288E-01	5.3176	2.8669	-0.4173E-01	0.9759E+00	0.3079E+00	0.1095E-01

NO. OF BLADES = 2 SIGT =0.0464 SIG =0.0464

Table 4. -Continued.

CT =0.00322 CP =0.000224 OBJ = -0.1440E+01

CTT =0.00471 CPI =0.000131 CVT1(LOCAL) =0.00050 CVT2(GLOBAL) =0.00500

ETA	CHORD	THETA	ALPHA	WLA	UT	CL	GAM
.150	0.7288E-01	17.9782	7.8252	-0.2686E-01	0.1524E+00	0.8294E+00	0.4606E-02
.250	0.7288E-01	16.9416	8.6264	-0.3654E-01	0.2527E+00	0.9207E+00	0.8478E-02
.350	0.7288E-01	14.6120	7.8725	-0.4136E-01	0.3524E+00	0.8427E+00	0.1082E-01
.450	0.7288E-01	11.3615	6.1111	-0.4135E-01	0.4519E+00	0.6552E+00	0.1079E-01
.600	0.7288E-01	8.4465	4.5263	-0.4112E-01	0.6014E+00	0.4858E+00	0.1065E-01
.750	0.7288E-01	6.7574	3.6194	-0.4112E-01	0.7511E+00	0.3886E+00	0.1064E-01
.825	0.7288E-01	5.8173	3.0637	-0.3968E-01	0.8260E+00	0.3290E+00	0.9904E-02
.875	0.7288E-01	5.7425	3.0671	-0.4089E-01	0.8760E+00	0.3294E+00	0.1052E-01
.925	0.7288E-01	5.5202	2.9626	-0.4132E-01	0.9259E+00	0.3182E+00	0.1074E-01
.975	0.7288E-01	4.9392	2.6035	-0.3977E-01	0.9758E+00	0.2797E+00	0.9945E-02

NO. OF BLADES = 2 SIGT =0.0464 SIG =0.0464

CT =0.00322 CP =0.000223 OBJ = -0.1440E+01

CTT =0.00471 CPI =0.000131 CVT1(LOCAL) =0.00050 CVT2(GLOBAL) =0.00500

ETA	CHORD	THETA	ALPHA	WLA	UT	CL	GAM
.150	0.7288E-01	18.5747	8.1927	-0.2748E-01	0.1525E+00	0.8681E+00	0.4824E-02
.250	0.7288E-01	17.5915	9.0693	-0.3746E-01	0.2528E+00	0.9679E+00	0.8916E-02
.350	0.7288E-01	14.5244	7.8110	-0.4120E-01	0.3524E+00	0.8361E+00	0.1074E-01
.450	0.7288E-01	10.6263	5.5992	-0.3958E-01	0.4517E+00	0.6004E+00	0.9883E-02
.600	0.7288E-01	8.3329	4.4471	-0.4075E-01	0.6014E+00	0.4773E+00	0.1046E-01
.750	0.7288E-01	6.6519	3.5459	-0.4070E-01	0.7511E+00	0.3807E+00	0.1042E-01
.825	0.7288E-01	6.1276	3.2791	-0.4105E-01	0.8260E+00	0.3521E+00	0.1060E-01
.875	0.7288E-01	5.8515	3.1432	-0.4139E-01	0.8760E+00	0.3376E+00	0.1078E-01
.925	0.7288E-01	5.4310	2.9004	-0.4088E-01	0.9259E+00	0.3115E+00	0.1051E-01
.975	0.7288E-01	5.2236	2.8011	-0.4125E-01	0.9759E+00	0.3009E+00	0.1070E-01

NO. OF BLADES = 2 SIGT =0.0464 SIG =0.0464

CT =0.00328 CP =0.000227 OBJ = -0.1441E+01

CTT =0.00471 CPI =0.000134 CVT1(LOCAL) =0.00050 CVT2(GLOBAL) =0.00500

ETA	CHORD	THETA	ALPHA	WLA	UT	CL	GAM
.150	0.7288E-01	20.0915	9.1422	-0.2902E-01	0.1528E+00	0.9680E+00	0.5389E-02
.250	0.7288E-01	19.0338	10.0648	-0.3946E-01	0.2531E+00	0.1074E+01	0.9903E-02
.350	0.7288E-01	14.3678	7.7012	-0.4091E-01	0.3524E+00	0.8244E+00	0.1059E-01
.450	0.7288E-01	10.6785	5.6354	-0.3971E-01	0.4517E+00	0.6042E+00	0.9947E-02
.600	0.7288E-01	8.5778	4.6182	-0.4153E-01	0.6014E+00	0.4956E+00	0.1086E-01
.750	0.7288E-01	6.8692	3.6976	-0.4156E-01	0.7512E+00	0.3970E+00	0.1087E-01
.825	0.7288E-01	6.4358	3.4952	-0.4238E-01	0.8261E+00	0.3753E+00	0.1130E-01
.875	0.7288E-01	5.4642	2.8742	-0.3958E-01	0.8759E+00	0.3087E+00	0.9854E-02
.925	0.7288E-01	5.3924	2.8735	-0.4069E-01	0.9259E+00	0.3086E+00	0.1041E-01
.975	0.7288E-01	5.1622	2.7583	-0.4093E-01	0.9759E+00	0.2963E+00	0.1054E-01

Table 5. Optimization Results Obtained by Using Free Wake Theory.

OBJ = CP/CT

NDV = 5 PITCH ANGLES WITH WAYNE JOHNSON ROTOR

NO. OF BLADES = 2 SIGT =0.0464 SIG =0.0464

CT =0.00459 CP =0.000336 OBJ = 0.7316E-01

CTT =0.00459 CPI =0.000229 CVT1(LOCAL) =0.00050 CVT2(GLOBAL) =0.00500

ETA	CHORD	THETA	ALPHA	WLA	UT	CL	GAM
.150	0.7288E-01	17.1314	7.7205	-0.2486E-01	0.1520E+00	0.8242E+00	0.4567E-02
.250	0.7288E-01	15.9110	8.5295	-0.3239E-01	0.2521E+00	0.9142E+00	0.8399E-02
.350	0.7288E-01	14.6906	8.3062	-0.3916E-01	0.3522E+00	0.8903E+00	0.1143E-01
.450	0.7288E-01	13.4645	7.5166	-0.4688E-01	0.4524E+00	0.8042E+00	0.1326E-01
.600	0.7288E-01	11.6310	5.8676	-0.6056E-01	0.6030E+00	0.6266E+00	0.1377E-01
.750	0.7288E-01	9.7976	4.8186	-0.6534E-01	0.7528E+00	0.5173E+00	0.1419E-01
.825	0.7288E-01	8.8808	4.5787	-0.6206E-01	0.8273E+00	0.4932E+00	0.1487E-01
.875	0.7288E-01	8.2735	5.2142	-0.4677E-01	0.8762E+00	0.5605E+00	0.1790E-01
.925	0.7288E-01	7.6604	5.8348	-0.2948E-01	0.9255E+00	0.6250E+00	0.2108E-01
.975	0.7288E-01	7.0474	4.6705	-0.4047E-01	0.9758E+00	0.5009E+00	0.1781E-01

NO. OF BLADES = 2 SIGT =0.0464 SIG =0.0464

CT =0.00442 CP =0.000314 OBJ = 0.7114E-01

CTT =0.00459 CPI =0.000210 CVT1(LOCAL) =0.00050 CVT2(GLOBAL) =0.00500

ETA	CHORD	THETA	ALPHA	WLA	UT	CL	GAM
.150	0.7288E-01	17.1314	7.4460	-0.2560E-01	0.1522E+00	0.7897E+00	0.4379E-02
.250	0.7288E-01	15.9110	8.3851	-0.3303E-01	0.2522E+00	0.8961E+00	0.8235E-02
.350	0.7288E-01	14.6906	8.2564	-0.3947E-01	0.3522E+00	0.8841E+00	0.1135E-01
.450	0.7288E-01	13.4645	7.5668	-0.4648E-01	0.4524E+00	0.8107E+00	0.1336E-01
.600	0.7288E-01	11.6310	6.0030	-0.5913E-01	0.6029E+00	0.6428E+00	0.1412E-01
.750	0.7288E-01	9.4344	4.6476	-0.6280E-01	0.7526E+00	0.4979E+00	0.1366E-01
.825	0.7288E-01	8.8605	4.4548	-0.6356E-01	0.8274E+00	0.4775E+00	0.1440E-01
.875	0.7288E-01	8.3073	5.1869	-0.4770E-01	0.8763E+00	0.5567E+00	0.1778E-01
.925	0.7288E-01	7.1922	5.4767	-0.2770E-01	0.9254E+00	0.5884E+00	0.1984E-01
.975	0.7288E-01	4.7098	3.6192	-0.1856E-01	0.9752E+00	0.3889E+00	0.1382E-01

NO. OF BLADES = 2 SIGT =0.0464 SIG =0.0464

CT =0.00442 CP =0.000313 OBJ = 0.7085E-01

CTT =0.00459 CPI =0.000209 CVT1(LOCAL) =0.00050 CVT2(GLOBAL) =0.00500

ETA	CHORD	THETA	ALPHA	WLA	UT	CL	GAM
.150	0.7288E-01	17.1314	7.4745	-0.2552E-01	0.1522E+00	0.7946E+00	0.4406E-02
.250	0.7288E-01	15.9110	8.4042	-0.3294E-01	0.2522E+00	0.8994E+00	0.8265E-02
.350	0.7288E-01	14.6906	8.2726	-0.3937E-01	0.3522E+00	0.8869E+00	0.1138E-01
.450	0.7288E-01	13.4645	7.5872	-0.4632E-01	0.4524E+00	0.8139E+00	0.1342E-01
.600	0.7288E-01	11.6310	6.0342	-0.5880E-01	0.6029E+00	0.6474E+00	0.1422E-01
.750	0.7288E-01	9.4242	4.6636	-0.6246E-01	0.7526E+00	0.5006E+00	0.1373E-01
.825	0.7288E-01	8.8527	4.4588	-0.6339E-01	0.8274E+00	0.4788E+00	0.1444E-01
.875	0.7288E-01	8.2881	5.1769	-0.4756E-01	0.8763E+00	0.5563E+00	0.1777E-01
.925	0.7288E-01	7.1482	5.4605	-0.2725E-01	0.9254E+00	0.5861E+00	0.1976E-01

Table 5. -Continued.

.975	0.7288E-01	4.6219	3.5849	-0.1765E-01	0.9752E+00	0.3842E+00	0.1365E-01

NO. OF BLADES = 2 SIGT =0.0464 SIG =0.0464

CT =0.00431 CP =0.000305 OBJ = 0.7070E-01

CTT =0.00459 CPI =0.000202 CVT1(LOCAL) =0.00050 CVT2(GLOBAL) =0.00500

ETA	CHORD	THETA	ALPHA	WLA	UT	CL	GAM
.150	0.7288E-01	17.1314	7.6227	-0.2512E-01	0.1521E+00	0.8131E+00	0.4506E-02
.250	0.7288E-01	15.9110	8.5099	-0.3247E-01	0.2521E+00	0.9126E+00	0.8385E-02
.350	0.7288E-01	14.6906	8.3584	-0.3884E-01	0.3521E+00	0.8980E+00	0.1152E-01
.450	0.7288E-01	13.4645	7.6603	-0.4574E-01	0.4523E+00	0.8242E+00	0.1359E-01
.600	0.7288E-01	11.6310	6.0920	-0.5819E-01	0.6028E+00	0.6561E+00	0.1441E-01
.750	0.7288E-01	9.2859	4.6155	-0.6127E-01	0.7525E+00	0.4964E+00	0.1361E-01
.825	0.7288E-01	8.6752	4.3239	-0.6277E-01	0.8274E+00	0.4645E+00	0.1400E-01
.875	0.7288E-01	8.0866	4.8187	-0.4996E-01	0.8764E+00	0.5159E+00	0.1648E-01
.925	0.7288E-01	6.7378	5.1065	-0.2634E-01	0.9254E+00	0.5480E+00	0.1848E-01
.975	0.7288E-01	3.8324	3.1679	-0.1131E-01	0.9751E+00	0.3403E+00	0.1209E-01

NO. OF BLADES = 2 SIGT =0.0464 SIG =0.0464

CT =0.00422 CP =0.000296 OBJ = 0.7008E-01

CTT =0.00459 CPI =0.000194 CVT1(LOCAL) =0.00050 CVT2(GLOBAL) =0.00500

ETA	CHORD	THETA	ALPHA	WLA	UT	CL	GAM
.150	0.7288E-01	17.1314	7.5981	-0.2519E-01	0.1521E+00	0.8096E+00	0.4488E-02
.250	0.7288E-01	15.9110	8.4854	-0.3258E-01	0.2521E+00	0.9096E+00	0.8357E-02
.350	0.7288E-01	14.6906	8.3222	-0.3906E-01	0.3522E+00	0.8939E+00	0.1147E-01
.450	0.7288E-01	13.4645	7.5991	-0.4623E-01	0.4524E+00	0.8176E+00	0.1348E-01
.600	0.7288E-01	11.6310	6.0573	-0.5855E-01	0.6029E+00	0.6521E+00	0.1433E-01
.750	0.7288E-01	9.1590	4.5814	-0.6005E-01	0.7524E+00	0.4929E+00	0.1351E-01
.825	0.7288E-01	8.5053	4.2667	-0.6114E-01	0.8273E+00	0.4590E+00	0.1384E-01
.875	0.7288E-01	7.9072	4.7948	-0.4758E-01	0.8763E+00	0.5153E+00	0.1645E-01
.925	0.7288E-01	6.3274	4.8796	-0.2338E-01	0.9253E+00	0.5240E+00	0.1767E-01
.975	0.7288E-01	3.0588	2.8007	-0.4391E-02	0.9750E+00	0.3008E+00	0.1069E-01

Table 6. Optimization Results From Free Wake Lifting Line Theory with the Constraint on $C_T = C_{TT}$.

OPT.DAT;2 17-JUN-1985 17:23 Page 1

OBJ = 10.*CP/CT + 100000.*(CTT-CT)**2

DESIGN VARIABLES = 5 TIP PITCH ANGLES

NO. OF BLADES = 2 SIGT =0.0464 SIG =0.0464

CT =0.00459 CP =0.000336 OBJ = 0.7454E+00

CTT =0.00422 CPI =0.000229 CVT1(LOCAL) =0.00050 CVT2(GLOBAL) =0.00500

ETA	CHORD	THETA	ALPHA	WLA	UT	CL	GAM
.150	0.7288E-01	17.1314	7.7205	-0.2486E-01	0.1520E+00	0.8242E+00	0.4567E-02
.250	0.7288E-01	15.9110	8.5295	-0.3239E-01	0.2521E+00	0.9142E+00	0.8399E-02
.350	0.7288E-01	14.6906	8.3062	-0.3916E-01	0.3522E+00	0.8903E+00	0.1143E-01
.450	0.7288E-01	13.4645	7.5166	-0.4688E-01	0.4524E+00	0.8042E+00	0.1326E-01
.600	0.7288E-01	11.6310	5.8676	-0.6056E-01	0.6030E+00	0.6266E+00	0.1377E-01
.750	0.7288E-01	9.7976	4.8186	-0.6534E-01	0.7528E+00	0.5173E+00	0.1419E-01
.825	0.7288E-01	8.8808	4.5787	-0.6206E-01	0.8273E+00	0.4932E+00	0.1487E-01
.875	0.7288E-01	8.2735	5.2142	-0.4677E-01	0.8762E+00	0.5605E+00	0.1790E-01
.925	0.7288E-01	7.6604	5.8348	-0.2948E-01	0.9255E+00	0.6250E+00	0.2108E-01
.975	0.7288E-01	7.0474	4.6705	-0.4047E-01	0.9758E+00	0.5009E+00	0.1781E-01

NO. OF BLADES = 2 SIGT =0.0464 SIG =0.0464

CT =0.00409 CP =0.000286 OBJ = 0.7008E+00

CTT =0.00422 CPI =0.000185 CVT1(LOCAL) =0.00050 CVT2(GLOBAL) =0.00500

ETA	CHORD	THETA	ALPHA	WLA	UT	CL	GAM
.150	0.7288E-01	17.1314	7.2817	-0.2604E-01	0.1522E+00	0.7722E+00	0.4285E-02
.250	0.7288E-01	15.9110	8.2775	-0.3351E-01	0.2522E+00	0.8847E+00	0.8132E-02
.350	0.7288E-01	14.6906	8.1825	-0.3993E-01	0.3523E+00	0.8762E+00	0.1125E-01
.450	0.7288E-01	13.4645	7.5223	-0.4684E-01	0.4524E+00	0.8057E+00	0.1328E-01
.600	0.7288E-01	11.6310	5.9566	-0.5962E-01	0.6030E+00	0.6379E+00	0.1402E-01
.750	0.7288E-01	7.6008	3.5196	-0.5351E-01	0.7519E+00	0.3781E+00	0.1036E-01
.825	0.7288E-01	7.9392	3.6599	-0.6173E-01	0.8273E+00	0.3936E+00	0.1187E-01
.875	0.7288E-01	7.4016	4.3872	-0.4608E-01	0.8762E+00	0.4735E+00	0.1512E-01
.925	0.7288E-01	6.2938	5.1088	-0.1913E-01	0.9252E+00	0.5489E+00	0.1851E-01
.975	0.7288E-01	5.4271	3.8443	-0.2694E-01	0.9754E+00	0.4129E+00	0.1468E-01

NO. OF BLADES = 2 SIGT =0.0464 SIG =0.0464

CT =0.00409 CP =0.000276 OBJ = 0.6765E+00

CTT =0.00422 CPI =0.000174 CVT1(LOCAL) =0.00050 CVT2(GLOBAL) =0.00500

ETA	CHORD	THETA	ALPHA	WLA	UT	CL	GAM
.150	0.7288E-01	17.1314	6.9606	-0.2691E-01	0.1524E+00	0.7356E+00	0.4085E-02
.250	0.7288E-01	15.9110	8.0774	-0.3440E-01	0.2524E+00	0.8622E+00	0.7929E-02
.350	0.7288E-01	14.6906	8.0663	-0.4065E-01	0.3524E+00	0.8633E+00	0.1108E-01
.450	0.7288E-01	13.4645	7.5024	-0.4700E-01	0.4524E+00	0.8038E+00	0.1325E-01
.600	0.7288E-01	11.6310	6.0393	-0.5874E-01	0.6029E+00	0.6474E+00	0.1422E-01
.750	0.7288E-01	8.8853	4.0030	-0.6406E-01	0.7527E+00	0.4283E+00	0.1175E-01
.825	0.7288E-01	5.4153	3.3089	-0.3034E-01	0.8256E+00	0.3572E+00	0.1075E-01
.875	0.7288E-01	9.0101	6.1797	-0.4326E-01	0.8761E+00	0.6648E+00	0.2123E-01

Table 6. -Continued.

OPT.DAT;2 17-JUN-1985 17:23 Page 2

.925	0.7288E-01	5.4406	4.5877	-0.1377E-01	0.9251E+00	0.4928E+00	0.1662E-01
.975	0.7288E-01	2.6227	2.5173	-0.1793E-02	0.9750E+00	0.2703E+00	0.9604E-02

NO. OF BLADES = 2 SIGT =0.0464 SIG =0.0464

CT =0.00416 CP =0.000269 OBJ = 0.6467E+00

CTT =0.00422 CPI =0.000166 CVT1(LOCAL) =0.00050 CVT2(GLOBAL) =0.00500

ETA	CHORD	THETA	ALPHA	WLA	UT	CL	GAM
.150	0.7288E-01	17.1314	7.8568	-0.2450E-01	0.1520E+00	0.8356E+00	0.4628E-02
.250	0.7288E-01	15.9110	8.6675	-0.3177E-01	0.2520E+00	0.9273E+00	0.8516E-02
.350	0.7288E-01	14.6906	8.5148	-0.3787E-01	0.3520E+00	0.9125E+00	0.1171E-01
.450	0.7288E-01	13.4645	7.9160	-0.4371E-01	0.4521E+00	0.8489E+00	0.1399E-01
.600	0.7288E-01	11.6310	6.5186	-0.5368E-01	0.6024E+00	0.6991E+00	0.1535E-01
.750	0.7288E-01	9.5550	4.5979	-0.6505E-01	0.7528E+00	0.4928E+00	0.1352E-01
.825	0.7288E-01	3.6253	1.9500	-0.2413E-01	0.8254E+00	0.2095E+00	0.6302E-02
.875	0.7288E-01	7.6037	5.4027	-0.3363E-01	0.8756E+00	0.5805E+00	0.1852E-01
.925	0.7288E-01	5.7371	4.8277	-0.1468E-01	0.9251E+00	0.5188E+00	0.1749E-01
.975	0.7288E-01	2.5673	2.6123	0.7659E-03	0.9750E+00	0.2807E+00	0.9975E-02

Table 7. Optimization Results with Free Wake Theory.
Design Variables = 2 tip pitch and 2 chord from 2 tip sections.

OPTIMIZATION OF WAYNE JOHNSON ROTOR

OBJ = -CT/CP

NO. OF BLADES = 2 SIGT =0.0464 SIG =0.0464

CT =0.00459 CP =0.000336 OBJ = -0.1367E+02

CTT =0.00459 CPI =0.000229 CVT1(LOCAL) =0.00050 CVT2(GLOBAL) =0.00500

ETA	CHORD	THETA	ALPHA	WLA	UT	CL	GAM
.150	0.7288E-01	17.1314	7.7206	-0.2486E-01	0.1520E+00	0.8242E+00	0.4567E-02
.250	0.7288E-01	15.9110	8.5296	-0.3239E-01	0.2521E+00	0.9142E+00	0.8399E-02
.350	0.7288E-01	14.6906	8.3062	-0.3916E-01	0.3522E+00	0.8903E+00	0.1143E-01
.450	0.7288E-01	13.4645	7.5166	-0.4688E-01	0.4524E+00	0.8042E+00	0.1326E-01
.600	0.7288E-01	11.6310	5.8676	-0.6056E-01	0.6030E+00	0.6266E+00	0.1377E-01
.750	0.7288E-01	9.7976	4.8186	-0.6534E-01	0.7528E+00	0.5173E+00	0.1419E-01
.825	0.7288E-01	8.8808	4.5786	-0.6206E-01	0.8273E+00	0.4932E+00	0.1487E-01
.875	0.7288E-01	8.2735	5.2140	-0.4677E-01	0.8762E+00	0.5605E+00	0.1790E-01
.925	0.7288E-01	7.6604	5.8349	-0.2948E-01	0.9255E+00	0.6250E+00	0.2108E-01
.975	0.7288E-01	7.0474	4.6706	-0.4047E-01	0.9758E+00	0.5009E+00	0.1781E-01

NO. OF BLADES = 2 SIGT =0.0442 SIG =0.0464

CT =0.00422 CP =0.000286 OBJ = -0.1475E+02

CTT =0.00459 CPI =0.000193 CVT1(LOCAL) =0.00050 CVT2(GLOBAL) =0.00500

ETA	CHORD	THETA	ALPHA	WLA	UT	CL	GAM
.150	0.7288E-01	17.1314	7.2951	-0.2601E-01	0.1522E+00	0.7738E+00	0.4293E-02
.250	0.7288E-01	15.9110	8.2649	-0.3356E-01	0.2522E+00	0.8835E+00	0.8122E-02
.350	0.7288E-01	14.6906	8.1380	-0.4020E-01	0.3523E+00	0.8716E+00	0.1119E-01
.450	0.7288E-01	13.4645	7.4369	-0.4752E-01	0.4525E+00	0.7966E+00	0.1314E-01
.600	0.7288E-01	11.6310	5.9244	-0.5996E-01	0.6030E+00	0.6343E+00	0.1394E-01
.750	0.7288E-01	9.7976	4.8378	-0.6509E-01	0.7528E+00	0.5187E+00	0.1423E-01
.825	0.7288E-01	8.8808	4.7976	-0.5889E-01	0.8271E+00	0.5143E+00	0.1550E-01
.875	0.7288E-01	8.2735	5.8958	-0.3633E-01	0.8758E+00	0.6317E+00	0.2016E-01
.925	0.6051E-01	7.1375	5.7162	-0.2295E-01	0.9253E+00	0.6135E+00	0.1717E-01
.975	0.2429E-01	4.2894	5.3775	0.1852E-01	0.9752E+00	0.5774E+00	0.6839E-02

NO. OF BLADES = 2 SIGT =0.0439 SIG =0.0464

CT =0.00416 CP =0.000283 OBJ = -0.1474E+02

CTT =0.00459 CPI =0.000192 CVT1(LOCAL) =0.00050 CVT2(GLOBAL) =0.00500

ETA	CHORD	THETA	ALPHA	WLA	UT	CL	GAM
.150	0.7288E-01	17.1314	7.2562	-0.2611E-01	0.1523E+00	0.7701E+00	0.4273E-02
.250	0.7288E-01	15.9110	8.2440	-0.3365E-01	0.2523E+00	0.8817E+00	0.8105E-02
.350	0.7288E-01	14.6906	8.1323	-0.4024E-01	0.3523E+00	0.8716E+00	0.1119E-01
.450	0.7288E-01	13.4645	7.4501	-0.4741E-01	0.4525E+00	0.7992E+00	0.1318E-01
.600	0.7288E-01	11.6310	5.9405	-0.5979E-01	0.6030E+00	0.6375E+00	0.1401E-01
.750	0.7288E-01	9.7976	4.8172	-0.6536E-01	0.7528E+00	0.5168E+00	0.1418E-01
.825	0.7288E-01	8.8808	4.9472	-0.5673E-01	0.8269E+00	0.5319E+00	0.1603E-01
.875	0.7288E-01	8.2735	5.9687	-0.3522E-01	0.8757E+00	0.6415E+00	0.2047E-01
.925	0.5858E-01	7.0602	5.6497	-0.2278E-01	0.9253E+00	0.6070E+00	0.1645E-01
.975	0.1715E-01	3.8903	5.5440	0.2815E-01	0.9754E+00	0.5956E+00	0.4981E-02

Table 8. Optimization Results Obtained by Using Free Wake Theory, with Constraint of $C_T = C_{TT}$.

3-D MOMENTUM THEORY

NO. OF BLADES = 2 SOLIDITY =0.0460

CT =0.00460 CP =0.000331

CTT =0.00459 CPI =0.000226

CVT1(LOCAL) =0.00050 CVT2(GLOBAL) =0.00500

ETA	CHORD	THETA	ALPHA	WLA	UT	CL	GAM
.150	.0729	0.1713E+02	0.7334E+01	-0.2590E-01	0.1522E+00	0.7778E+00	0.4315E-02
.250	.0729	0.1591E+02	0.7955E+01	-0.3494E-01	0.2524E+00	0.8493E+00	0.7813E-02
.350	.0729	0.1469E+02	0.7948E+01	-0.4138E-01	0.3524E+00	0.8508E+00	0.1093E-01
.450	.0729	0.1346E+02	0.7628E+01	-0.4600E-01	0.4523E+00	0.8176E+00	0.1348E-01
.600	.0729	0.1163E+02	0.6838E+01	-0.5031E-01	0.6021E+00	0.7337E+00	0.1610E-01
.750	.0729	0.9798E+01	0.5834E+01	-0.5197E-01	0.7518E+00	0.6263E+00	0.1716E-01
.825	.0729	0.8881E+01	0.5283E+01	-0.5187E-01	0.8266E+00	0.5672E+00	0.1709E-01
.875	.0729	0.8274E+01	0.4906E+01	-0.5148E-01	0.8765E+00	0.5268E+00	0.1683E-01
.925	.0692	0.7452E+01	0.4363E+01	-0.4992E-01	0.9263E+00	0.4685E+00	0.1501E-01
.975	.0666	0.6524E+01	0.3738E+01	-0.4744E-01	0.9762E+00	0.4015E+00	0.1306E-01

NB = 2 KIT = 20 RES. = 0.7754E-04

ZT =	0.0000E+00	RT =	0.1000E+00
ZT =	0.0000E+00	RT =	0.5899E+00
ZT =	0.0000E+00	RT =	0.9905E+00
ZT =	-0.7300E-01	RT =	0.8236E-01
ZT =	-0.1837E+00	RT =	0.5181E+00
ZT =	-0.4927E-01	RT =	0.8814E+00
ZT =	-0.1404E+00	RT =	0.6755E-01
ZT =	-0.3852E+00	RT =	0.5065E+00
ZT =	-0.1778E+00	RT =	0.8089E+00
ZT =	-0.2167E+00	RT =	0.5839E-01
ZT =	-0.5996E+00	RT =	0.4836E+00
ZT =	-0.3401E+00	RT =	0.7792E+00
ZT =	-0.2988E+00	RT =	0.5061E-01
ZT =	-0.8194E+00	RT =	0.4552E+00
ZT =	-0.5063E+00	RT =	0.7747E+00
ZT =	-0.3810E+00	RT =	0.5061E-01
ZT =	-0.1039E+01	RT =	0.4552E+00
ZT =	-0.6725E+00	RT =	0.7747E+00

OPTIMIZATION OF ROTOR OF REF. 35

OBJ = 100.*(CP+10000.*(CTT-CT)**2)

2 TIP PITCH AND 2 CHORDS DESIGN VARIABLES

Table 8. -Continued.

NO. OF BLADES = 2 SOLIDITY =0.0460

CT =0.00450 CP =0.000324

CTT =0.00459 CPI =0.000221

CVT1(LOCAL) =0.00050 CVT2(GLOBAL) =0.00500

ETA	CHORD	THETA	ALPHA	WLA	UT	CL	GAM
.150	.0729	0.1713E+02	0.7707E+01	−0.2490E−01	0.1521E+00	0.8228E+00	0.4559E−02
.250	.0729	0.1591E+02	0.8503E+01	−0.3251E−01	0.2521E+00	0.9112E+00	0.8371E−02
.350	.0729	0.1469E+02	0.8251E+01	−0.3951E−01	0.3522E+00	0.8840E+00	0.1135E−01
.450	.0729	0.1346E+02	0.7414E+01	−0.4770E−01	0.4525E+00	0.7926E+00	0.1307E−01
.600	.0729	0.1163E+02	0.5816E+01	−0.6110E−01	0.6031E+00	0.6215E+00	0.1366E−01
.750	.0729	0.9798E+01	0.4860E+01	−0.6480E−01	0.7528E+00	0.5220E+00	0.1432E−01
.825	.0729	0.8881E+01	0.4602E+01	−0.6172E−01	0.8273E+00	0.4961E+00	0.1496E−01
.875	.0729	0.8274E+01	0.5176E+01	−0.4735E−01	0.8763E+00	0.5568E+00	0.1778E−01
.925	.0692	0.7452E+01	0.5829E+01	−0.2620E−01	0.9254E+00	0.6244E+00	0.1998E−01
.975	.0666	0.6524E+01	0.4621E+01	−0.3239E−01	0.9755E+00	0.4955E+00	0.1611E−01

Table 9. Optimization Results Obtained Using Free Wake Theory for Rotor of Fig.(4-3) with Design Variable Set(8)

OPTIMIZATION OF ROTOR OF FIG.(4-3) WITH DESIGN VARIABLE SET (8)

OBJ=CP/CT+WFN*(CTT-CT)**2, WFN=1.3*WFO, AND WF(INITIAL)=100000.0

NO. OF BLADES = 2 SIGT =0.0464 SIG =0.0464

CT =0.00452 CP =0.000339 FM =0.635 CT/CP =13.348 OBJ = 0.7552E-01

CTT =0.00459 CPI =0.000233 CVT1(LOCAL) =0.00050 CVT2(GLOBAL) =0.00500

ETA	CHORD	THETA	ALPHA	WLA	UT	CL	GAM
.150	0.7290E-01	17.1337	8.0549	-0.2397E-01	0.1519E+00	0.8658E+00	0.4794E-02
.225	0.7290E-01	16.2170	8.6486	-0.2990E-01	0.2270E+00	0.9300E+00	0.7695E-02
.275	0.7290E-01	15.6058	8.8532	-0.3256E-01	0.2769E+00	0.9517E+00	0.9606E-02
.350	0.7290E-01	14.6891	8.4609	-0.3820E-01	0.3521E+00	0.9079E+00	0.1165E-01
.500	0.7290E-01	12.8556	6.8070	-0.5298E-01	0.5028E+00	0.7261E+00	0.1331E-01
.670	0.7290E-01	10.7777	5.3578	-0.6357E-01	0.6730E+00	0.5755E+00	0.1412E-01
.760	0.7290E-01	9.6776	4.9156	-0.6331E-01	0.7626E+00	0.5295E+00	0.1472E-01
.800	0.7290E-01	9.1888	4.8084	-0.6128E-01	0.8023E+00	0.5187E+00	0.1517E-01
.840	0.7290E-01	8.6999	4.8508	-0.5652E-01	0.8419E+00	0.5231E+00	0.1605E-01
.880	0.7290E-01	8.2110	5.2666	-0.4526E-01	0.8812E+00	0.5639E+00	0.1811E-01
.910	0.7290E-01	7.8443	5.4927	-0.3737E-01	0.9108E+00	0.5860E+00	0.1945E-01
.930	0.7290E-01	7.5998	5.4204	-0.3539E-01	0.9307E+00	0.5783E+00	0.1962E-01
.950	0.7290E-01	7.3554	5.0828	-0.3770E-01	0.9507E+00	0.5427E+00	0.1881E-01
.970	0.7290E-01	7.1110	4.4563	-0.4497E-01	0.9710E+00	0.4762E+00	0.1686E-01
.990	0.7290E-01	6.8665	3.3239	-0.6129E-01	0.9919E+00	0.3552E+00	0.1284E-01

NO. OF BLADES = 2 SIGT =0.0457 SIG =0.0464

CT =0.00459 CP =0.000344 FM =0.639 CT/CP =13.344 OBJ = 0.7494E-01

CTT =0.00459 CPI =0.000238 CVT1(LOCAL) =0.00050 CVT2(GLOBAL) =0.00500

ETA	CHORD	THETA	ALPHA	WLA	UT	CL	GAM
.150	0.7177E-01	17.3528	8.2672	-0.2399E-01	0.1519E+00	0.8889E+00	0.4845E-02
.225	0.7177E-01	16.4366	8.8607	-0.2992E-01	0.2270E+00	0.9530E+00	0.7762E-02
.275	0.7177E-01	15.8258	9.0662	-0.3259E-01	0.2769E+00	0.9748E+00	0.9687E-02
.350	0.7177E-01	14.9095	8.6666	-0.3829E-01	0.3521E+00	0.9302E+00	0.1175E-01
.500	0.7177E-01	13.0771	6.9926	-0.5330E-01	0.5028E+00	0.7462E+00	0.1346E-01
.670	0.7177E-01	11.0003	5.5469	-0.6396E-01	0.6730E+00	0.5958E+00	0.1439E-01
.760	0.7177E-01	9.8971	5.0961	-0.6383E-01	0.7627E+00	0.5489E+00	0.1502E-01
.800	0.7177E-01	9.3931	4.9821	-0.6171E-01	0.8024E+00	0.5374E+00	0.1547E-01
.840	0.7176E-01	8.8892	5.0195	-0.5682E-01	0.8419E+00	0.5412E+00	0.1635E-01
.880	0.7176E-01	8.3853	5.4270	-0.4548E-01	0.8812E+00	0.5811E+00	0.1837E-01
.910	0.7176E-01	8.0073	5.6382	-0.3765E-01	0.9108E+00	0.6017E+00	0.1966E-01
.930	0.7176E-01	7.7554	5.5557	-0.3572E-01	0.9307E+00	0.5928E+00	0.1980E-01
.950	0.7176E-01	7.5034	5.2075	-0.3809E-01	0.9508E+00	0.5561E+00	0.1897E-01
.970	0.7176E-01	7.2515	4.5667	-0.4549E-01	0.9711E+00	0.4881E+00	0.1701E-01
.990	0.7176E-01	6.9995	3.4089	-0.6212E-01	0.9919E+00	0.3643E+00	0.1297E-01

NO. OF BLADES = 2 SIGT =0.0453 SIG =0.0464

CT =0.00457 CP =0.000342 FM =0.639 CT/CP =13.373 OBJ = 0.7482E-01

Table 9. -Continued

CTT =0.00459 CPI =0.000237 CVT1(LOCAL) =0.00050 CVT2(GLOBAL) =0.00500

ETA	CHORD	THETA	ALPHA	WLA	UT	CL	GAM
.150	0.7111E-01	17.3806	8.3138	-0.2394E-01	0.1519E+00	0.8940E+00	0.4829E-02
.225	0.7111E-01	16.4647	8.9087	-0.2985E-01	0.2270E+00	0.9583E+00	0.7733E-02
.275	0.7111E-01	15.8541	9.1147	-0.3250E-01	0.2769E+00	0.9801E+00	0.9650E-02
.350	0.7111E-01	14.9382	8.7142	-0.3817E-01	0.3521E+00	0.9354E+00	0.1171E-01
.500	0.7111E-01	13.1065	7.0345	-0.5319E-01	0.5028E+00	0.7507E+00	0.1342E-01
.670	0.7111E-01	11.0305	5.5836	-0.6389E-01	0.6730E+00	0.5998E+00	0.1435E-01
.760	0.7111E-01	9.9270	5.1300	-0.6378E-01	0.7627E+00	0.5525E+00	0.1498E-01
.800	0.7111E-01	9.4209	5.0133	-0.6166E-01	0.8024E+00	0.5408E+00	0.1543E-01
.840	0.7111E-01	8.9149	5.0474	-0.5679E-01	0.8419E+00	0.5442E+00	0.1629E-01
.880	0.7111E-01	8.4088	5.4546	-0.4541E-01	0.8812E+00	0.5841E+00	0.1830E-01
.910	0.7111E-01	8.0293	5.6692	-0.3751E-01	0.9108E+00	0.6050E+00	0.1959E-01
.930	0.7111E-01	7.7763	5.5876	-0.3554E-01	0.9307E+00	0.5962E+00	0.1973E-01
.950	0.7111E-01	7.5232	5.2385	-0.3790E-01	0.9508E+00	0.5595E+00	0.1891E-01
.970	0.7110E-01	7.2702	4.5952	-0.4532E-01	0.9711E+00	0.4911E+00	0.1696E-01
.990	0.7110E-01	7.0172	3.4320	-0.6203E-01	0.9919E+00	0.3668E+00	0.1293E-01

NO. OF BLADES = 2 SIGT =0.0451 SIG =0.0464

CT =0.00457 CP =0.000341 FM =0.640 CT/CP =13.386 OBJ = 0.7480E-01

CTT =0.00459 CPI =0.000237 CVT1(LOCAL) =0.00050 CVT2(GLOBAL) =0.00500

ETA	CHORD	THETA	ALPHA	WLA	UT	CL	GAM
.150	0.7084E-01	17.3843	8.3291	-0.2391E-01	0.1519E+00	0.8957E+00	0.4819E-02
.225	0.7084E-01	16.4703	8.9253	-0.2980E-01	0.2270E+00	0.9601E+00	0.7719E-02
.275	0.7084E-01	15.8609	9.1320	-0.3245E-01	0.2769E+00	0.9820E+00	0.9632E-02
.350	0.7084E-01	14.9468	8.7320	-0.3811E-01	0.3521E+00	0.9373E+00	0.1169E-01
.500	0.7084E-01	13.1187	7.0513	-0.5315E-01	0.5028E+00	0.7526E+00	0.1340E-01
.670	0.7084E-01	11.0468	5.6020	-0.6386E-01	0.6730E+00	0.6018E+00	0.1435E-01
.760	0.7084E-01	9.9445	5.1474	-0.6378E-01	0.7627E+00	0.5544E+00	0.1498E-01
.800	0.7084E-01	9.4356	5.0287	-0.6165E-01	0.8024E+00	0.5424E+00	0.1542E-01
.840	0.7084E-01	8.9267	5.0601	-0.5677E-01	0.8419E+00	0.5456E+00	0.1627E-01
.880	0.7084E-01	8.4177	5.4662	-0.4537E-01	0.8812E+00	0.5854E+00	0.1827E-01
.910	0.7083E-01	8.0361	5.6813	-0.3742E-01	0.9108E+00	0.6063E+00	0.1956E-01
.930	0.7083E-01	7.7816	5.5994	-0.3544E-01	0.9307E+00	0.5975E+00	0.1969E-01
.950	0.7083E-01	7.5272	5.2494	-0.3779E-01	0.9508E+00	0.5606E+00	0.1888E-01
.970	0.7083E-01	7.2727	4.6048	-0.4520E-01	0.9711E+00	0.4922E+00	0.1693E-01
.990	0.7083E-01	7.0183	3.4396	-0.6192E-01	0.9919E+00	0.3676E+00	0.1291E-01

Table 10. Optimization Results Obtained by Using Free Wake Theory for Rotor of Fig.(4-7) with Design Variable Set(8)

OPTIMIZATION OF ROTOR OF FIG.(4-7) WITH DESIGN VARIABLE SET(8)

OBJ=CP/CT + WFN*(CTT-CT)**2, WFN=1.3*WFO, AND WF(INITIAL)=100000.0

NO. OF BLADES = 2 SIGT =0.0419 SIG =0.0464

CT =0.00333 CP =0.000213 FM =0.638 CT/CP =15.639 OBJ = 0.6766E-01

CTT =0.00350 CPI =0.000138 CVT1(LOCAL) =0.00050 CVT2(GLOBAL) =0.00500

ETA	CHORD	THETA	ALPHA	WLA	UT	CL	GAM
.150	0.7290E-01	20.0535	8.9666	-0.2939E-01	0.1529E+00	0.9498E+00	0.5292E-02
.225	0.7290E-01	18.6211	9.1570	-0.3751E-01	0.2281E+00	0.9753E+00	0.8109E-02
.275	0.7290E-01	17.6662	9.0014	-0.4191E-01	0.2782E+00	0.9602E+00	0.9736E-02
.350	0.7290E-01	16.2338	8.2461	-0.4911E-01	0.3534E+00	0.8801E+00	0.1134E-01
.500	0.7290E-01	13.3690	6.9206	-0.5651E-01	0.5032E+00	0.7406E+00	0.1358E-01
.670	0.7290E-01	10.1223	5.4363	-0.5492E-01	0.6722E+00	0.5836E+00	0.1430E-01
.760	0.7086E-01	8.2506	4.7952	-0.4589E-01	0.7614E+00	0.5150E+00	0.1389E-01
.800	0.6269E-01	6.8755	4.7642	-0.2949E-01	0.8005E+00	0.5099E+00	0.1279E-01
.840	0.5453E-01	5.5004	4.5124	-0.1449E-01	0.8401E+00	0.4814E+00	0.1103E-01
.880	0.4636E-01	4.1253	3.8999	-0.3461E-02	0.8800E+00	0.4159E+00	0.8485E-02
.910	0.4024E-01	3.0940	3.2755	0.2884E-02	0.9100E+00	0.3493E+00	0.6396E-02
.930	0.3616E-01	2.4064	2.7238	0.5151E-02	0.9300E+00	0.2905E+00	0.4884E-02
.950	0.3208E-01	1.7189	2.1690	0.7463E-02	0.9500E+00	0.2312E+00	0.3522E-02
.970	0.2799E-01	1.0313	1.5877	0.9420E-02	0.9700E+00	0.1690E+00	0.2295E-02
.990	0.2391E-01	0.3438	0.9585	0.1062E-01	0.9901E+00	0.1018E+00	0.1205E-02

NO. OF BLADES = 2 SIGT =0.0417 SIG =0.0464

CT =0.00332 CP =0.000212 FM =0.638 CT/CP =15.662 OBJ = 0.6711E-01

CTT =0.00350 CPI =0.000138 CVT1(LOCAL) =0.00050 CVT2(GLOBAL) =0.00500

ETA	CHORD	THETA	ALPHA	WLA	UT	CL	GAM
.150	0.7251E-01	20.0551	8.9866	-0.2934E-01	0.1528E+00	0.9520E+00	0.5275E-02
.225	0.7251E-01	18.6231	9.1776	-0.3743E-01	0.2281E+00	0.9775E+00	0.8084E-02
.275	0.7251E-01	17.6684	9.0208	-0.4182E-01	0.2782E+00	0.9624E+00	0.9705E-02
.350	0.7251E-01	16.2364	8.2629	-0.4902E-01	0.3534E+00	0.8820E+00	0.1130E-01
.500	0.7251E-01	13.3723	6.9345	-0.5642E-01	0.5032E+00	0.7421E+00	0.1354E-01
.670	0.7251E-01	10.1264	5.4477	-0.5483E-01	0.6722E+00	0.5848E+00	0.1425E-01
.760	0.7048E-01	8.2551	4.8044	-0.4583E-01	0.7614E+00	0.5159E+00	0.1384E-01
.800	0.6236E-01	6.8796	4.7726	-0.2943E-01	0.8005E+00	0.5108E+00	0.1275E-01
.840	0.5424E-01	5.5041	4.5201	-0.1443E-01	0.8401E+00	0.4823E+00	0.1099E-01
.880	0.4612E-01	4.1286	3.9059	-0.3421E-02	0.8800E+00	0.4166E+00	0.8452E-02
.910	0.4003E-01	3.0970	3.2798	0.2904E-02	0.9100E+00	0.3498E+00	0.6371E-02
.930	0.3596E-01	2.4093	2.7270	0.5158E-02	0.9300E+00	0.2908E+00	0.4863E-02
.950	0.3190E-01	1.7215	2.1713	0.7457E-02	0.9500E+00	0.2314E+00	0.3507E-02
.970	0.2784E-01	1.0338	1.5892	0.9403E-02	0.9700E+00	0.1692E+00	0.2285E-02
.990	0.2378E-01	0.3461	0.9593	0.1060E-01	0.9901E+00	0.1019E+00	0.1199E-02

NO. OF BLADES = 2 SIGT =0.0328 SIG =0.0464

CT =0.00351 CP =0.000221 FM =0.667 CT/CP =15.918 OBJ = 0.6284E-01

Table 10. -Continued

CTT =0.00350 CPI =0.000152 CVT1(LOCAL) =0.00050 CVT2(GLOBAL) =0.00500

ETA	CHORD	THETA	ALPHA	WLA	UT	CL	GAM
.150	0.5671E-01	20.8817	10.6997	-0.2694E-01	0.1524E+00	0.1139E+01	0.4923E-02
.225	0.5671E-01	19.6395	11.1200	-0.3370E-01	0.2275E+00	0.1189E+01	0.7669E-02
.275	0.5671E-01	18.8113	11.0855	-0.3731E-01	0.2775E+00	0.1187E+01	0.9336E-02
.350	0.5671E-01	17.5691	10.2567	-0.4491E-01	0.3529E+00	0.1097E+01	0.1098E-01
.500	0.5671E-01	15.0846	8.6077	-0.5676E-01	0.5032E+00	0.9213E+00	0.1314E-01
.670	0.5671E-01	12.2689	7.3022	-0.5822E-01	0.6725E+00	0.7833E+00	0.1494E-01
.760	0.5671E-01	10.7782	6.5586	-0.5607E-01	0.7621E+00	0.7035E+00	0.1520E-01
.800	0.5049E-01	9.3121	6.4549	-0.3993E-01	0.8010E+00	0.6910E+00	0.1397E-01
.840	0.4381E-01	7.7846	6.2544	-0.2244E-01	0.8403E+00	0.6674E+00	0.1228E-01
.880	0.3712E-01	6.2571	5.7031	-0.8509E-02	0.8800E+00	0.6083E+00	0.9934E-02
.910	0.3210E-01	5.1114	5.0532	-0.9243E-03	0.9100E+00	0.5392E+00	0.7876E-02
.930	0.2876E-01	4.3477	4.4456	0.1590E-02	0.9300E+00	0.4745E+00	0.6345E-02
.950	0.2541E-01	3.5839	3.8176	0.3875E-02	0.9500E+00	0.4076E+00	0.4920E-02
.970	0.2207E-01	2.8202	3.1285	0.5219E-02	0.9700E+00	0.3340E+00	0.3575E-02
.990	0.1873E-01	2.0564	2.2803	0.3868E-02	0.9900E+00	0.2433E+00	0.2256E-02

NO. OF BLADES = 2 SIGT =0.0328 SIG =0.0464

CT =0.00349 CP =0.000219 FM =0.666 CT/CP =15.946 OBJ = 0.6274E-01

CTT =0.00350 CPI =0.000150 CVT1(LOCAL) =0.00050 CVT2(GLOBAL) =0.00500

ETA	CHORD	THETA	ALPHA	WLA	UT	CL	GAM
.150	0.5668E-01	20.7863	10.6279	-0.2688E-01	0.1524E+00	0.1132E+01	0.4887E-02
.225	0.5668E-01	19.5482	11.0516	-0.3361E-01	0.2275E+00	0.1182E+01	0.7618E-02
.275	0.5668E-01	18.7229	11.0182	-0.3720E-01	0.2775E+00	0.1179E+01	0.9274E-02
.350	0.5668E-01	17.4848	10.1926	-0.4479E-01	0.3529E+00	0.1091E+01	0.1091E-01
.500	0.5668E-01	15.0088	8.5516	-0.5659E-01	0.5032E+00	0.9153E+00	0.1305E-01
.670	0.5668E-01	12.2026	7.2534	-0.5802E-01	0.6725E+00	0.7780E+00	0.1483E-01
.760	0.5668E-01	10.7170	6.5146	-0.5584E-01	0.7620E+00	0.6987E+00	0.1509E-01
.800	0.5048E-01	9.2574	6.4121	-0.3976E-01	0.8010E+00	0.6864E+00	0.1388E-01
.840	0.4380E-01	7.7349	6.2150	-0.2229E-01	0.8403E+00	0.6632E+00	0.1220E-01
.880	0.3711E-01	6.2125	5.6658	-0.8397E-02	0.8800E+00	0.6043E+00	0.9867E-02
.910	0.3209E-01	5.0706	5.0173	-0.8477E-03	0.9100E+00	0.5353E+00	0.7817E-02
.930	0.2875E-01	4.3094	4.4112	0.1653E-02	0.9300E+00	0.4708E+00	0.6294E-02
.950	0.2541E-01	3.5482	3.7851	0.3927E-02	0.9500E+00	0.4041E+00	0.4876E-02
.970	0.2206E-01	2.7870	3.0984	0.5272E-02	0.9700E+00	0.3307E+00	0.3539E-02
.990	0.1872E-01	2.0257	2.2549	0.3960E-02	0.9900E+00	0.2406E+00	0.2230E-02

Table 11. Optimization Results Obtained by Using Free Wake Theory

NO. OF BLADES = 2 SIGT =0.0464 SIG =0.0464

CT =0.00455 CP =0.000342 FM =0.635 CT/CP =13.309 OBJ = 0.7532E-01

CTT =0.00459 CPI =0.000236 CVT1(LOCAL) =0.00050 CVT2(GLOBAL) =0.00500

ETA	CHORD	THETA	ALPHA	WLA	UT	CL	GAM
.150	0.7290E-01	17.1337	10.1922	-0.1826E-01	0.1511E+00	0.1103E+01	0.6073E-02
.225	0.7290E-01	16.2170	10.0533	-0.2430E-01	0.2263E+00	0.1085E+01	0.8951E-02
.275	0.7290E-01	15.6038	9.8621	-0.2766E-01	0.2764E+00	0.1063E+01	0.1071E-01
.350	0.7290E-01	14.6891	8.9327	-0.3526E-01	0.3518E+00	0.9607E+00	0.1232E-01
.500	0.7290E-01	12.8556	6.8348	-0.5274E-01	0.5028E+00	0.7344E+00	0.1346E-01
.670	0.7290E-01	10.7777	5.8762	-0.5746E-01	0.6725E+00	0.6323E+00	0.1550E-01
.760	0.7288E-01	9.4776	5.3966	-0.5689E-01	0.7621E+00	0.5803E+00	0.1612E-01
.800	0.7288E-01	9.1888	5.2268	-0.5541E-01	0.8019E+00	0.5616E+00	0.1641E-01
.840	0.7288E-01	8.6999	5.0641	-0.5339E-01	0.8417E+00	0.5432E+00	0.1666E-01
.880	0.7288E-01	8.2110	4.9132	-0.5071E-01	0.8815E+00	0.5257E+00	0.1689E-01
.910	0.7288E-01	7.8443	4.7604	-0.4902E-01	0.9113E+00	0.5083E+00	0.1688E-01
.930	0.7288E-01	7.5998	4.5963	-0.4880E-01	0.9313E+00	0.4900E+00	0.1663E-01
.950	0.7288E-01	7.3554	4.3185	-0.5040E-01	0.9513E+00	0.4601E+00	0.1595E-01
.970	0.7288E-01	7.1110	3.8346	-0.5553E-01	0.9716E+00	0.4083E+00	0.1446E-01
.990	0.7288E-01	6.8665	2.9052	-0.6856E-01	0.9924E+00	0.3091E+00	0.1118E-01

NO. OF BLADES = 2 SIGT =0.0464 SIG =0.0464

CT =0.00458 CP =0.000344 FM =0.636 CT/CP =13.298 OBJ = 0.7521E-01

CTT =0.00459 CPI =0.000239 CVT1(LOCAL) =0.00050 CVT2(GLOBAL) =0.00500

ETA	CHORD	THETA	ALPHA	WLA	UT	CL	GAM
.150	0.7290E-01	17.2022	10.2497	-0.1829E-01	0.1511E+00	0.1109E+01	0.6107E-02
.225	0.7290E-01	16.2850	10.1098	-0.2434E-01	0.2263E+00	0.1091E+01	0.9001E-02
.275	0.7290E-01	15.6736	9.9198	-0.2771E-01	0.2764E+00	0.1069E+01	0.1077E-01
.350	0.7290E-01	14.7564	8.9906	-0.3534E-01	0.3518E+00	0.9670E+00	0.1240E-01
.500	0.7290E-01	12.9221	6.8857	-0.5287E-01	0.5028E+00	0.7399E+00	0.1356E-01
.670	0.7290E-01	10.8432	5.9245	-0.5767E-01	0.6725E+00	0.6374E+00	0.1562E-01
.760	0.7288E-01	9.5410	5.4413	-0.5714E-01	0.7621E+00	0.5851E+00	0.1625E-01
.800	0.7288E-01	9.2449	5.2685	-0.5561E-01	0.8019E+00	0.5661E+00	0.1654E-01
.840	0.7288E-01	8.7489	5.1015	-0.5355E-01	0.8417E+00	0.5473E+00	0.1679E-01
.880	0.7288E-01	8.2528	4.9482	-0.5081E-01	0.8815E+00	0.5295E+00	0.1701E-01
.910	0.7288E-01	7.8808	4.7921	-0.4910E-01	0.9113E+00	0.5116E+00	0.1699E-01
.930	0.7288E-01	7.6328	4.6242	-0.4884E-01	0.9313E+00	0.4930E+00	0.1673E-01
.950	0.7288E-01	7.3848	4.3424	-0.5049E-01	0.9513E+00	0.4626E+00	0.1604E-01
.970	0.7288E-01	7.1368	3.8538	-0.5564E-01	0.9716E+00	0.4104E+00	0.1453E-01
.990	0.7288E-01	6.8887	2.9183	-0.6871E-01	0.9924E+00	0.3105E+00	0.1123E-01

NO. OF BLADES = 2 SIGT =0.0464 SIG =0.0464

CT =0.00454 CP =0.000332 FM =0.631 CT/CP =13.666 OBJ = 0.7349E-01

CTT =0.00459 CPI =0.000227 CVT1(LOCAL) =0.00050 CVT2(GLOBAL) =0.00500

_DUA1:[USER.FLUIDS.CHUNG]OPT.DAT;3 24-AUG-1985 20:42

ETA	CHORD	THETA	ALPHA	WLA	UT	CL	GAM
.150	0.7290E-01	17.2769	9.9348	-0.1933E-01	0.1512E+00	0.1073E+01	0.5915E-02
.225	0.7290E-01	16.3692	9.9085	-0.2548E-01	0.2264E+00	0.1069E+01	0.8822E-02
.275	0.7290E-01	15.7641	9.7692	-0.2888E-01	0.2765E+00	0.1053E+01	0.1062E-01
.350	0.7290E-01	14.8565	8.9021	-0.3650E-01	0.3519E+00	0.9591E+00	0.1230E-01
.500	0.7290E-01	13.0412	6.9935	-0.5297E-01	0.5028E+00	0.7521E+00	0.1378E-01
.670	0.7290E-01	10.9839	6.0710	-0.5759E-01	0.6725E+00	0.6528E+00	0.1600E-01
.760	0.7288E-01	9.8395	5.5408	-0.5713E-01	0.7621E+00	0.5954E+00	0.1653E-01
.800	0.7284E-01	9.1630	5.2866	-0.5421E-01	0.8018E+00	0.5676E+00	0.1658E-01
.840	0.7281E-01	8.4864	5.0427	-0.5055E-01	0.8415E+00	0.5405E+00	0.1656E-01
.880	0.7277E-01	7.8098	4.8236	-0.4591E-01	0.8812E+00	0.5155E+00	0.1653E-01
.910	0.7275E-01	7.3023	4.6091	-0.4281E-01	0.9110E+00	0.4916E+00	0.1629E-01
.930	0.7273E-01	6.9640	4.3907	-0.4180E-01	0.9309E+00	0.4679E+00	0.1584E-01
.950	0.7271E-01	6.6257	4.0630	-0.4252E-01	0.9510E+00	0.4328E+00	0.1496E-01
.970	0.7270E-01	6.2874	3.5488	-0.4610E-01	0.9711E+00	0.3780E+00	0.1334E-01
.990	0.7268E-01	5.9491	2.6440	-0.5717E-01	0.9916E+00	0.2815E+00	0.1014E-01

TABLE OF OPTIMIZATION

Table 4	Momentum, -Optimized	CT/CP=14.4	CT=0.00328	
Table 3	Constant Downwash. Free Wake	CT/CP=13.4	CT=0.00376	
Table 3	Variable Downwash. Momentum	CT/CP=13.8	CT=0.00471	
Table 5	Constant CH. Var. Twist	CT/CP=14.25	CT=0.00422	
Table 6	Same as 5, Constrained	CT/CP=15.46	CT=0.00416	*
Table 7	Tapered and Double Twisted	CT/CP=14.7	CT=0.00416	
Table 8	Same as 7, Constrained	CT/CP=13.9	CT=0.00450	
Fig.4-3	Johnson Rotor	CT/CP=13.6	CT=0.00459	
Table 9	Same as 8 with Var. Solidity	CT/CP=13.39	CT=0.00457	
Table 10	Same as 9 with Double Twist	CT/CP=15.946	CT=0.0035	**

* Questionable Result - Optimization Gave Erratic Values

** Compare to CT/CP = 15.78 at CT=0.0033 from Heuristically Optimized Rotor Geometry (Fig. 4-7)

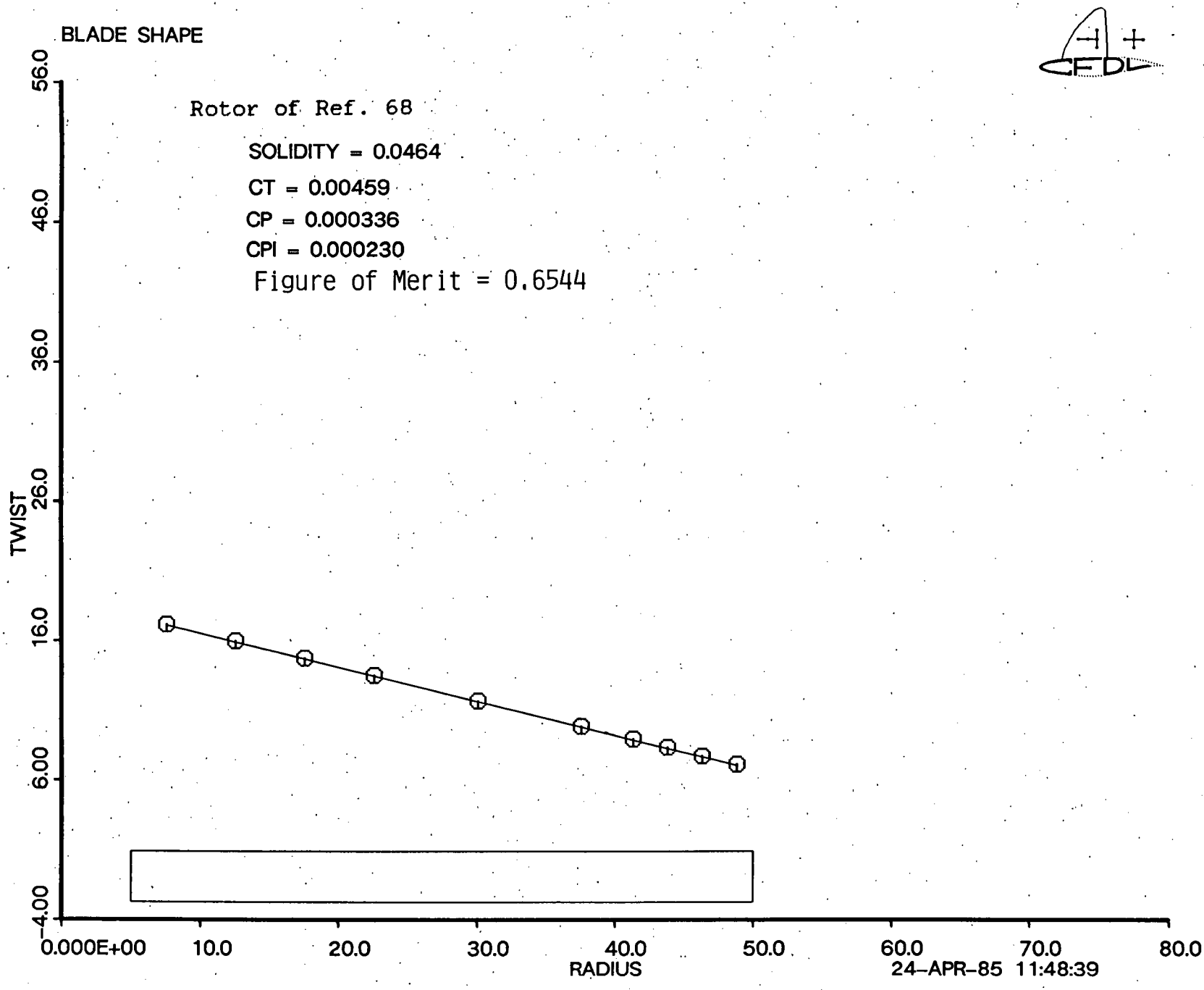

Figure 4-1 Blade Geometry of ROTOR OF REF. 68

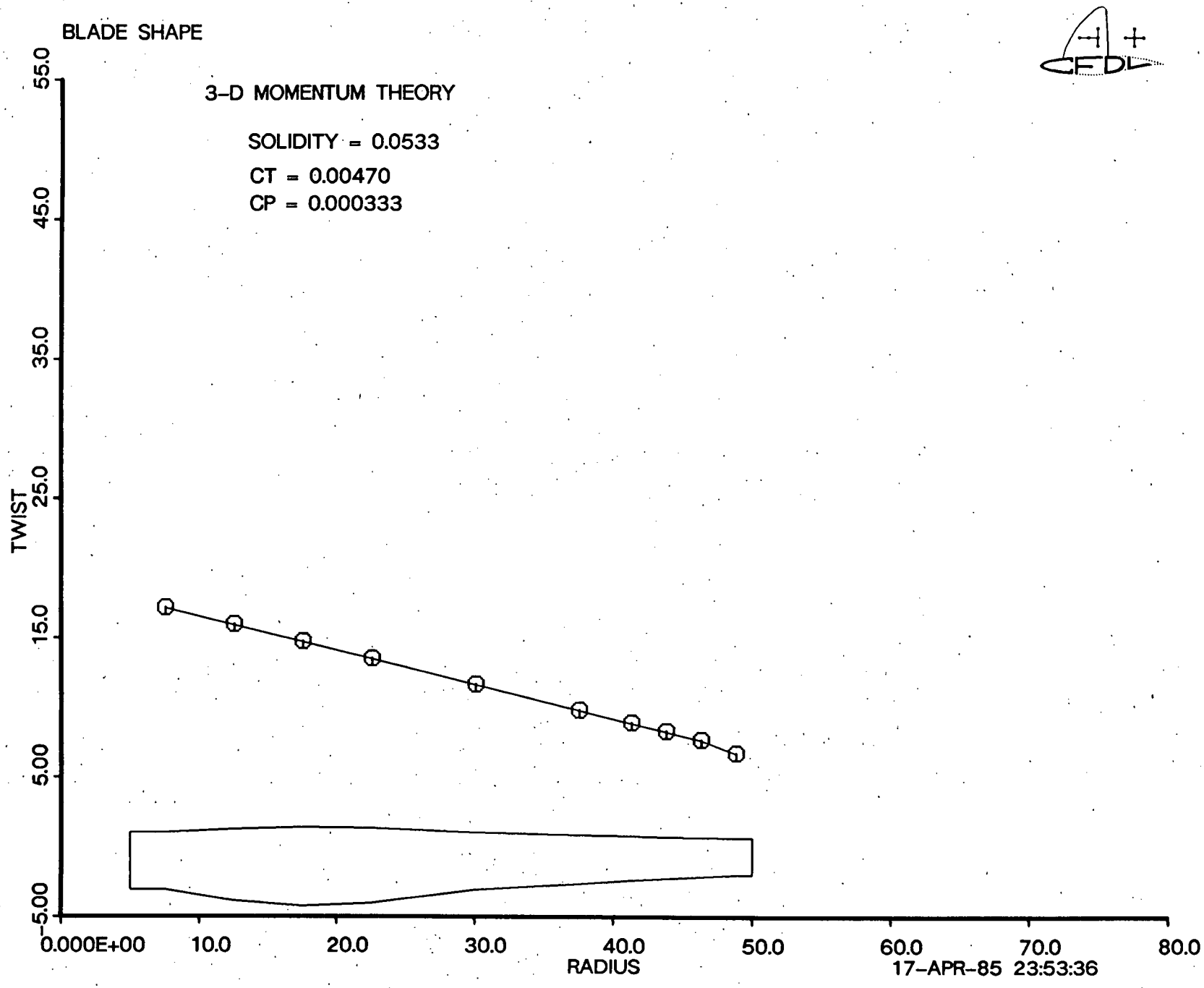

Figure 4-2. Chord Distribution Obtained by Optimization Using 3-D Momentum Theory.

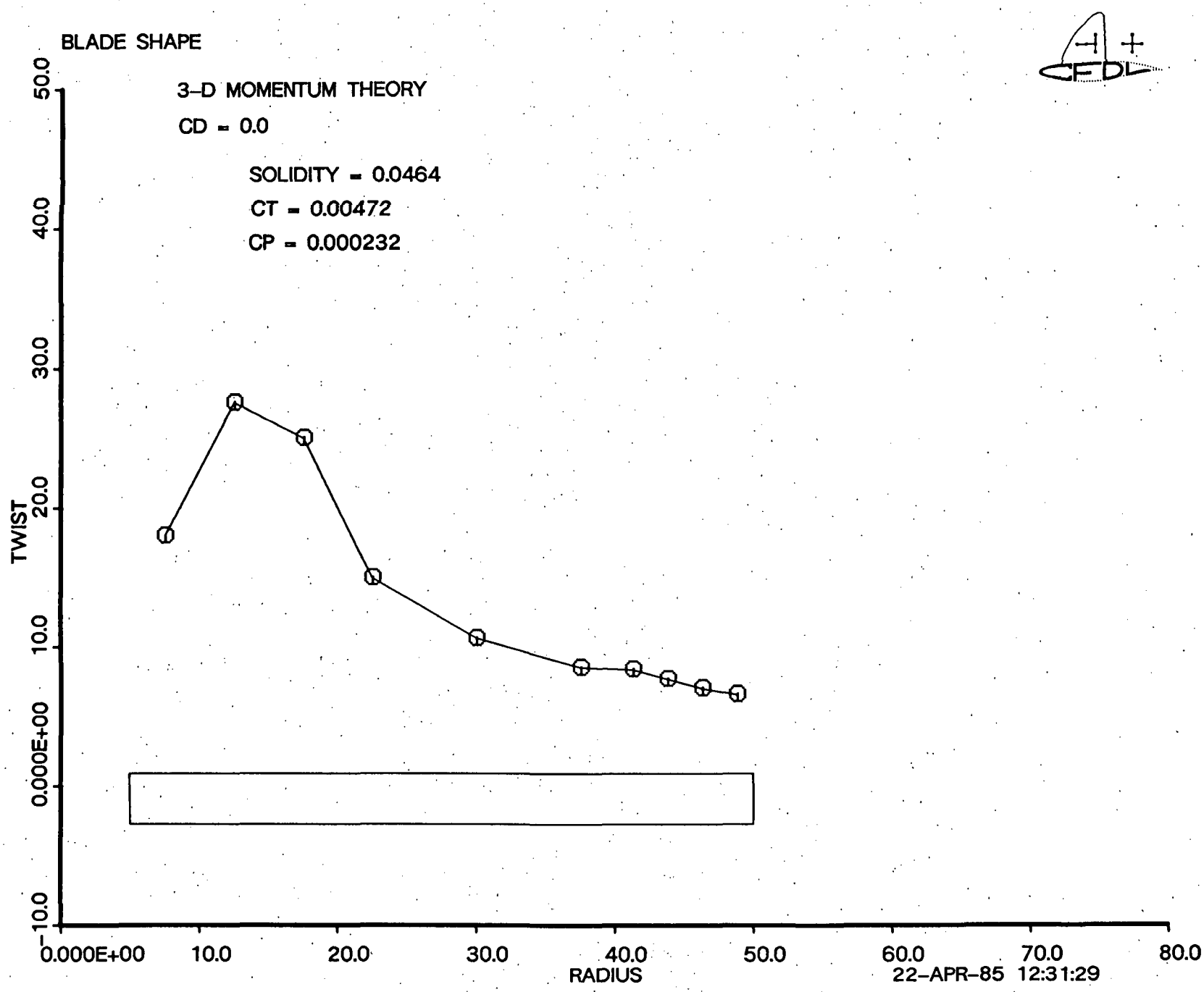

Figure 4-3. Pitch Distribution Obtained by Optimization for Fixed Chord and by Using 3-D Momentum Theory at Zero Profile Drag.

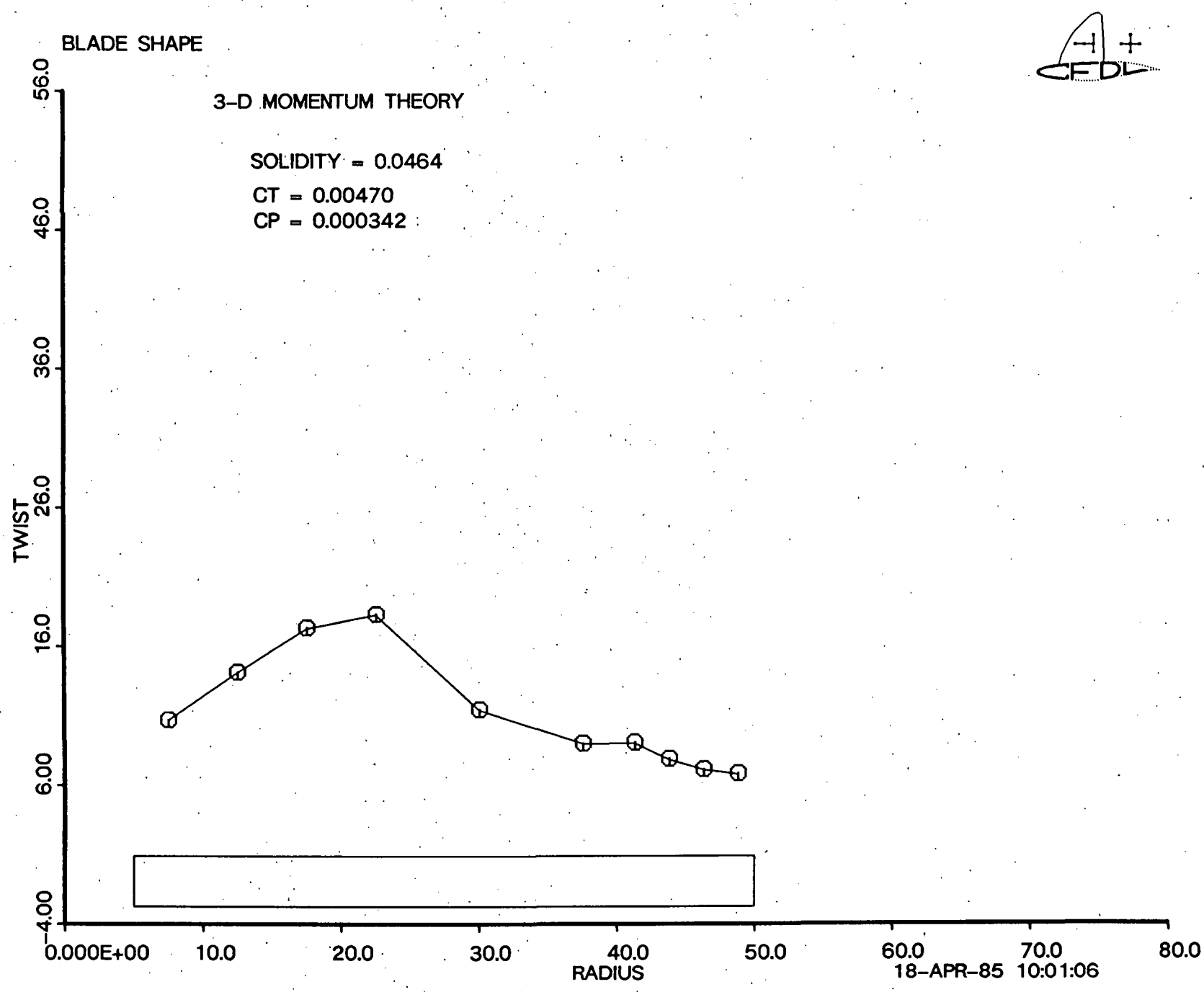

Figure 4-4. Pitch Distribution Obtained by Optimization Using 3-D Momentum Theory for Fixed Chord with $C_D = C_{DO} + C_{dk} \cdot \alpha^2$

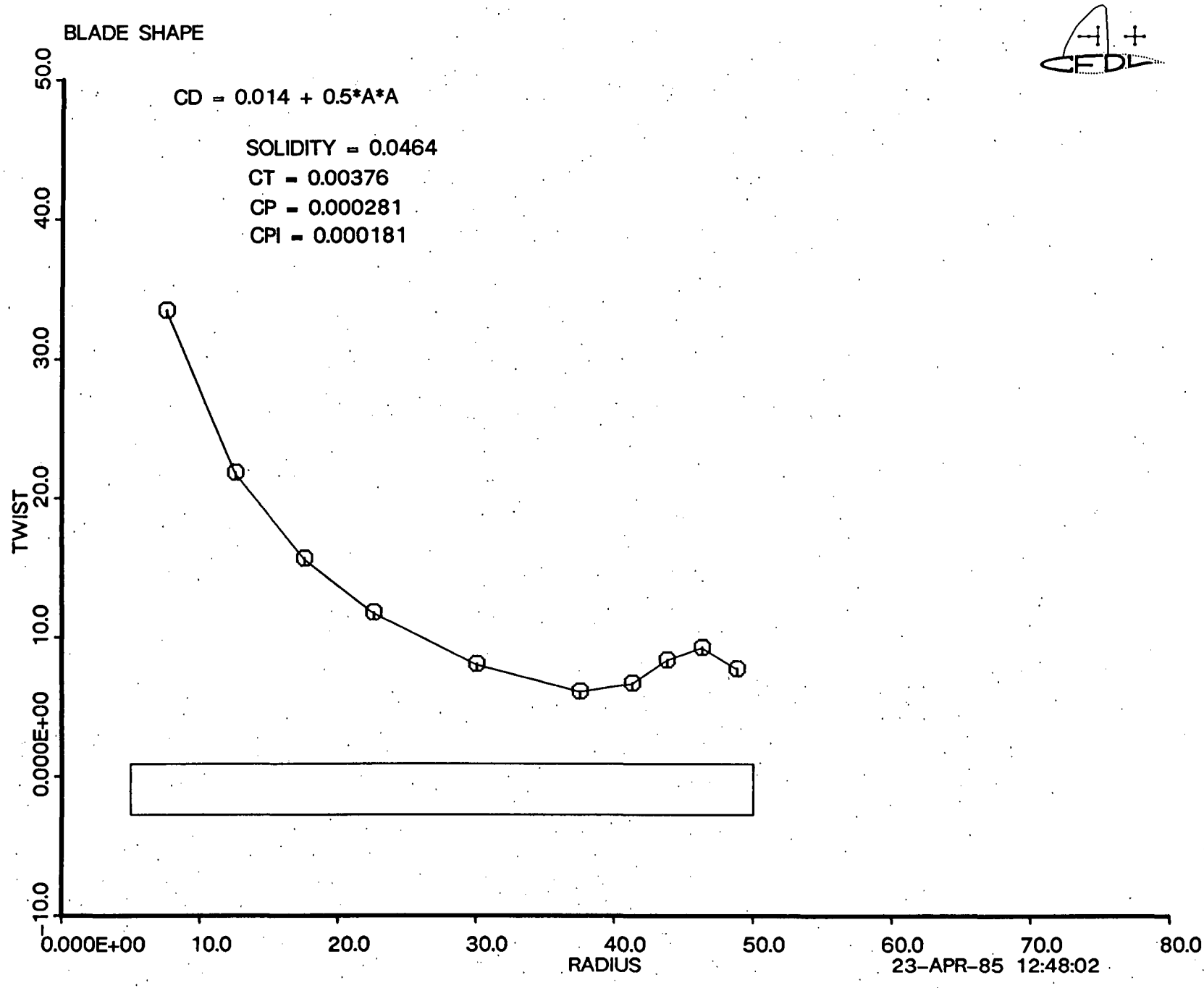

Figure 4-5. Pitch Distribution to Give A Constant Downwash.

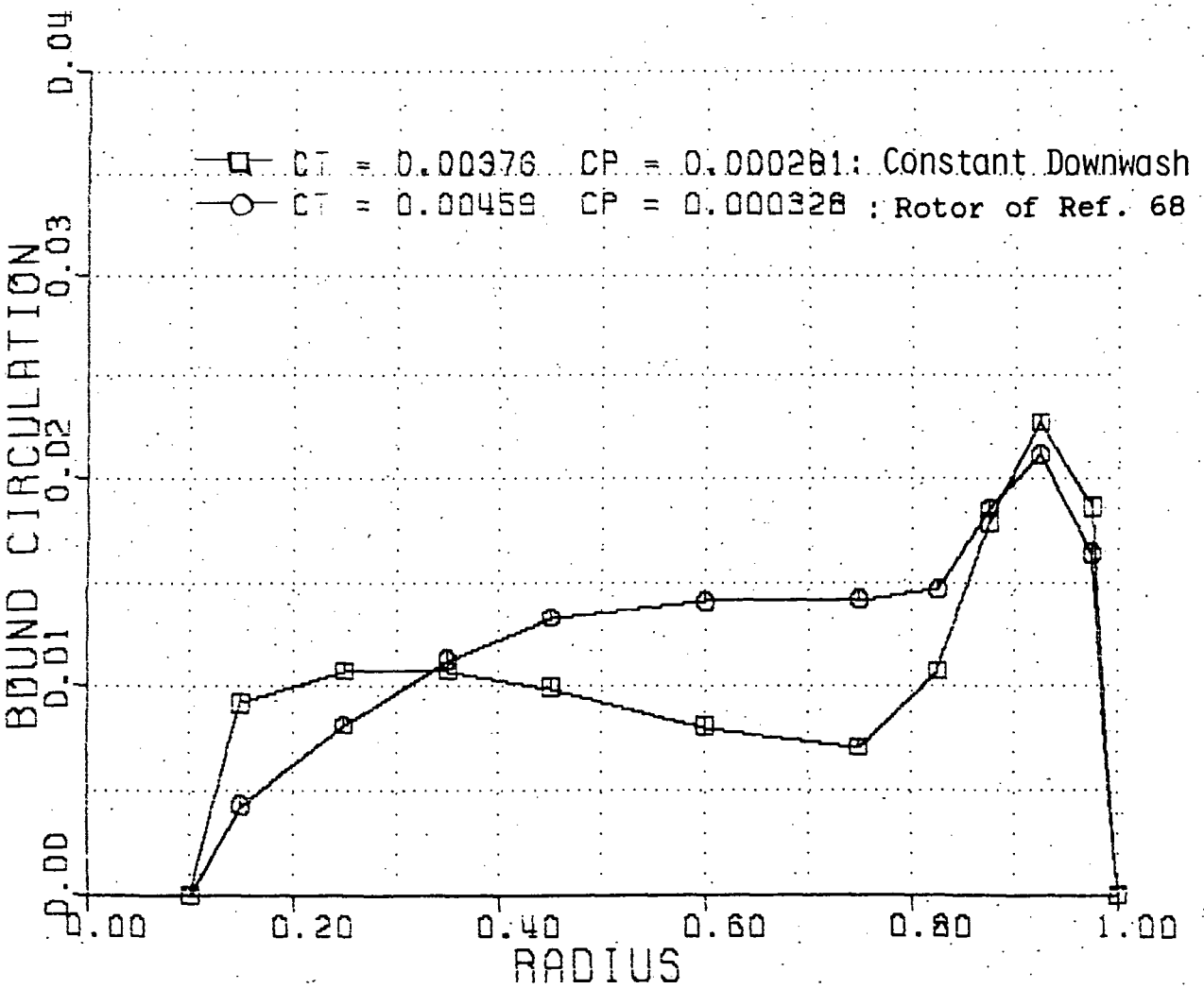

Figure 4-6. Comparison of Bound Circulation Between Rotor of Ref.35 and Rotor of Constant Downwash.

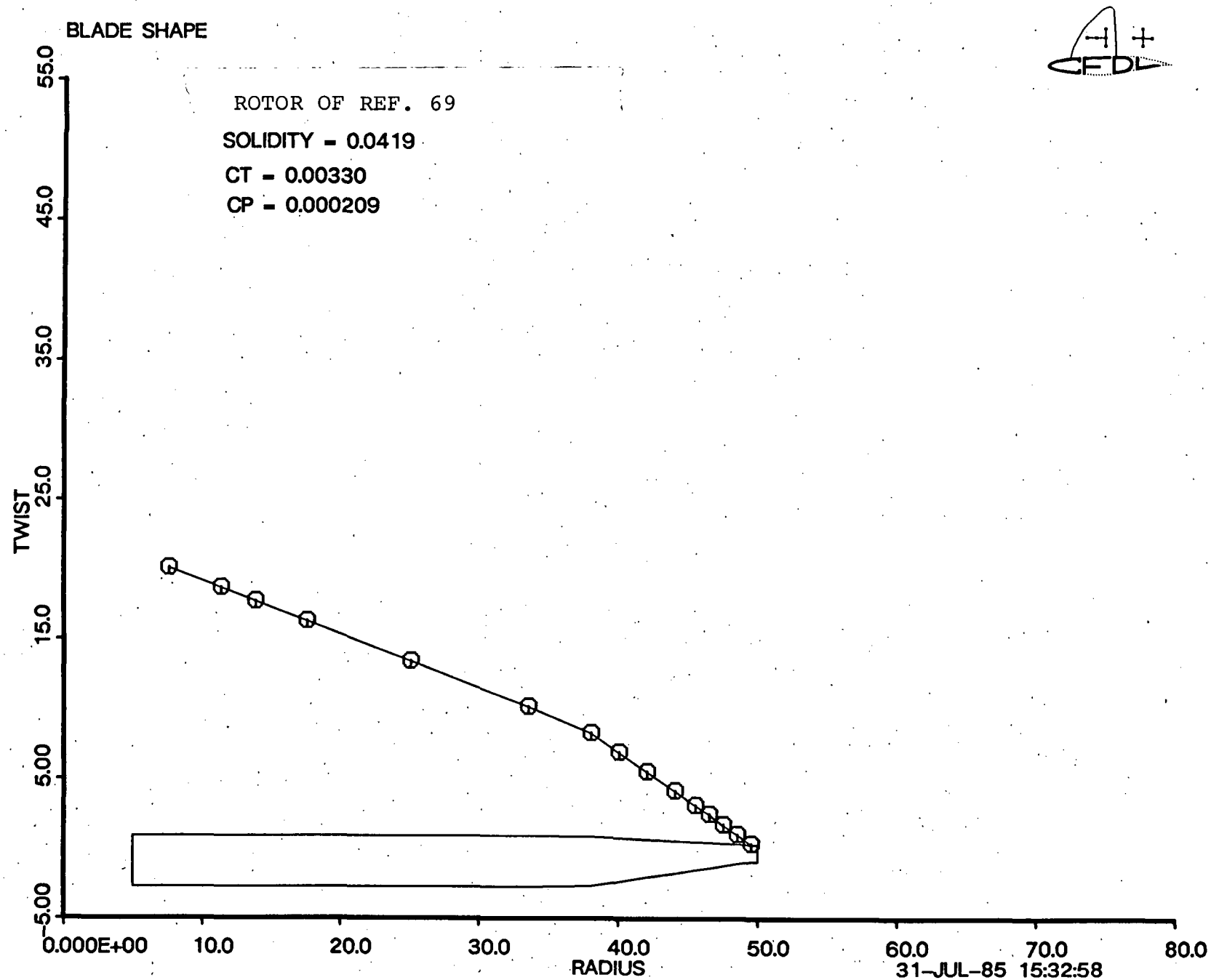

Figure 4-7. A Double Twisted and Tapered Rotor Used for Formal Optimization.

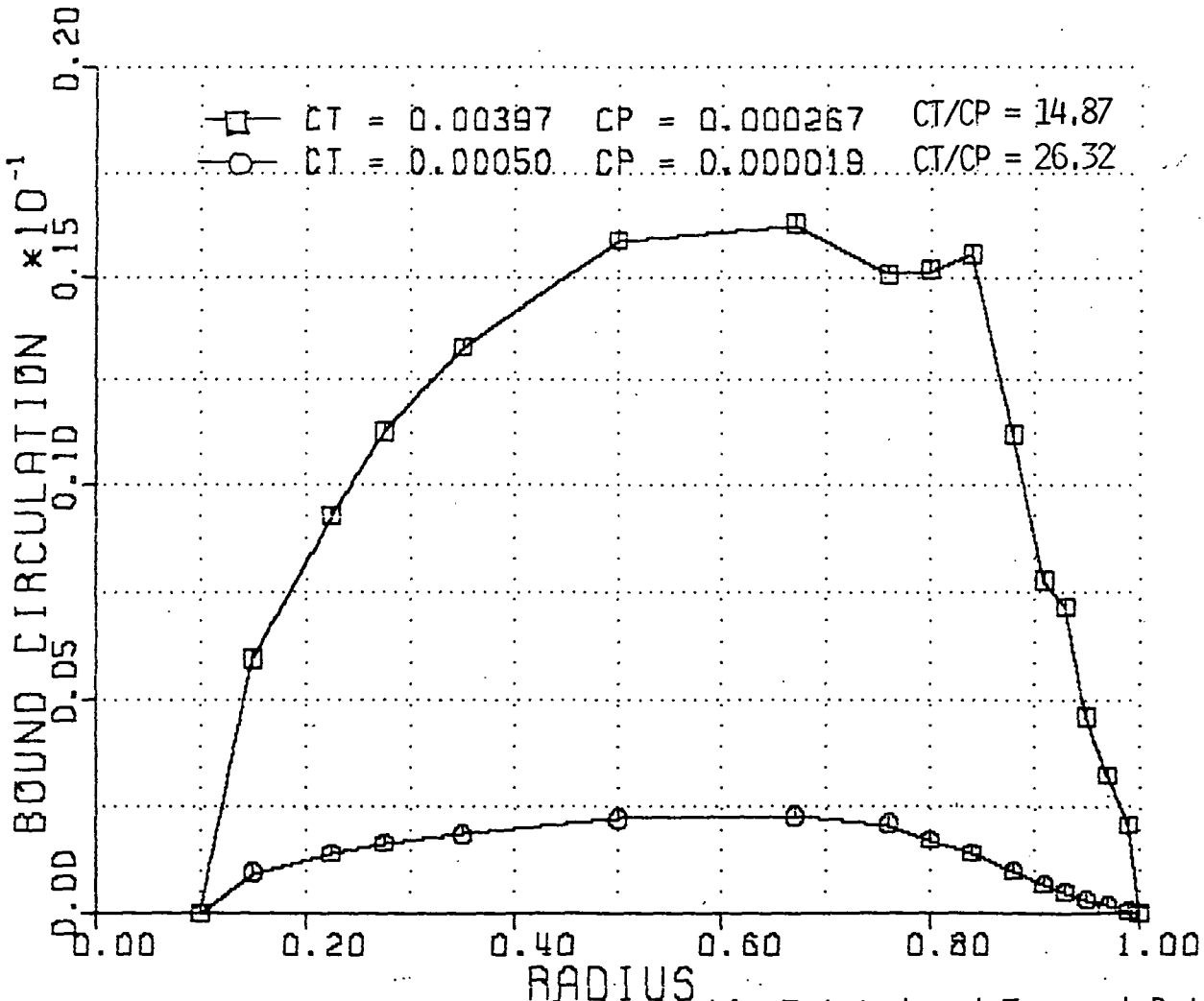

Figure 4-8. Bound Circulation of the Double Twisted and Tapered Rotor for Different Root Chord.

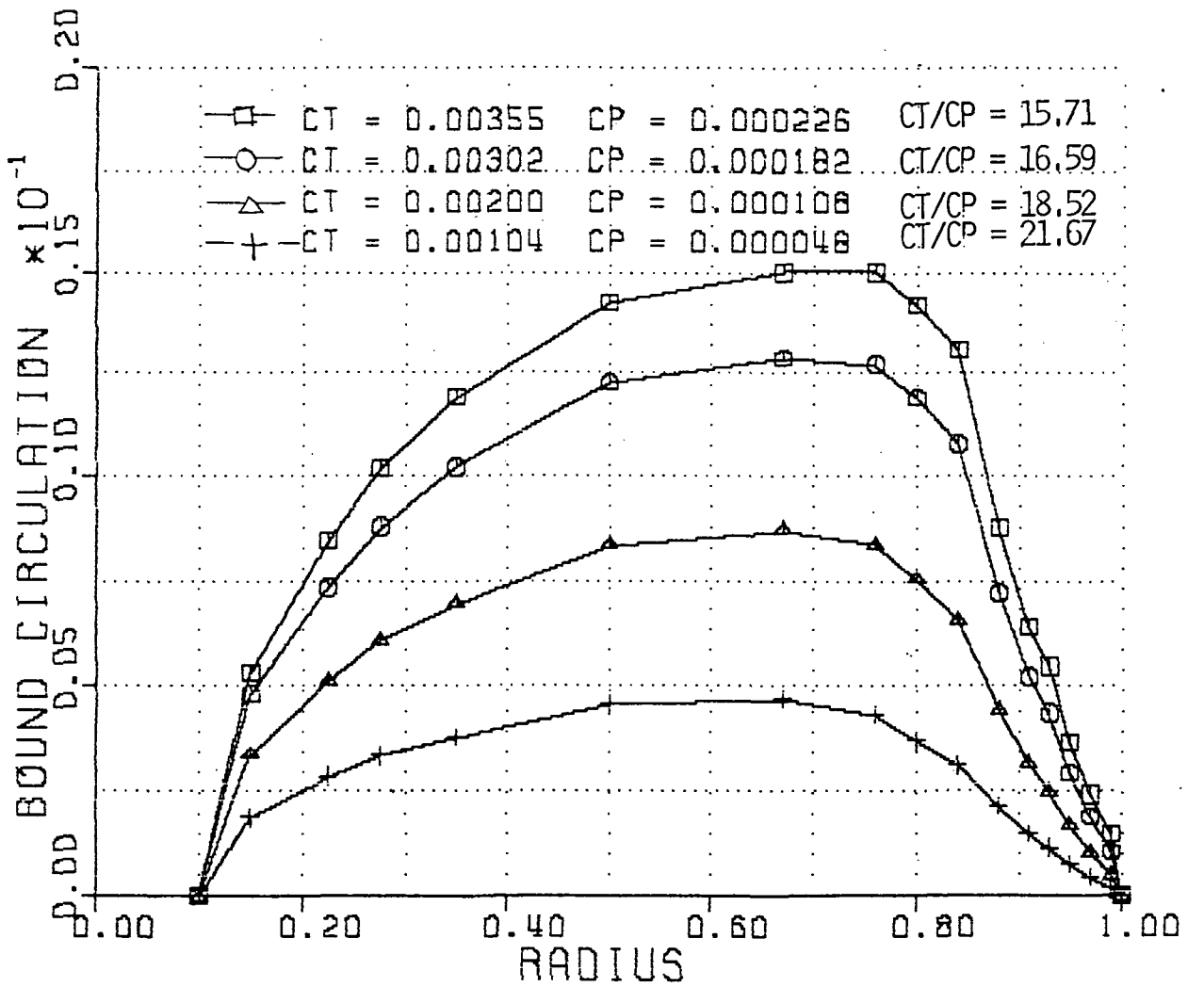

Figure 4-9. Bound Circulation of the Double Twisted and Tapered Rotor for Different Chord.

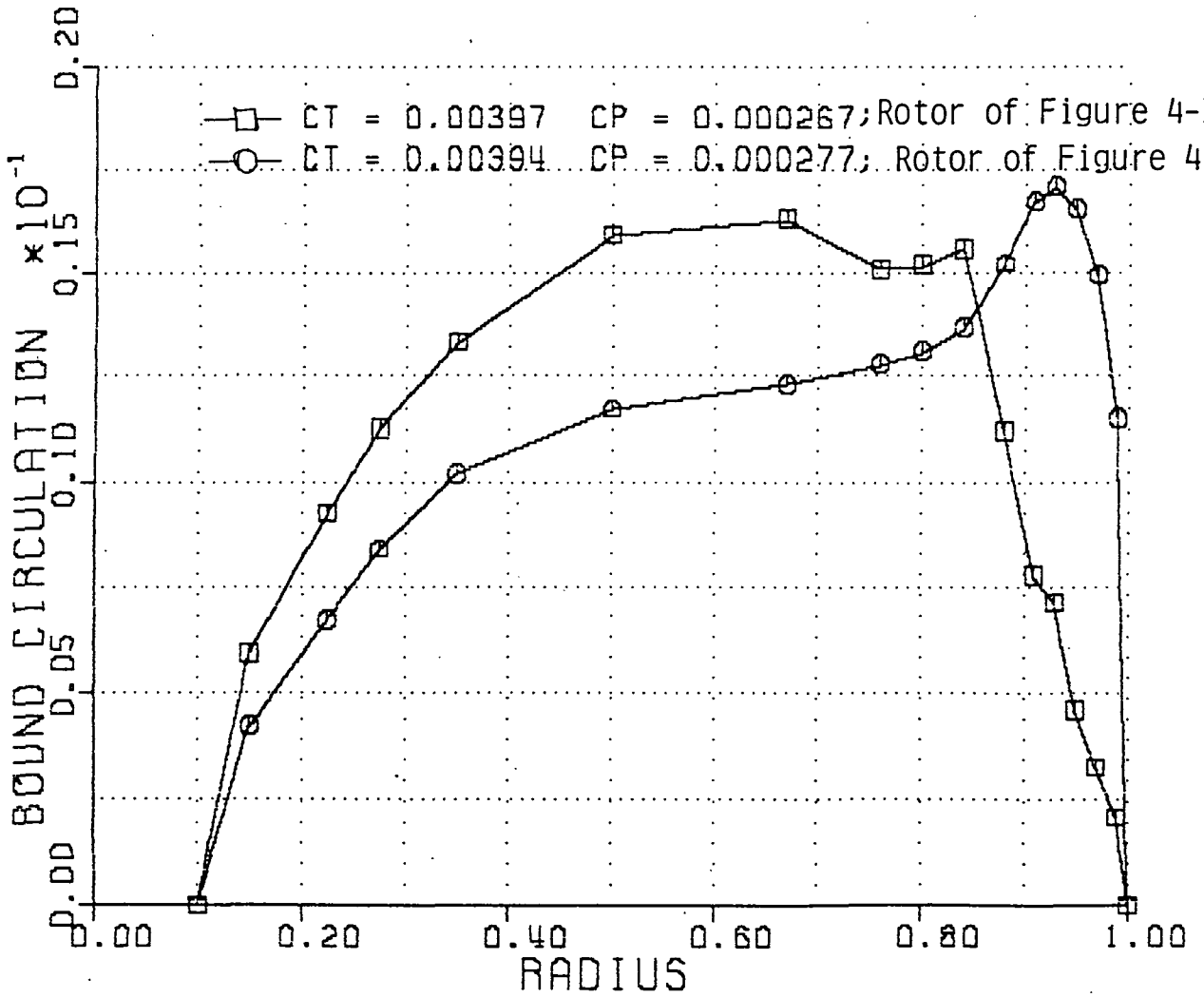

Figure 4-10. Bound Circulations of the Double Twisted and Tapered Rotor and of the Straight Twisted and Constant Chord Rotor.

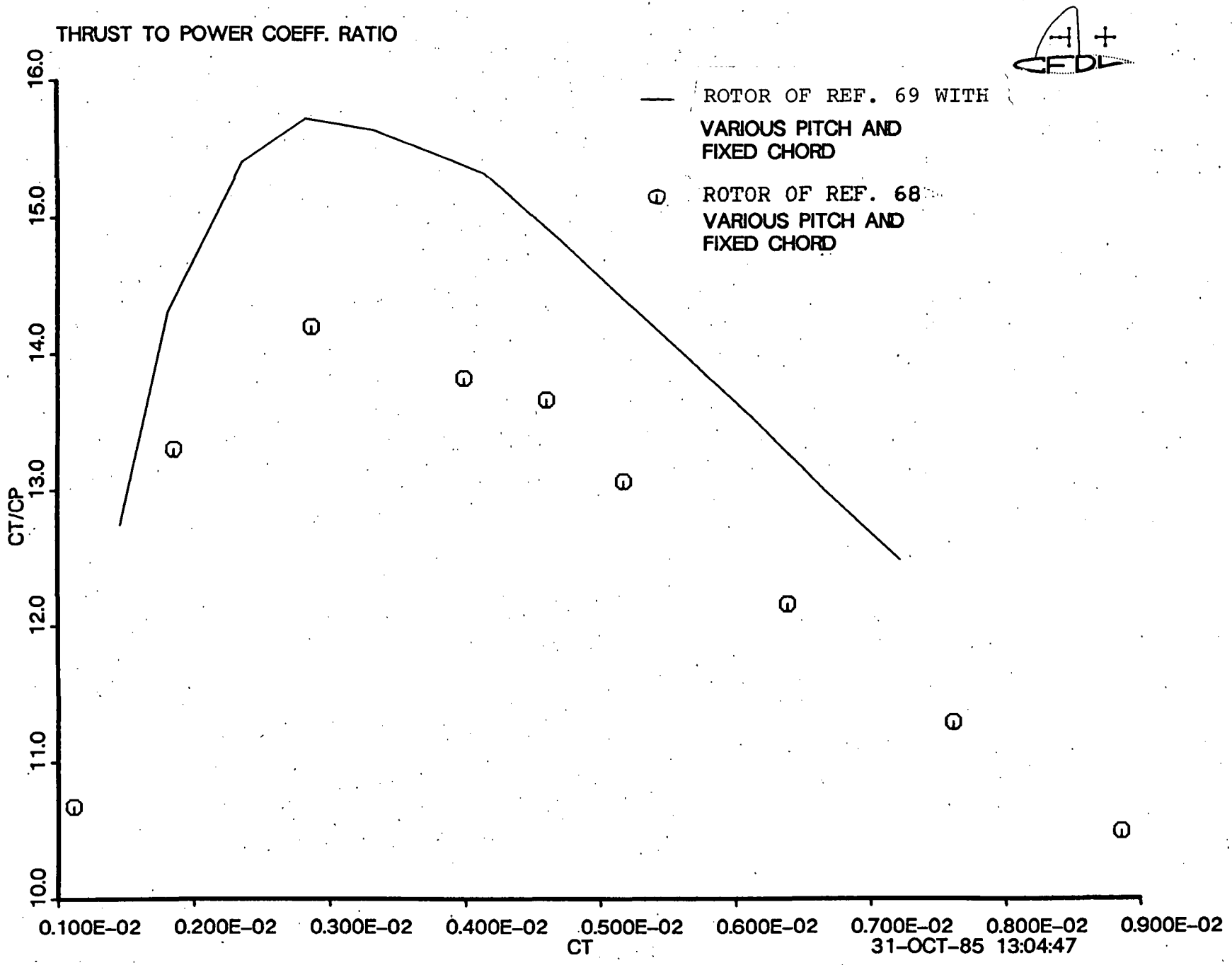

Figure 4-11A. Thrust to Power Coefficient Ratio vs Thrust Coeff.

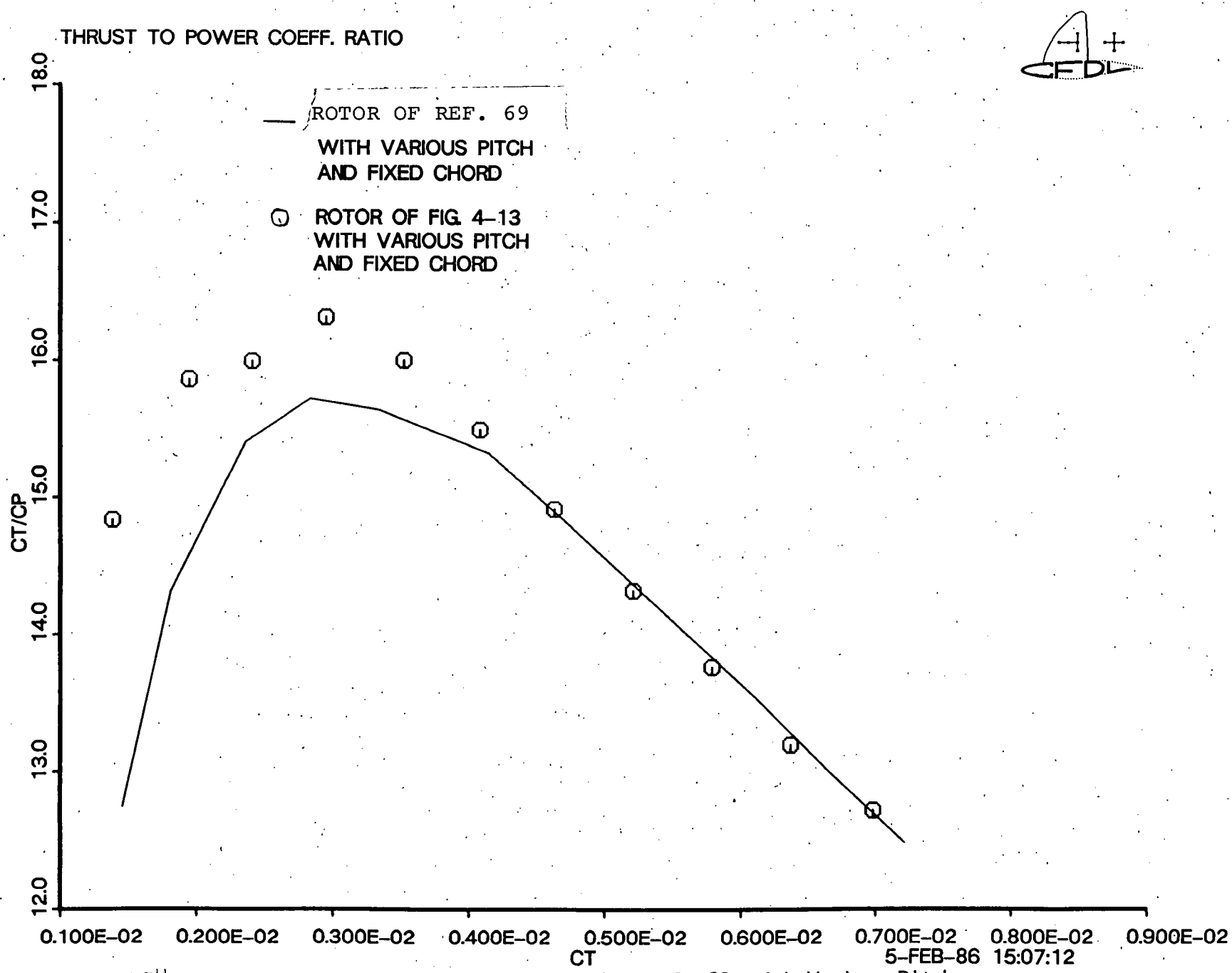

Figure 4-11B, Thrust to Power Coefficient Ratio vs Thrust Coeff. with Various Pitch.

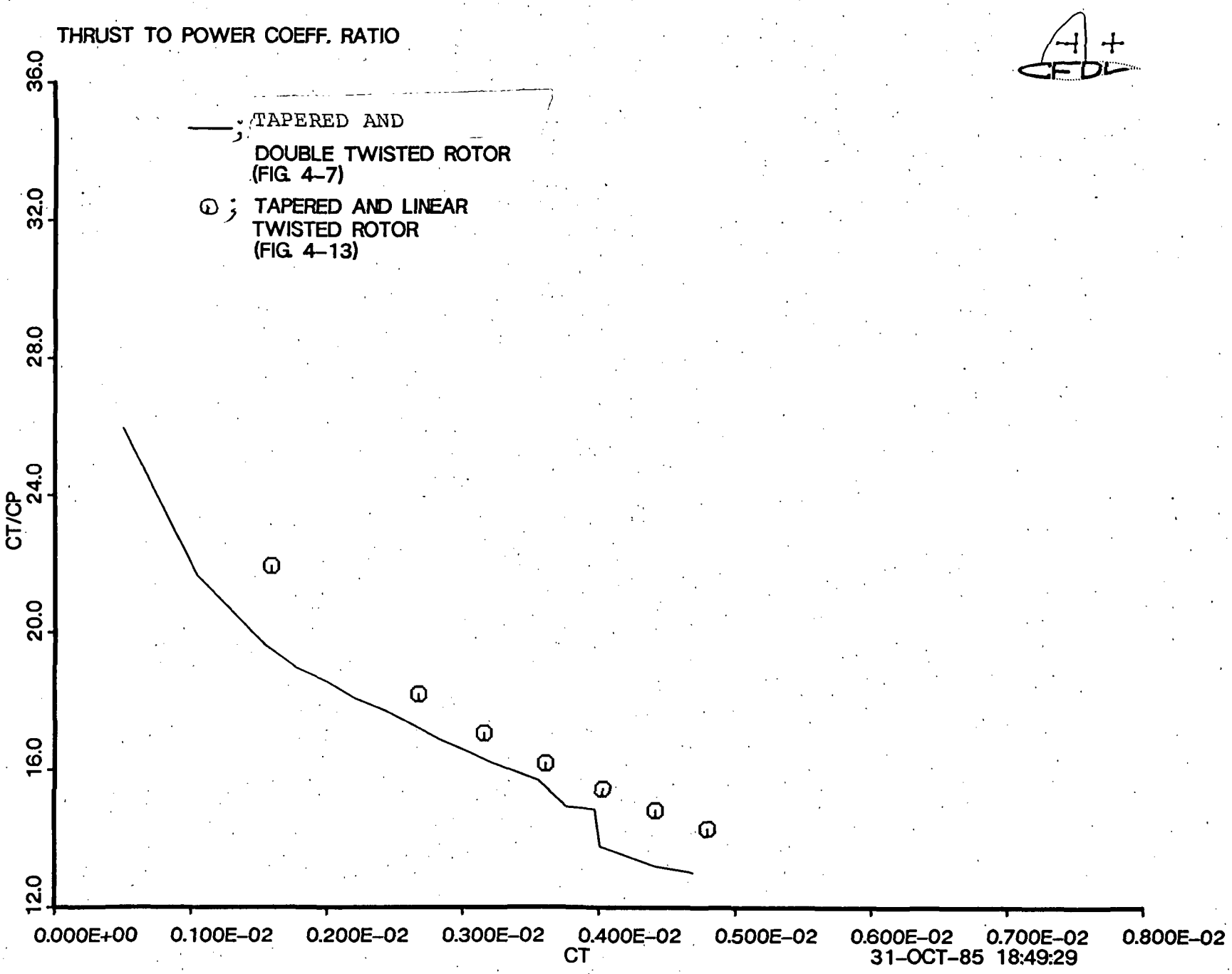

Figure 4-12. Thrust to Power Coeff. Ratio vs Thrust Coeff. Obtained by Varying Chord.

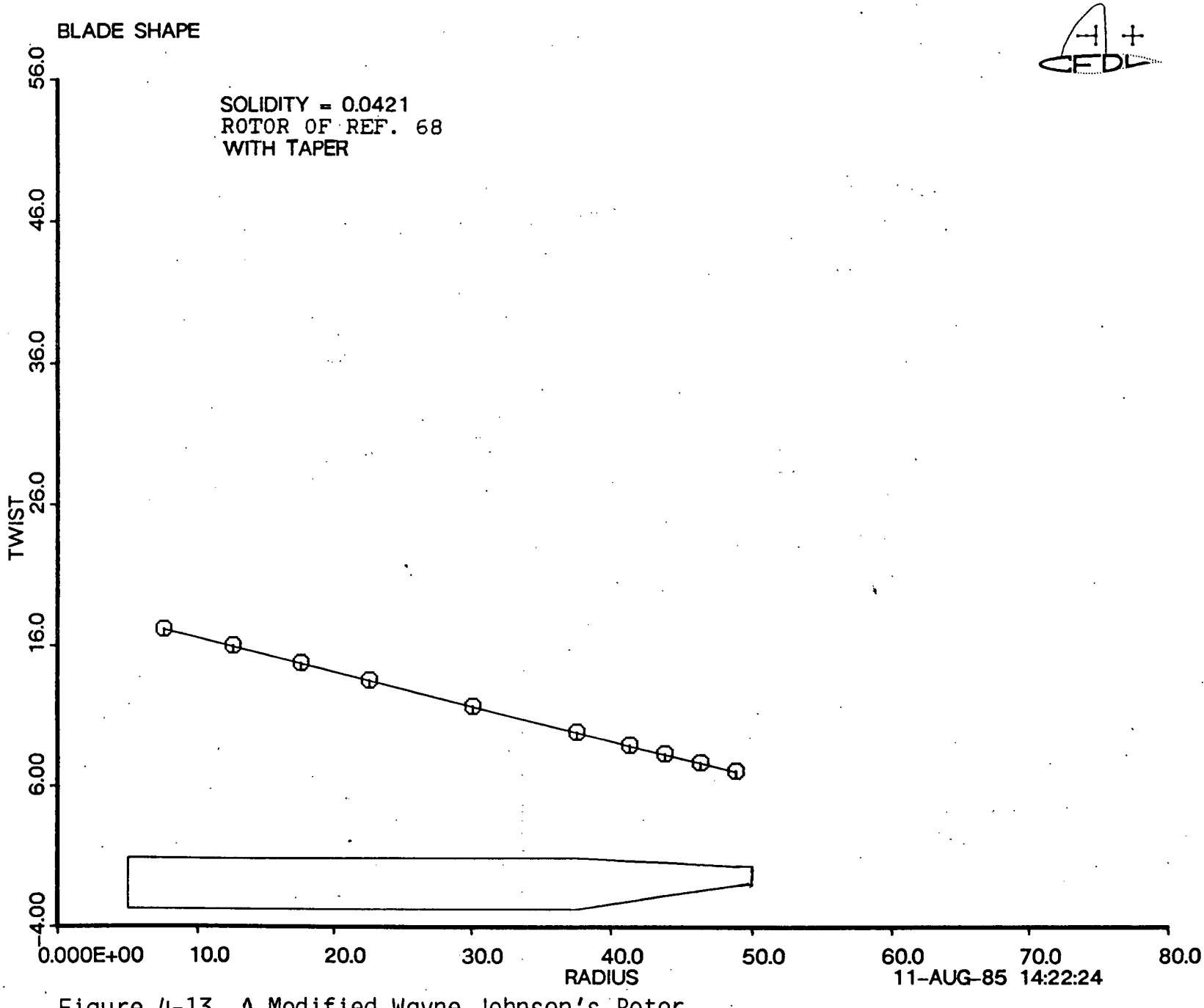

Figure 4-13. A Modified Wayne Johnson's Rotor.

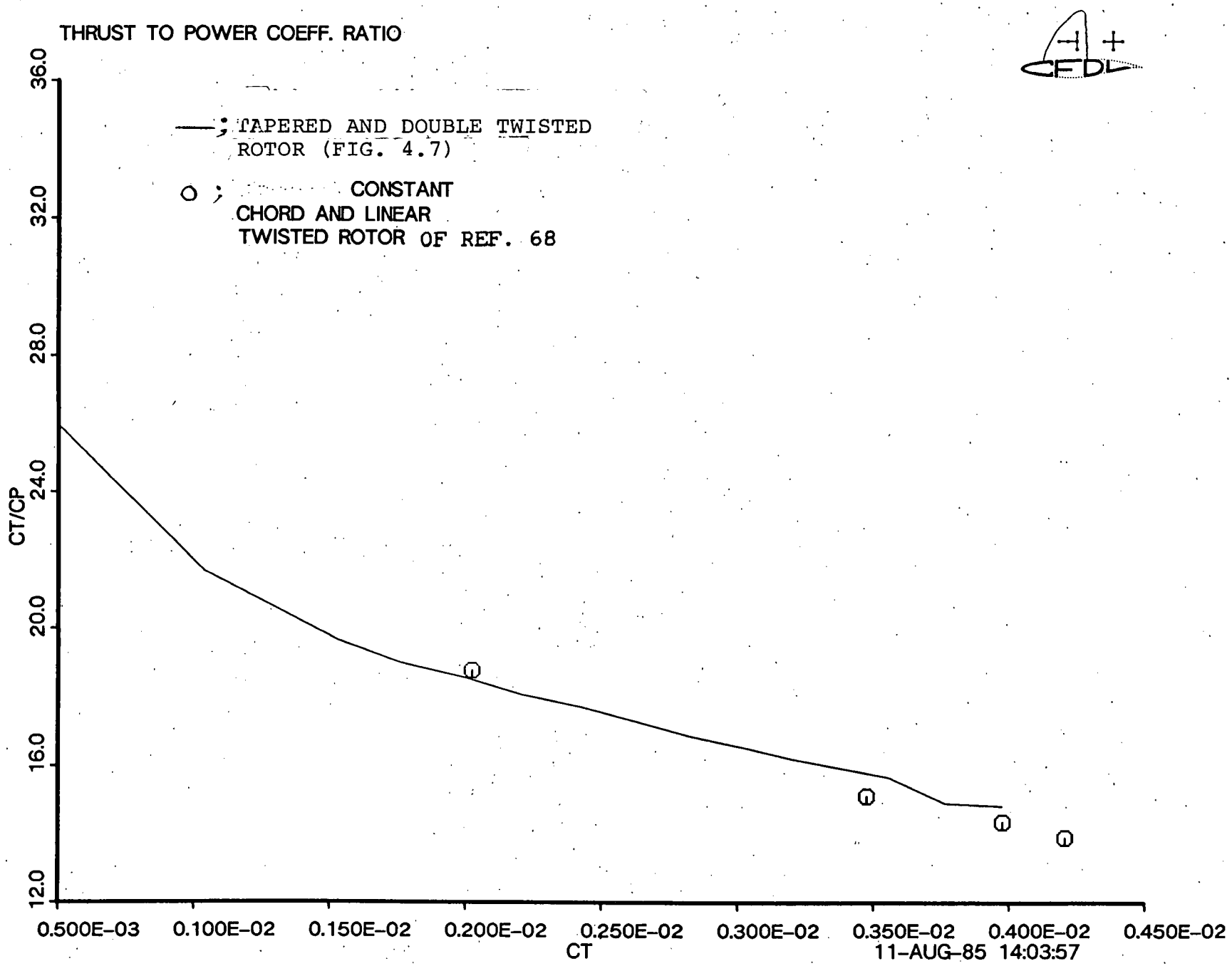

Figure 4-14. Thrust to Power Coefficient Ratio vs Thrust Coeff.

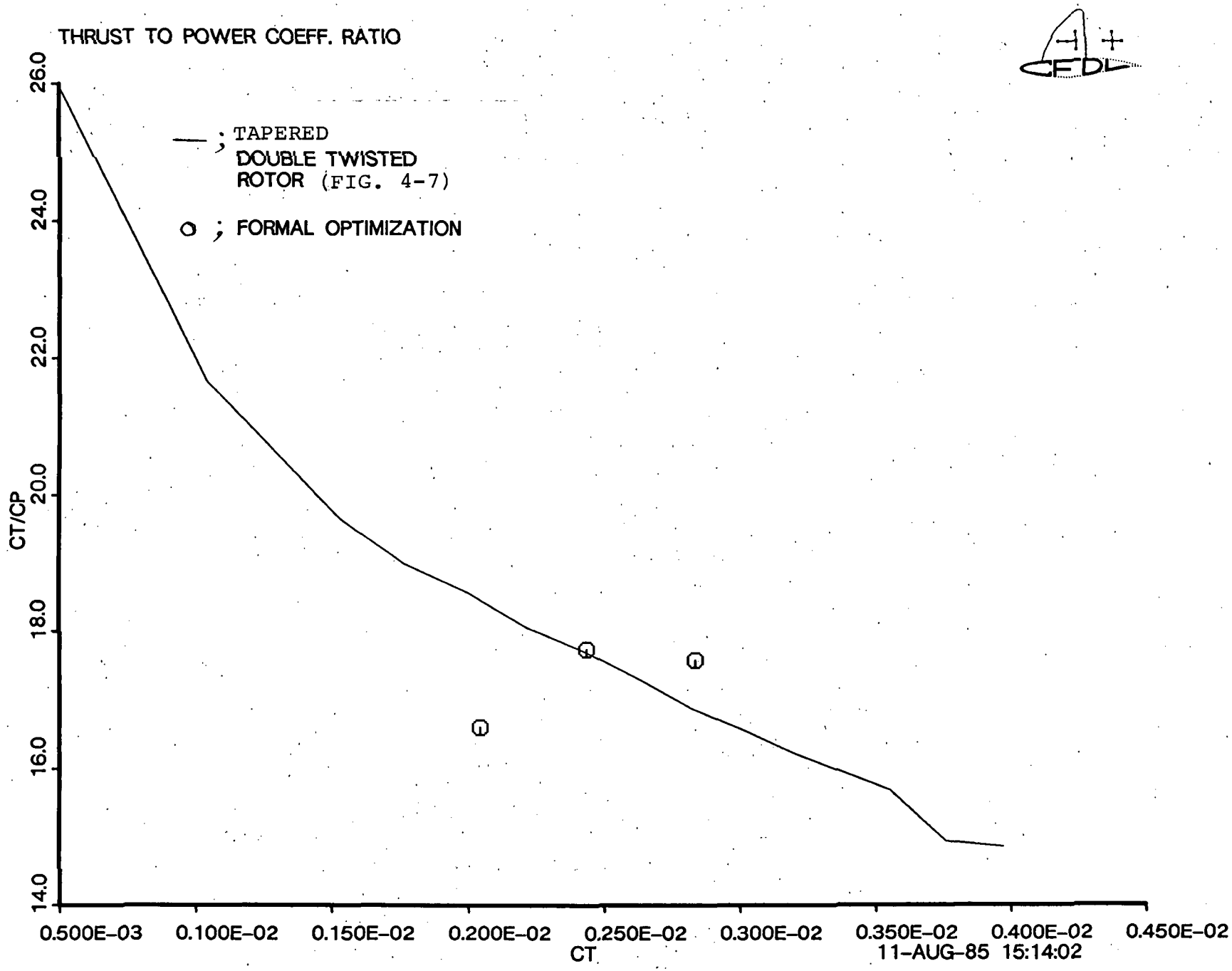

Figure 4-15. Thrust to Power Coefficient Ratio vs Thrust Coeff.

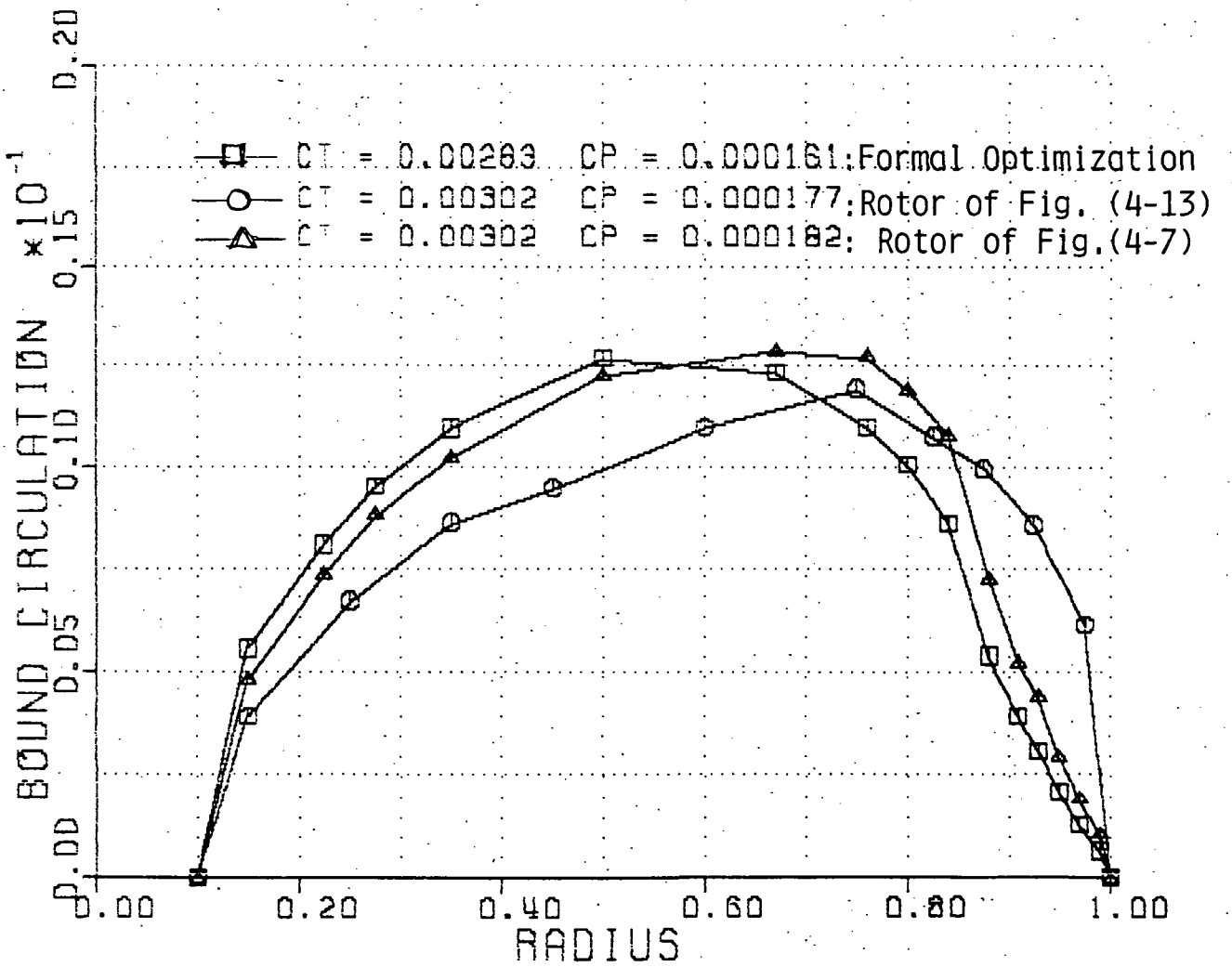

Figure 4-16. Comparison of Bound Circulations for three Different Rotors.

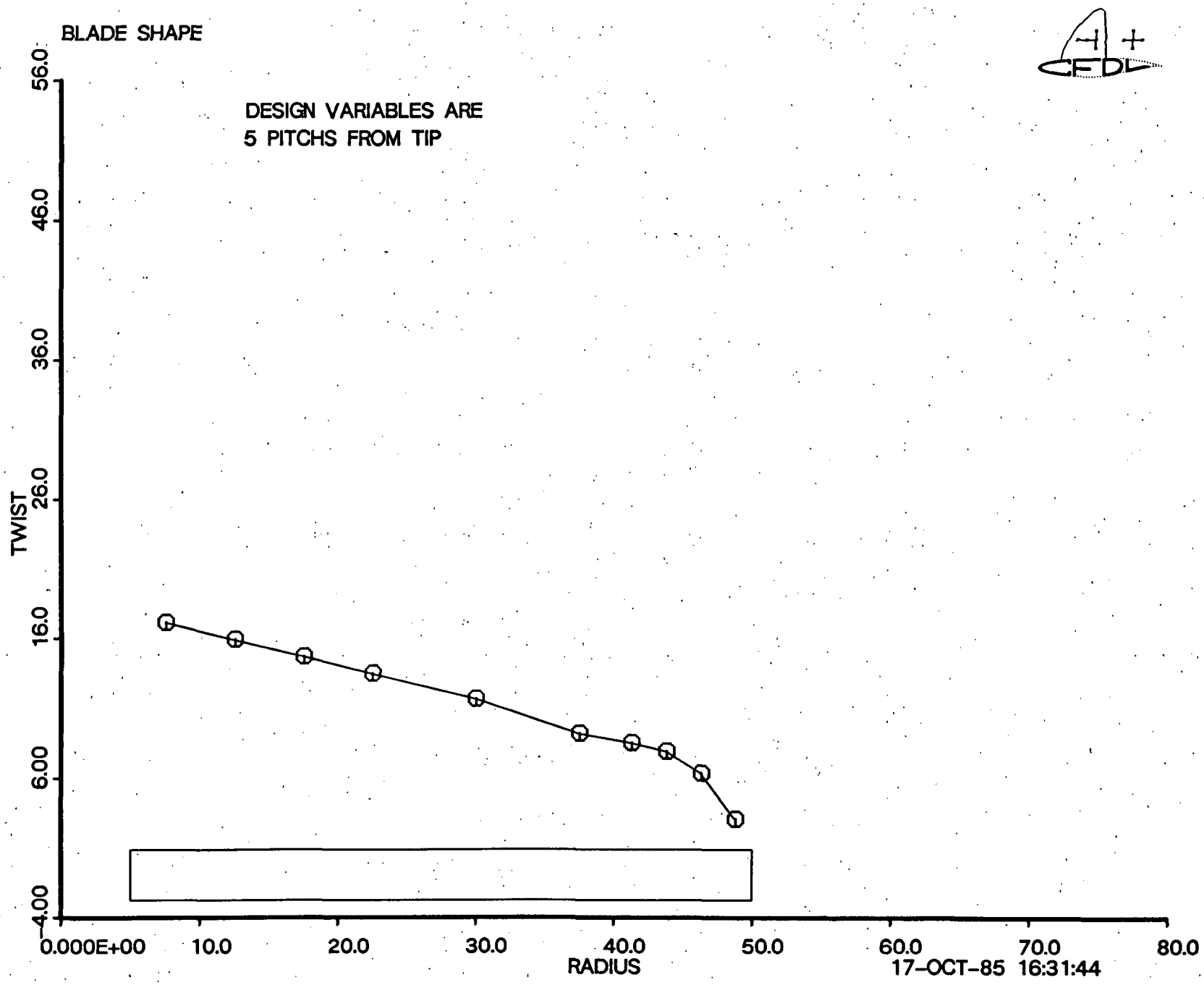

Fig.(4-17) Pitch Distribution Obtained by Optimization for Rotor of Fig.(4-1)

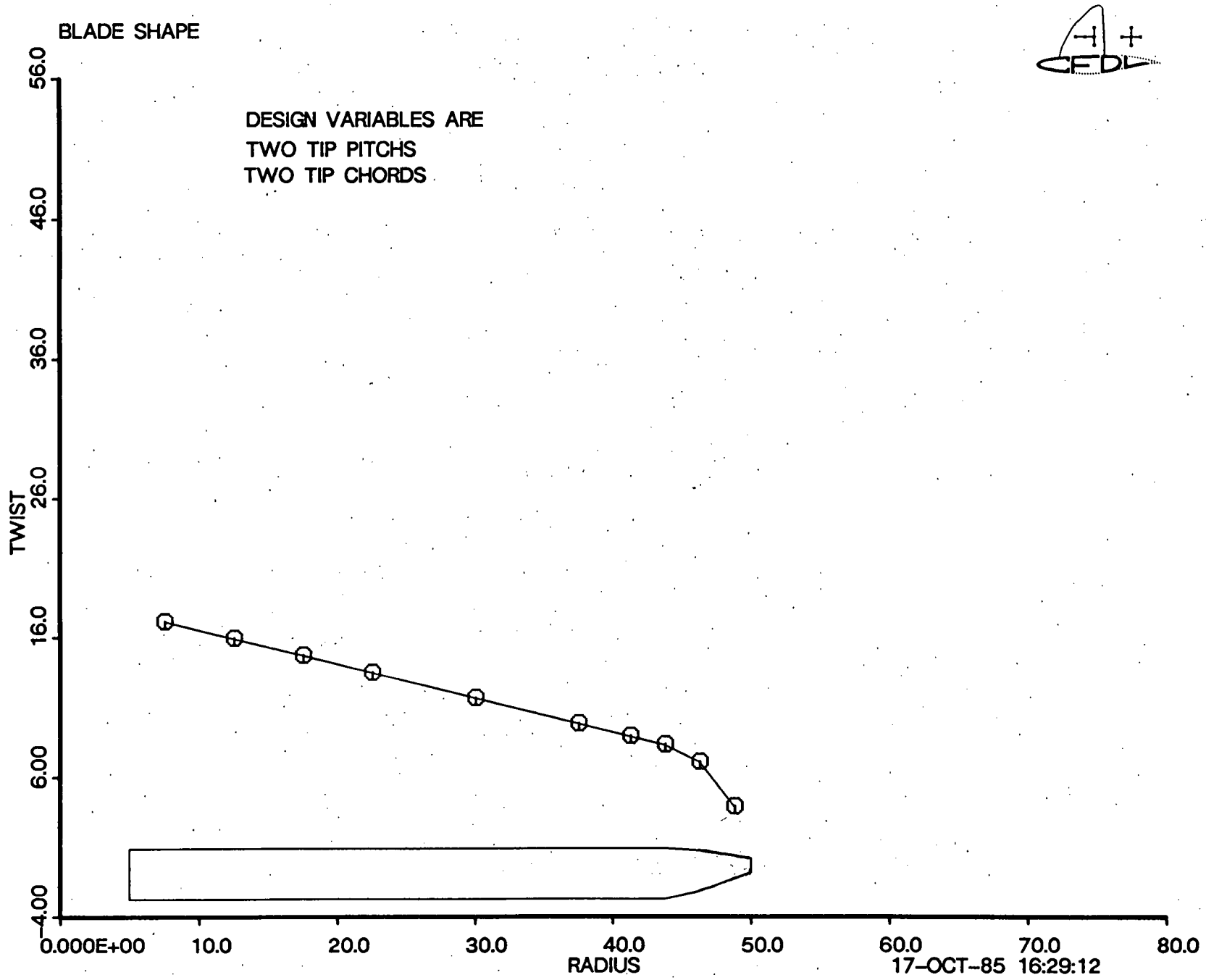

Fig.(4-18). Pitch and Chord Distribution Obtained by Optimization for Rotor of Fig.(4-1)

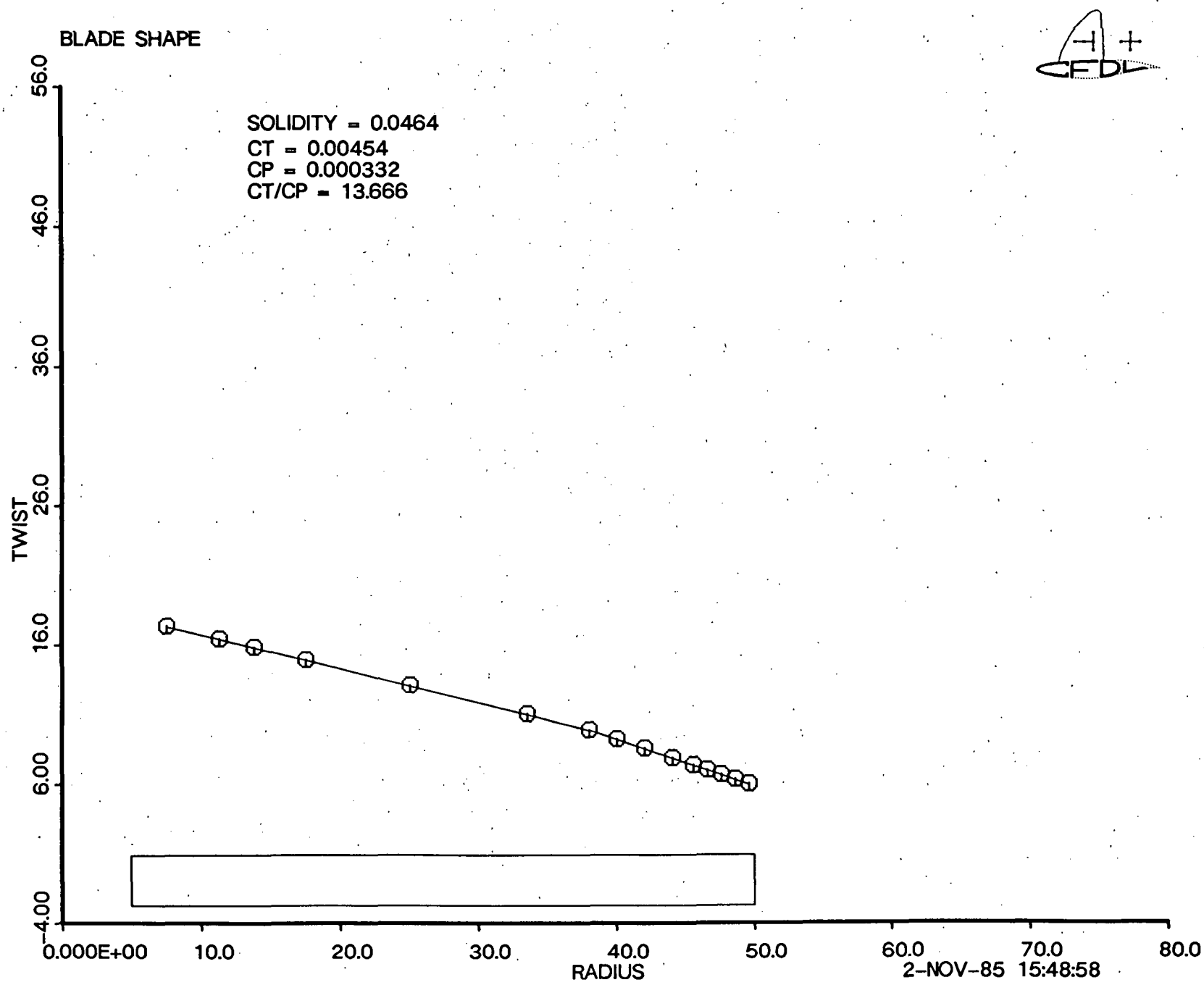

Fig.(4-20). Pitch and Chord Distribution Results of Optimization for Rotor of Fig.(4-3)

CHAPTER 5. CONCLUSIONS AND RECOMMENDATIONS

As a test of the optimization program constant downwash is obtained by using momentum theory and optimization using the Quasi-Newton method. The uniform downwash or uniform circulation is found to be not the optimum condition because of the highly concentrated tip vortex for the maximum thrust to power coefficient of a rotor. The classical vortex or momentum theory can not be used for the hovering performance optimization.

Free wake lifting line theory is found to agree better with the experimental results in Ref.(35) than lifting surface theory for performance analysis. The lifting body theory which uses the superposition of source and vortex sheets is developed and compares well in performance prediction with other methods such as Euler solution in Ref.(32) or panel method solution in Ref.(33) of a wing.

The free wake geometries obtained by free wake lifting line theory is in good agreement with experimental results in Ref.(35).

For the calculation of the self-induced velocity of a ring vortex the formula given in Ref.(4) is used with the vortex core size of 2 % of the rotor radius.

It is shown that the fast free wake techniques used in Ref.s(7-11) give the real flow field and is necessary to compute the rotor hovering performance because the free wake geometry is very different from the rigid wake geometry and hence momentum theory is not accurate. 10 to 15 spanwise divisions of the blade are found to be sufficient for the analysis and optimization.

The vortex core size of the ring vortices below the rotor are calculated by the conservation of the kinetic energy, circulation, and momentum. The work done by the rotor is found to appear as the kinetic energy due to the wake vortices. The core size is shown to grow because the flow outside of the core containes more energy as the ring vortices move downward from the rotor.

During the formal optimization of the hovering performance it is found that the sensitive parameter to the performance is the root chord, the collective pitch, the taper ratio, and the degree of twist in the order of the relative importance. When the initially linear twisted blade is optimized with constant chord and varying pitch only over the outer 20 % of the blade, the optimization without constraint on CT gives a double twisted blade. With design variables of taper and spanwise location of the start of taper, optimization indicated no change in geometry for the straight twisted blade with the constraint on current

CT. With design variables of taper and twist and spanwise location of the start of taper and twist, the optimization indicated a doubly twisted and tapered geometry with an increase in CT/CP of 5%.

It is demonstrated that the formal optimization can be used with the implicit and nonlinear objective or cost function such as the performance of hovering rotors. The formal optimization can be extended to the performance optimization of forward flights of rotors with a robust analysis code. By the addition of the free stream velocity and the swirl loss correction the present optimization can be extended to the propeller or wind turbine. Although the close blade and first ring vortex encounter occurs outside of the vortex core, a better definition of the vorticity distribution from the roll-up of the near wake is needed.

APPENDIX

A. A Surface Singularity Method for Computing the Potential Flow of Thick Airfoils in Subsonic Flow

For solving the potential flow of two dimensional lifting airfoils a superposition method which uses elementary singularities at body surfaces is presented. The strengths of these singularities are determined by the flow tangency condition on body surface and the Kutta condition.

This method was developed in Ref.(34) for three-dimensional lifting flows using three-dimensional singularities, source and doublet, distribution on body surface. There the nonlifting flow was solved first and then a linearly varying doublet around the wing curve surface at each section was added to the nonlifting flow to satify the Kutta condition and hence to create lift. The two-dimensional version of this approach was tested in this analysis. It was found that for the nonlifting flow the flow velocity at the trailing edge was infinite and therefore a finite vorticity could not be added to the nonlifting flow to cancel this infinite velocity. The lifting flow is solved here independently of the nonlifting flow.

Hess and Smith (ref.55) computed exactly the two, axisymmetric, or three-dimensional nonlifting flows by using the surface source distribution. For two-dimensional lifting flows they used three basic flows, that is, the nonlifting flows due to uniform streams at α =0 degree and α =90 degree and the flow due to a pure circulation about airfoil, to generate the flows corresponding to a set of angles of attack or lift coefficients. In Ref.s (56) and (57) the doublet distribution on camber surface and the source distribution on body surface were used and their strengths were determined by the flow tangency condition on each surface. There linearly varying source or quadratically varying doublet was distributed on curved panels obtained by fitting a paraboloid to corner points. Also, the design problem of determining the body geometry to have a given tangential velocity distribution was considered first and analysis or design formulation was given by the Green's solution of the potential Laplace equation. Basu and Hancock (ref.58) solved the transient problem of a sudden airfoil incidence change or an airfoil passing through a sharp-edged gust. They employed the distribution of sources and constant strength vorticity around airfoil curve. The position of shed vortices were calculated from the resultant velocities on free vortices at each time increment. In Ref.(59) linearly varying vortex panels and a

constant source around airfoil curve were employed together with a vortex sheet to represent the seperated region. There the boundary layer effect was modelled by source distribution due to the boundary layer displacement and the shape of the vortex sheet representing the seperated region was calculated iteratively. Maskew (ref.10) used the Green's function solution to compute the pressure for four blade tip shapes which are oscillating in pitch as semi-span wings. He applied Green's theorem outside and inside of the blade independently and set the potential inside the blade to be the free stream potential. In Ref.(61) the two-dimensioanl lifting airfoil was solved by Green's function formula and the superposition of potential due to circulation and non-circulatory flow. There the total potential instead of the perturbation potential was employed and hence needed the far field potential approximation which used the potential due to uniform flow past a unit circular cylinder with given circulation. In Ref.(62) constant source panels on body surface and constant doublets panels on camber surface were employed with the flow tangency condition on each surface. Also, the compressibility correction method ws given according to Gothert coordinate transformation. In Ref.(63) the Green's function formula for compressible and steady or unsteady potential flow was derived. There the strengths of source on body surface were

known from normal boundary condition and linear system of equation for the potential strength on body surface was derived by influence coefficient method. Since the derivative of potential which is velocity is relatively large, the potential which was assumed to be constant within each element in Ref.(63) varies much from panel to panel. The accuracy becomes poor as reflected in the comparison of the calculated results with experiments in Ref.(10). The approach written in Ref.(64) for the pressure calculation of two-dimensional lifting airfoil was tried in the analysis. It was found that the vortex panel superposition to nonlifting flow was not appropriate.

The method used in this analysis is same as the one developed in Ref.(34). But the lifting flow is solved directly by the superposition of N sources and 1 constant vorticity around airfoil curve with the N flow tangency and 1 Kutta conditions. The compressibility is handled by the Gothert coordinate transformation used in Ref.(62). The influence coefficient matrix for N sources and 1 vortex is same for one airfoil with different angles of attack. Hence it can be inverted for all angles of attacks at once. This method was extended to three-dimensional wing and hovering rotor problem with free wake geometry and is applied for the optimization of performance.

A.1 DERIVATION OF METHOD

A.1.1 Green's Solution of Laplace Equation

The second form of Green's theorem is

$$\iiint_R (\phi_1 \nabla^2 \phi_2 - \phi_2 \nabla^2 \phi_1)\, dV$$

$$= \iint_S \vec{n} \cdot (\phi_1 \nabla \phi_2 - \phi_2 \nabla \phi_1)\, dS \qquad \text{---} \quad (A\text{-}1)$$

where R is the region bounded by the closed surface S and $\vec{n}$ is the outward unit normal. Let's consider the region outside a two-dimensional airfoil as shown in figure.

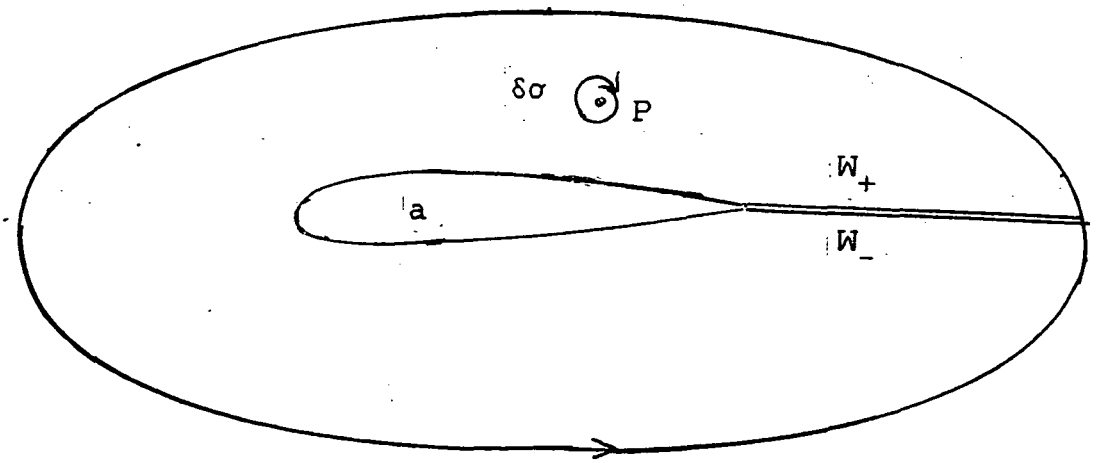

Let's consider the unit length along the axis of airfoil

cylinder. Then $dV = d\sigma\, dz$ and $dS = d\ell\, dz$. Let $\phi_1 = \phi$ and $\phi_2 = \chi = \ell n\ r$. Then $\nabla^2\phi_1 = 0$ in region R and $\nabla^2\phi_2 = 0$ except at a point P.

$$\int_{d\sigma} \vec{n} \cdot (\phi\ \nabla\chi\ - \chi\nabla\phi\ )\ d\ell\ + \int_{S} \vec{n} \cdot (\phi\nabla\chi\ - \chi\nabla\phi)\ d\ell = 0 \quad \text{---- (A-2)}$$

At the point P $\nabla\chi = \frac{1}{r}\,\vec{e}_r$ and $\vec{n} = \vec{e}_r$. The first integral in equation (A-2) becomes

$$\lim_{r\to 0} \int_{2\pi}^{0} \left\{ \phi\ \frac{1}{r} - \ell n\ r \cdot \nabla\phi \right\} r\ d\theta = -\ 2\pi\ \phi_p \quad \text{---- (A-3)}$$

If the point P is located on the airfoil surface, the first integral becomes $-\pi\phi_p$. From equations (A-2) and (A-3),

$$2\pi\ \phi_p\beta_p = \int (\phi\ \frac{\partial\chi}{\partial n} - \chi\ \frac{\partial\phi}{\partial n}\ )\ d\ell \quad \text{where } \beta = 1 \text{ or } 1/2 \quad \text{---- (A-4)}$$

Since $\Phi_{total} = \Phi_\infty + \phi$ and $\nabla\Phi_T = U_\infty\,\vec{i} + \nabla\phi$, $\phi \to 0$ as $r \to \infty$.

$$2\pi\ \phi\beta = \int_a \left[\ \phi\ \frac{\partial\chi}{\partial n} - \chi\ \frac{\partial\phi}{\partial n}\ \right] d\ell + \int_{W_+} (\phi_u - \phi_\ell\ )\ \frac{\partial\chi}{\partial n}\ d\ell$$

$$\int \nabla\phi \cdot \overrightarrow{d\ell} = \phi_u - \phi_\ell = \Gamma$$

$$2\pi\phi\beta = \int_a \left[\phi\ \frac{\partial\chi}{\partial n} - \chi\ \frac{\partial\phi}{\partial n}\ \right] d\ell + \Gamma \int_{W_+} \frac{\partial\chi}{\partial n}\ d\ell \quad \text{---- (A-5)}$$

For the point in region R,

$$\phi_p = \int_S \sigma(Q)\left(-\frac{1}{2\pi} \ell n\ r \right) d\ell + \int_S \mu(Q) \frac{\partial}{\partial n_Q}\left(\frac{1}{2\pi} \ell n\ r\right) d\ell \quad \text{—— (A-6)}$$

where $\phi_s = \frac{1}{2\pi} \ell n\ r$ is the potential due to a two-dimensional source of unit strength and $\frac{\partial}{\partial n}(\phi_s)$ is the doublet. Also, $\sigma(Q)$ and $\mu(Q)$ are the strengths of sources and doublet each. For analysis boundary conditions we have

$$\frac{\partial \phi}{\partial n_p} = \int_S \sigma(Q) \frac{\partial}{\partial n_p}\left(-\frac{1}{2\pi} \ell n r\right) d\ell + \int_S \mu(Q) \frac{\partial}{\partial n_p} \frac{\partial}{\partial n_Q} \left(\frac{1}{2\pi} \ell n\ r\right) d\ell \quad \text{—— (A-7)}$$

For design conditions we have

$$\frac{\partial \phi}{\partial t_p} = \int_S \sigma(Q) \frac{\partial}{\partial t_p}\left(-\frac{1}{2\pi} \ell n\ r\right) d\ell + \int_S \mu(Q) \frac{\partial}{\partial t_p} \frac{\partial}{\partial n_Q}\left(\frac{1}{2\pi} \ell n\ r\right) d\ell \quad \text{—— (A-8)}$$

Here, $\frac{\partial}{\partial n_p}$ is the derivative in a normal direction and $\frac{\partial}{\partial t_p}$ is the derivative in a selected tangential direction. S includes the airfoil and the branch cut surfaces.

A.1.2 Methods Using the Continuity of Potential

We use the equation (A-5) to obtain the linear system of equations for the body surface potential ϕ . The body surface S is divided into segmenta S_K and ϕ is approximated to be constant ϕ_K on each segment.

$$\frac{\partial \Phi_T}{\partial n} = \vec{U}_\infty \cdot \vec{n} + \frac{\partial \phi}{\partial n} = 0 \text{ on body surface.}$$

$$\Gamma = \Delta\phi_{T.E.} \qquad \frac{\partial \phi}{\partial n} = - \vec{U}_\infty \cdot \vec{n} \qquad \text{—— (A.9)}$$

From equation (A-5),

$$[\ \delta_{pk} - C_{pk} - W_{pk}]\ \{\phi_k\} = [\ b_{pk}\ ]\ \left\{ \left(\frac{\partial \phi}{\partial n} \right)_K \right\} \qquad \text{—— (A-10)}$$

where δ_{pk} is the kronecker delta,

$$C_{pk} = \left[\frac{1}{\pi} \int_{S_k} \frac{\partial}{\partial n} (\ell n\ r)\ dS_k \right] \qquad \text{—— (A-11)}$$

$$b_{pk} = \left[- \frac{1}{\pi} \int_{S_k} \ell n\ r\ dS_k \right] \qquad \text{—— (A-12)}$$

and $W_{pk} = 0$ for the segments not in contact with the trailing edge. For the segments in contact with the trailing edge,

$$W_{pk} = \left[\pm \frac{1}{\pi} \int_{S_W} \frac{\partial}{\partial n_u} (\ell n\ r)\ dS_W \right] \qquad \text{—— (A-13)}$$

where S_u is the surface of the branch cut. The upper (lower) sign must be used for the upper (lower) side of the airfoil.

It may be noted that $\Gamma = \Delta\phi_{T.E.}$ is the Kutta condition.

A.1.3 Superposition Method of Source and Vortex or Doublet

We use the equation (A-7) to obtain the linear equations for source strengths and one constant vortex or one linearly varying doublet around the body. Since vortex strength is the derivative of normal doublet, $\gamma(Q) = \nabla \mu(Q)$, one constant vortex around airfoil curve is used here instead of doublet. The body surface S is divided into segments S_k and $\sigma(Q)$ is approximated to be constant $\sigma(k)$.

$$\left[C_{p,k} \;,\; C_{p,N+1} \right] \begin{Bmatrix} \sigma_k \\ \gamma_{N+1} \end{Bmatrix} = \left\{ \frac{\partial \phi}{\partial n_p} \right\} \text{ for } p = 1,2,\cdots,N \qquad \text{—— (A-14)}$$

where $C_{p,k}$ is the normal velocity at p due to source segment k of unit strength and $C_{p,N+1}$ is the normal velocity at p due to the unit constant vortex around the airfoil curve. One additional equation is obtained from Kutta condition. That is,

$$\vec{U}_\infty \cdot \vec{t}_1 + \frac{\partial \phi}{\partial t_1} = \vec{U}_\infty \cdot \vec{t}_N + \frac{\partial \phi}{\partial t_N}$$

where 1 is the point on the lower surface of airfoil nearest to the trailing edge and N is the point on the upper surface of airfoil nearest to the trailing edge.

$$\left[C'_{1,k} \;,\; C'_{1,N+1} \right] \begin{Bmatrix} \sigma_k \\ \gamma_{N+1} \end{Bmatrix} + \vec{U}_\infty \cdot \vec{t}_1$$

$$= \left[C'_{N,k} \;,\; C'_{N,N+1} \right] \begin{Bmatrix} \sigma_k \\ \gamma_{N+1} \end{Bmatrix} + \vec{U}_\infty \cdot \vec{t}_N \qquad \text{—— (A-15)}$$

$$\left[\left(C'_{1,k} - C'_{N,k} \right) \;,\; \left(C'_{1,N+1} - C'_{N,N+1} \right) \right] \begin{Bmatrix} \sigma_k \\ \gamma_{N+1} \end{Bmatrix}$$

$$= \vec{U}_\infty \cdot \vec{t}_N - \vec{U}_\infty \cdot \vec{t}_1 \qquad \text{—— (A-16)}$$

$$k = 1,2, \cdots, N$$

$$C'_{p,k} = \int_{S_k} \frac{\partial}{\partial t_p} \left(\frac{1}{2\pi} \ell n \; r_p \right) d\ell_k$$

$$C'_{p,N+1} = \int_{S_a} \frac{\partial}{\partial t_p} \left(\frac{1}{2\pi} \tan^{-1} \frac{y_p}{x_p} \right) d\ell$$

Let $\quad C_{N+1,k} = C'_{1,k} - C'_{N,k}$

$$C_{N+1,N+1} = C'_{1,N+1} - C'_{N,N+1}$$

and $\quad \frac{\partial \phi}{\partial n_{N+1}} = \vec{U}_\infty \cdot \vec{t}_N - \vec{U}_\infty \cdot \vec{t}_1$

Then

$$\left[C_{p,k} \;,\; C_{p,N+1} \right] \begin{Bmatrix} \sigma_k \\ \gamma_{N+1} \end{Bmatrix} = \left\{ \frac{\partial \phi}{\partial n_p} \right\} \quad , \; p=1,2,\cdots,N+1 \qquad \text{——(A-17)}$$

Here, $\quad C_{p,k} = \int_{S_k} \frac{\partial}{\partial n_p} \left(\frac{1}{2\pi} \ell n \; r_p \right) d\ell_k$

$$C_{p,N+1} = \int_{S_a} \frac{\partial}{\partial n_p} \left(\frac{1}{2\pi} \tan^{-1} \frac{y_p}{x_p} \right) d\ell_a \qquad \text{—— (A-19)}$$

A.1.4 Calculation of Influence Coefficients

Let's drop 2π from equations (A-18) and (A-19).

$$\phi_S = \int_j \ln r_{ij}\, dS_j$$

$$\nabla\phi_s = \int_j \left\{ \vec{i}\, \frac{\partial}{\partial x_i} \ln r_{ij} + \vec{j}\, \frac{\partial}{\partial y_i} \ln r_{ij} \right\} dS_j \quad \text{—— (A-20)}$$

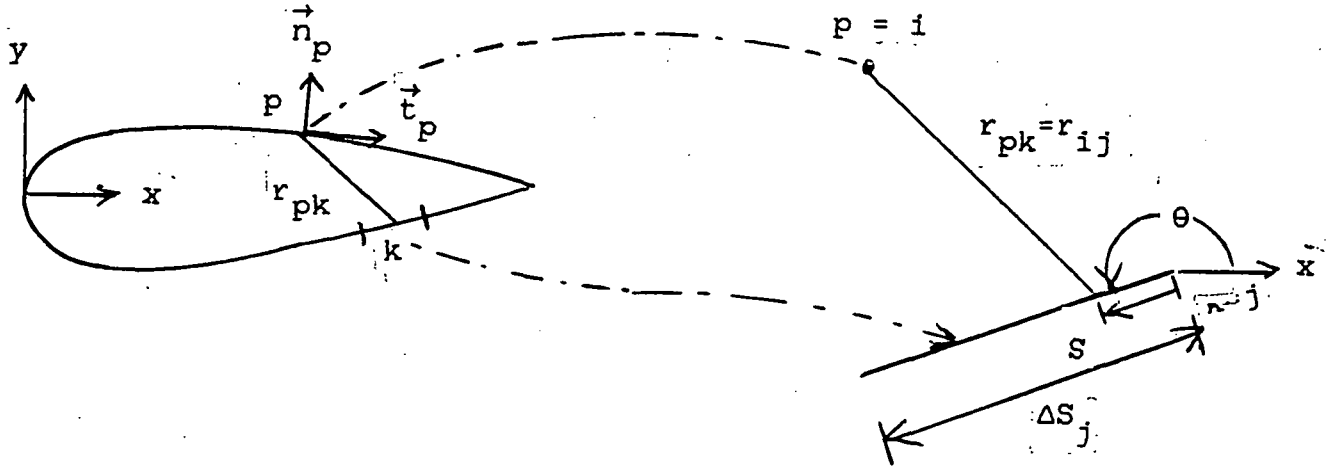

$$r_{ij} = \sqrt{(x_i - x_j - S\cos\theta_j)^2 + (y_i - y_j - S\sin\theta_j)^2}$$

$$\nabla\phi_s = \int_0^{\Delta S_j} \frac{[(x_i - x_j - S\cos\theta_j)\,\vec{i} + (y_i - y_j - S\sin\theta_j)\,\vec{j}\,]\, dS_j}{(x_i - x_j - S\cos\theta_j)^2 + (y_i - y_j - S\sin\theta_j)^2}$$

$$\nabla\phi_s = \int_0^{\Delta S_j} \frac{(AS + B)\,\vec{i} + (CS + D)\,\vec{j}}{\alpha + 2\beta S + S \cdot S}\, dS = C_{xi,j}\,\vec{i} + C_{yi,j}\,\vec{j} \quad \text{—— (A-21)}$$

where

$$\alpha = (x_i - x_j)^2 + (y_i - y_j)^2$$

$$\beta = -\{ (x_i - x_j) \cos\theta_j + (y_i - y_j) \sin\theta_j \}$$

$$A = -\cos\theta_j \quad , \quad C = -\sin\theta_j$$

$$B = x_i - x_j \quad , \quad D = y_i - y_j$$

$$C_{p,k} = (C_{xp,k}\,\vec{i} + C_{yp,k}\,\vec{j}) \cdot \vec{n}_p \quad \text{—— (A-22)}$$

$$\phi_v = \int_j \tan^{-1} \frac{(y_i - y_j - S \sin\theta_j)}{(x_i - x_j - S \cos\theta_j)}\, dS_j$$

$$\nabla\phi_v = \int_j \left(\vec{i}\,\frac{\partial}{\partial x_i} + \vec{j}\,\frac{\partial}{\partial y_i}\right) \tan^{-1} \frac{(y_i - y_j - S \sin\theta_j)}{(x_i - x_j - S \cos\theta_j)}\, dS_j \quad \text{—— (A-23)}$$

$$= \int \frac{\Delta S_j \; -(y_i - y_j - S \sin\theta_j)\,\vec{i} + (x_i - x_j - S \cos\theta_j)\,\vec{j}}{(x_i - x_j - S \cos\theta_j)^2 + (y_i - y_j - S \sin\theta_j)^2}\, dS_j$$

$$\nabla\phi_v = \int_0^{\Delta S_j} \frac{(AS + B)i + (CS + D)j}{\alpha + 2\beta S + S \cdot S}\, dS = C_{xi,j}\,\vec{i} + C_{yi,j}\,\vec{j} \quad \text{—— (A-24)}$$

Here,

$$\alpha = (x_i - x_j)^2 + (y_i - y_j)^2$$

$$\beta = -\{ (x_i - x_j) \cos\theta_j + (y_i - y_j) \sin\theta_j \}$$

$$A = \sin\theta_j \ , \ C = -\cos\theta_j$$

$$B = -(y_i - y_j) \ , \ D = x_i - x_j$$

$$C_{p,N+1} = \sum_{k=1}^{N} (C_{xp,k}\,\vec{i} + C_{yp,k}\,\vec{j}) \cdot \vec{n}_p \qquad \text{—— (A-25)}$$

$$I = \int_0^{\Delta S_j} \frac{(AS + B)\vec{i} + (CS + D)\vec{j}}{\alpha + 2\beta S + S \cdot S}\, dS = \int_0^{\Delta S_j} \frac{(AS + B)\vec{i} + (CS + D)\vec{j}}{R}\, dS$$

$$= \left[\frac{A}{2} \ell n\, R - A\beta \int \frac{dS}{R} + B \int \frac{dS}{R} \right]_0^{\Delta S_j} \vec{i}$$

$$+ \left[\frac{C}{2} \ell n\, R - C\beta \int \frac{dS}{R} + D \int \frac{dS}{R} \right]_0^{\Delta S_j} \vec{j}$$

$$I = \left[\frac{A}{2} \ell n\{(\alpha + 2\beta\Delta S_j + \Delta S_j^2)/\alpha\} + (B - A\beta) \int_0^{\Delta S_j} \frac{dS}{R} \right] \vec{i}$$

$$+ \left[\frac{C}{2} \ell n\{(\alpha + 2\beta\Delta S_j + \Delta S_j^2)/\alpha\} + (D - C\beta) \int_0^{\Delta S_j} \frac{dS}{R} \right] \vec{j} \qquad \text{—— (A-26)}$$

Let $\Delta = (\alpha - \beta)^2$

$$= \{(x_i - x_j)^2 (1 - \cos^2\theta_j) + (y_i - y_j) (1 - \sin^2\theta_j)$$

$$- 2 (x_i - x_j) (y_i - y_j) \cos\theta_j \sin\theta_j\}$$

$$= \{(x_i - x_j) \sin\theta_j - (y_i - y_j) \cos\theta_j\}^2 \geq 0$$

$$\int_0^{\Delta S_j} \frac{dS}{R} = \frac{\Delta S_j}{\beta(\beta + \Delta S_j)} \quad \text{if} \quad \Delta = 0 \quad \text{—— (A-27)}$$

$$\int_0^{\Delta S_j} \frac{dS}{R} = \frac{1}{\sqrt{\Delta}} \left\{ \tan^{-1}\frac{\beta + \Delta S_j}{\sqrt{\Delta}} - \tan^{-1}\frac{\beta}{\sqrt{\Delta}} \right\} \quad , \Delta > 0$$

The velocity on panel itself due to source is obtained as follows.

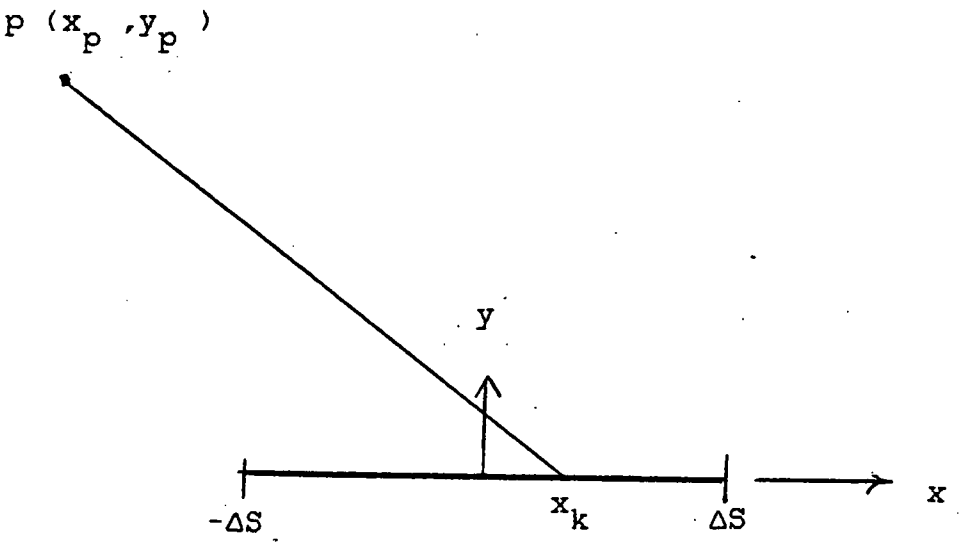

$$\phi_s = \frac{\lambda}{2\pi} \int_{\Delta S}^{\Delta S} \ell n \sqrt{(x_p - x_k)^2 + y_p^2}\, dx_k$$

$$\nabla\phi_s = \frac{\lambda}{2\pi} \int_{-\Delta S}^{\Delta S} \left\{ \frac{x_p - x_k}{(x_p - x_k)^2 + y_p^2} \vec{i} + \frac{y_p}{(x_p - x_k)^2 + y_p^2} \vec{j} \right\} dx_k$$

$$= \frac{\lambda}{2\pi} \left\{ \left[-\ln \sqrt{(x_p - x_k)^2 + y_p^2} \right]_{-\Delta S}^{\Delta S} \vec{i} + \left[-\tan^{-1} \left(\frac{x_p - x_k}{y_p} \right) \right]_{-\Delta S}^{\Delta S} \vec{j} \right\}$$

At $x_p = y_p = 0$,

$$V_x = \frac{\lambda}{2\pi} \{ -\ln \Delta S + \ln \Delta S \} = 0 \qquad \text{—— (A-29)}$$

$$V_y = \frac{\lambda}{2\pi} \left\{ -\tan^{-1} \frac{-\Delta S}{y_p} + \tan^{-1} \frac{\Delta S}{y_p} \right\} = \pm \frac{\lambda}{2} \text{ , } y_p = \pm 0 \qquad \text{—— (A-30)}$$

The veocity on panel itself due to vortex is as follows.

$$\phi_v = \frac{\gamma}{2\pi} \int_{-\Delta S}^{\Delta S} \tan^{-1} \frac{y_p}{x_p - x_k} dx_k$$

$$\nabla \phi_v = \frac{\gamma}{2\pi} \int_{-\Delta S}^{\Delta S} \left\{ \frac{-y_p \vec{i} + (x_p - x_k) \vec{j}}{(x_p - x_k)^2 + y_p^2} \right\} dx_k$$

$$= \frac{\gamma}{2\pi} \left\{ \left[\tan^{-1} \left(\frac{x_p - x_k}{y_p} \right) \right]_{-\Delta S}^{\Delta S} \vec{i} + \left[-\ln \sqrt{(x_p - x_k)^2 + y_p^2} \right]_{-\Delta S}^{\Delta S} \vec{j} \right\}$$

At $x_p = y_p = 0$,

$$V_x = \frac{\gamma}{2\pi} \left\{ \tan^{-1} \frac{-\Delta S}{y_p} - \tan^{-1} \frac{\Delta S}{y_p} \right\} = \mp \frac{\gamma}{2} \text{ , } y_p = \pm 0 \qquad \text{—— (A-31)}$$

$$V_y = \frac{\gamma}{2\pi} \{ -\ell n\ \Delta S + \ell n\ \Delta S \} = 0 \qquad \text{—— (A-32)}$$

A.1.5 Compressibility Correction

The governing equation for linearized subsonic flow is

$$(1 - M_\infty^2)\ \phi_{xx} + \phi_{yy} = 0 \qquad \text{—— (A-33)}$$

Let $x' = x,\ y' = y \sqrt{1-M_\infty^2} = y\ \beta$ —— (A-34)

Then

$$(1 - M_\infty^2)\ \phi_{x'x'} + (1- M_\infty^2)\ \phi_{y'y'} = 0$$

Let $\phi' = (1 - M_\infty^2)\ \phi$ —— (A-35)

$$\phi'_{x'x'} + \phi'_{y'y'} = 0$$

We compute the geometry for the equivalent body using the Gothert transformation (A-34). We compute the perturbation potential of the equivalent body. Then the perturbation to the real body geometry is

$$\frac{\partial \phi}{\partial x} = \frac{\partial \phi'}{\partial x'} \frac{1}{\beta^2}\ ,\ \frac{\partial \phi}{\partial y} = \frac{\partial \phi'}{\partial y'} \frac{1}{\beta} \qquad \text{—— (A-36)}$$

This procedure can be drawn as follows.

body $\longrightarrow$ M_∞ $\longrightarrow$ equivalent body

$\longrightarrow$ influence functions $(C_{ij})_a$ on the equivalent body

$\longrightarrow$ boundary value problem on real body

$\longrightarrow$ $\vec{n}_i \cdot \vec{C}_{ij} = n_{ix} (\vec{i} \cdot \vec{C}_{ij})_a / \beta^2 + n_{iy} (\vec{j} \cdot \vec{C}_{ij})_a / \beta$

: $- \vec{n} \cdot \dfrac{\vec{U_\infty}}{U_\infty} = \sum_j \vec{n}_i \cdot \vec{C}_{ij} X_j = \sum_j \vec{n}_i \cdot (C_{xij} \vec{i} + C_{yij} \vec{j}) X_j$

$\longrightarrow$ perturbation velocities on the real body

: $u = \sum_j \vec{i} \cdot \vec{C}_{ij} X_j$

: $v = \sum_j \vec{j} \cdot \vec{C}_{ij} X_j$

where X_j are the strengths of sources and vortex.

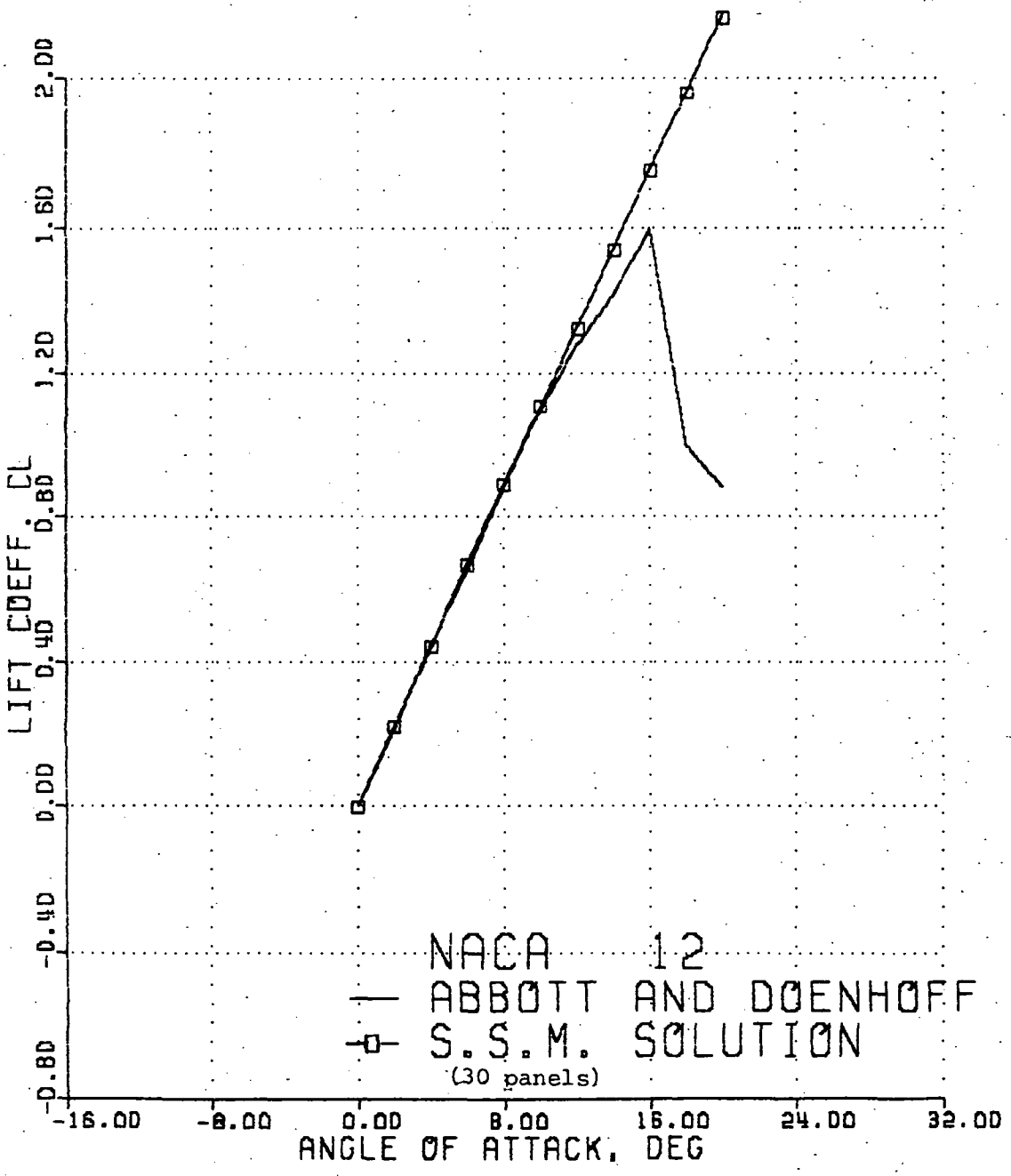
LIFT COEFF, CL
2.00
1.60
1.20
0.80
0.40
0.00
-0.40
-0.80
-16.00
-8.00
0.00
8.00
16.00
24.00
32.00
ANGLE OF ATTACK, DEG
NACA 12
ABBOTT AND DOENHOFF
S.S.M. SOLUTION
(30 panels)

Figure A-1.

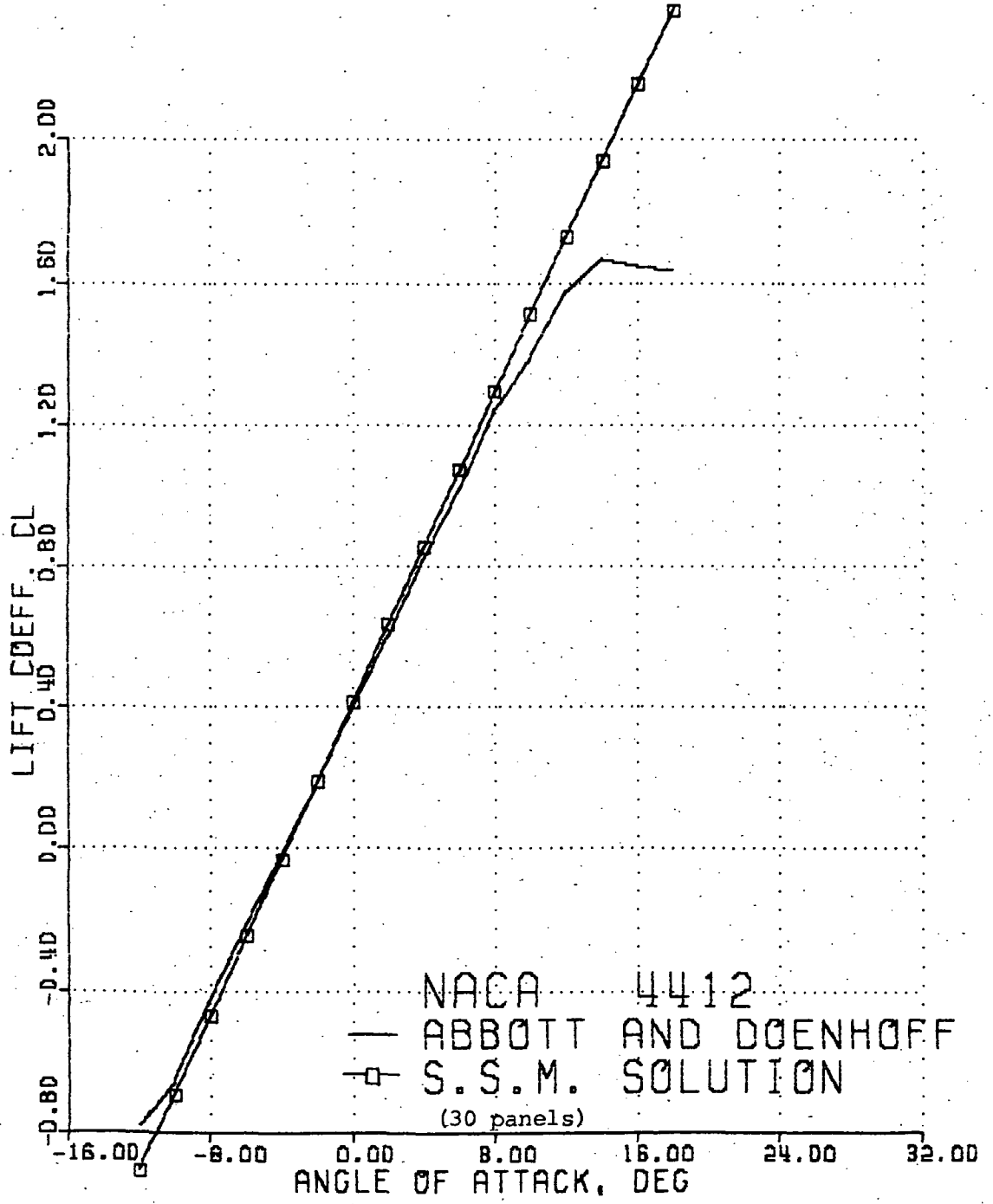
LIFT COEFF., CL
2.00
1.60
1.20
0.80
0.40
0.00
-0.40
-0.80
-16.00
-8.00
0.00
8.00
16.00
24.00
32.00
ANGLE OF ATTACK, DEG
NACA 4412
ABBOTT AND DOENHOFF
S.S.M. SOLUTION
(30 panels)

Figure A-2.

C-3

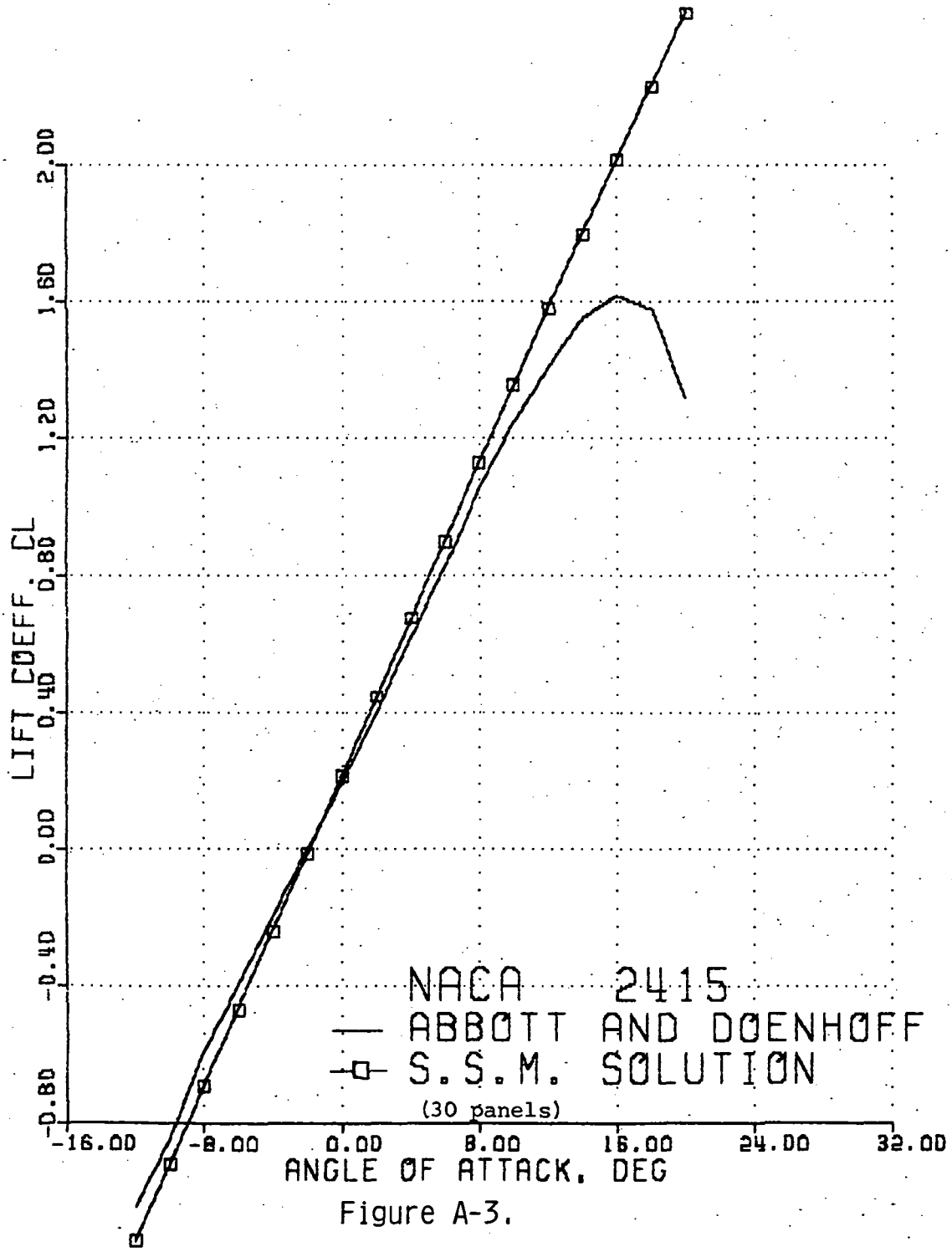
LIFT COEFF, CL
2.00
1.60
1.20
0.80
0.40
0.00
-0.40
-0.80
-16.00
-8.00
0.00
8.00
16.00
24.00
32.00
ANGLE OF ATTACK, DEG
NACA 2415
ABBOTT AND DOENHOFF
S.S.M. SOLUTION
(30 panels)

Figure A-3.

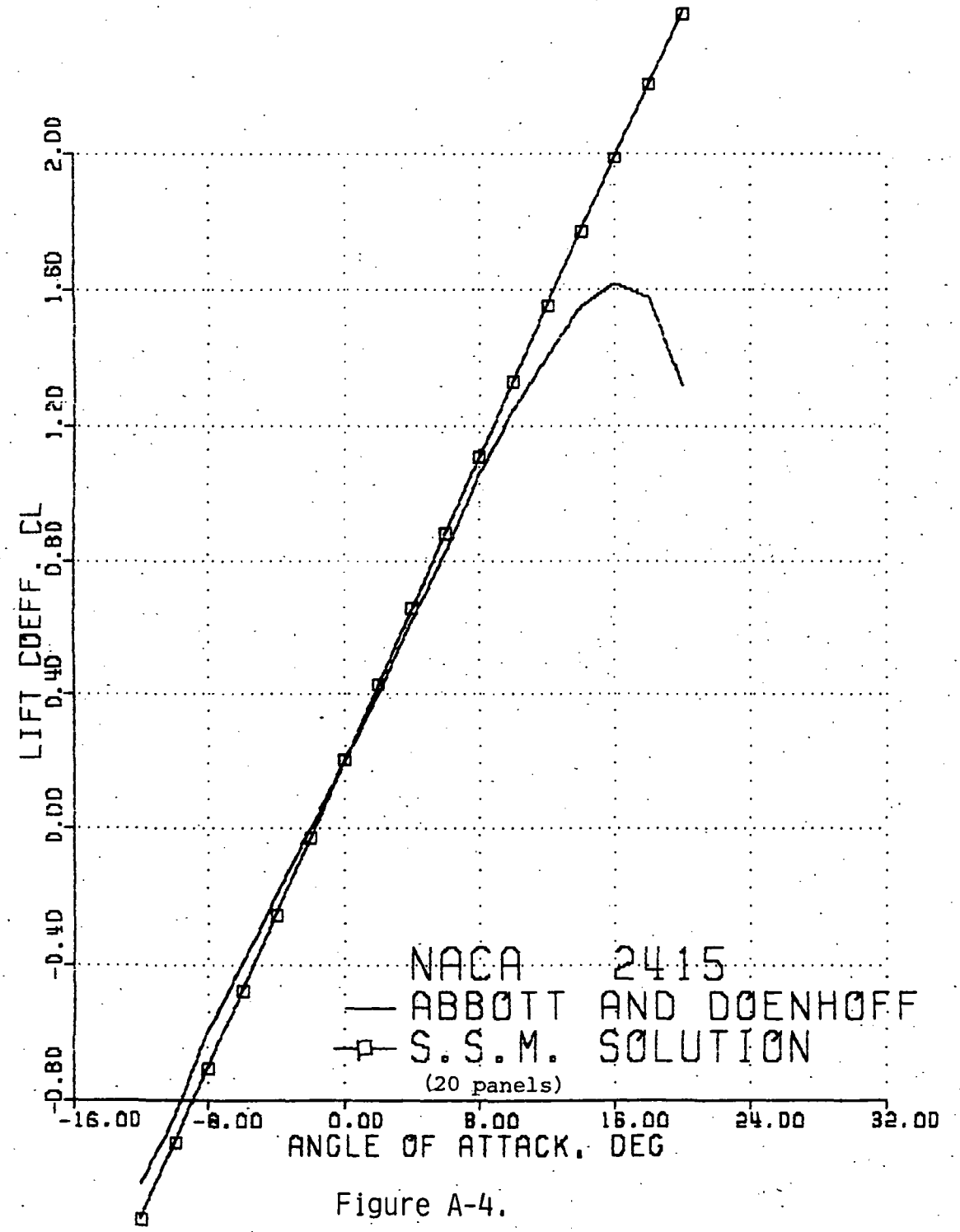
LIFT COEFF. CL
2.00
1.60
1.20
0.80
0.40
0.00
-0.40
-0.80
-16.00
-8.00
0.00
8.00
16.00
24.00
32.00
ANGLE OF ATTACK, DEG
NACA 2415
ABBOTT AND DOENHOFF
S.S.M. SOLUTION
(20 panels)

Figure A-4.

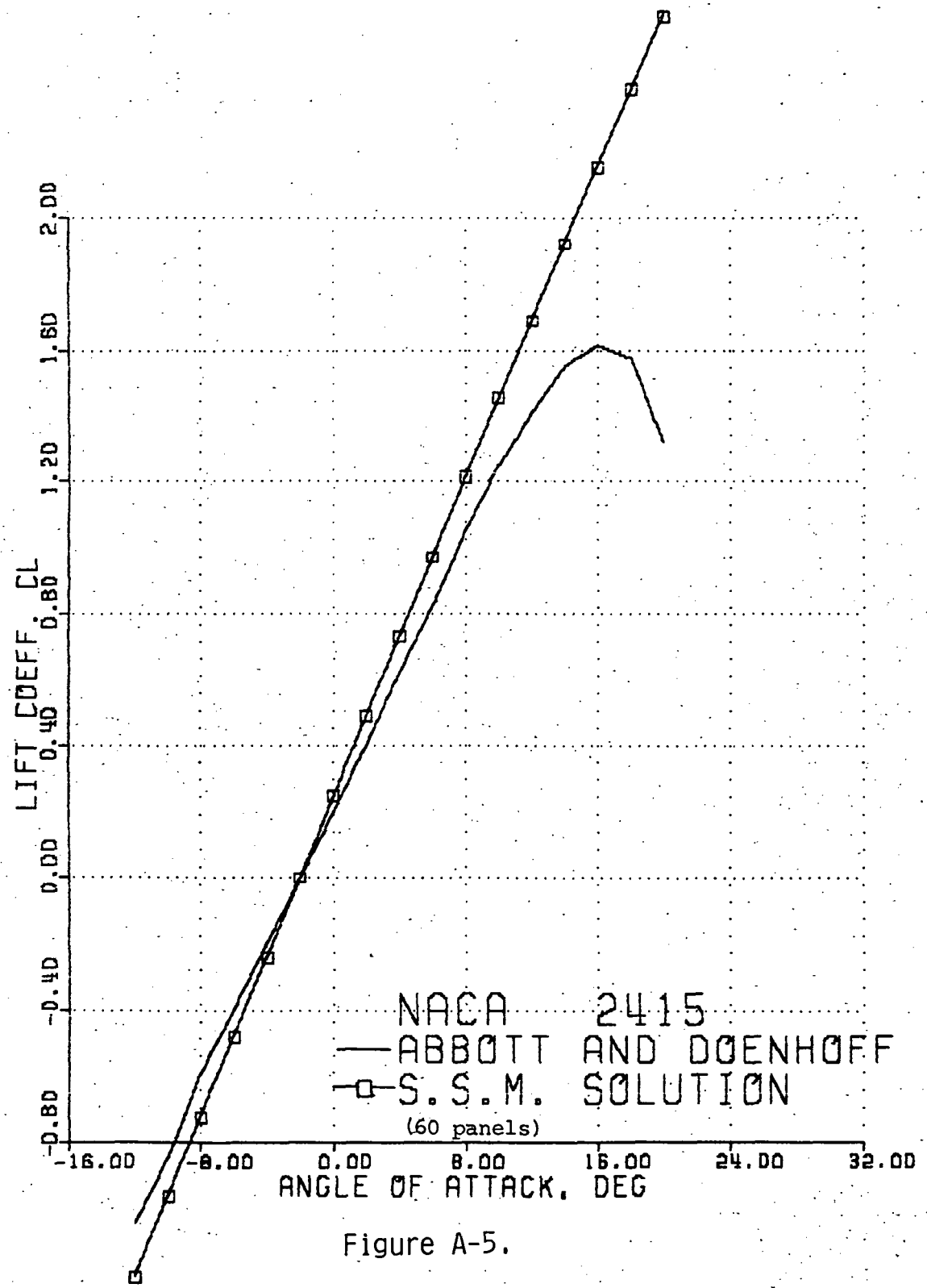
LIFT COEFF, CL
2.00
1.60
1.20
0.80
0.40
0.00
-0.40
-0.80
-16.00
-8.00
0.00
8.00
16.00
24.00
32.00
ANGLE OF ATTACK, DEG
NACA 2415
ABBOTT AND DOENHOFF
S.S.M. SOLUTION
(60 panels)

Figure A-5.

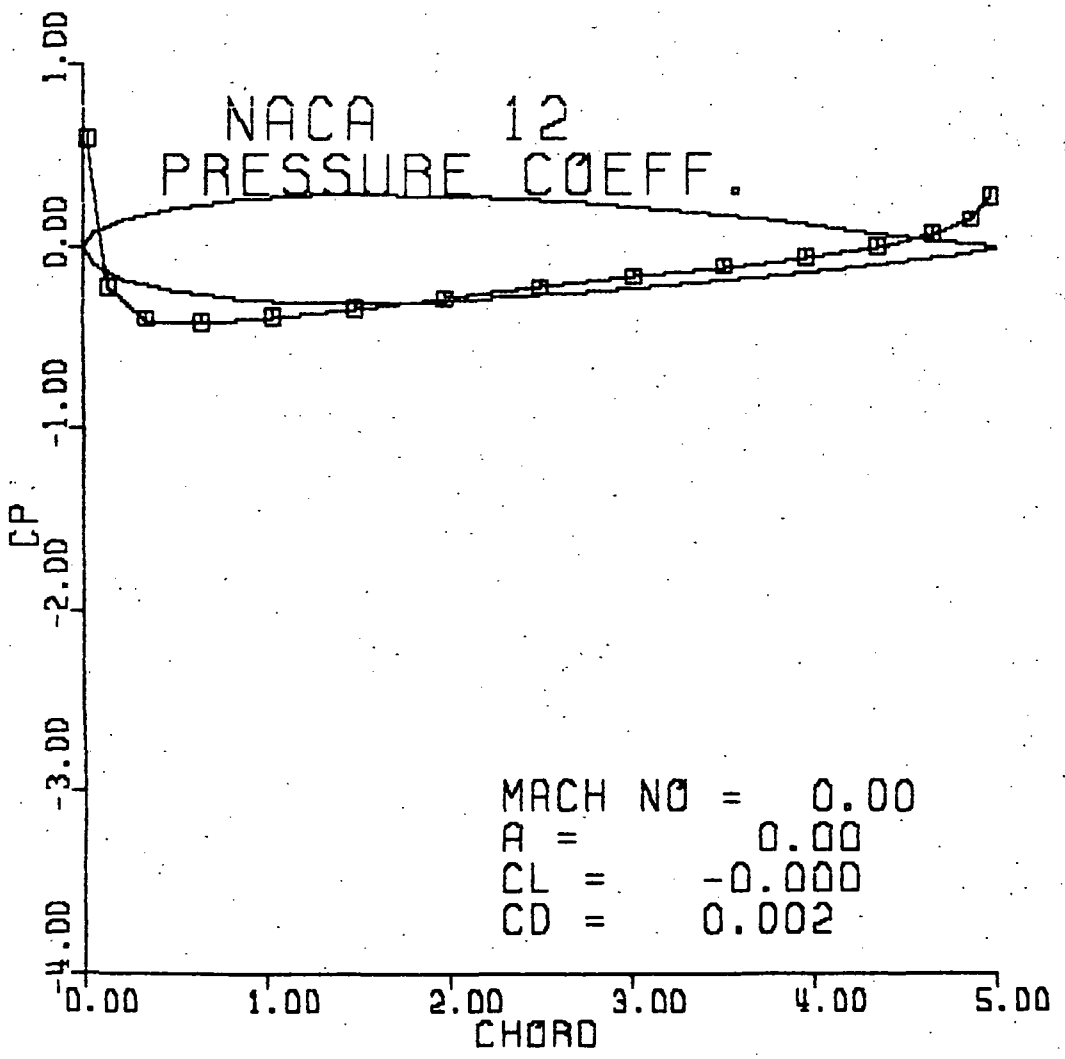
NACA 12
PRESSURE COEFF.
MACH NO = 0.00
A = 0.00
CL = -0.000
CD = 0.002
CP
1.00
0.00
-1.00
-2.00
-3.00
-4.00
0.00
1.00
2.00
3.00
4.00
5.00
CHORD

Figure A-6.

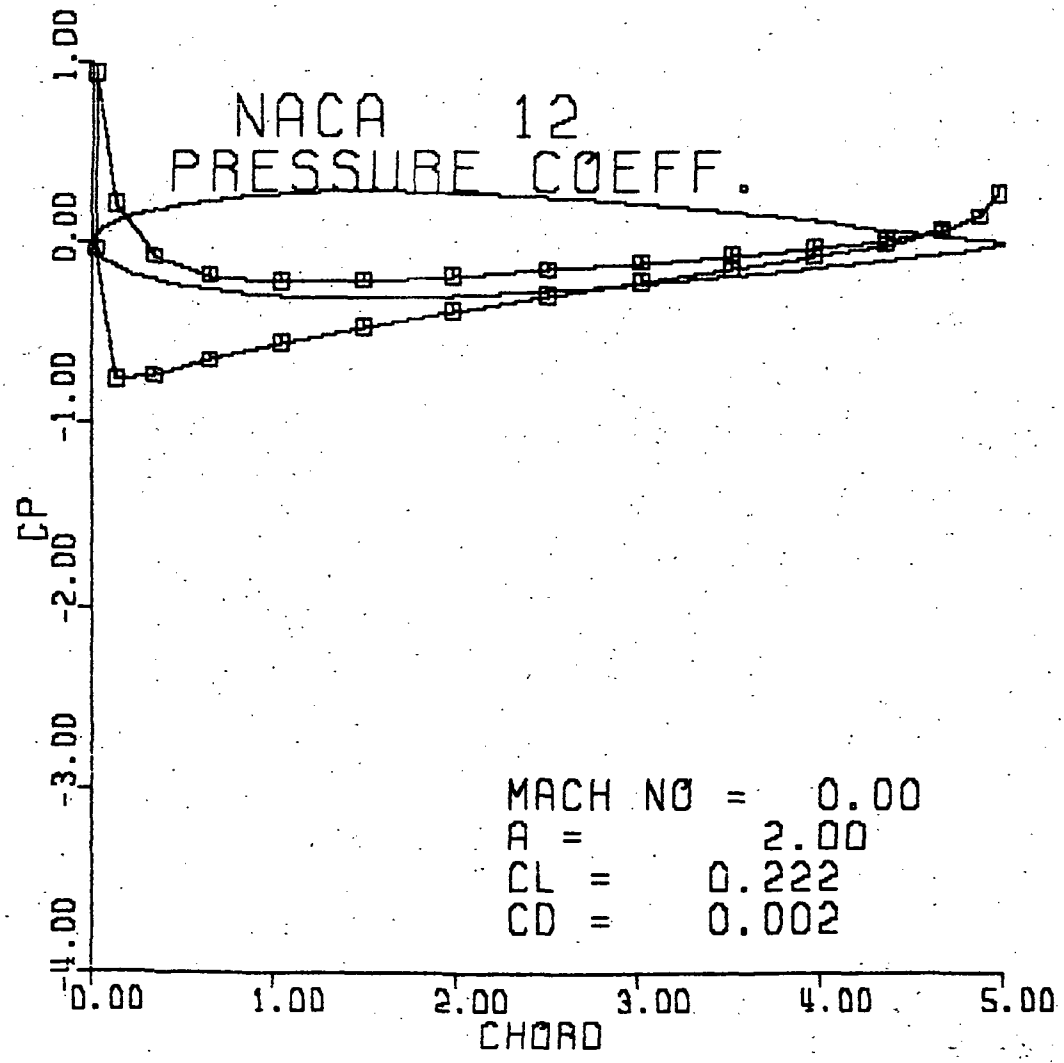
NACA 12
PRESSURE COEFF.
MACH NO = 0.00
A = 2.00
CL = 0.222
CD = 0.002
CP
1.00
0.00
-1.00
-2.00
-3.00
-4.00
0.00
1.00
2.00
3.00
4.00
5.00
CHORD

Figure A-7.

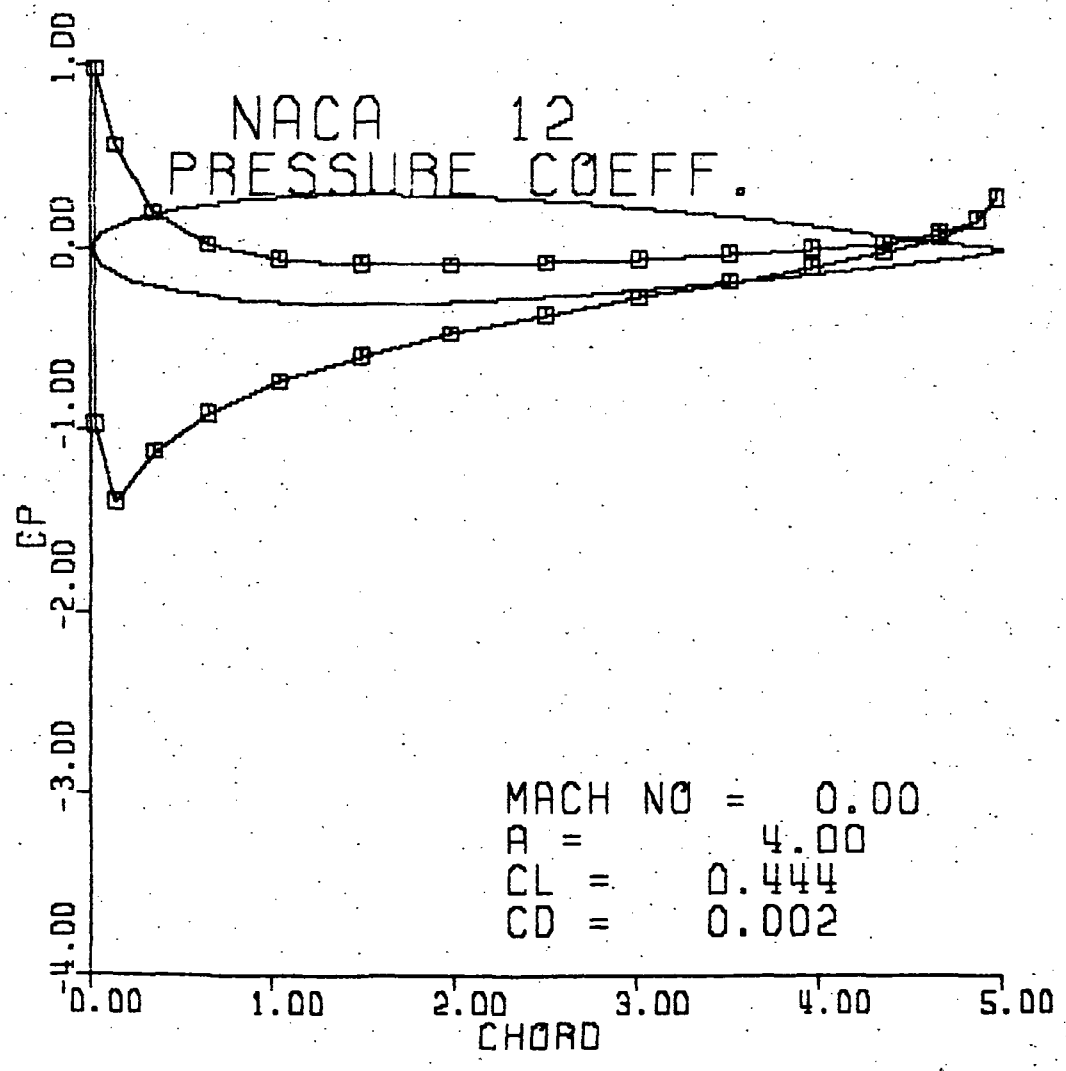
NACA 12
PRESSURE COEFF.
MACH NO = 0.00
A = 4.00
CL = 0.444
CD = 0.002
CP
1.00
0.00
-1.00
-2.00
-3.00
-4.00
0.00
1.00
2.00
3.00
4.00
5.00
CHORD

Figure A-8.

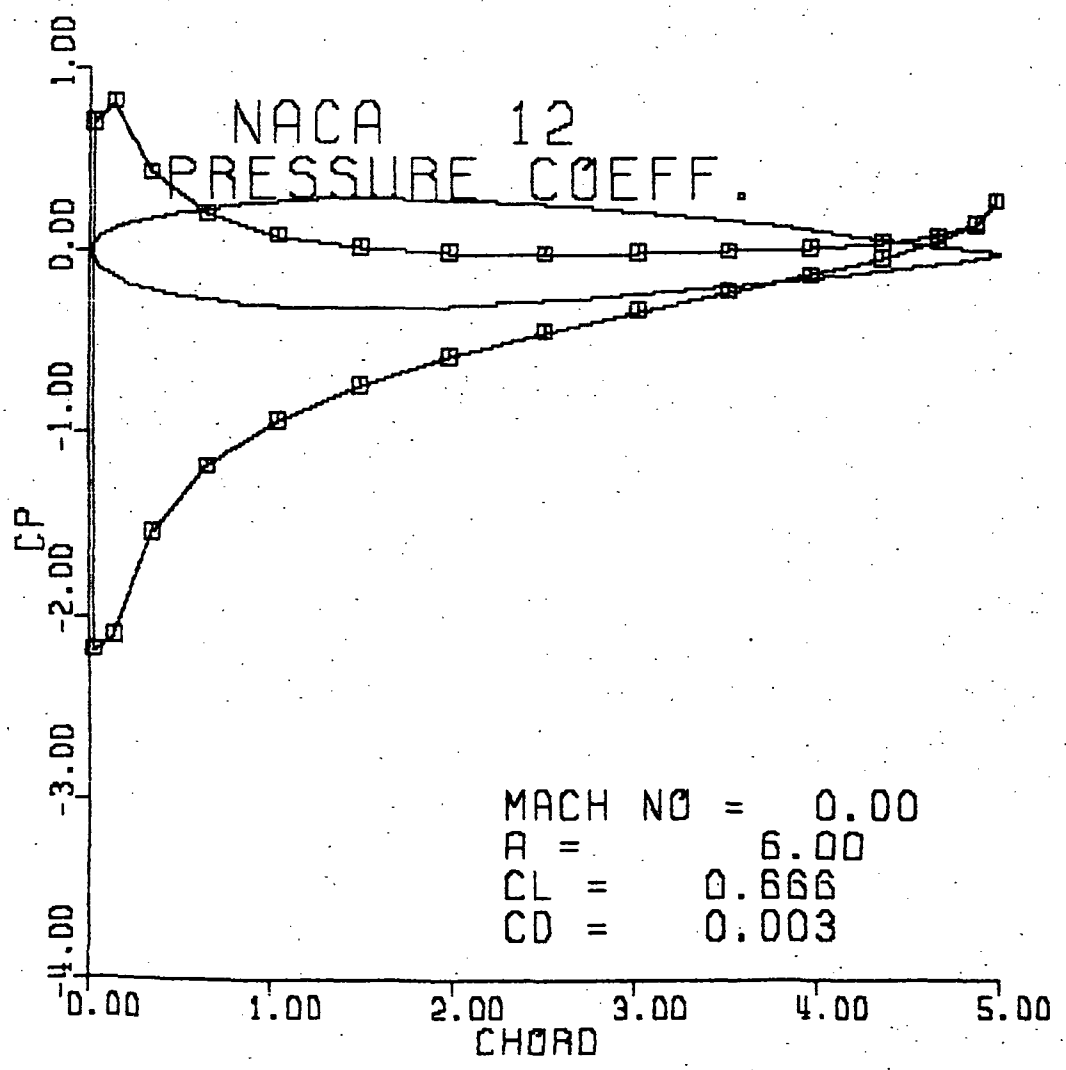
NACA 12
PRESSURE COEFF.
MACH NO = 0.00
A = 6.00
CL = 0.666
CD = 0.003
CP
CHORD
1.00
0.00
-1.00
-2.00
-3.00
-4.00
0.00
1.00
2.00
3.00
4.00
5.00

Figure A-9.

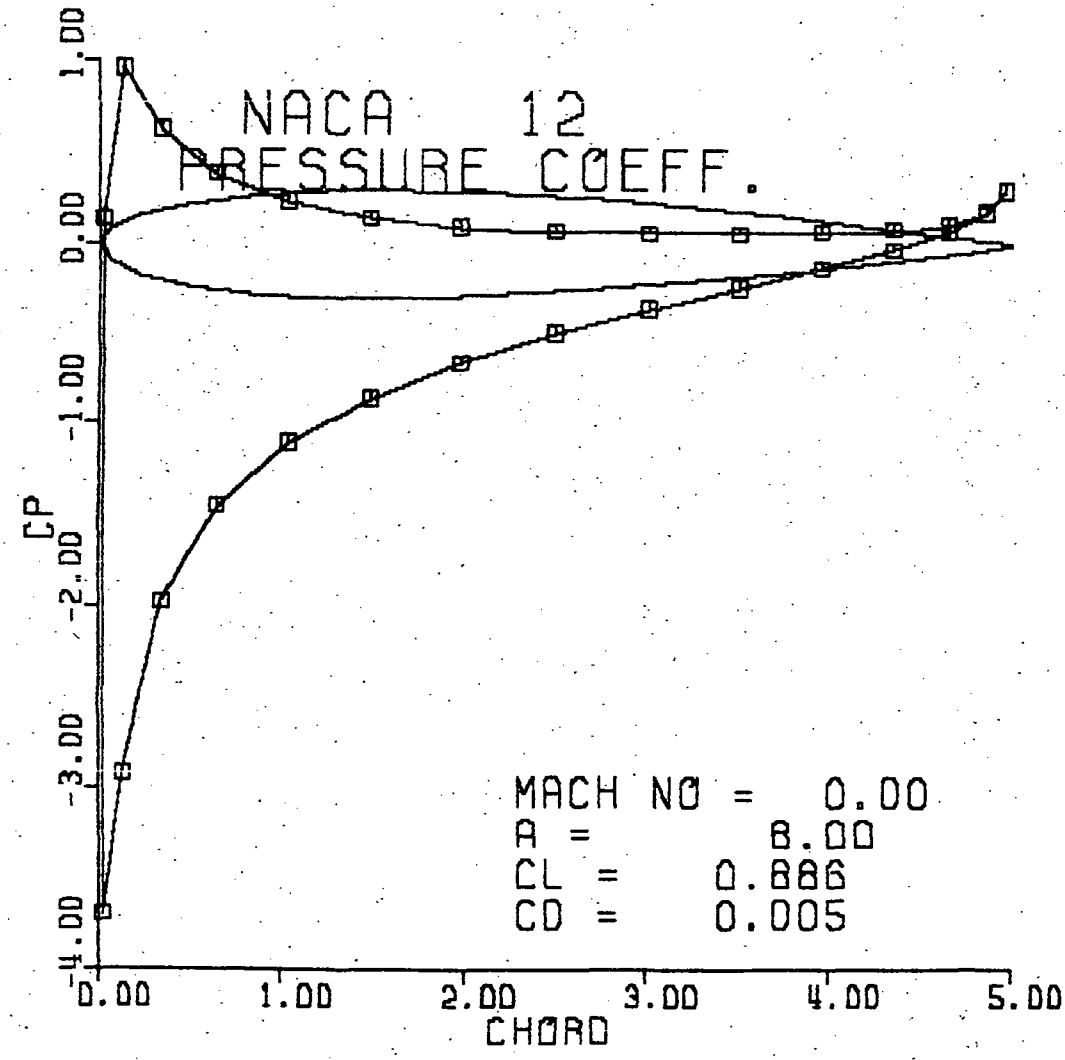
NACA 12
PRESSURE COEFF.
MACH NO = 0.00
A = 8.00
CL = 0.886
CD = 0.005
CP
1.00
0.00
-1.00
-2.00
-3.00
-4.00
0.00
1.00
2.00
3.00
4.00
5.00
CHORD

Figure A-10.

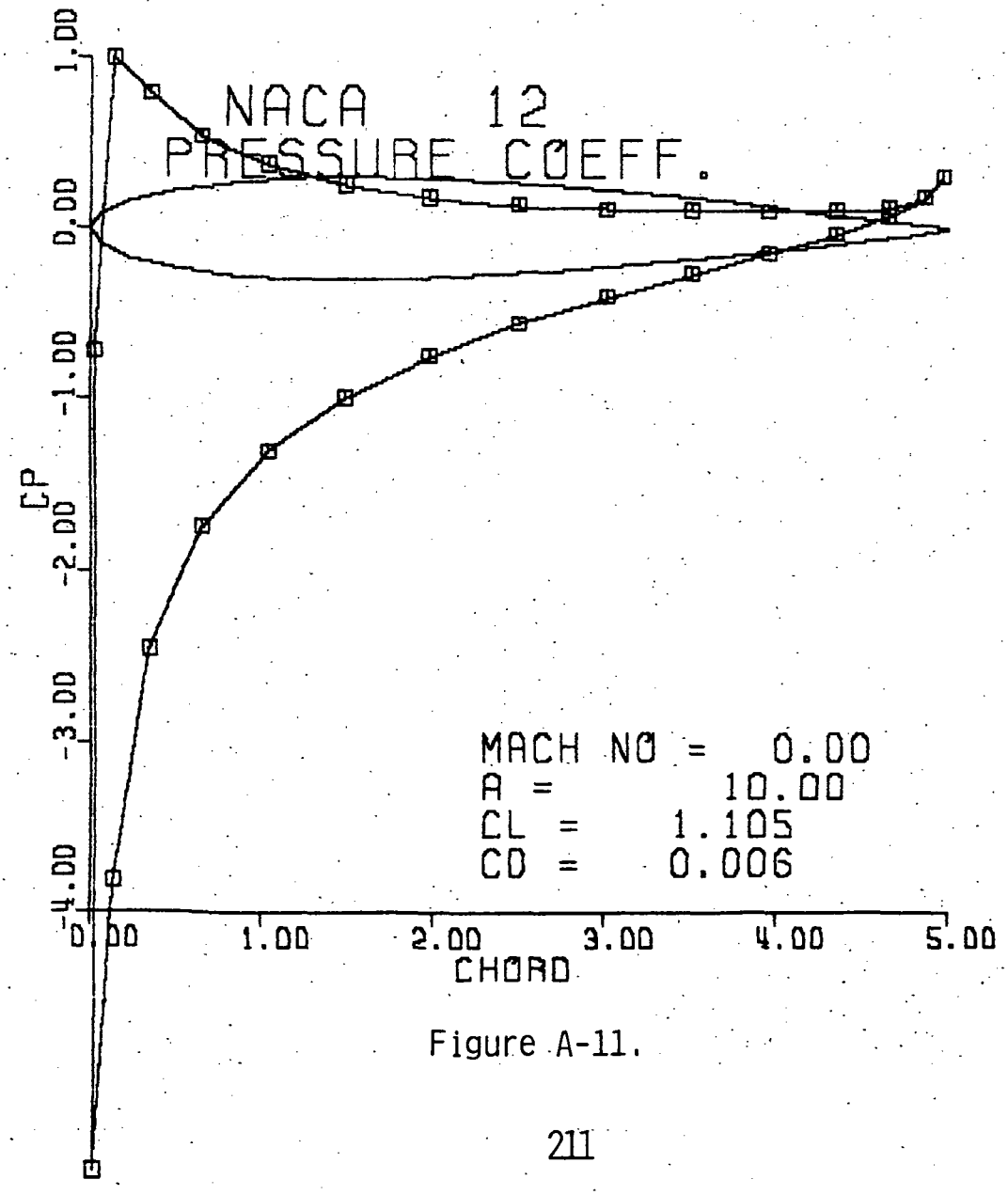
NACA 12
PRESSURE COEFF.
MACH NO = 0.00
A = 10.00
CL = 1.105
CD = 0.006
CP
1.00
0.00
-1.00
-2.00
-3.00
-4.00
0.00
1.00
2.00
3.00
4.00
5.00
CHORD

Figure A-11.

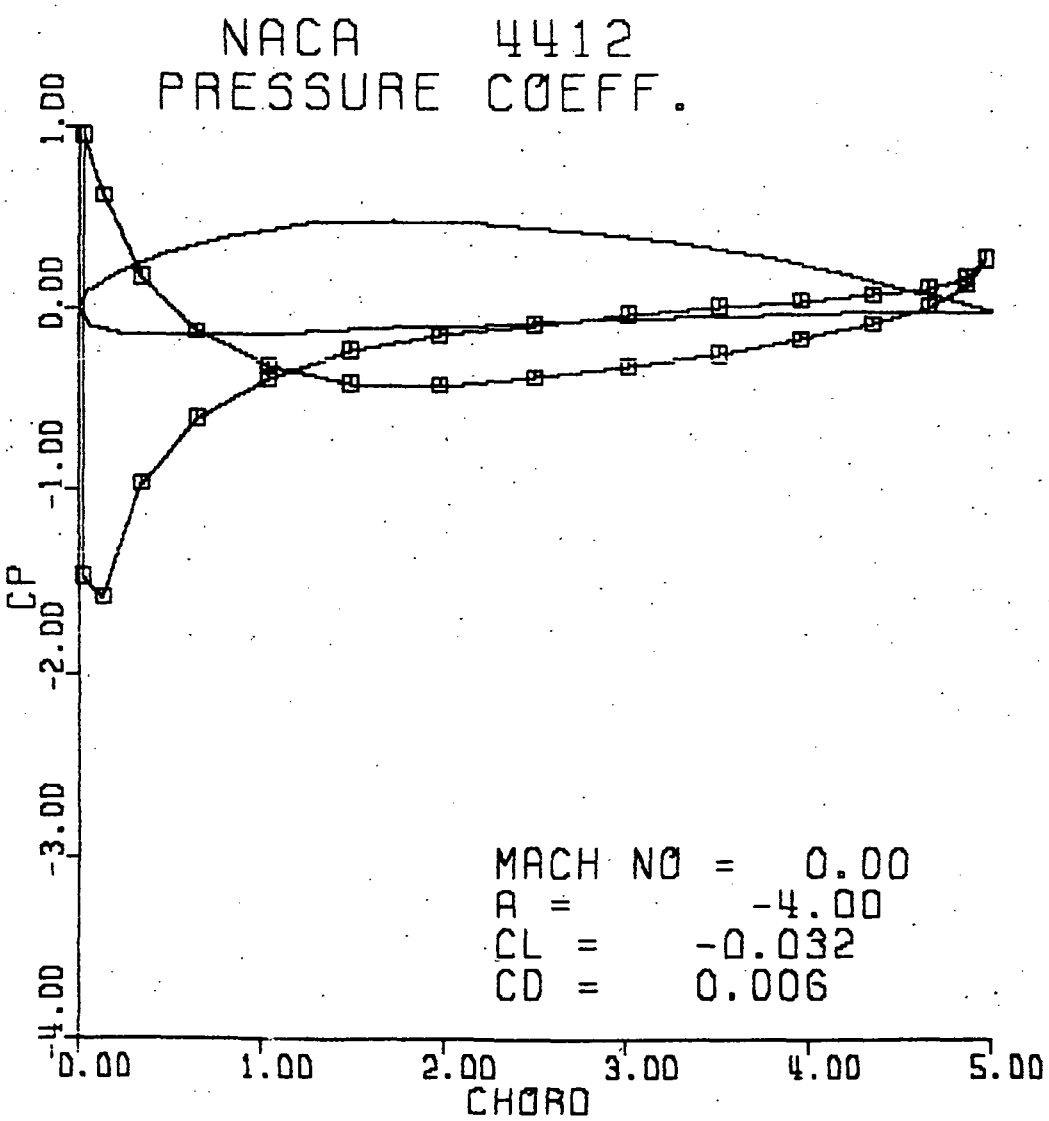
NACA 4412
PRESSURE COEFF.
1.00
0.00
-1.00
-2.00
-3.00
-4.00
CP
0.00
1.00
2.00
3.00
4.00
5.00
CHORD
MACH NO = 0.00
A = -4.00
CL = -0.032
CD = 0.006

Figure A-12.

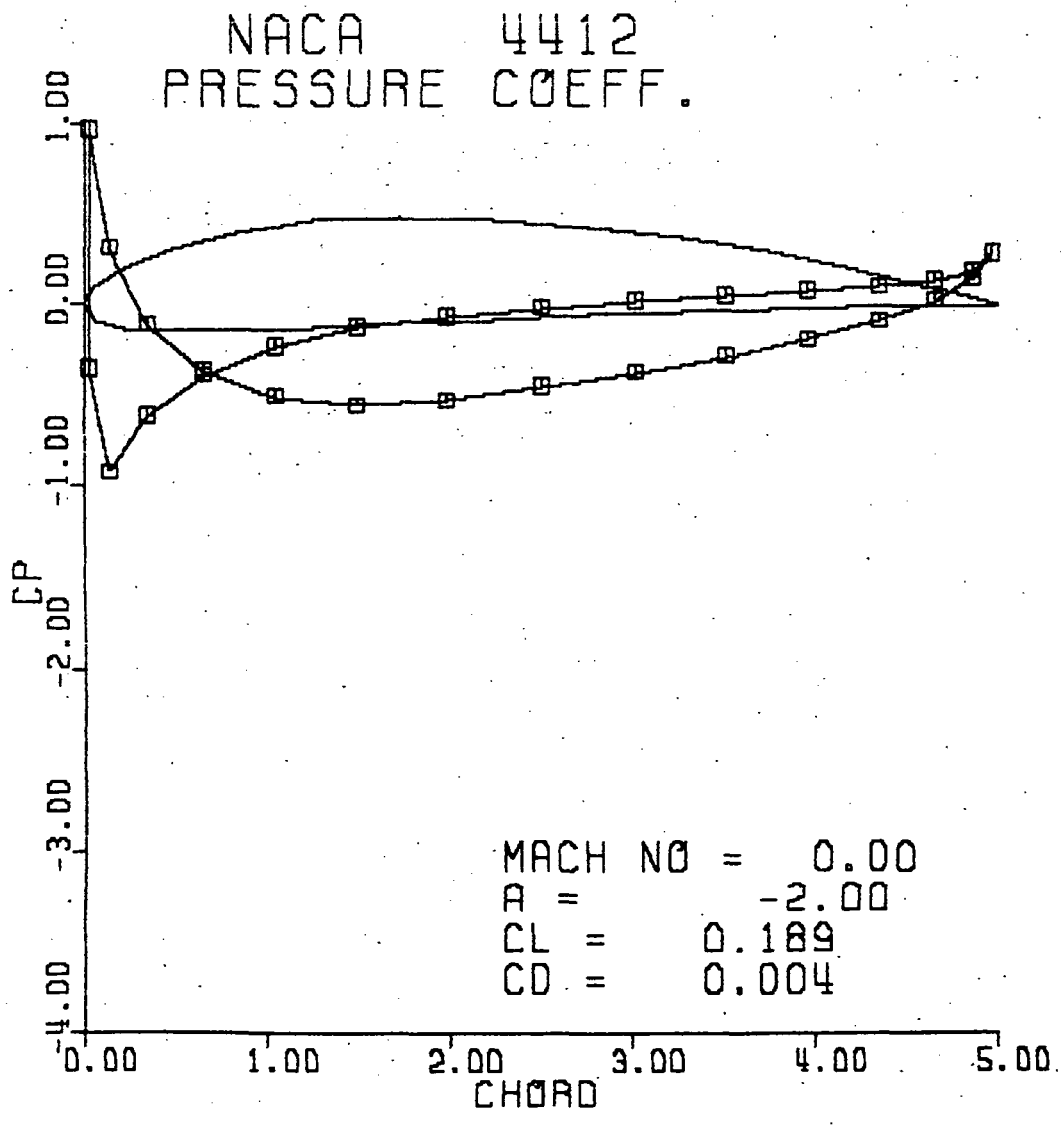
NACA 4412
PRESSURE COEFF.
1.00
0.00
-1.00
-2.00
-3.00
-4.00
CP
0.00
1.00
2.00
3.00
4.00
5.00
CHORD
MACH NO = 0.00
A = -2.00
CL = 0.189
CD = 0.004

Figure A-13.

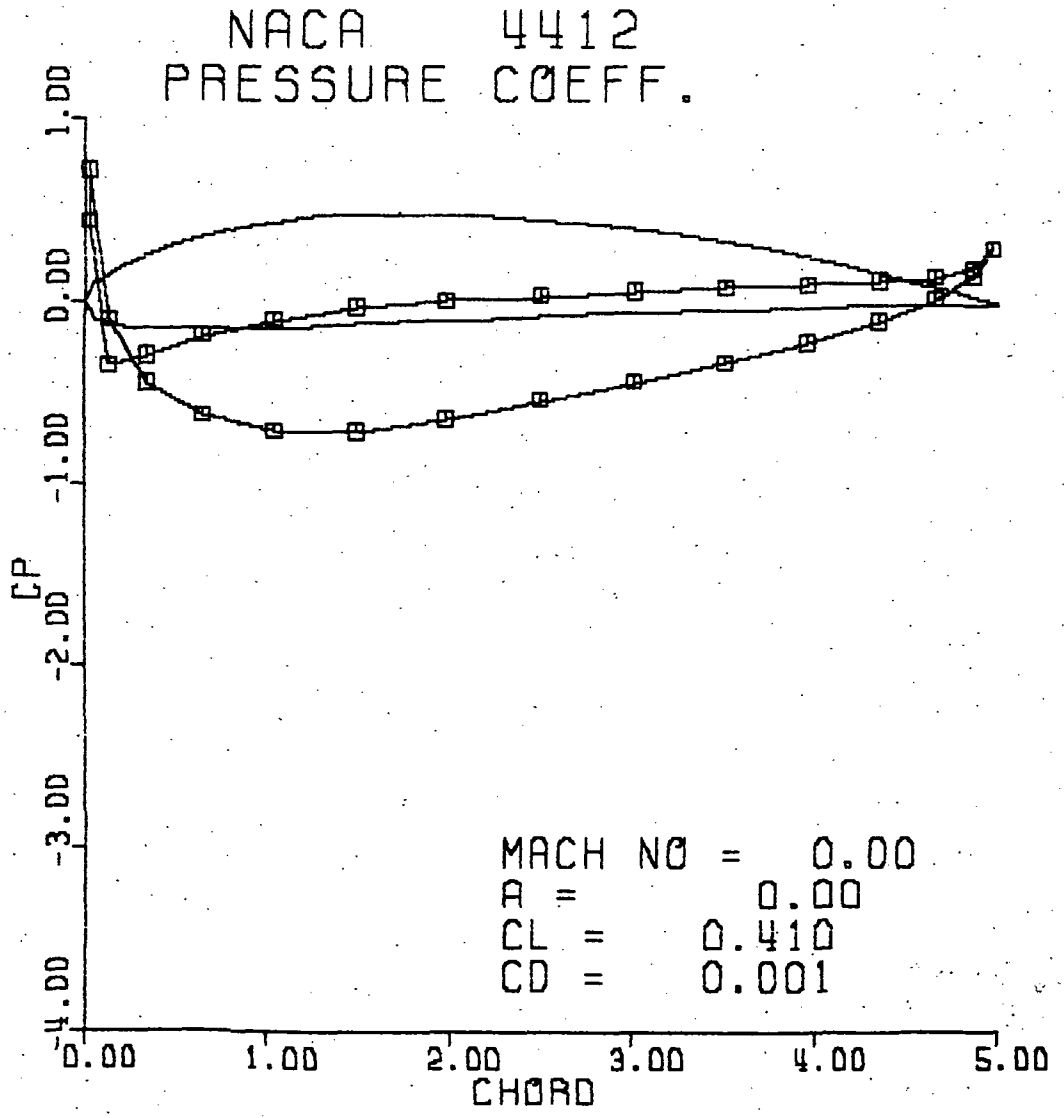
NACA 4412
PRESSURE COEFF.
1.00
0.00
-1.00
-2.00
-3.00
-4.00
CP
MACH NO = 0.00
A = 0.00
CL = 0.410
CD = 0.001
0.00
1.00
2.00
3.00
4.00
5.00
CHORD

Figure A-14.

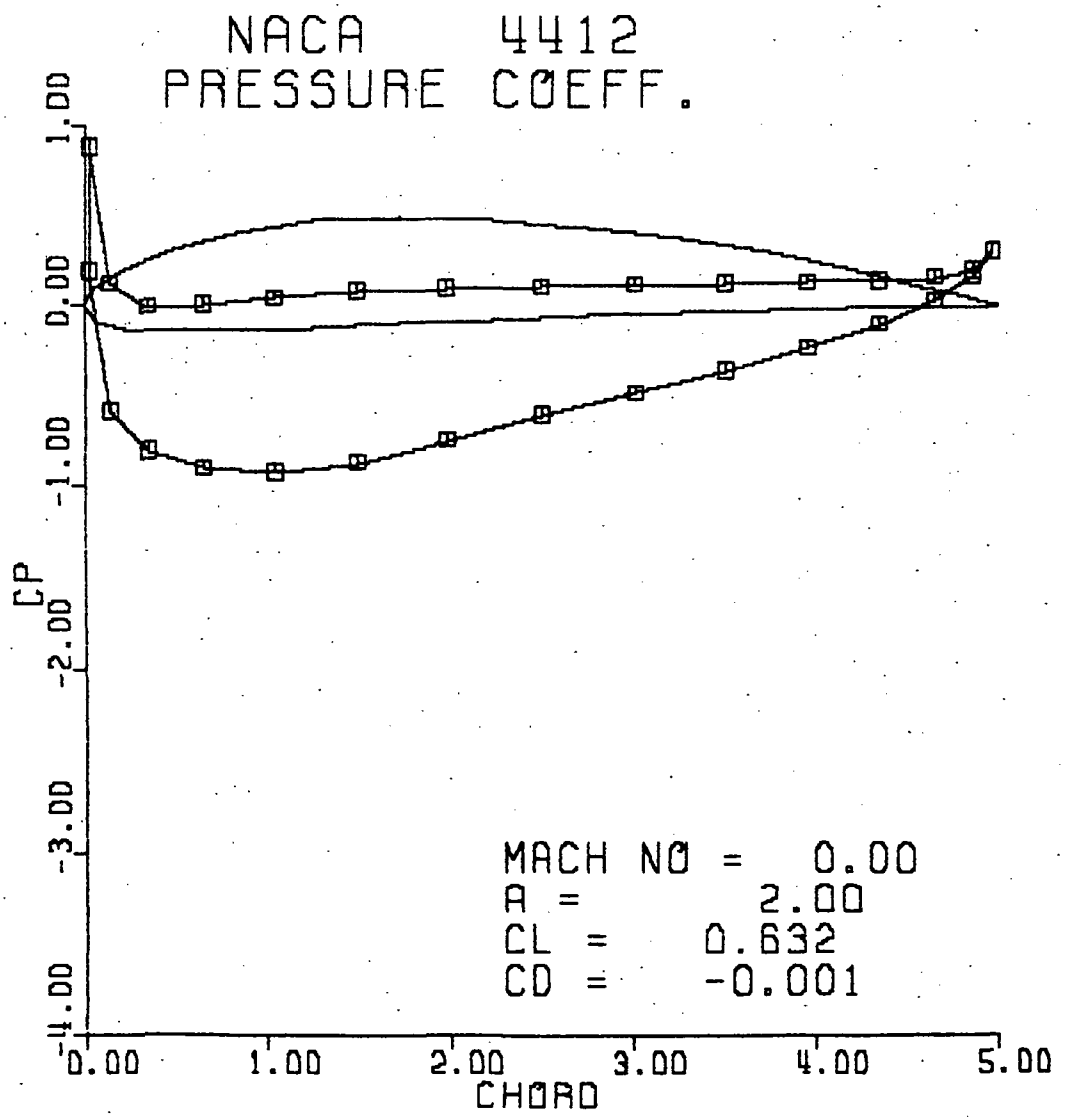
NACA 4412
PRESSURE COEFF.
1.00
0.00
-1.00
-2.00
-3.00
-4.00
CP
0.00
1.00
2.00
3.00
4.00
5.00
CHORD
MACH NO = 0.00
A = 2.00
CL = 0.632
CD = -0.001

Figure A-15.

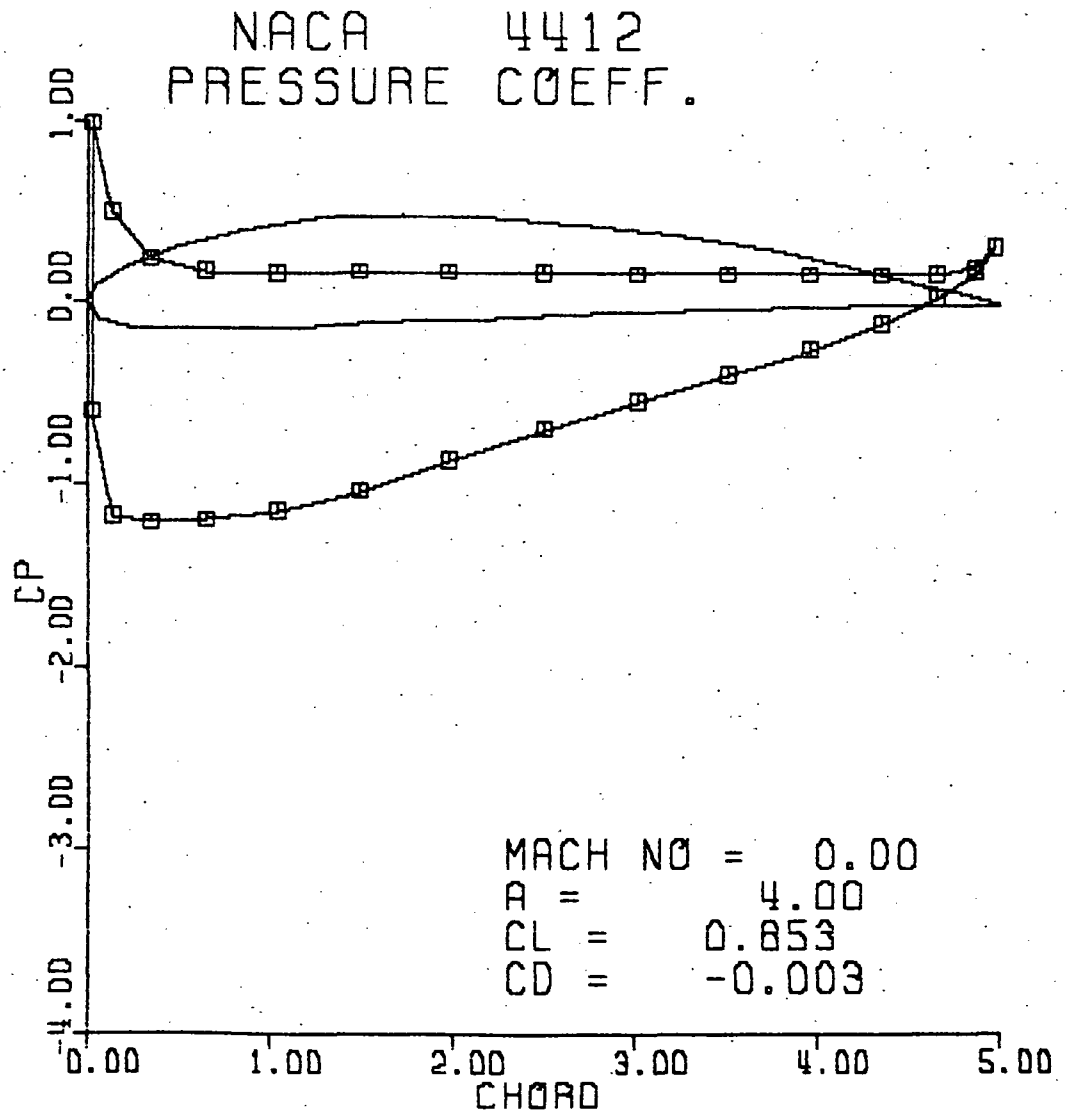
NACA 4412
PRESSURE COEFF.
1.00
0.00
-1.00
-2.00
-3.00
-4.00
CP
0.00
1.00
2.00
3.00
4.00
5.00
CHORD
MACH NO = 0.00
A = 4.00
CL = 0.853
CD = -0.003

Figure A-16.

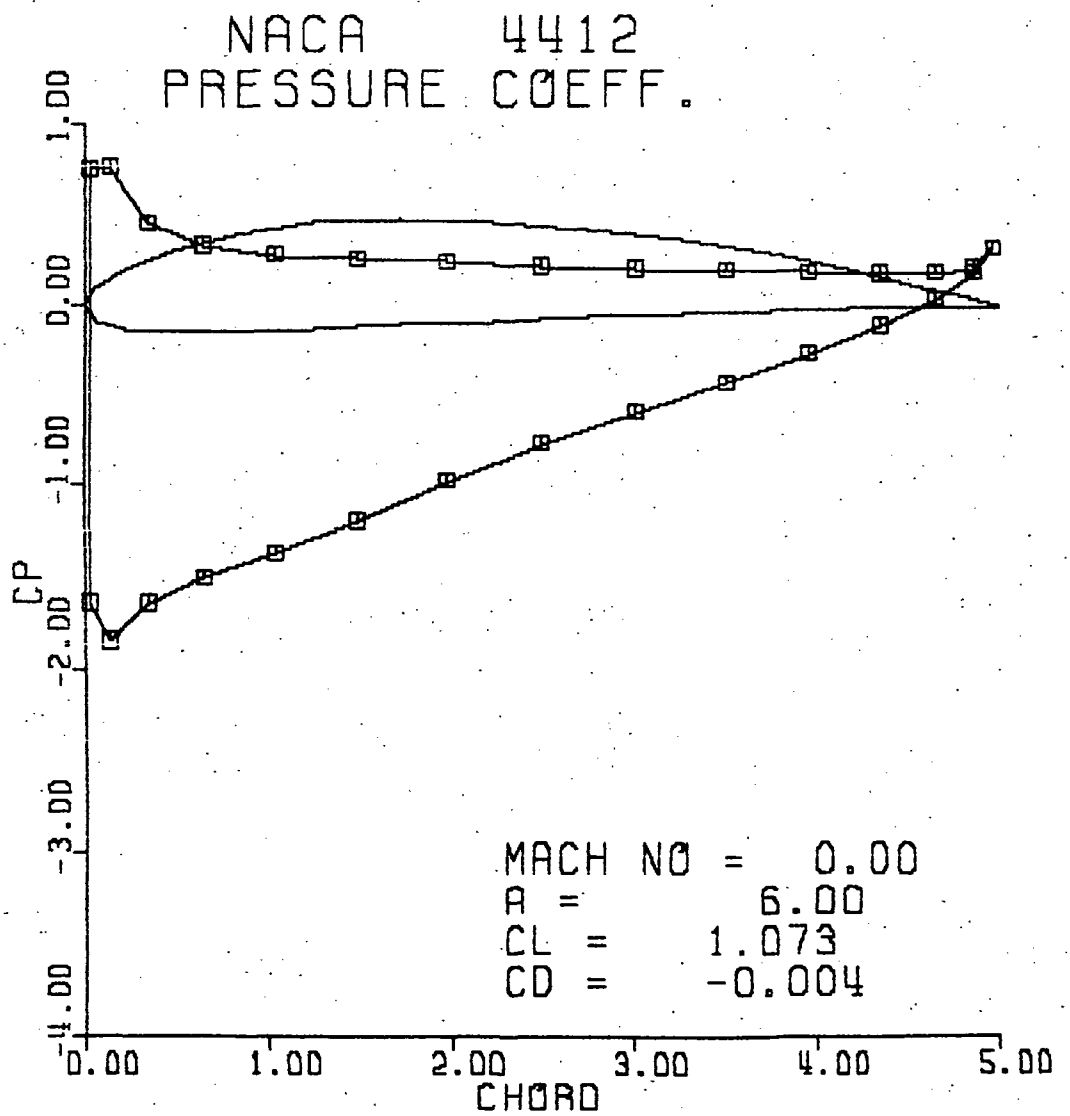
NACA 4412
PRESSURE COEFF.
1.00
0.00
-1.00
-2.00
-3.00
-4.00
CP
0.00
1.00
2.00
3.00
4.00
5.00
CHORD
MACH NO = 0.00
A = 6.00
CL = 1.073
CD = -0.004

Figure A-17.

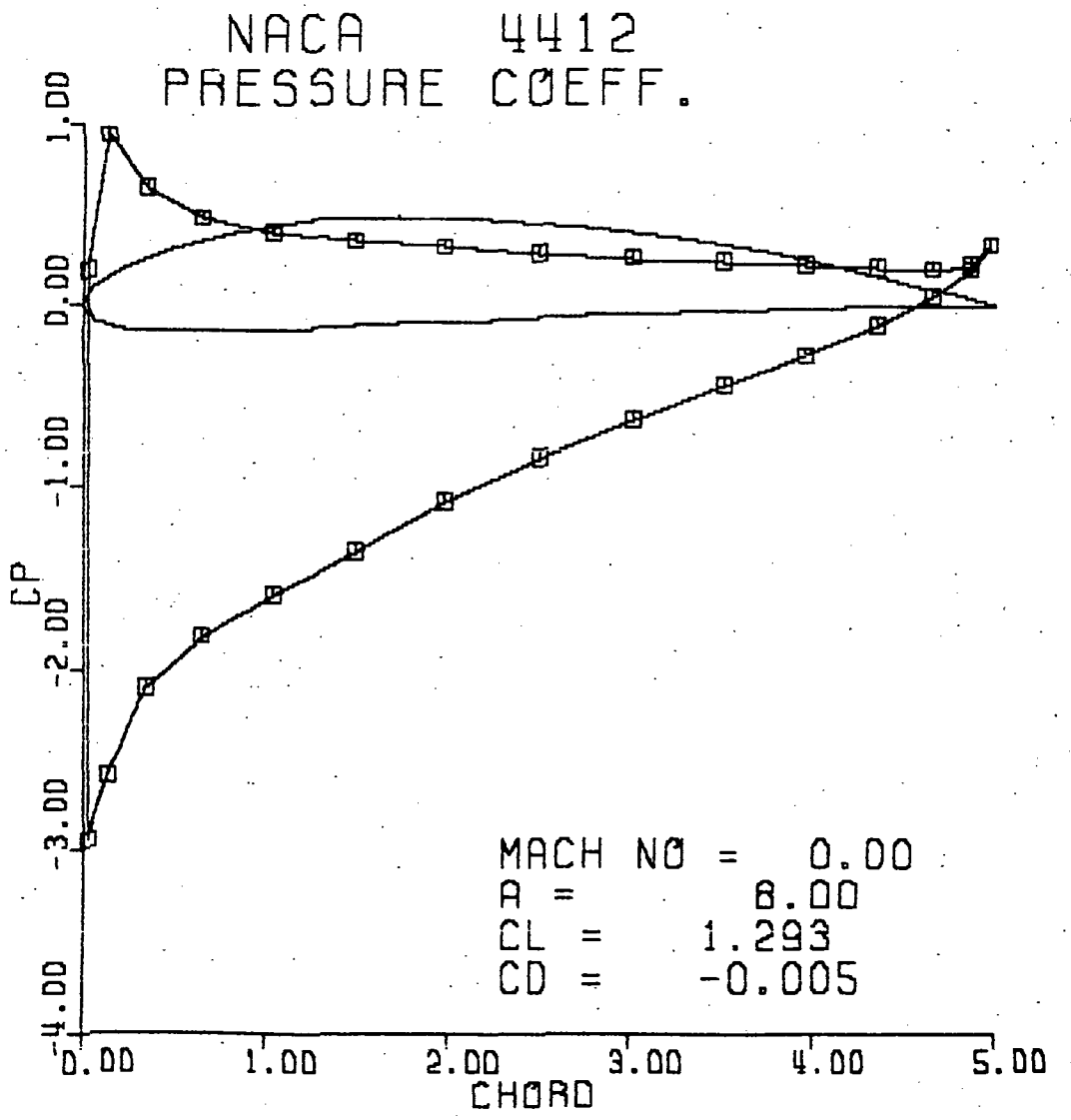
NACA 4412
PRESSURE COEFF.
1.00
0.00
-1.00
-2.00
-3.00
-4.00
CP
0.00
1.00
2.00
3.00
4.00
5.00
CHORD
MACH NO = 0.00
A = 8.00
CL = 1.293
CD = -0.005

Figure A-18.

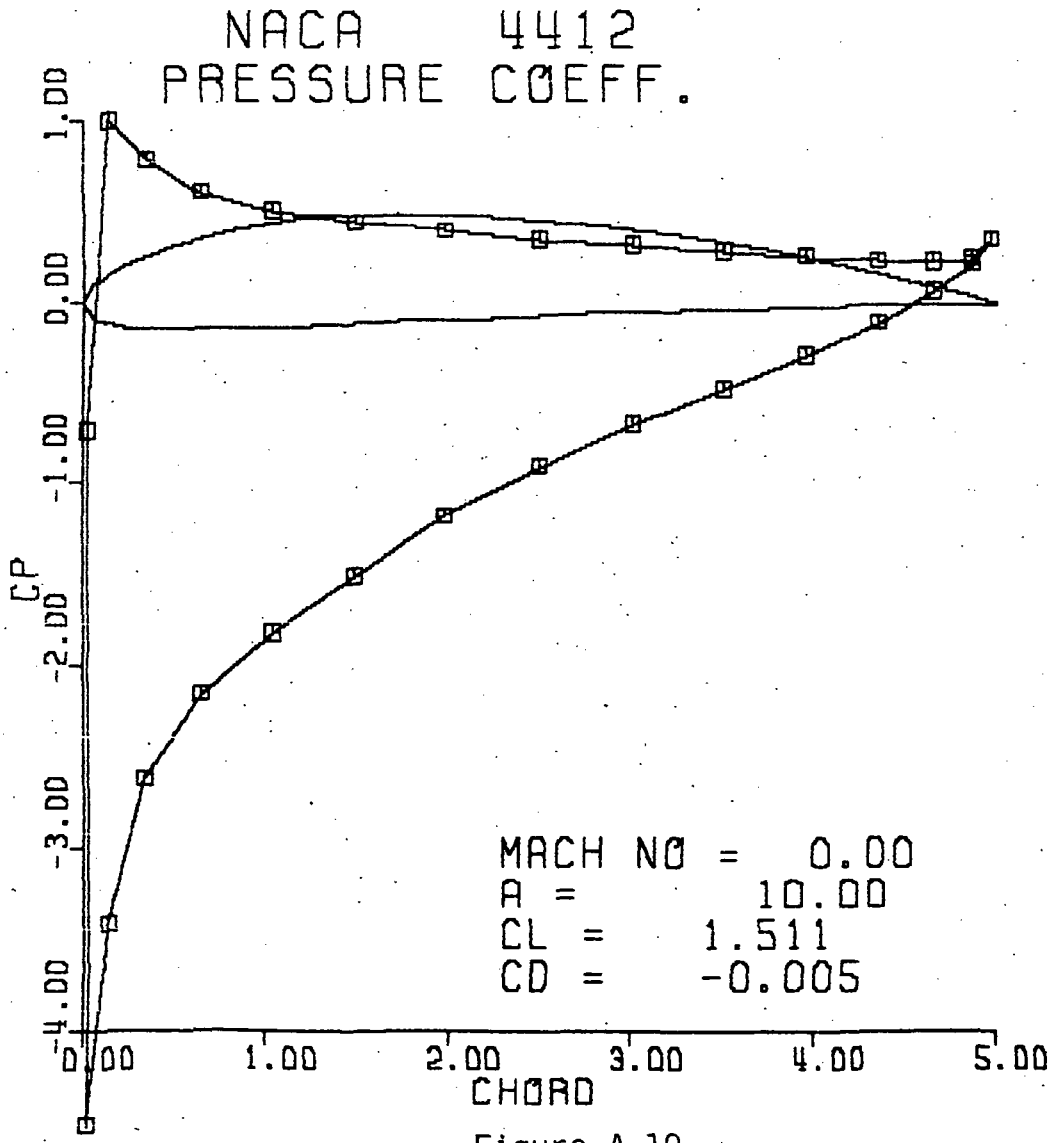
NACA 4412
PRESSURE COEFF.
1.00
0.00
-1.00
-2.00
-3.00
-4.00
CP
0.00
1.00
2.00
3.00
4.00
5.00
CHORD
MACH NO = 0.00
A = 10.00
CL = 1.511
CD = -0.005

Figure A-19.

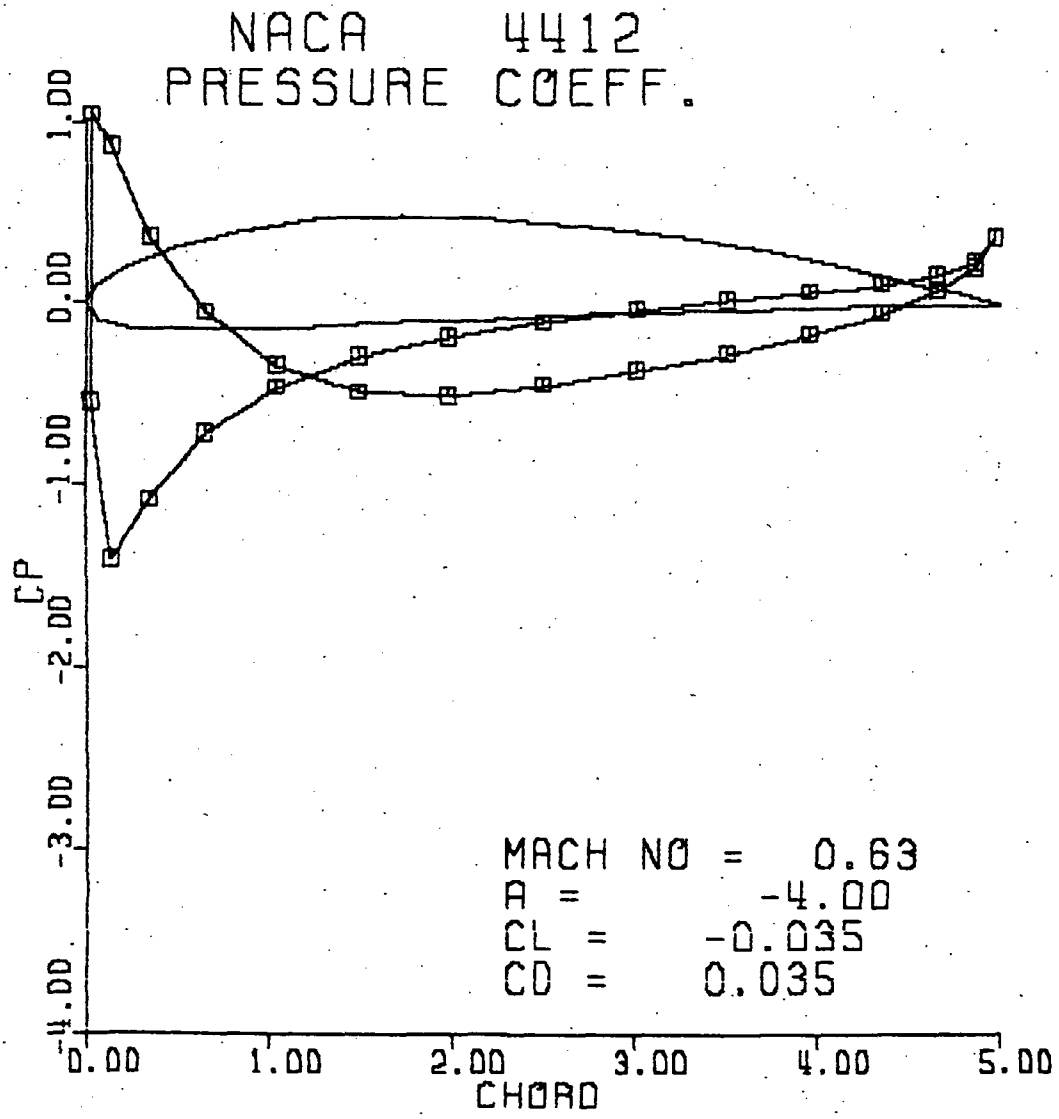
NACA 4412
PRESSURE COEFF.
1.00
0.00
-1.00
-2.00
-3.00
-4.00
CP
0.00
1.00
2.00
3.00
4.00
5.00
CHORD
MACH NO = 0.63
A = -4.00
CL = -0.035
CD = 0.035

Figure A-20.

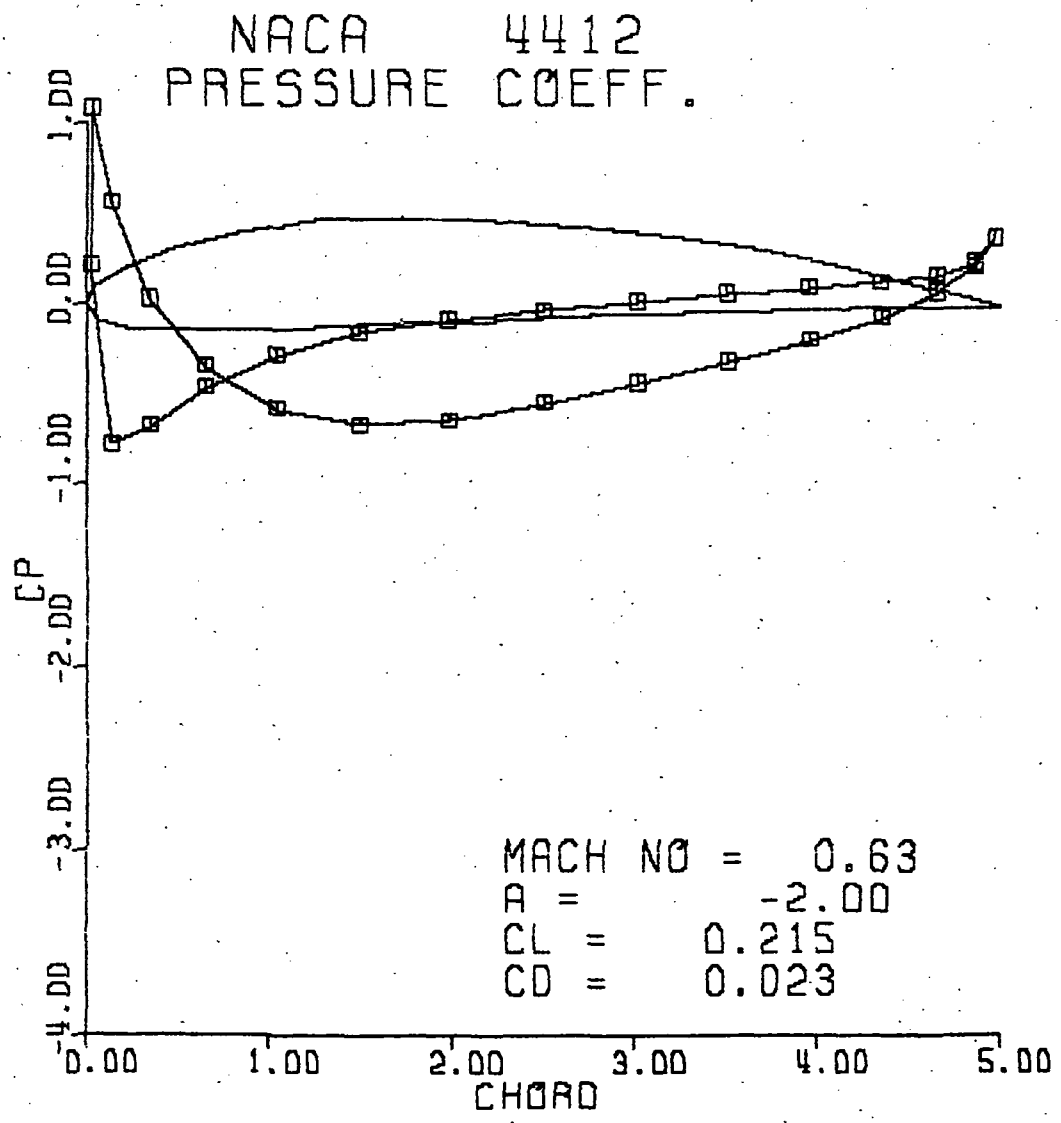
NACA 4412
PRESSURE COEFF.
1.00
0.00
-1.00
-2.00
-3.00
-4.00
CP
0.00
1.00
2.00
3.00
4.00
5.00
CHORD
MACH NO = 0.63
A = -2.00
CL = 0.215
CD = 0.023

Figure A-21.

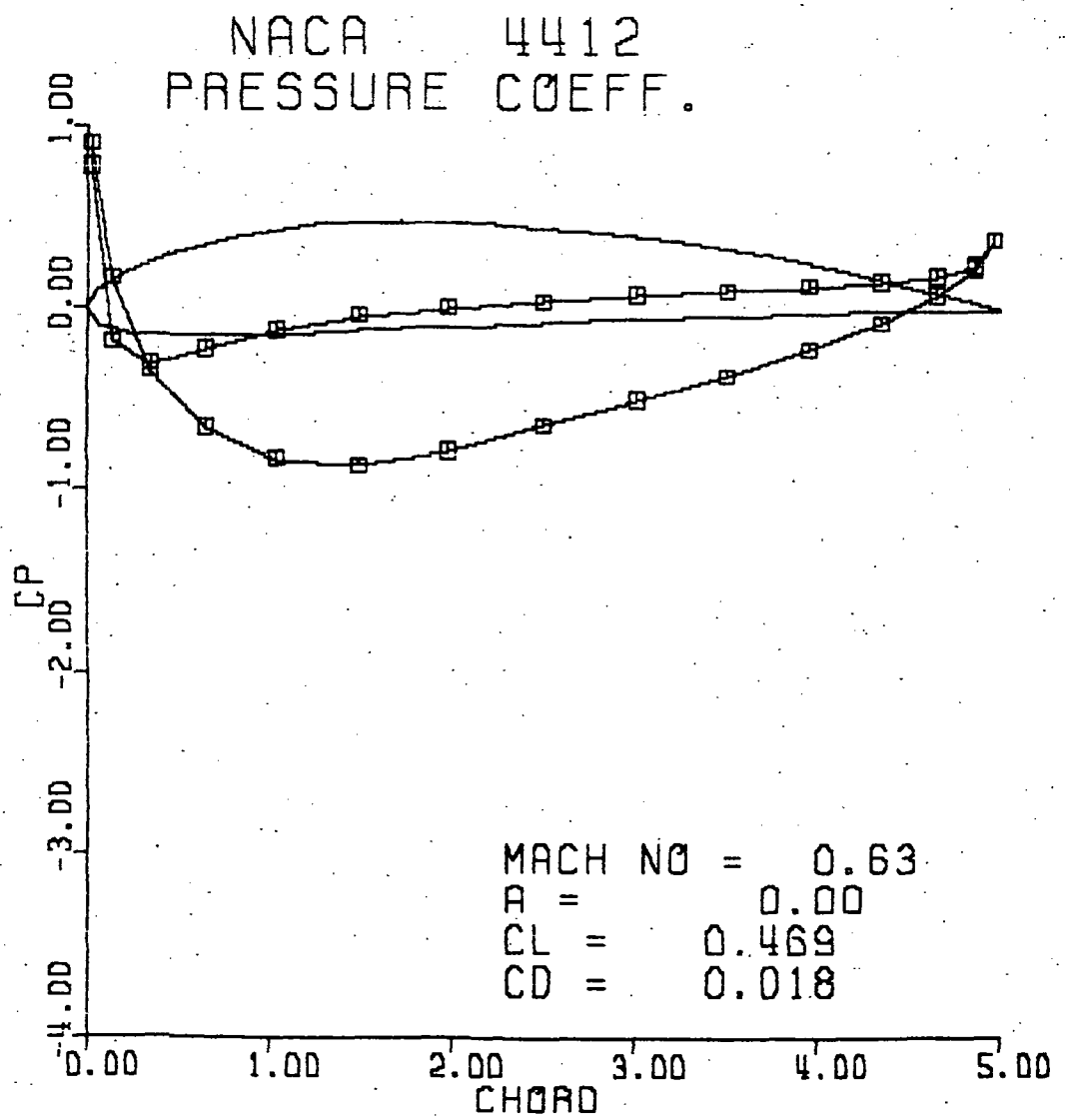
NACA 4412
PRESSURE COEFF.
CP
1.00
0.00
-1.00
-2.00
-3.00
-4.00
0.00
1.00
2.00
3.00
4.00
5.00
CHORD
MACH NO = 0.63
A = 0.00
CL = 0.469
CD = 0.018

Figure A-22.

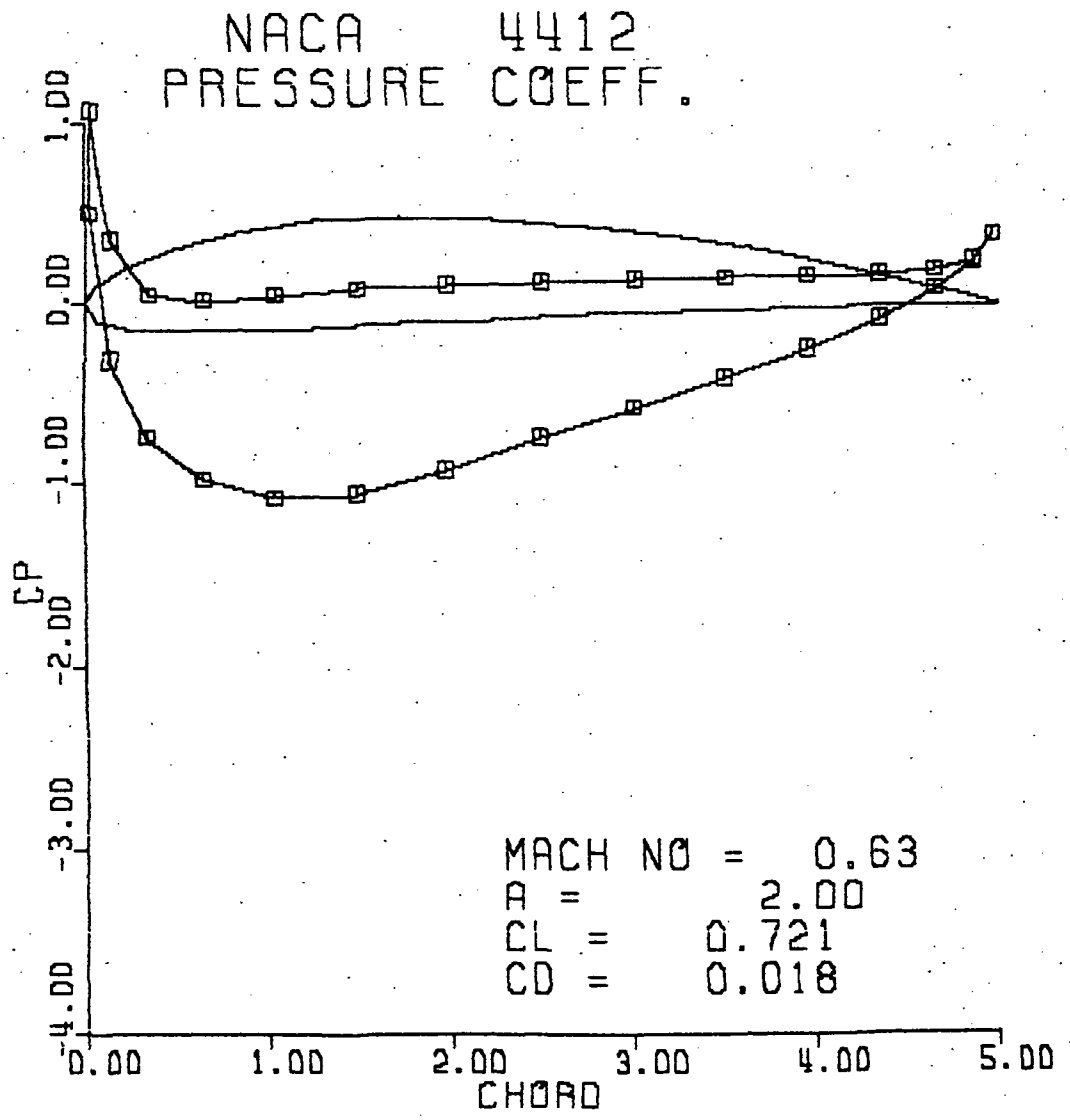
NACA 4412
PRESSURE COEFF.
1.00
0.00
-1.00
-2.00
-3.00
-4.00
CP
0.00
1.00
2.00
3.00
4.00
5.00
CHORD
MACH NO = 0.63
A = 2.00
CL = 0.721
CD = 0.018

Figure A-23.

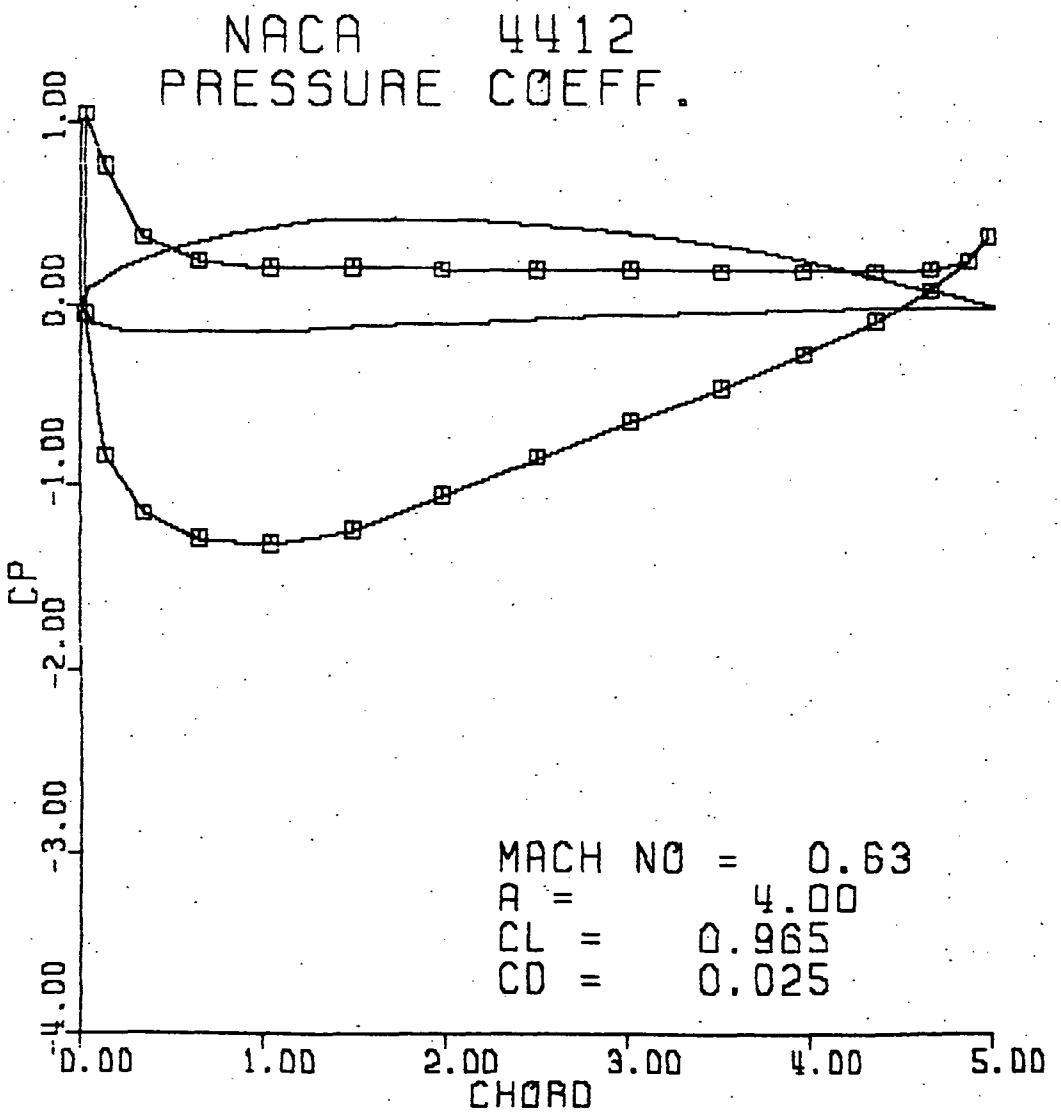
NACA 4412
PRESSURE COEFF.
1.00
0.00
-1.00
-2.00
-3.00
-4.00
CP
0.00
1.00
2.00
3.00
4.00
5.00
CHORD
MACH NO = 0.63
A = 4.00
CL = 0.965
CD = 0.025

Figure A-24 .

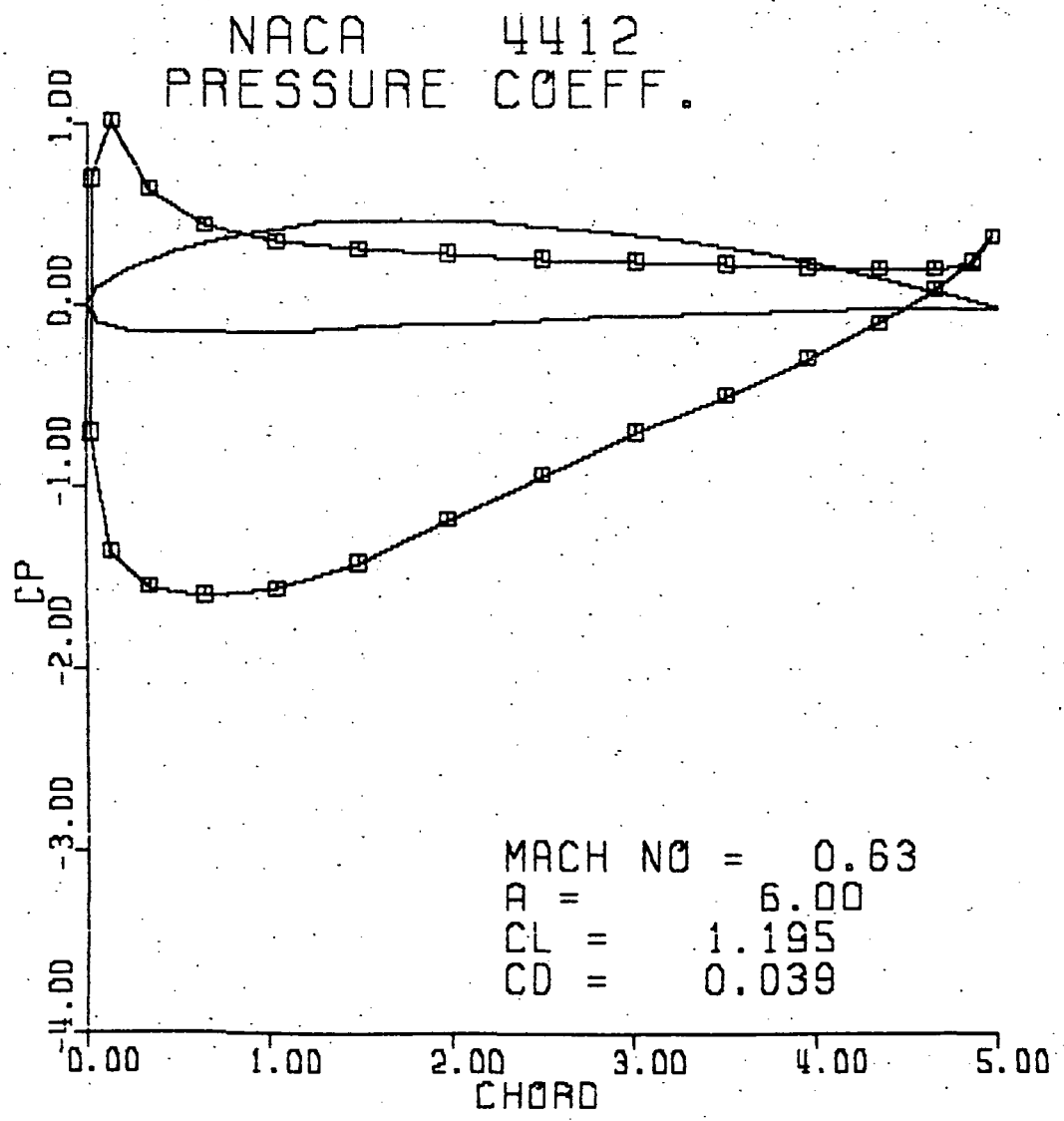
NACA 4412
PRESSURE COEFF.
1.00
0.00
-1.00
-2.00
-3.00
-4.00
CP
0.00
1.00
2.00
3.00
4.00
5.00
CHORD
MACH NO = 0.63
A = 6.00
CL = 1.195
CD = 0.039

Figure A-25.

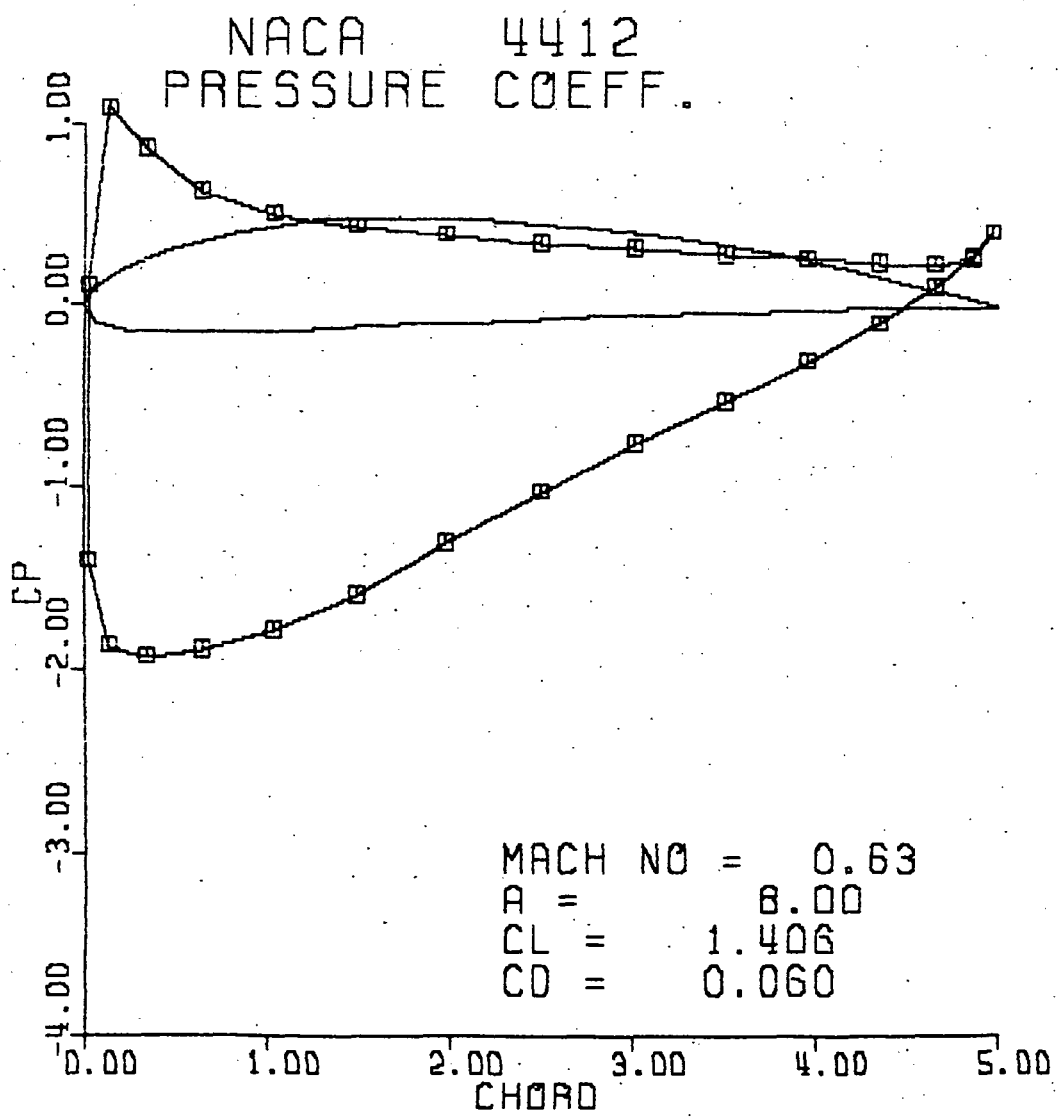
NACA 4412
PRESSURE COEFF.
1.00
0.00
-1.00
-2.00
-3.00
-4.00
CP
0.00
1.00
2.00
3.00
4.00
5.00
CHORD
MACH NO = 0.63
A = 8.00
CL = 1.406
CD = 0.060

Figure A-26.

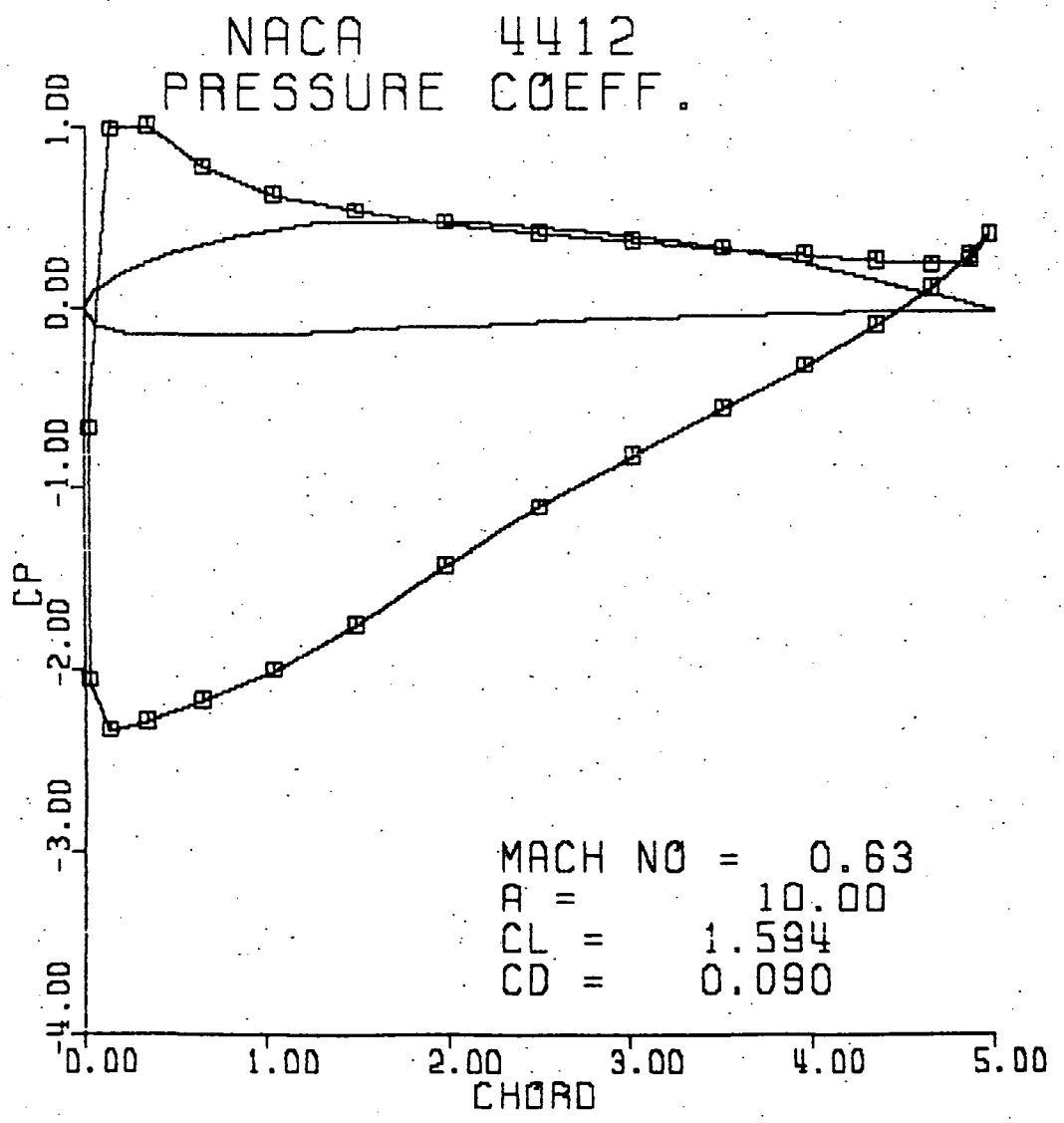
NACA 4412
PRESSURE COEFF.
1.00
0.00
-1.00
-2.00
-3.00
-4.00
CP
0.00
1.00
2.00
3.00
4.00
5.00
CHORD
MACH NO = 0.63
A = 10.00
CL = 1.594
CD = 0.090

Figure A-27.

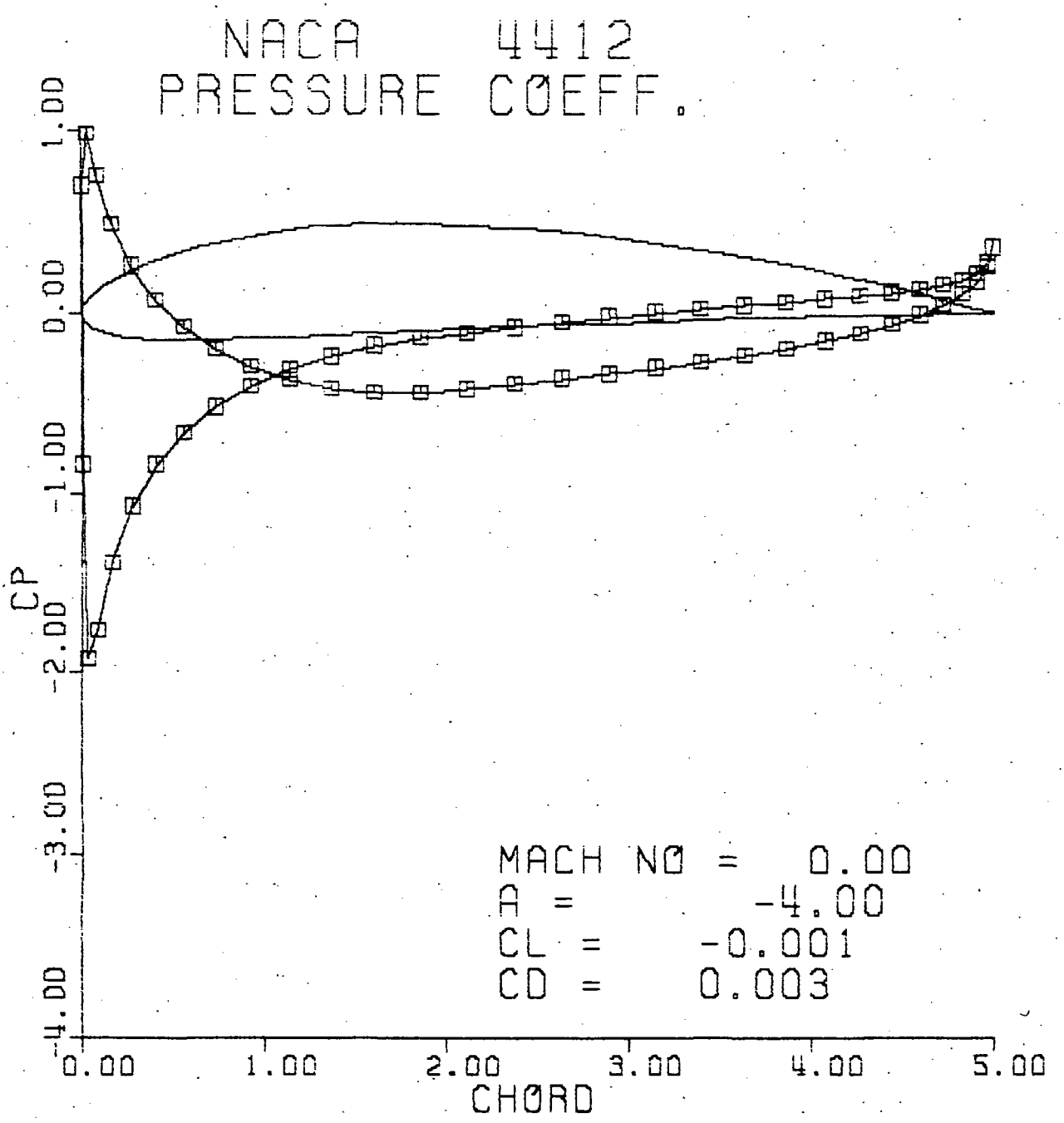
NACA 4412
PRESSURE COEFF.
1.00
0.00
-1.00
-2.00
-3.00
-4.00
CP
0.00
1.00
2.00
3.00
4.00
5.00
CHORD
MACH NO = 0.00
A = -4.00
CL = -0.001
CD = 0.003

Figure A-28.

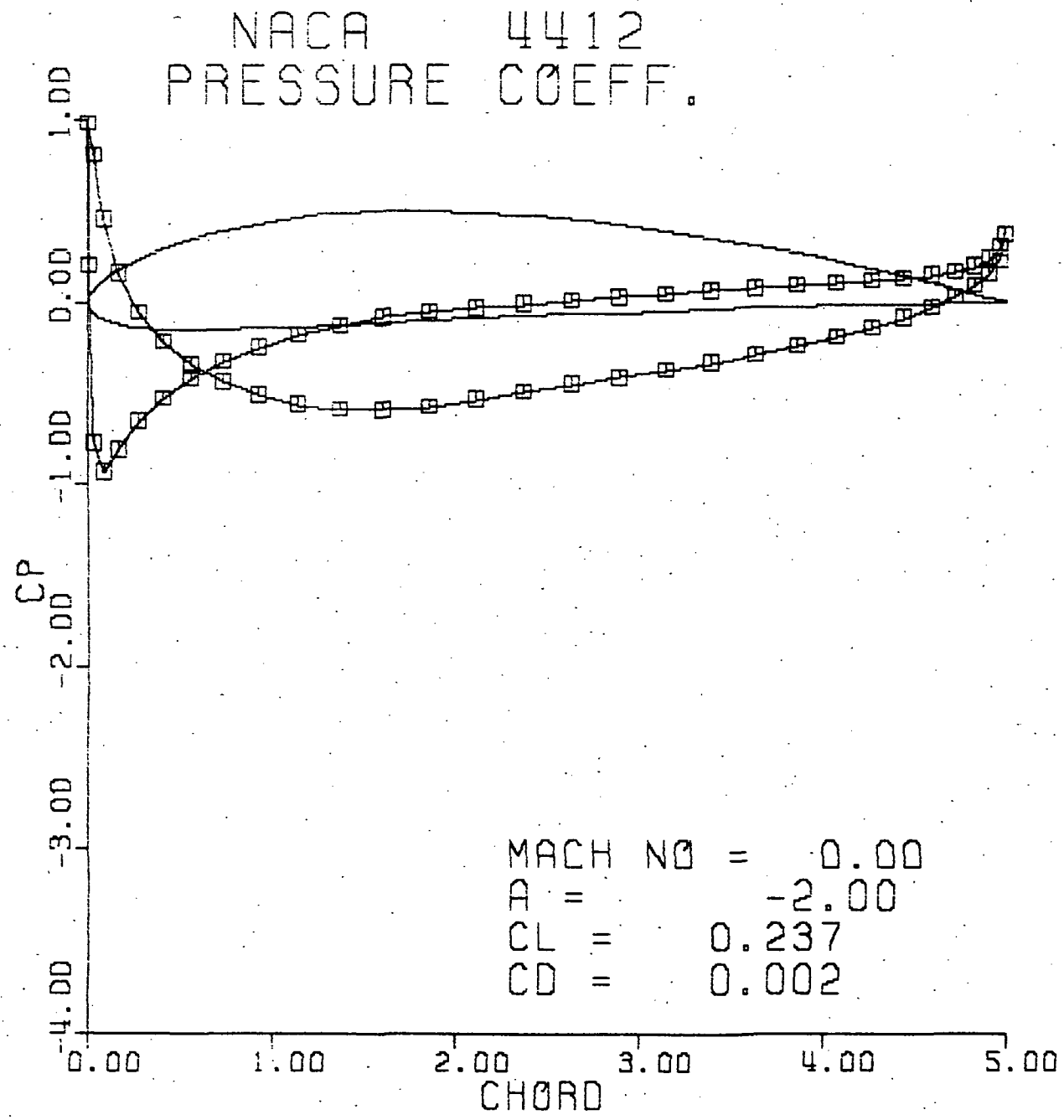
NACA 4412
PRESSURE COEFF.
1.00
0.00
-1.00
-2.00
-3.00
-4.00
CP
MACH NO = 0.00
A = -2.00
CL = 0.237
CD = 0.002
0.00
1.00
2.00
3.00
4.00
5.00
CHORD

Figure A-29.

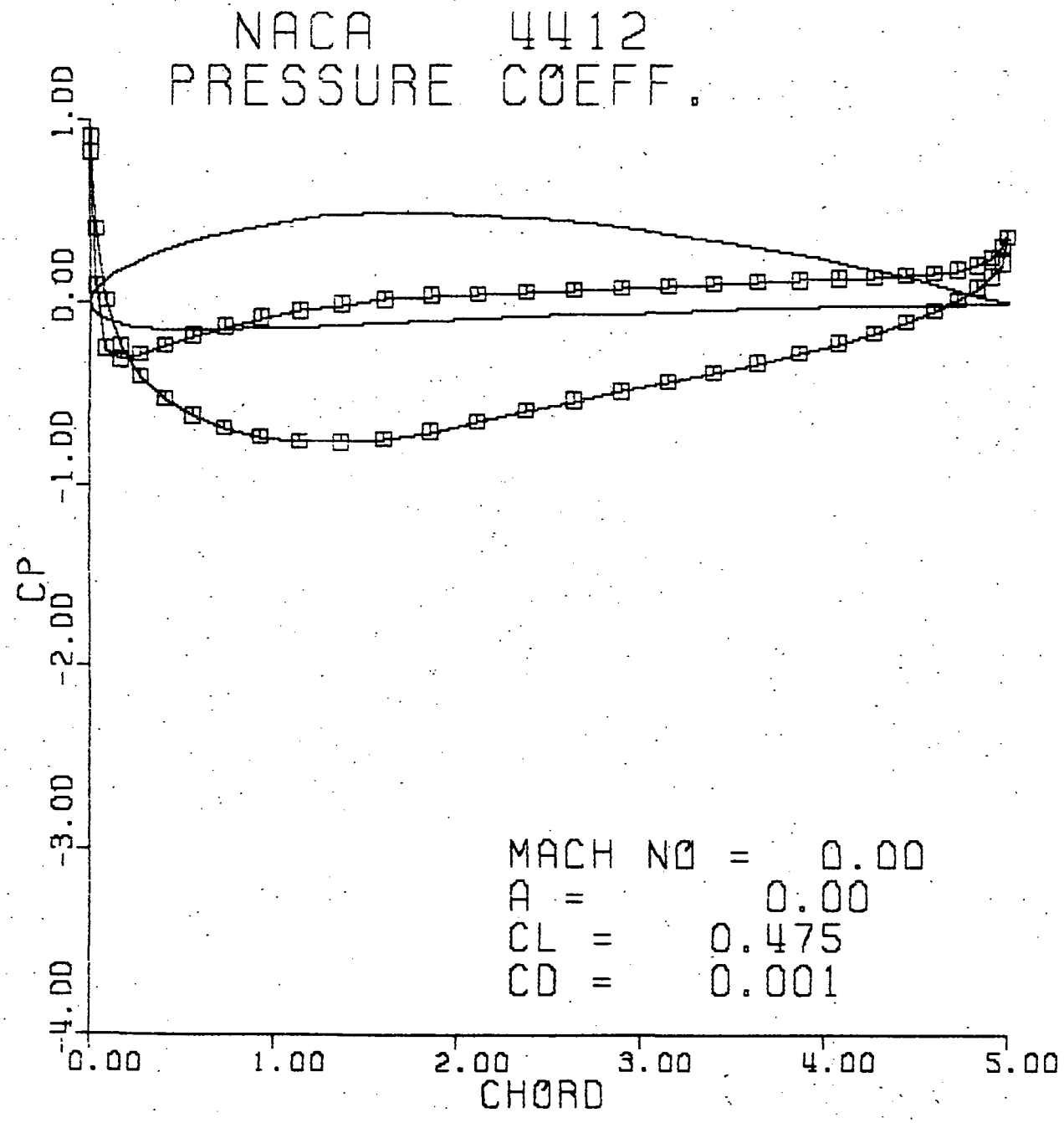
NACA 4412
PRESSURE COEFF.
1.00
0.00
-1.00
-2.00
-3.00
-4.00
CP
0.00
1.00
2.00
3.00
4.00
5.00
CHORD
MACH NO = 0.00
A = 0.00
CL = 0.475
CD = 0.001

Figure A-30.

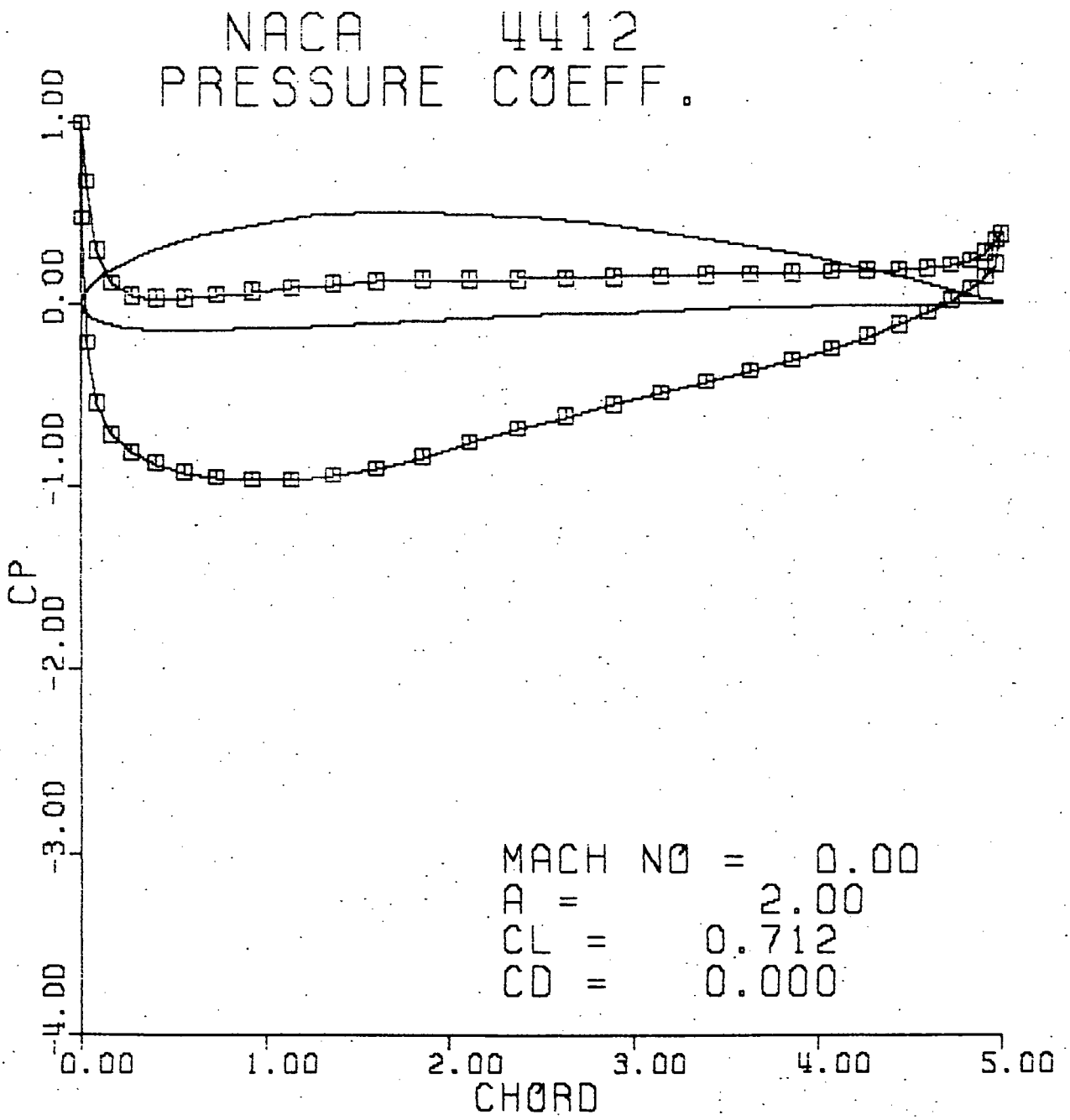
NACA 4412
PRESSURE COEFF.
1.00
0.00
-1.00
-2.00
-3.00
-4.00
CP
0.00
1.00
2.00
3.00
4.00
5.00
CHORD
MACH NO = 0.00
A = 2.00
CL = 0.712
CD = 0.000

Figure A-31.

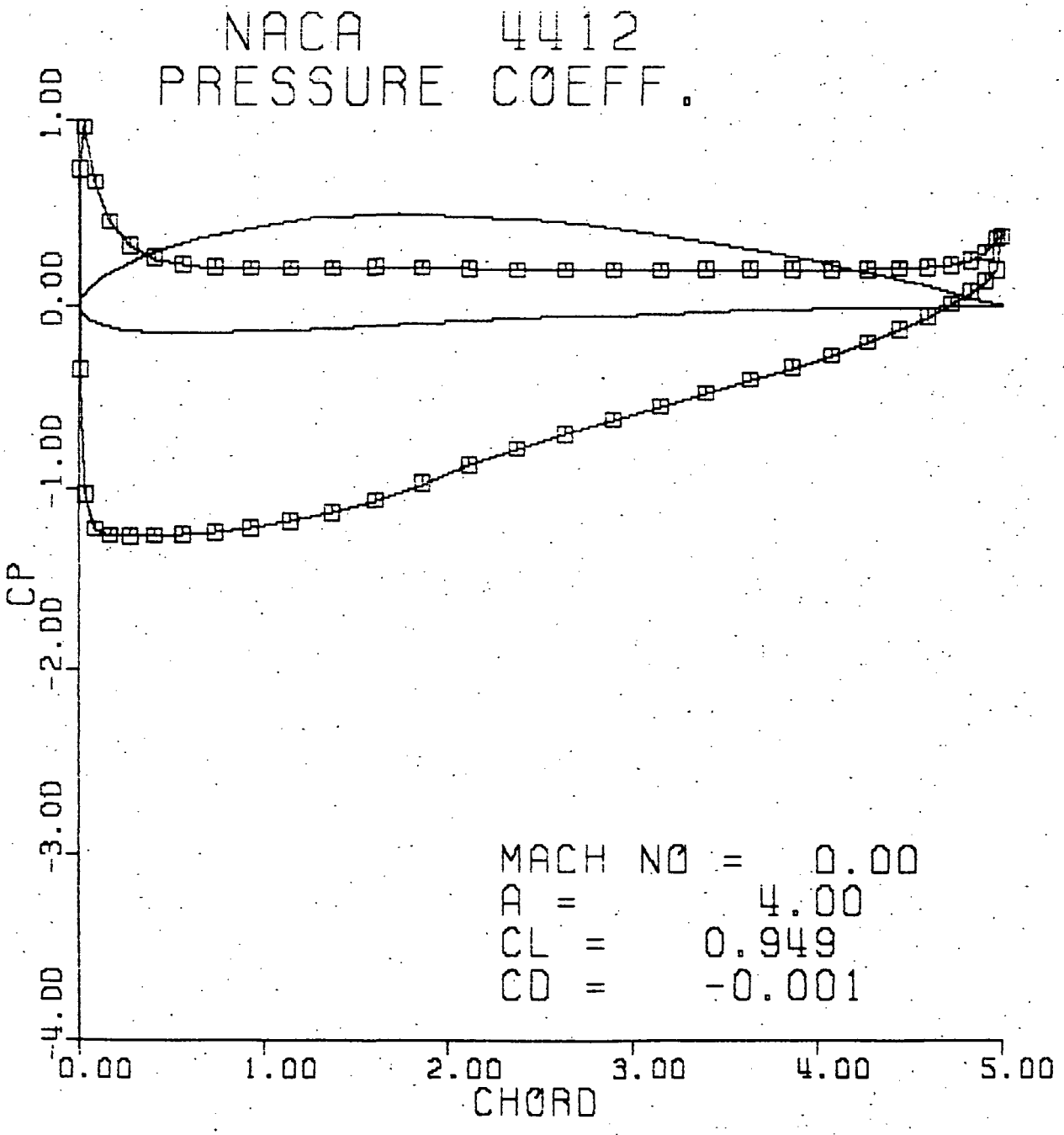
NACA 4412
PRESSURE COEFF.
1.00
0.00
-1.00
-2.00
-3.00
-4.00
CP
0.00
1.00
2.00
3.00
4.00
5.00
CHORD
MACH NO = 0.00
A = 4.00
CL = 0.949
CD = -0.001

Figure A-32.

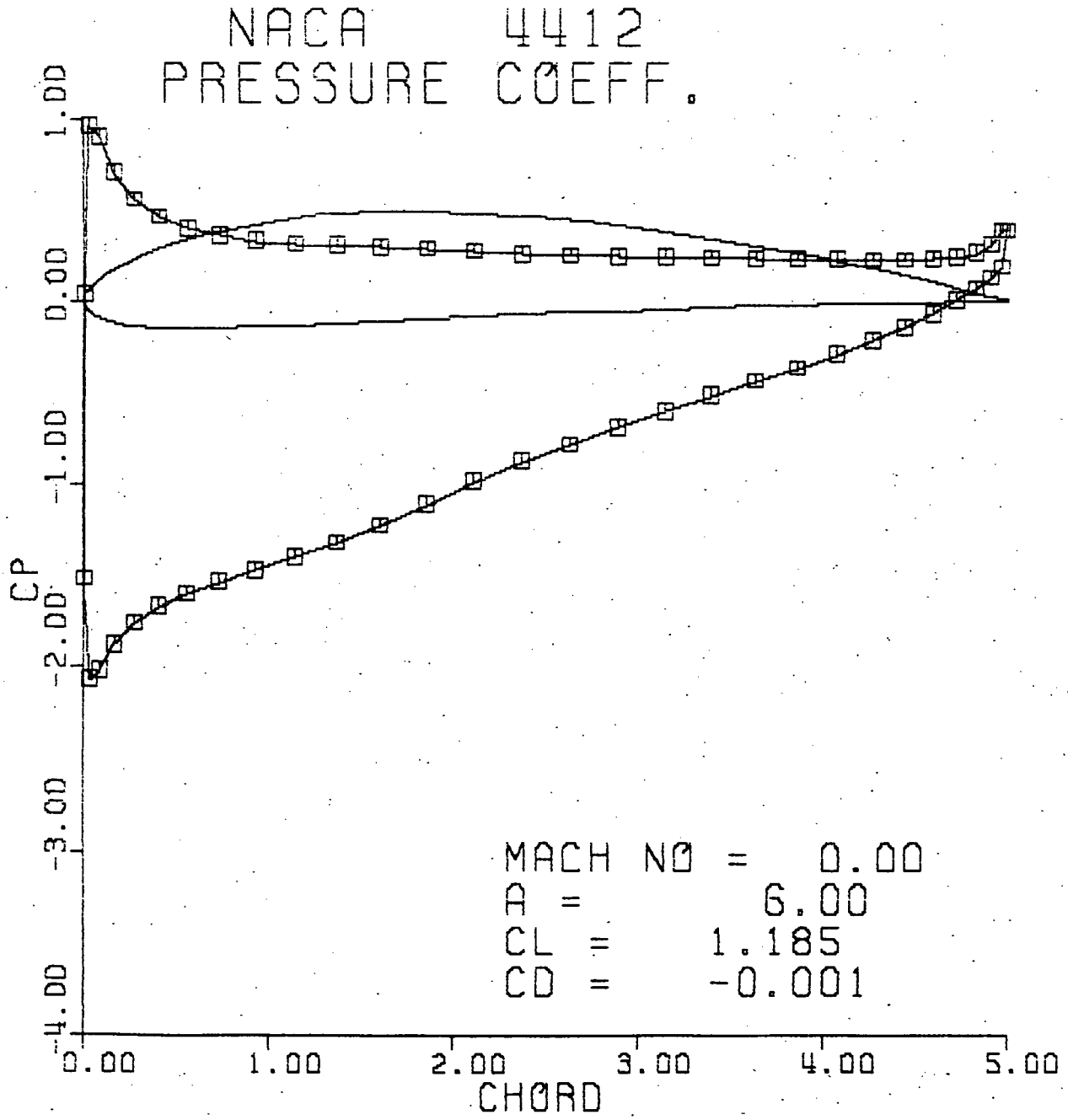
NACA 4412
PRESSURE COEFF.
1.00
0.00
-1.00
-2.00
-3.00
-4.00
CP
0.00
1.00
2.00
3.00
4.00
5.00
CHORD
MACH NO = 0.00
A = 6.00
CL = 1.185
CD = -0.001

Figure A-33.

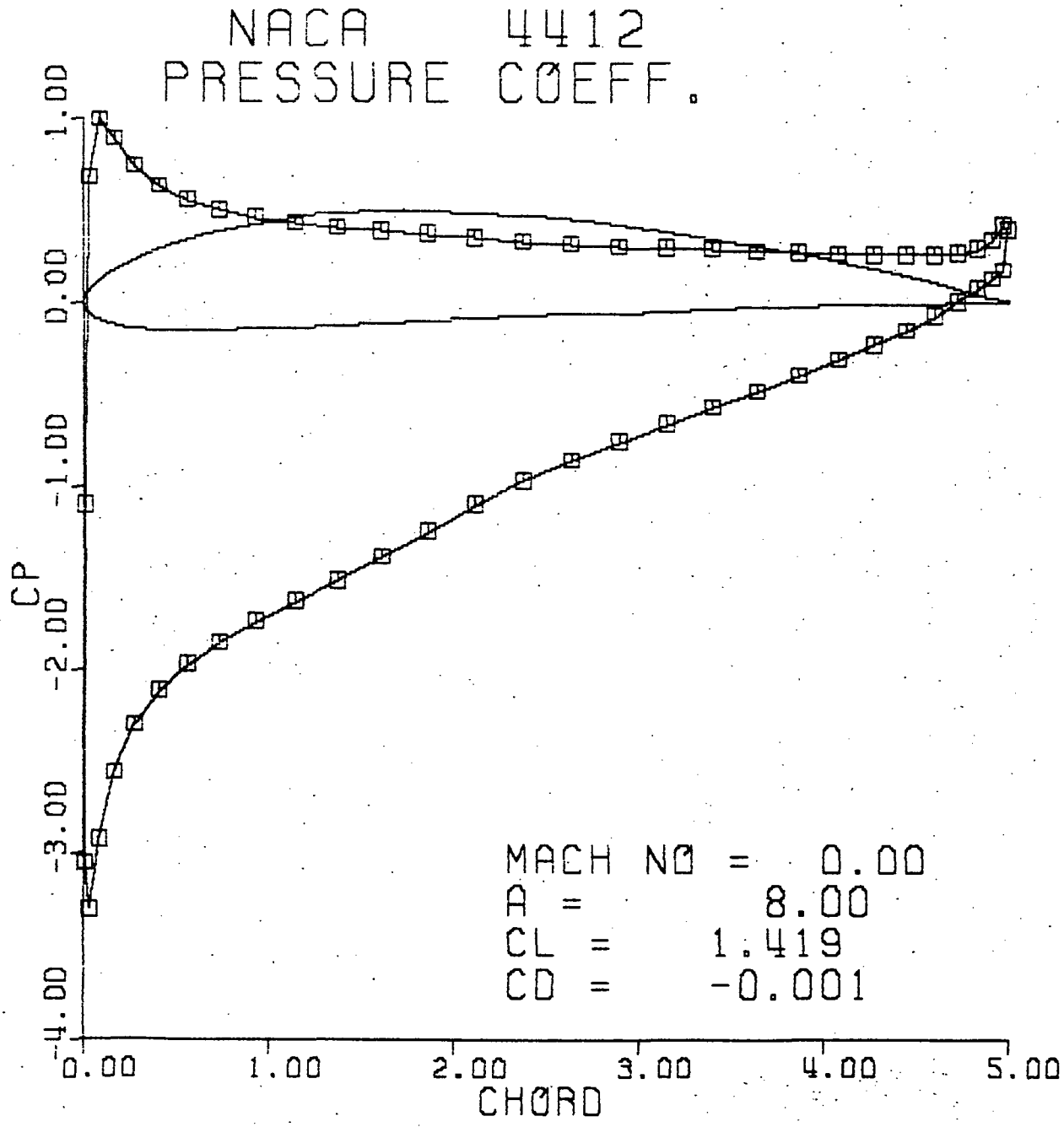
NACA 4412
PRESSURE COEFF.
1.00
0.00
-1.00
-2.00
-3.00
-4.00
CP
0.00
1.00
2.00
3.00
4.00
5.00
CHORD
MACH NO = 0.00
A = 8.00
CL = 1.419
CD = -0.001

Figure A-34.

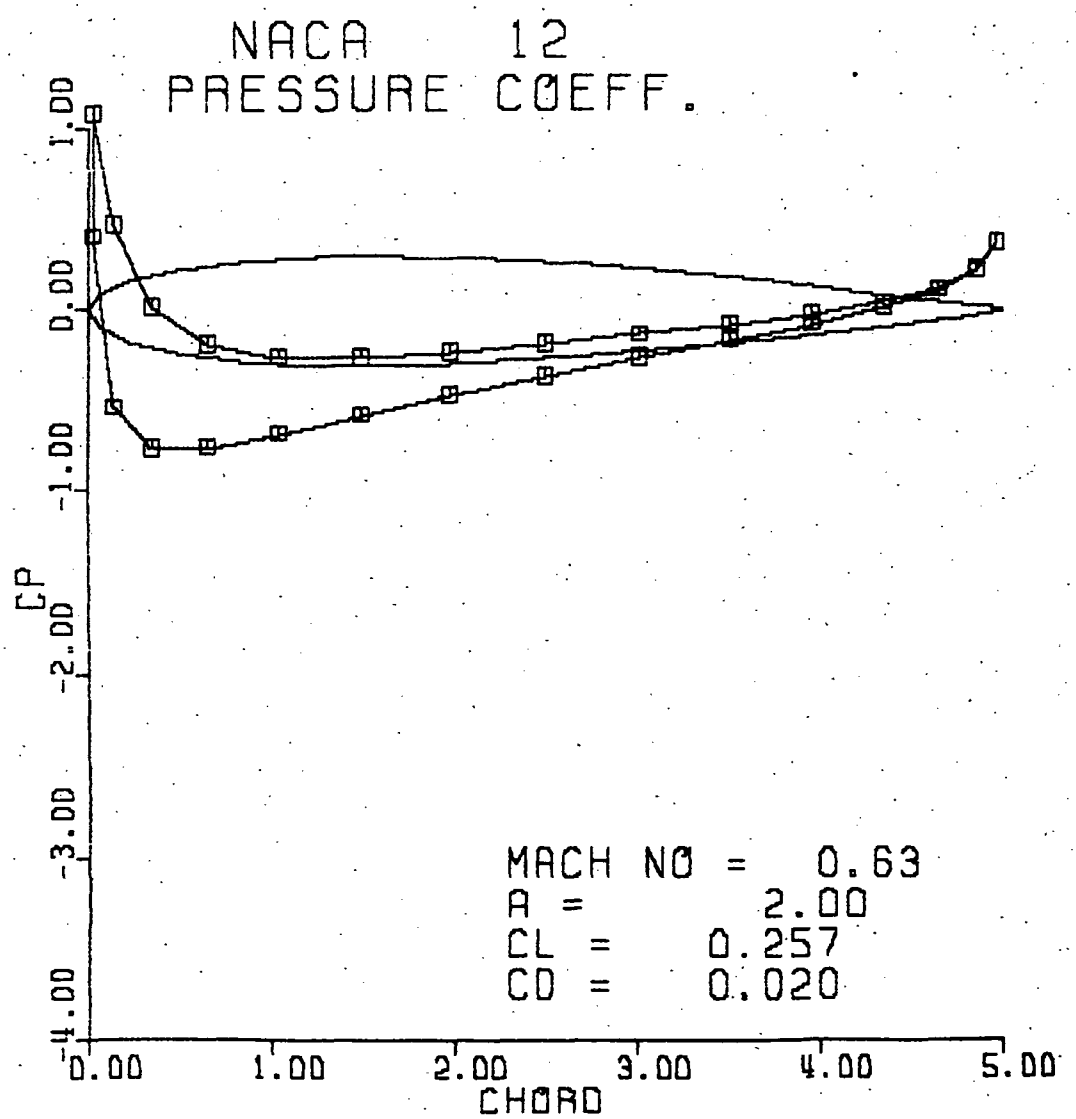

Figure A-36.

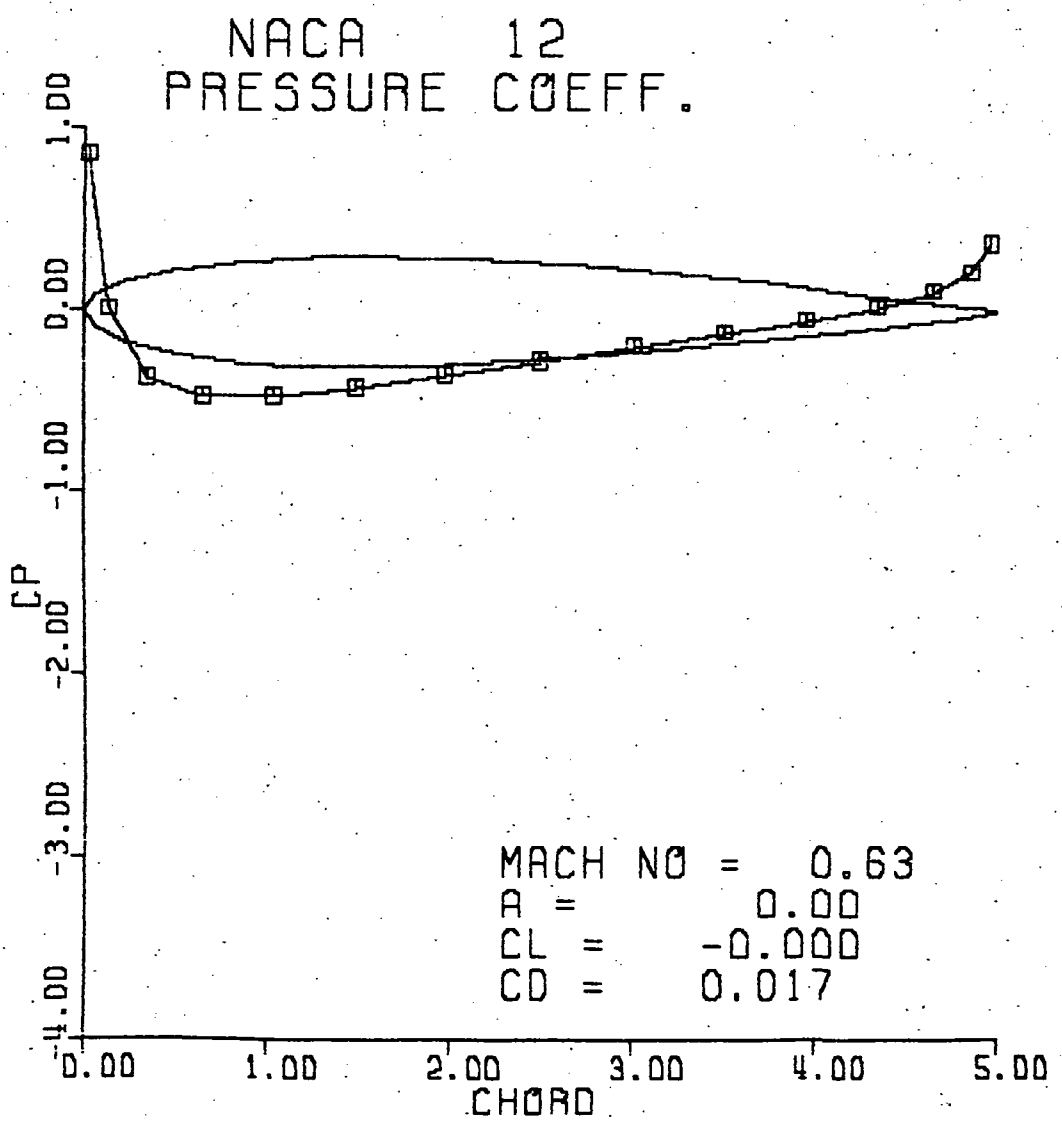
NACA 12
PRESSURE COEFF.
1.00
0.00
-1.00
-2.00
-3.00
-4.00
CP
0.00
1.00
2.00
3.00
4.00
5.00
CHORD
MACH NO = 0.63
A = 0.00
CL = -0.000
CD = 0.017

Figure A-37.

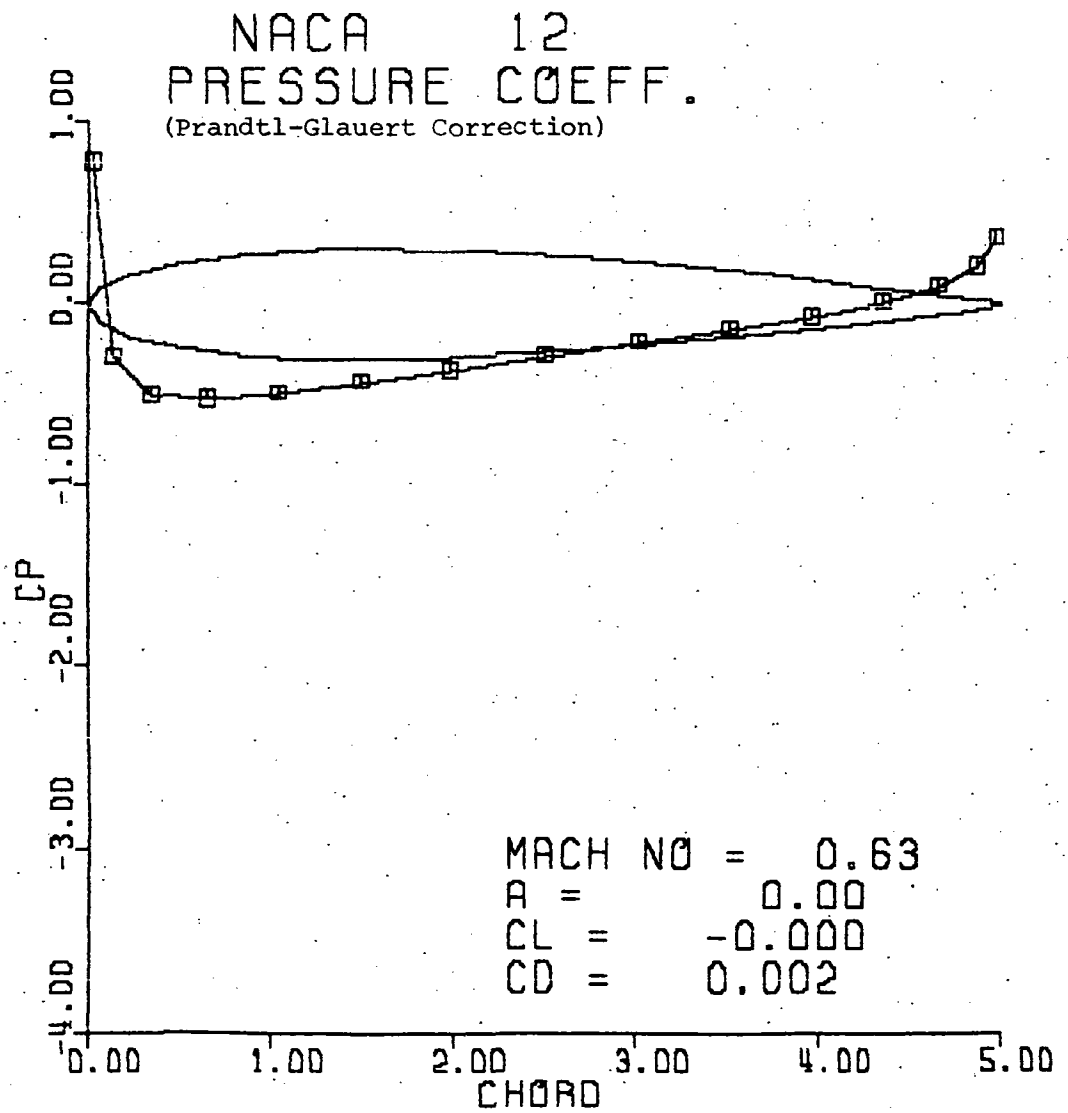
NACA 12
PRESSURE COEFF.
(Prandtl-Glauert Correction)
1.00
0.00
-1.00
-2.00
-3.00
-4.00
CP
0.00
1.00
2.00
3.00
4.00
5.00
CHORD
MACH NO = 0.63
A = 0.00
CL = -0.000
CD = 0.002

Figure A-38.

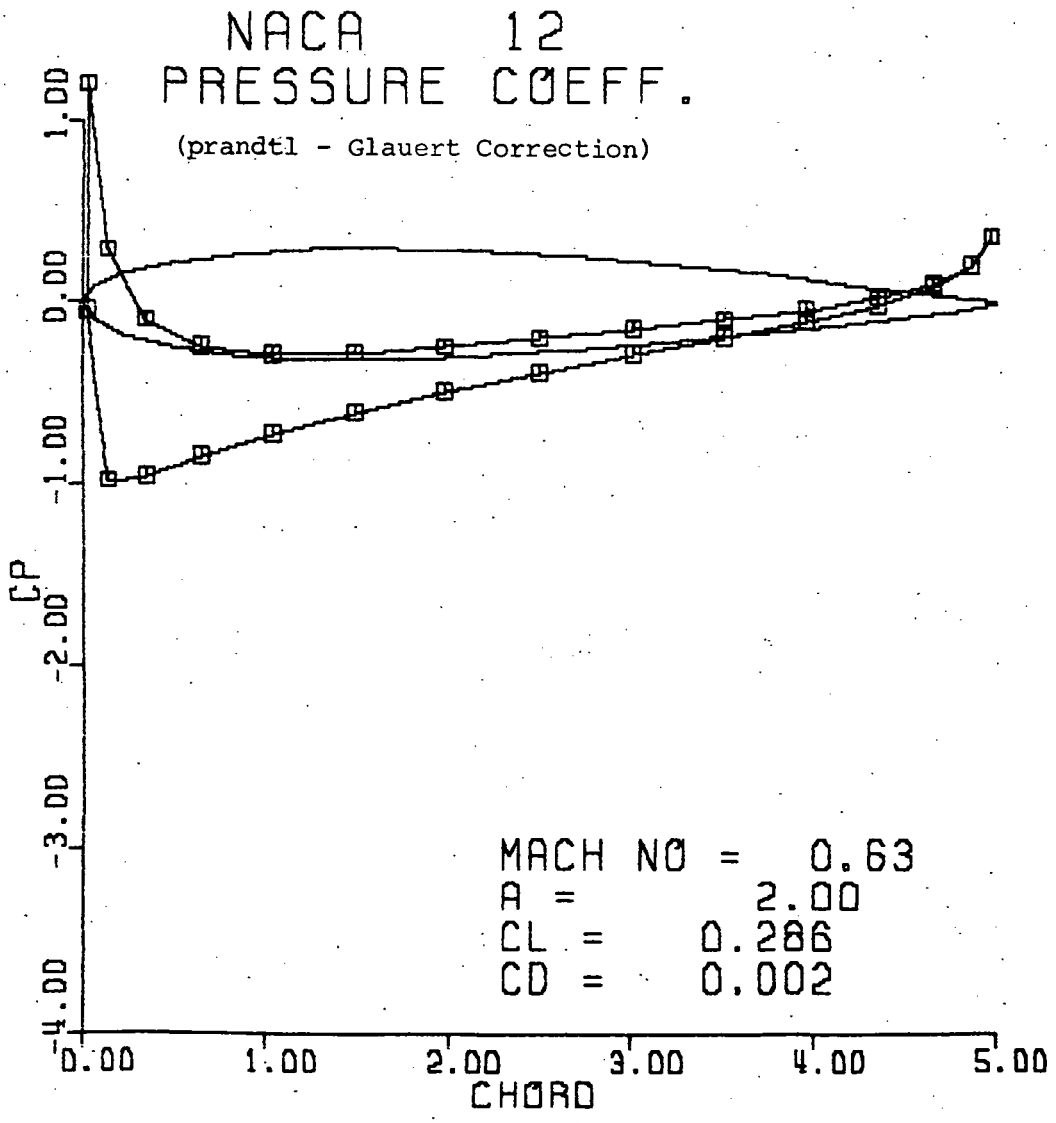
NACA 12
PRESSURE COEFF.
(prandtl - Glauert Correction)
MACH NO = 0.63
A = 2.00
CL = 0.286
CD = 0.002
CP
1.00
0.00
-1.00
-2.00
-3.00
-4.00
0.00
1.00
2.00
3.00
4.00
5.00
CHORD

Figure A-39.

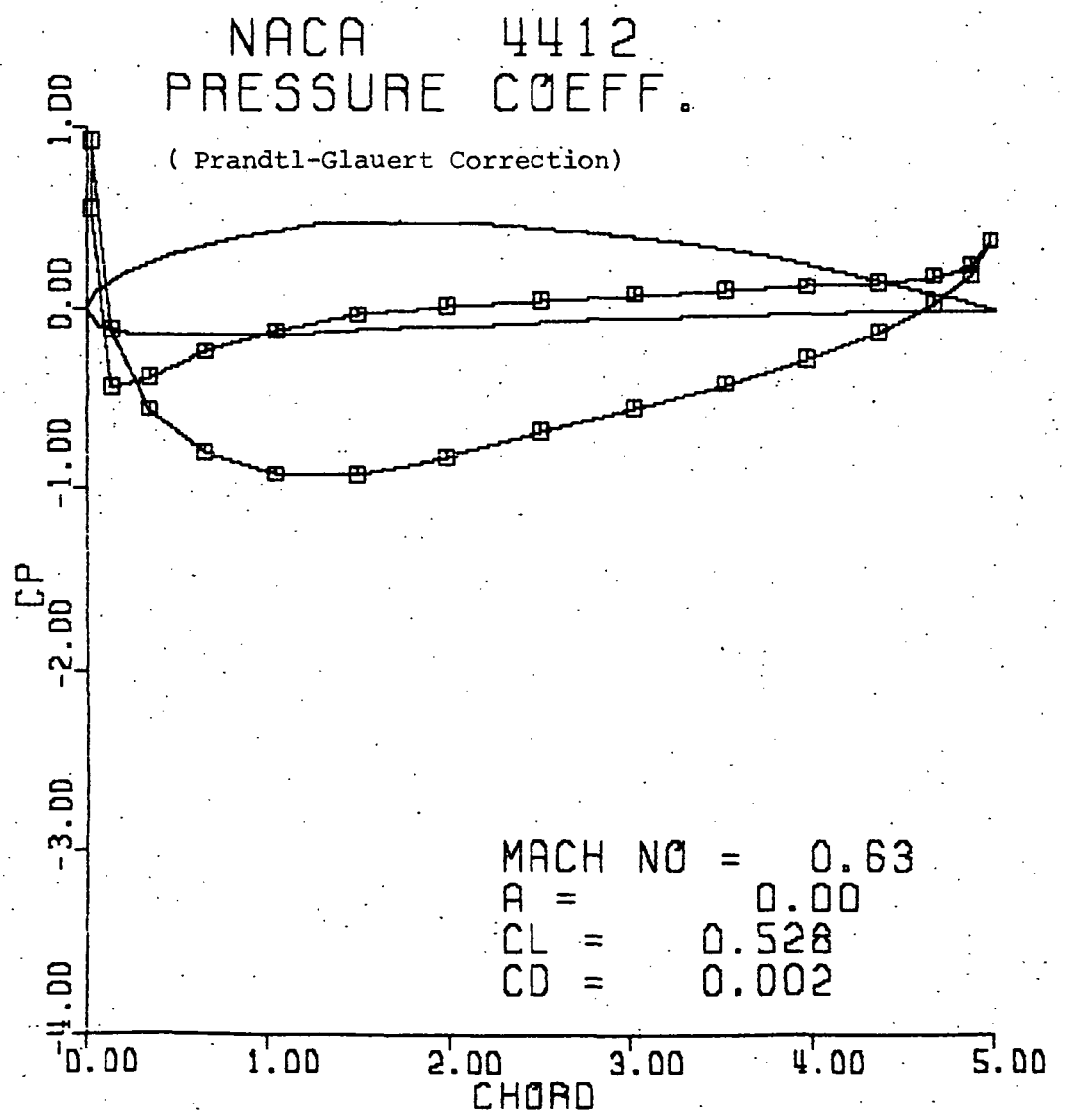
NACA 4412
PRESSURE COEFF.
(Prandtl-Glauert Correction)
1.00
0.00
-1.00
-2.00
-3.00
-4.00
CP
0.00
1.00
2.00
3.00
4.00
5.00
CHORD
MACH NO = 0.63
A = 0.00
CL = 0.528
CD = 0.002

Figure A-40.

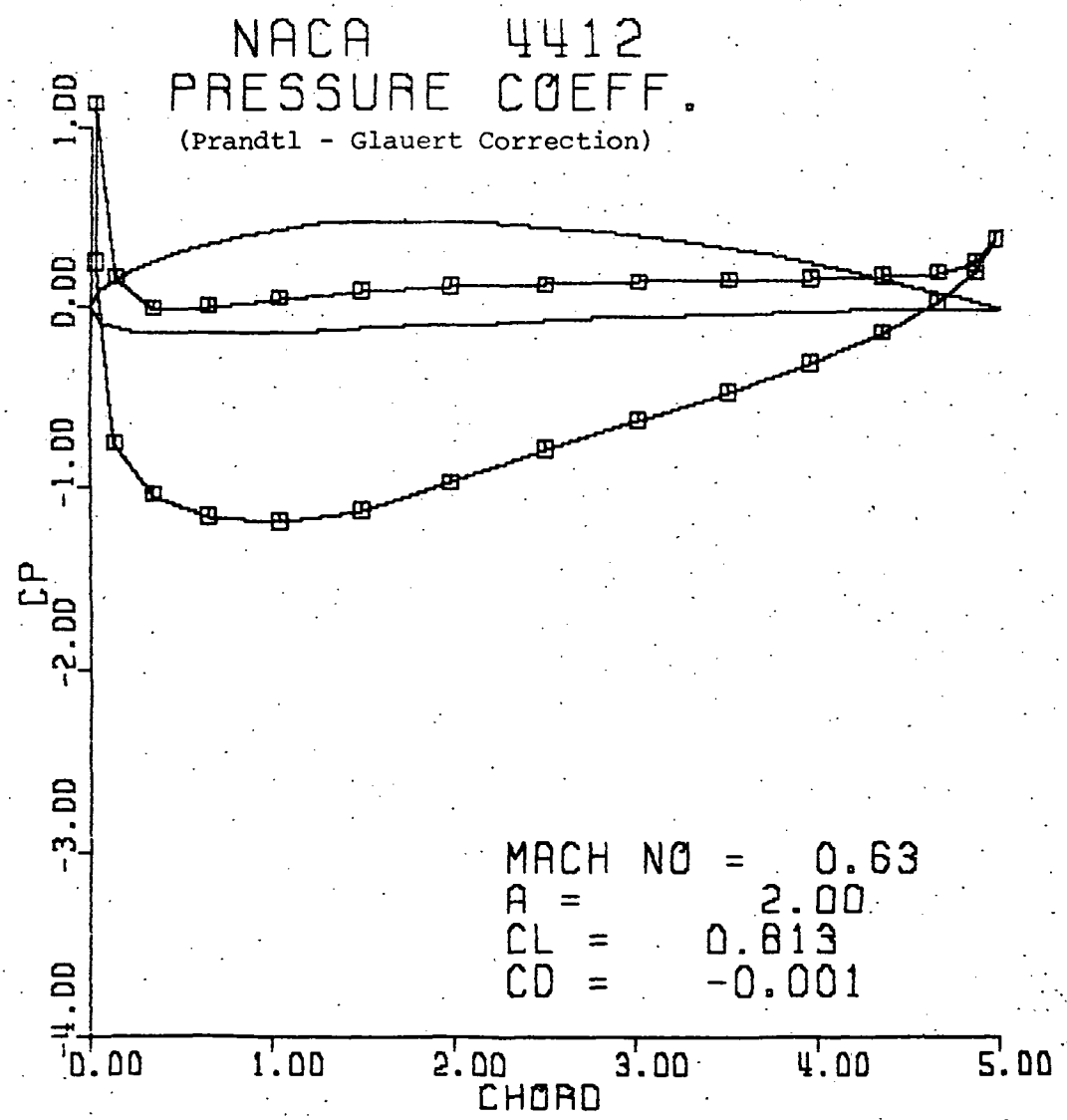
NACA 4412
PRESSURE COEFF.
(Prandtl - Glauert Correction)
CP
1.00
0.00
-1.00
-2.00
-3.00
-4.00
0.00
1.00
2.00
3.00
4.00
5.00
CHORD
MACH NO = 0.63
A = 2.00
CL = 0.813
CD = -0.001

Figure A-41.

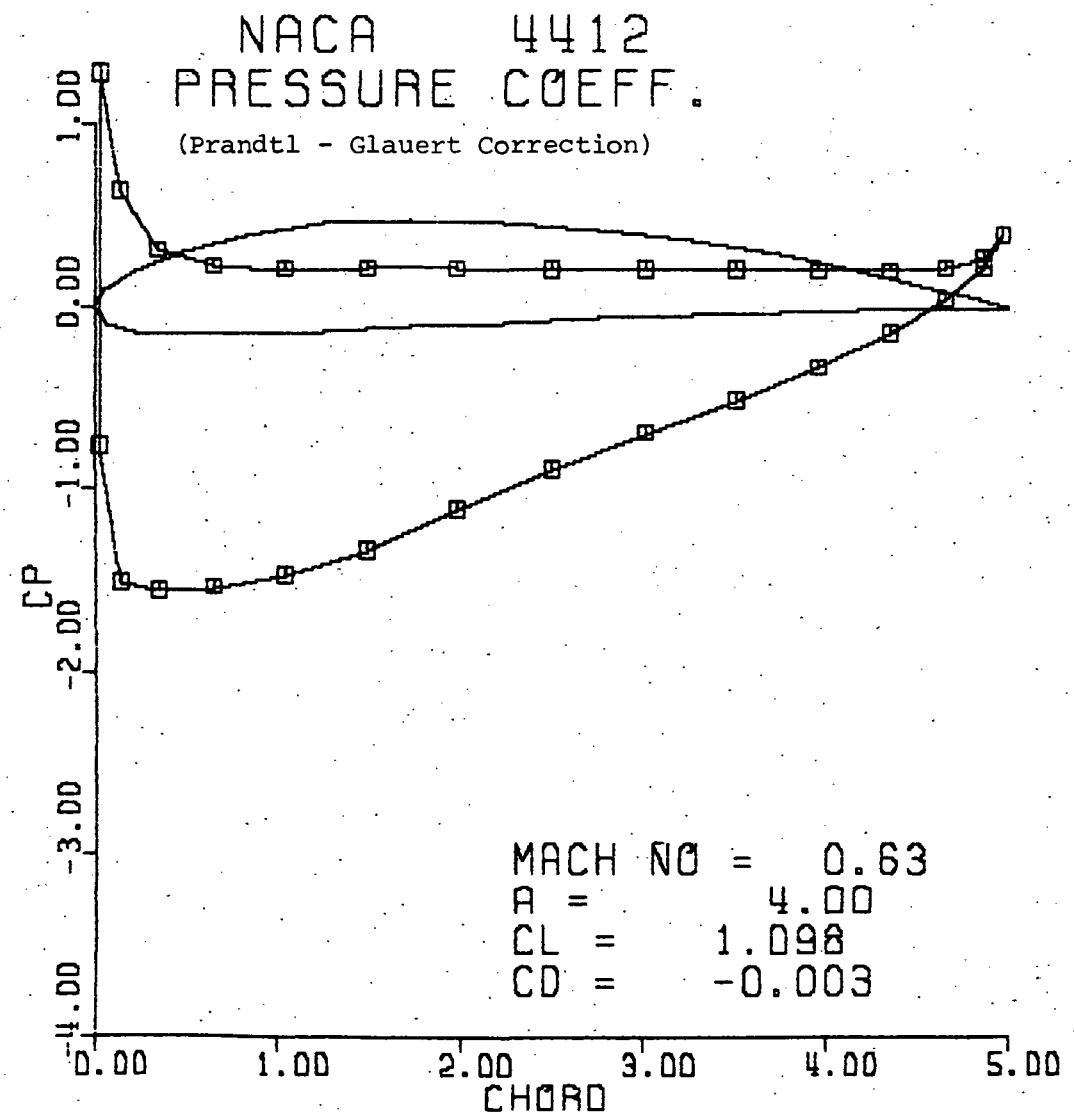
NACA 4412
PRESSURE COEFF.
(Prandtl - Glauert Correction)
CP
1.00
0.00
-1.00
-2.00
-3.00
-4.00
0.00
1.00
2.00
3.00
4.00
5.00
CHORD
MACH NO = 0.63
A = 4.00
CL = 1.098
CD = -0.003

Figure A-42.

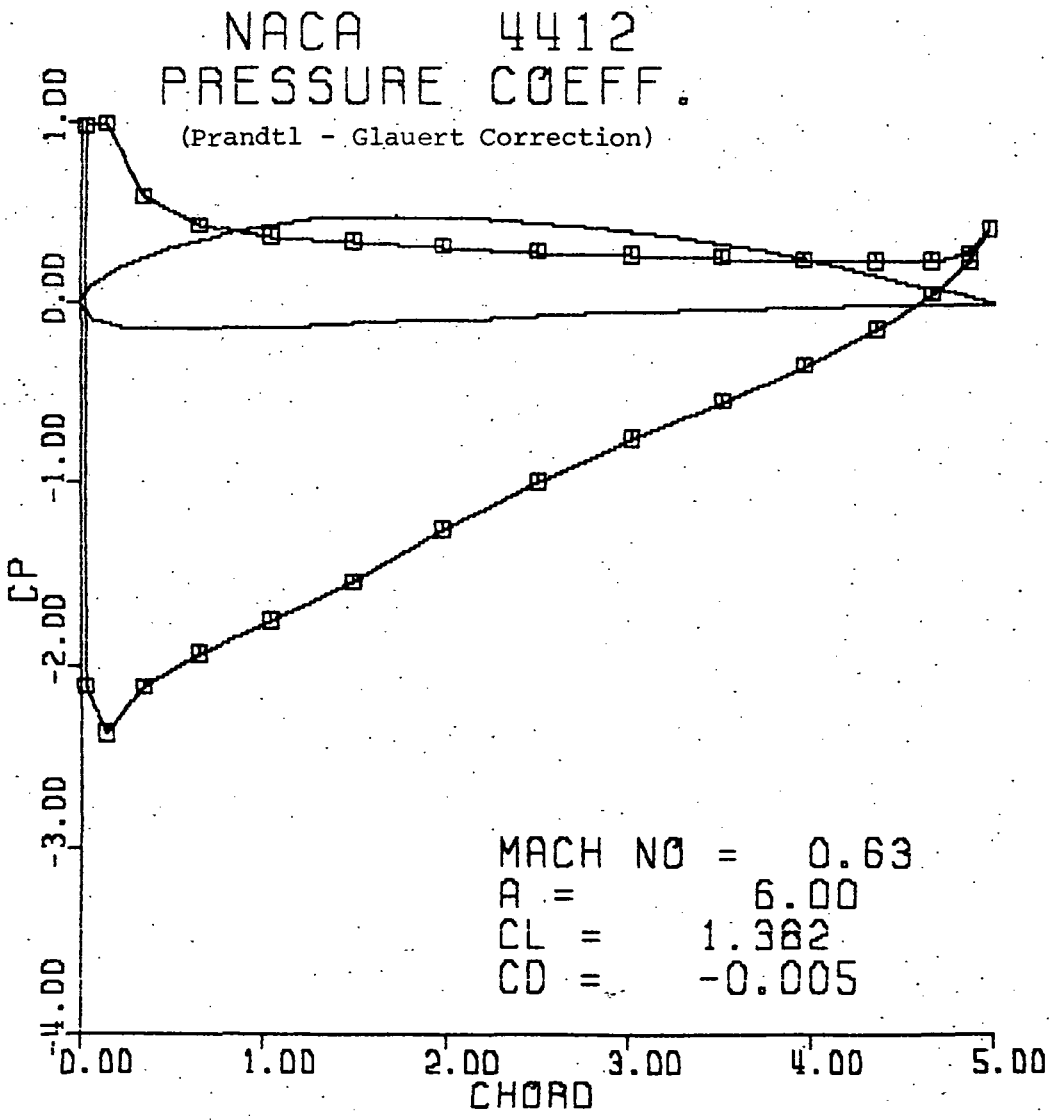
NACA 4412
PRESSURE COEFF.
(Prandtl - Glauert Correction)
1.00
0.00
-1.00
-2.00
-3.00
-4.00
CP
0.00
1.00
2.00
3.00
4.00
5.00
CHORD
MACH NO = 0.63
A = 6.00
CL = 1.382
CD = -0.005

Figure A-43.

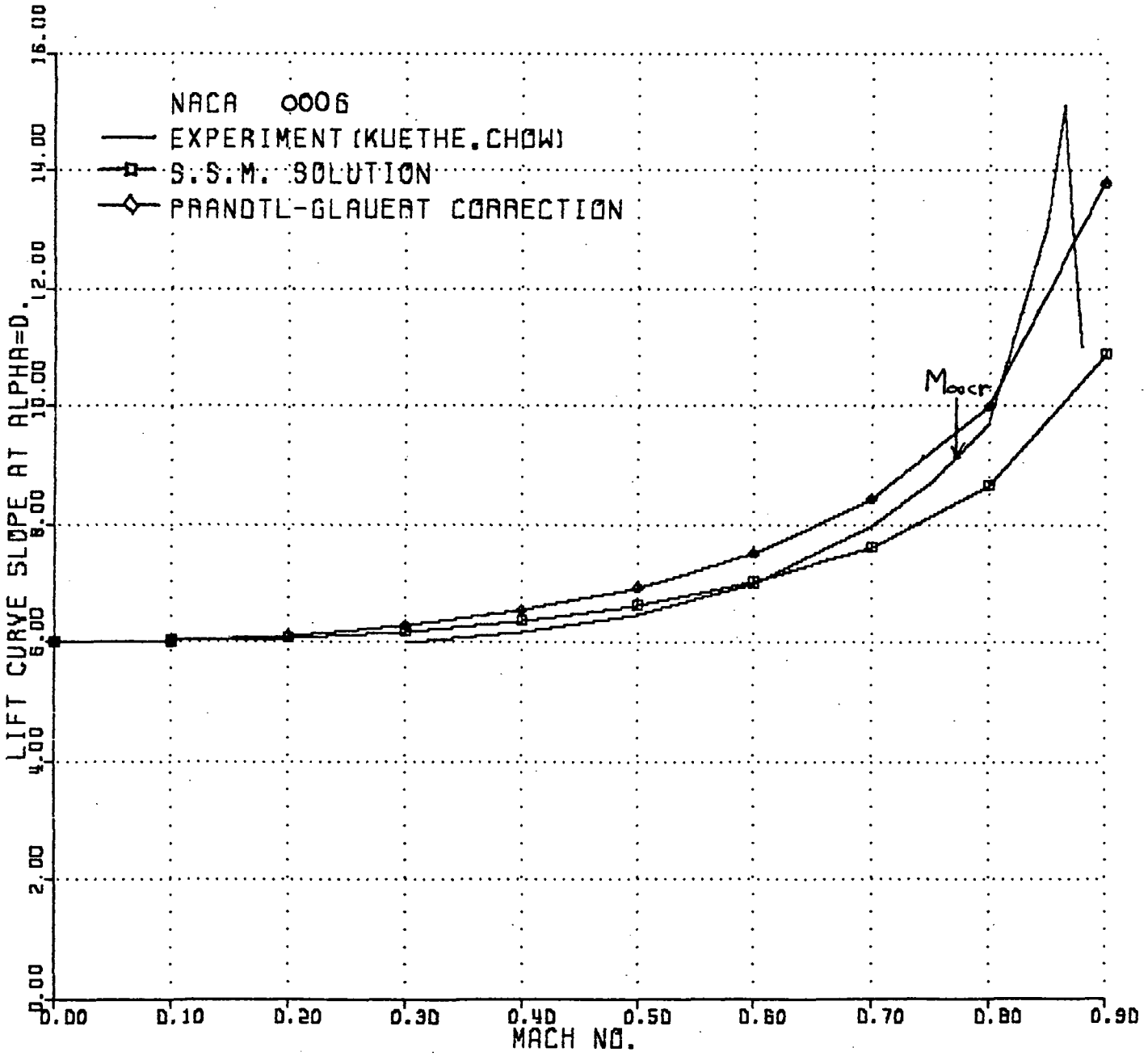
NACA 0006
EXPERIMENT (KUETHE, CHOW)
S.S.M. SOLUTION
PRANDTL-GLAUERT CORRECTION
LIFT CURVE SLOPE AT ALPHA=0.
MACH NO.
M_cr
0.00
2.00
4.00
6.00
8.00
10.00
12.00
14.00
16.00
0.00
0.10
0.20
0.30
0.40
0.50
0.60
0.70
0.80
0.90

Figure A-44.

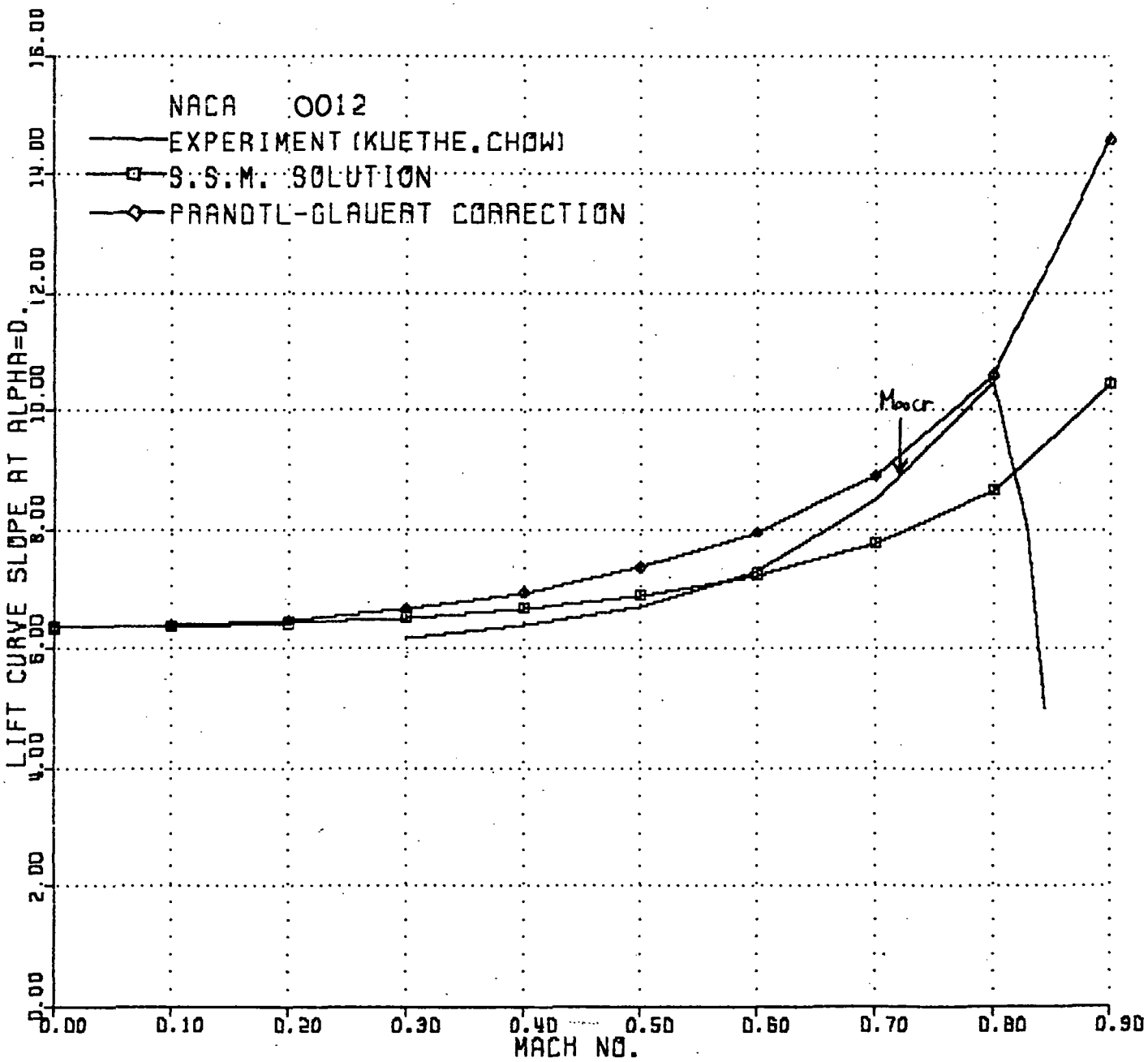
NACA 0012
EXPERIMENT (KUETHE, CHOW)
S.S.M. SOLUTION
PRANDTL-GLAUERT CORRECTION
Mcr
LIFT CURVE SLOPE AT ALPHA=0.
MACH NO.
0.00
2.00
4.00
6.00
8.00
10.00
12.00
14.00
16.00
0.00
0.10
0.20
0.30
0.40
0.50
0.60
0.70
0.80
0.90

Figure A-45.

A.2 Results and Discussion

In this section we discuss results from the investigation of the capabilities of the surface singularity method applied to thick airfoils in subsonic flow. In figures (A-1) to (A-3) lift coefficients vs angle of attack are shown for three NACA four digit airfoils. The airfoils were divided into 30 straight segements along their surface curve according to cosine spacing. The experimental results from Ref.(65) are shown together. For the symmetrical airfoil of figure (A-1) theory and experiment agree exactly up to 10 degree angle of attack. After 16 degree angle of attack the experimental lift coefficient drops because of boundary layer seperation contrast to the continuing increase of the theoretical result. For the cambered airfoils of figures (A-2) and (A-3) the upper airfoil boundary loses more total pressure than lower airfoil boundary. Hence, the conservation of total pressure is less accurate there. Figures (A-4) and (A-5) show the effect of the number of segments used on lift coefficient. With 60 segments figure (A-5) is the exact potential flow solution. When the smaller number of segments is used, the lift coefficient is smaller. Figure (A-4) shows that results

obtained with 20 segments are in very good agreement with experiment.

Figure (A-6) to (A-11) show pressure coefficients, lift coefficients, and drag coefficients for several angles of attack of NACA 0012 airfoil at Mach no. = 0.0. In all cases chord direction forces are negative, but drag coefficients are slightly positive. The drag coefficient which should be zero in exact solution and is the numerical error increases with angle of attack for this symmetrical airfoil. Figures (A-12) to (A-19) show pressure, lift, and drag coefficients for several angle of attack of NACA 4412 airfoil at Mach no. =0.0. The drag coefficient decreases with angle of attack due to the leading edge suction of the camber effect. The larger boundary layer growth and hence the bigger displacement thickness on upper airfoil surface than on lower airfoil surface makes the theoretical result less accurate on the upper surface than on the lower surface. Figures (A-20) to (A-27) show pressure, lift, and drag coefficients for several angles of attack of NACA 4412 airfoil at Mach no. =0.63. The increase of lift coefficient due to compressibility effect are shown in all figures. But the leading edge suction decreases for compressible flow. Unlike incompressible flow results the numerical drag coefficients are all positive. For example, the numerical drag coefficient increases from -0.005 to

0.090 due to compressibility effect for 10 degree angle of attack. Figures (A-28) to (A-35) show results obtained with 60 segments fo NACA 4412 airfoil at Mach no. =0.0. Lift coefficients are higer with 60 segments than with 30 segments due to the better resolution of the leading edge suction. The overall shape and local value of pressure coefficients in all figures are similar to the results obtained with 30 segments. Figures (A-36) to (A-39) compare the compressible flow results obtained by Prandtl-Glauert correction from incompressible flow results to the linear compressible flow results. They show that Prandtl-Glauert corection overpredicts lift coefficients. Figures (A-40) to (A-43) show Prandtl-Glauert correction results from incompressible flow results for NACA 4412 airfoil. Compared to figures (A-22) to (A-25) they overpredicts lift coefficients and underpredicts drag coefficients. Figures (A-44) and (A-45) show lift curve slope at zero angle of attack with respect to free stream Mach no. The agreement between theory and experiment is good below the critical Mach no., M_{cr} . When the critical mach number is reached, the neglected terms in deriving subsonic potential equation is important. They show that Prandtl-Glauert correction overpredicts lift curve slope.

B. Numerical Method for Solving Nonlinear Simultaneous Equations.

Let f_1 , $\cdots$, f_N be N nonlinear simultaneous equations.

$$f_i(X) = 0 = \frac{dF}{dX_i} \quad , i = 1, \cdots, N$$

The residuals of the functions f_1 , $\cdots$, f_N replace the the gradients of the objective function, F, in the numerical optimization and the Jacobian of the functions, $f_1 \cdots f_N$, replace the Hessian of the objective function, F.
The direction vector, S, which drives the residuals to be zero, is given as follows according to Broyden in Ref. (49).

$$S^{p+1} = - [\, J^p \,]^{-1} R^p$$

where $R_i^p = f_i(X^p)$ and $J^p = \frac{df_i}{dX_j}(X^p)$.

A quasi-Newton or the conjugate gradient method of section (4.3) can be used to approximate the inverse of Jacobian.
The solution vector at p th iteration is given as follows.

$$X^{p+1} = X^p + \alpha S^p$$

α is determined by one dimensional line search in such a way that the norm of residuals attains its minimum with respect positive α. The initial estimate of α is obtained as follows.

$$\alpha \,||\, J_{ij}\, R_j \,||\, = 0 \;-\; ||\, R_i \,||$$

$$\alpha \;=\; \frac{-\,||\, R_i \,||}{||\, J_{ij}\, R_j \,||}$$

|| || denotes the norm of the vector. We can choose the individual α .

$$\alpha_i \;=\; \frac{-\,R_i}{J_{ij}\, R_j}$$

Then, $\alpha \;=\; ||\, \alpha_i \,||$

Let's consider the system of equations F which are the function of the independent variable vector U.

Then,

$$F\,(U^n) \;+\; \frac{dF}{dU}\,(U^{n+1} - U^n) = 0$$

$$U^{n+1} = U^n - \left[\frac{dF}{dU}\right]^{-1} F\,(U^n)$$

$F\,(U^n)$ is the residual vector, R and $\frac{dF}{dU}\,(U^n)$ is the Jacobian, J. When J and J^{-1} are computed exactly, the above formula becomes the Newton's method. We can put in the following form.

$$U^{n+1} = U^n - \alpha \left[\frac{dF}{dU}\right]^{-1} F\,(U^n)$$

α is chosen such that the norm of the residual vector $F\,(U^n)$ attains its minimum with respect to the positive α.
When the Jacobian J is nonsingular and symmetric, the above method is exact in that the solution vector, U converges

in a finite number of iterations. Also, we can use the approximation formula for the inverse of J given in section (4.3) during each iteration. Then the solution vector U converges quadratically. In the above method the Jacobian or the inverse of the Jacobian does not have to have all eigen values which are less than one in absolute magnitude. In the case of Euler equations the differential equations should be discretized with respect to all field points ,including the boundary conditions, Then U vector becomes mass, momentum, and energy densities at all field and boundary points. For the N field points and K boundary conditions there are a system of (N +K) equations for each component of mass, momentum, and energy densities. Denpending on the discretization these system of equations are grouped with respect to cell nodes or centers. Further discussions are beyond the present study and can be found in many publications.

C. 3-D Momentum Theory

Three dimensional momentum theory assumes the independence of each annulus of rotor radius, dr. 3-D momentum theory equates the thrust produced by the momentum change in an annulus of rotor, dr , to the thrust obtained by the blade element.

$$dT = 2\, w(r)\, dm$$

where $dm = 2\,\Pi\, r\, \rho\, w(r)\, dr$

Also, for the blade element of dr,

$$dT = 0.5\, \rho\, \Omega\, (\Omega r)^2\, a \left[\Theta(r) - \frac{w(r)}{\Omega r}\right] C(r)\, dr$$

which leads to

$$\lambda\,(r) = \frac{a}{8}\left[-\frac{\sigma(r)}{2} + \sqrt{\left(\frac{\sigma(r)}{2}\right)^2 + \frac{8\,\eta\sigma(r)\,\Theta(r)}{a}}\right]$$

$$\text{for} \quad \Theta(r) > -\frac{\sigma(r)a}{32\,\eta}$$

$$\lambda\,(r) = \frac{a}{8}\left[\frac{\sigma(r)}{2} - \sqrt{\left(\frac{\sigma(r)}{2}\right)^2 - \frac{8\eta\,\sigma(r)\,\Theta(r)}{a}}\right]$$

$$\text{for} \quad \Theta\,(r) < -\frac{\sigma(r)a}{32\,\eta}$$

where $\lambda\,(r) = \frac{w(r)}{\Omega R}$ and $\sigma(r) = \frac{Q\, C(r)}{\Pi R}$

The work done by the rotor can be calculated by the account of the energy change in the wake.

$$dT \cdot w(r) = dm\ 0.5\ (2w)^2$$

$$dT = dm\ 2\ w(r)$$

REFERENCES

(1) Spreiter,J. and Sacks, A.H.,"The Rolling up of the Trailing Vortex Sheet and Its Effect on Downwash Behind Wings", Journal of Aeronautical Sciences 18, 21.

(2) Ferziger, J., "Energetics of Vortex Rollup and Pairing", Physics of Fluids 23 (1), 1980.

(3) Landahl, M.,"Roll Up Model for Rotor Wake Vorices", The Aeronautical Research Institute of Sweden, TN HU-2262, 1981.

(4) Widnall, S.E., "The Structure and Dynamics of Vortex Filaments", Annual Review of Fluid Mechanics, 7. 141, 1975.

(5) Wu,J.C., Sanker,N.L. and Hsu, T.M.,"Some Applications of a Generalized Aerodynamic Forces and Moments Theory", AIAA paper 83-0543.

(6) Felker, F.F., Maisel, M.D., and Betzina, M.D., "Full Scale Tilt Rotor Hover Performance", 41st Annual Forum of the American Helicopter Society, Ft. Worth, TX, May 15-17,1985.

(7) Miller,R.H.,"Simplified Free Wake Analysis for Rotors", FFA(Sweden) TN 1982-7; also MIT ASRL TR 194-3.

(8) Miller,R.H.,"Free Wake Techniques for Rotor Aerodynamic Analysis, Volume I : Summary of Results and Background Theory", NASA CR-166434, 1983.

(9) Miller,R.H.,"Factors Influencing Rotor Aerodynamics in Hover and Forward Flight", 10th European Rotorcraft Forum, paper No.11, August 28-31, 1984.

(10)Miller,R.H.,"A Simplified Approach to the Free Wake Analysis of a Hovering Rotor", Vertica, Vol. 6, pp 89-95, 1982.

(11)Miller,R.H.,"Application of Fast Free Wake Analysis Techniques to Rotors", Vertica. Vol.8, No.3, pp255-261,1984.

(12)Brower,M.,"Lifting Surface and Lifting Line Solutions for Rotor Blade Interaction with Curved and Straight Vortex Lines", MIT ASRL TR 194-5, November 1981.

(13)Brower,M.,"Free wake Techniques for Rotor Aerodynamic Analysis, Volume III : Vortex Filament Models", NASA CR -166434, 1983.

(14)Tanuwidjaja,A.,"Free Wake Techniques for Rotor Aerodynamic Analysis, Volume II : Vortex Sheet Models", NASA CR -166434, 1983.

(15)Kocurek,J.D.,Berkowitz,L.F., and Harris,F.D., "Hover Performance Methodology at Bell Helicopter Textron", 36th Annual Forum, American Helicopter Society, May 1980.

(16)Shenoy,K.R. and Gray,R.B., "An Iterative Lifting Surface Method for Thick Bladed Hovering Helicopter Rotors", AIAA paper 79-

(17)Djojodihardjo,R.H. and Widnall, S.E., "A Numerical Method for the Calculation of Nonlinear, Unsteady Lifting Potential Flow Problems", AIAA Journal, Vol.7, No.10,October 1969.

(18)Preuss,R.D., Suciu,E.O., and Morino,L.,"Unsteady Potential Aerodynamics of Rotors with Applications to Horizontal-Axis Windmills", AIAA Journal, Vol.18, No.4, April 1980.

(19)Clark,D.R., "Development of Aerodynamic Modelling Method to Include Seperated Flow", Journal of American Helicopter

Society, October 1980.

(20)Johansson,B.C.A.,"Compressible Flow about Helicopter Rotors" ,Vertica, 1978, Vol.2, pp 1-9.

(21)Johnson,W., "A Lifting Surface Solution for Vortex Induced Airloads", AIAA Journal, Vol.9, No.4, April 1971.

(22)Bristow,D.R., Hawk, J.D., and Thomas,J.L.,"Subsonic 3-D Surface Panel Method for Rapid Analysis of Mutiple Geometry Perturbations", AIAA paper 82-993.

(23)Mcveigh,M.A. and Mchugh, F.J.,"Influence of Tip Shape, Chord, Blade Numbers, and Airfoil on Advanced Rotor Performance", Journal of American Helicopter Society, October 1984.

(24)Roberts,T.W. and Murman, E.M., "A Computational Method for Helicopter Vortex Wakes", AIAA paper 84-1554.

(25)Tai,T.C., Kidwell,G.H., and Vanderplaats,G.W., "Numerical Optimization of Circulation Control Airfoils", AIAA paper 81-0016.

(26)Liu,C.H., Thomas,J.L., and Tung,C.,"Navier-Stokes Calculation for the Vortex Wake of a Rotor in Hover", AIAA paper 83-1676.

(27)Hess,J.L. and Smith,A.M.O., "Calculation of Non-lifting Potential Flow about Arbitrary Three-dimensional Bodies", Report No. E.S. 40622, McDonnell Douglas Corporation, March 1962.

(28)Gohard,J.D.,"Free Wake Analysis of Wind Turbine Aerodynamics" ,MIT ASRL TR 184-14, September 1978.

(29)Chung,S.Y., "Aerodynamics of Wind Turbine with Tower Disturbines", MIT ASRL TR 184-15, September 1978.

(30)Teng,Z.H.,"Elliptic-Vortex Method for Incompressible Flow

at High Reynolds Number", J. Comput. Pyysics, Vol. 1982.

(31)Inoue,O.,"Vortex Simulation of a Turbulent Mixing Layer", AIAA Journal, Vol.23, No.3, March 1985.

(32)Roberts,T.W. and Murman, E.M.,"Solution Method for a Hovering Helicopter Rotor using the Euler Equations", AIAA paper 85-0436.

(33)Johnson, F.T.,"A General Panel Method for the Analysis and Design of Arbitrary Configurations in Incompressible Flows", NASA-CP-3079, 1980.

(34)Hess,J.L.,"Calculation of Potential Flow about Arbitrary Three-dimensional Lifting Bodies", Final Technical Report, MDC J5679-01,McDonnell Douglas Corporation, Long Beach, California, October 1972.

(35)Johnson,W.,"Comparison of Calculated and Measured Model Rotor Loading and Wake Geometry", NASA TM 81189, April 1980.

(36)Lan,C.E., "Quasi-Vortex-Lattice Method in Thin Wing Theory", J. Aircraft, Sept. 1974.

(37)Liebst,B.S., "A Pitch Control System for Large Scale Wind Turbines", Ph.D. Thesis, M.I.T., August 1981.

(38)McCormick,B.W., "The Application of Vortex Theory to the Optimum Swept Propellers", AIAA paper 84-0036.

(39)Chang,L.K. and Sullivan,J.P., "Optimization of Propeller Blade Twist by an Analytical Method", AIAA Journal Vol.22, No. 2, February 1984.

(40)Ashley,H., "On Making Things the Best - Aeronautical Uses of Optimizations", J. Aircraft, Vol. 19, No.1,January 1982.

(41)Murman, E.M. and Chapman,G.T., "Aerodynamic Design Using

Numerical Optimization", MIT CFDL-TR-93-2, February 1983.

(42)Vanderplaats,G.N., Hicks,R.N., and Murman, E.M., "Application of Numerical Optimization Techniques to Airfoil Design", NASA-SP-347, Part II, March 1975.

(43)Peeters,M.F., "Computational Methods for Aerodynamic Design Using Numerical Optimization", M.S. Thesis, M.I.T., Feb. 1983.

(44)Larson,G.L., "Acceration of Aerodynamic Design Optimization through Interleaving of Aerodynamic and Optimization Iterations", M.S. Thesis, M.I.T., May 1983.

(45)Miura,H., "Application of Numerical Optimization Methods to Helicopter Design Problems", 10th European Rotorcraft Forum, August 28-31, 1984.

(46)Friedman,P.P. and Shanthakumaran,"Optimum Design of Rotor Blade for Vibration Reduction in Forward Flight", Journal of the American Helicopter Society, October 1984.

(47)Walsh,J.L., Bingham,G.J., and Riley, M.F.,"Optimization Methods Applied to the Aerodynamic Design of Helicopter Rotor Blades", AIAA 26th Structures, Structural Dynamics and Materials Conference, April 15-17, 1985.

(48)Consentino,G.B. and Holst, T.L., "Numerical Optimization Design of Advanced Transonic Wing Configurations", AIAA paper 85-0424

(49)Broyden,C.G., "Quasi-Newton Methods and Their Application to Function Minimization", Math. of Comp. ,Vol. 21, No.99, 1967, pp 368-380.

(50)Fletcher,R. and Reeves, C.M., "Function Minimization by Conjugate Gradients', Computer J. Vol.7, No.2, July 1964, pp 149-154.

(51)Fletcher,R. and Powell,M.J.D., "A Rapidly Convergent Descent Method for Minimization", Computer J., Vol.6, No. 2, July 1963, pp 163-168.

(52)Vanderplaats, G.N., "Numerical Optimization Techniques for Engineering Design", McGraw-Hill Book Comp., 1984.

(53)Vanderplaats,G.N., "CONMIN-A FORTRAN Program for Constrained Function Minimization User's Manual", NASA TM X-62282, Aug., 1973.

(54)Topping,B.H.V. and Robinson,D.J., "Selecting Non-linear Optimization Techniques for Structural Design", Eng. Comput., 1984, Vol. 1, September.

(55)Hess,J.L. and Smith,A.M.O., "Calculation of Potential Flow about Arbitrary Bodies", Progress in Aeronautical Sciences, Vol.8, Pergaman Press, 1967.

(56)Johnson, Forrester T. and Rubbert, Paul E.," Advanced Panel -Type Influence Coefficients Methods Applied to Subsonic Flows", AIAA Paper 75-50.

(57)Rubbert, P.E. and Sarris,G.R.,"Review and Evaluation of a Three-Dimensional Lifting Potential Flow Computation Method for Arbitrary Configurations", AIAA paper 72-188.

(58)Basu, B.C. and Hancock, G.J., "The Unsteady Motion of a Two-Dimensional Aerofoil in Incompressible Inviscid Flow", J. Fluid Mech. (1978) Vol.87, part 1, pp 159-178.

(59)Maskew, Brian. and Dvorak, Frank A.,"The Prediction of Cl Using a Seperated Flow Model", Journal of the American Helicopter Society, April 1978.

(60)Maskew,B., "Influence of Rotor Blade Tip Shape on Tip Vortex Shedding -- An Unsteady, Inviscid Analysis", 36th

Annual Forum of the American Helicopter Society, Washington D.C. May 1980.

(61)Carey, G.F. and Kim, S.W., "Lifting Aerofoil Calculation Using th Boundary Element Method", International Journal for Numerical Methods in Fluids, Vol.3, 481-492(1983).

(62)Kraus,Werner, "Panel Method in Aerodynamics", A Von Karman Institute Book : Numerical Methods in Fluid Dynamics. Hemisphere Publishing Corporation (1978)

(63)Chen, Lee-Tzong, Suciu, Emil O., and Morino, Luigi, "A Finite Element Method for Potential Aerodynamics around Complex Configurations", AIAA paper 74-107.

(64)Kuethe, Arnold M. and Chow, Chen-Yen, "Foundations of Aerodynamics", John WileySons, Inc. (1976).

(65)Abbot,I.H. and Doenhoff, A.E., "Theory of Wing Sections", Dover, 1958.

(66)Lamb, H., "Hydrodynamics", Dover, 1945.

(67)Experimental Data Obtained by Weston, R. and Supplied by Roberts, Thomas.

(68)Ballard, John D.; Orloff, Kenneth L.; and Luebs, Alan B., "Effect of Tip Shape on Blade Loading Characteristics for a Two-Bladed Rotor in Hover," 35th Annual National Forum of the American Helicopter Society, Washington, D.C., May 1979.

(69)Miller, R.H., unpublished communication.